

NASA-CR-167,978

DOE/NASA/0059-1  
NASA CR-167978  
SRD-81-088

NASA-CR-167978  
19830002079

# Improved Transistorized ac Motor Controller for Battery Powered Urban Electric Passenger Vehicles

Steven C. Peak  
Corporate Research and Development  
General Electric Company

**September 1982**

Prepared for  
NATIONAL AERONAUTICS AND SPACE ADMINISTRATION  
Lewis Research Center  
Under Contract DEN 3-59

for  
**U.S. DEPARTMENT OF ENERGY  
Conservation and Renewable Energy  
Office of Vehicle and Engine R&D**

**LIBRARY COPY**

JUN 15 1983

LANGLEY RESEARCH CENTER  
LIBRARY, NASA  
HAMPTON, VIRGINIA



NF01860

#### **NOTICE**

This report was prepared to document work sponsored by the United States Government. Neither the United States nor its agent, the United States Department of Energy, nor any Federal employees, nor any of their contractors, subcontractors or their employees, makes any warranty, express or implied, or assumes any legal liability or responsibility for the accuracy, completeness, or usefulness of any information, apparatus, product, or process disclosed, or represents that its use would not infringe privately owned rights.

DOE/NASA/0059-1  
NASA CR-167978  
SRD-81-088

# **Improved Transistorized ac Motor Controller for Battery Powered Urban Electric Passenger Vehicles**

Steven C Peak  
Power Electronics Laboratory  
Corporate Research and Development  
General Electric Company  
Schenectady, New York 12345

September 1982

Prepared for  
National Aeronautics and Space Administration  
Lewis Research Center  
Cleveland, Ohio 44135  
Under Contract DEN 3-59

for  
U S DEPARTMENT OF ENERGY  
Conservation and Renewable Energy  
Office of Vehicle and Engine R&D  
Washington, D.C. 20585  
Under Interagency Agreement DE-AI01-77CS51044

*N83-10349#*

**All Blank Pages  
Intentionally Left Blank  
To Keep Document Continuity**

## TABLE OF CONTENTS

Section	Page
1 SUMMARY	1
2 INTRODUCTION	2
2 1 Background	2
2 2 The AC Propulsion System	2
2 3 Objectives	2
2 4 Scope	3
3 ANALYSIS AND DESIGN	4
3 1 Propulsion System Requirements Review and Analysis	4
3 2 Motor Requirements Review and Analysis	8
3 2 1 Induction Motor Characteristics	8
3 2 2 Motor Tractive Effort and Speed Requirement	10
3 2 3 Motor Torque and Speed Requirement	12
3 2 4 Equivalent Motor Rating	13
3 3 Motor Design	14
3 3 1 Motor Description	14
3 3 2 Advantages of the GE Optimized Motor	18
3 4 System Design and Controller Requirements	19
3 4 1 System Voltage	19
3 4 2 Motoring Corner Point Speed	19
3 4 3 Motor Voltage and Current Schedules	19
3 4 4 Motor Performance	21
3 4 5 Effects of Pulse Width Modulation (PWM)	24
3 4 6 Motor Leakage Reactance and Harmonics	29
3 4 7 Controller and Power Module Requirements	30
3 5 Drive System Description	32
3 5 1 Control Strategy	32
3 5 2 Current-Controlled PWM	34
3 5 3 System Control	36
3 5 4 Power Inverter	40
3 6 Control Electronics	41
3 6 1 Current Control Loop	45
3 6 2 Outer Loop Controls	46
3 6 2 1 Flux regulator	46
3 6 2 2 Angle regulator	47
3 6 2 3 Real current regulator	47
3 6 3 Motor Reversing	48
3 6 4 Other Functions	49
3 6 5 Control Performance	49
3 7 Power Inverter	50
3 7 1 Power Circuit	50
3 7 2 Inverter Switching Frequency	54
3 7 3 Inverter Packaging	54
3 7 4 Power Darlington Transistor Base Drive	55
3 7 5 Power Darlington Transistor Snubber	57
3 7 6 Power Inverter Performance	59

## TABLE OF CONTENTS (Cont'd)

Section	Page
3 8 Transistor Power Modules	60
3 8 1 Available Transistors	60
3 8 2 Power Darlington Chip	60
3 8 3 Power Darlington Substrate	62
3 8 4 Thermal Resistance and Thermal Cycling	63
3 8 5 Electrical Performance	65
3 8 6 Power Module	66
3 8 7 Half-Phase Module Testing	68
3 9 Controller Family Expansion	70
3 9 1 Assumptions	70
3 9 2 Input Capacitor Scaling	70
3 9 2 1 Summary	70
3 9 2 2 Assumptions	71
3 9 2 3 Calculations	71
3 9 3 Motor Parameter Scaling	73
3 9 3 1 Summary	73
3 9 3 2 Assumptions	73
3 9 3 3 Calculations	73
3 9 4 Power Module Scaling	75
3 9 4 1 Summary	75
3 9 4 2 Assumptions	75
3 9 4 3 Calculations	75
3 9 5 Power Module Snubber Scaling	78
3 9 5 1 Summary	78
3 9 5 2 Assumptions	78
3 9 5 3 Calculations	78
3 9 6 Base Drive Scaling	80
3 9 6 1 Summary	80
3 9 6 2 Calculations	81
3 9 7 Base Drive Power Supply Scaling	83
3 9 7 1 Summary	83
3 9 7 2 Calculations	84
3 9 8 Control Scaling	85
3 9 8 1 Summary	85
3 9 8 2 Control timing considerations	86
3 9 8 3 Driver command and jerk limit	88
3 9 8 4 Lockout and waveform generator	89
3 9 8 5 Flux control	89
3 9 8 6 Angle regulator	89
3 9 8 7 Current magnitude, limit, and controller	89
3 9 8 8 Zero speed detector and protective circuits	90
3 9 8 9 Current interface and summing, and torque	90
3 9 9 Logic Power Supplies	90
3 10 Controller Family Life Cycle Cost Estimates	92
3 10 1 Life Cycle Cost Estimates Summary	92
3 10 2 Description of Life Cycle Cost Analysis	93
3 10 3 Elements of Capital Cost	97
3 10 3 1 Power circuit cost estimate summary	97
3 10 3 2 Control circuit cost estimate summary	98

**TABLE OF CONTENTS (Cont'd)**

<b>Section</b>	<b>Page</b>
3 10 3 3 Controller cost estimate summary	99
3 10 3 4 Salvage credit	100
3 10 4 Elements of Recurring Cost .. . . .	100
3 10 4 1 Maintenance and repair costs	100
3 10 4 2 Controller weight	100
3 10 5 Economic Parameters	102
3 11 Battery Charger	103
3 11 1 On-Board Battery Charging	103
3 11 2 Battery Charger Maximum Power Specifications	103
3 11 3 Boost Chopper Approach	104
3 11 4 Charger Operation	105
3 11 5 Major Component Sizing	107
3 11 5 1 Inductor	107
3 11 5 2 Transformer	110
3 11 6 Efficiency Estimates	110
3 11 6 1 Transformer	111
3 11 6 2 Transistor switching loss	111
3 11 6 3 Transistor saturation loss	111
3 11 6 4 Blocking diode loss	112
3 11 6 5 Inductor losses	112
3 11 6 6 Control power losses	112
3 11 6 7 Summary losses	113
<b>4 TEST AND EVALUATION</b>	<b>114</b>
4 1 Test Plan	114
4 1 1 Steady-State Tests	114
4 1 2 System Cyclic Tests	114
4 2 Test Instrumentation	116
4 3 Controller Transfer Functions	123
4 4 Motor No-Load Excitation	130
4 5 Motor Flux Operating Point	131
4 6 AC Current Waveforms	132
4 7 AC Voltage Waveforms	137
4 8 Power Module Waveforms	141
4 9 Controller Performance Characterization	144
4 10 Controller Loss Separation	147
4 11 Efficiency Mapping	149
4 12 Drive System Performance Recordings	163
<b>5 RESULTS AND CONCLUSIONS</b> . . . . .	<b>166</b>
<b>6 APPENDICES</b>	<b>169</b>
Appendix A — ELECTRIC VEHICLE PERFORMANCE ANALYSIS AND SPECIFICATION	169
Appendix B — DESCRIPTION OF INDIVIDUAL CONTROL CARD OPERATION	177

## TABLE OF CONTENTS (Cont'd)

Section		Page
	Appendix C – SETUP INSTRUCTIONS FOR AC CONTROLLER OPERATION	185
	Appendix D – AC CONTROLLER DRAWINGS	189
	Appendix E – AC CONTROLLER PRODUCTION MODEL COSTING	215
7	DEFINITIONS	226
8	REFERENCES	228

## Section 1

### SUMMARY

The objectives of this NASA/DOE sponsored program for an improved ac motor controller for battery powered urban electric passenger vehicles were the design, fabrication, test, evaluation and cost analysis of an engineering model controller for an ac induction motor drive system, the investigation of a power level expansion to a family of horsepower and battery system voltages, and the investigation of the applicability of the ac controller for use as an on-board battery charger and for providing the function of motor reversal

Additional vehicle specifications, e g , acceleration and pulling out of potholes, were added to the NASA vehicle specifications. Then, a vehicle performance analysis was done to establish the vehicle tractive effort-speed requirements. These requirements were then converted into a set of ac motor and ac controller requirements. The General Electric ac induction motor used in the drive is optimized to operate as a vehicle traction motor with a pulse width modulated (PWM) inverter as a power source. The motor is nominally rated 20 hp and 41 hp peak. The power inverter design is a three-phase transistorized bridge configuration with feedback diodes. The transistors are a special design General Electric high-power Darlington transistor rated 450 volts and 200 amps. The battery system voltage chosen was 108 volts. The control strategy is a constant torque profile by PWM operation to base speed and a constant horsepower profile by square-wave operation to maximum speed. A gear shifting transmission is not required. An advanced current-controlled PWM technique is used to control the motor voltage. The primary feedback control is a motor angle control, with voltage and torque outer loop controls. These advanced controls do not require a tachometer, allow a transition from PWM to square wave operation, and reduce motor flux (open loop) at light load to optimize motor efficiency. This drive system approach is scaled to a family of ac controllers over a range of 10-50 horsepower and 84-300 volts dc. Motor reversal is easily accomplished by electronic reversal of the inverter phase sequence. The battery charging function can be implemented with a boost chopper using two phases of the inverter.

The principal results and conclusions are

- The feasibility of the transistorized ac inverter-induction motor drive was demonstrated
- The current-controlled PWM method has improved motor current waveforms.
- The life cycle cost of the ac controller is 2.4¢/km (3.9¢/mile)
- The ac controller cost, size, and efficiency favor a higher system voltage
- Suitable power transistors are becoming more readily available but are costly, however market forces and volume production are expected to alleviate this in the future
- Future development work should be directed toward snubbers, high-voltage power transistors, inverter packaging, transistor base drives, and control design and hardware implementation

## Section 2 INTRODUCTION

### 2.1 BACKGROUND

A very large portion of the petroleum consumed in the United States is used for transportation. The introduction of electric vehicles could significantly shift the transportation energy base to other energy sources, e.g., coal, nuclear, or solar sources.

In 1976, the Electric and Hybrid Vehicle Program was initiated within the Energy Research and Development Administration (ERDA), now the Department of Energy (DOE). In September of that same year, Congress passed the Electric and Hybrid Vehicle Research, Development, and Demonstration Act of 1976 (Public Law 94-413). This Act and its amendments are intended to accelerate the integration of electric and hybrid vehicles into our transportation system and to stimulate growth in the electric vehicle industry.

The NASA Lewis Research Center has been given the authority by DOE to issue contracts for Research and Development of Propulsion Systems and Components for Electric and Hybrid Vehicles. This contract was one element of parallel efforts involving transmissions, motors, controllers, and other propulsion system components, as such, it represented the first step in the development of improved and/or advanced vehicle power train technology.

### 2.2 THE AC PROPULSION SYSTEM

Presently the dc motor and dc controller combination is the dominant electric vehicle drive system configuration, with only a few vehicles using an ac system. However, recent studies comparing various electric vehicle propulsion system approaches have concluded that the most promising drive system for near term electric vehicle use is the ac induction motor with a pulse width modulated (PWM) transistor inverter based controller<sup>(1)</sup>. The dc drive system has been the logical choice because of the maturity of the dc chopper technology, the performance available from well-understood control strategies, and the suitability of the dc motor to traction drives. The impetus behind the ac drive system is the cost, maintenance, size, reliability, and efficiency advantages of the ac induction motor. The size, cost, and complexity of the controller for this motor represent the technical challenge to the potential and desirable advantages of the ac induction motor. Much of the complexity of the controller exists in the signal level controls, where advances in microelectronics technology will play a significant role in reducing cost and parts count. The evolution and downward price trend in high-power transistors will allow the power inverter to be economically feasible and reliable.

### 2.3 OBJECTIVES

The specific objectives of the contract were.

1. To develop a cost-effective, lightweight, efficient, and highly reliable engineering model controller for a variable speed traction ac polyphase induction motor, using current microcircuit logic and the best state-of-the-art dc-to-ac inverter technology available.
2. To investigate expanding the power level capability of the engineering model controller by means of modularization and/or scaling, and to define a family of controllers for conventional polyphase motor sizes ranging from 10 hp to 50 hp (nominal 60 Hz, synchronous speed ratings).
3. To examine and characterize the applicability of the engineering model controller for use as an on-board battery charger, and for providing the function of motor reversal.

## 2.4 SCOPE

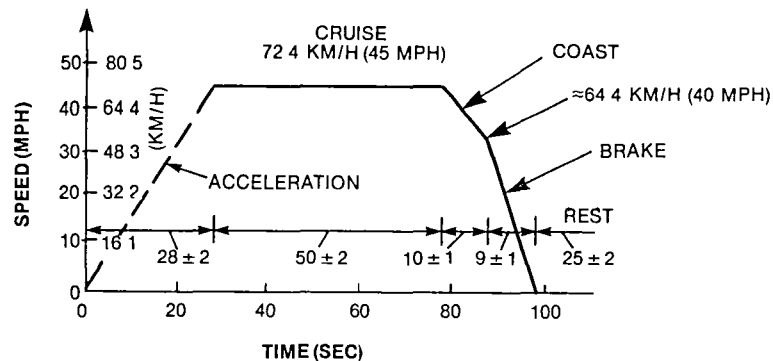
The scope of the work accomplished consists of the design, fabrication, test, evaluation, and cost analysis of an engineering model controller for conventional polyphase ac motors used in battery-powered electric vehicle applications. Additional work included the investigation and characterization of the controller's potential for growth. This program combined design and hardware. A set of general requirements were specified for a class, or family, of controllers applicable to a range of motor power ratings. The design and fabrication of a controller from this family to operate a specific motor size occurred during the hardware phase and the operation was demonstrated by tests on a dynamometer. The controller was further analyzed and evaluated relative to scaling for a wider power range, cost effectiveness, and impact on overall motor-controller energy efficiency.

### Section 3 ANALYSIS AND DESIGN

This section details all the analysis and design of the ac controller and ac induction motor. This section is organized to present first the drive system design aspects, then the power inverter and control electronics design aspects and lastly the separate tasks of controller scaling, life cycle cost and battery charging. The first section is a review of the vehicle performance requirements and the analysis of these requirements to obtain the vehicle tractive effort and speed requirements at the vehicle wheels (Section 3.1). These requirements are then translated into a drive system specification of the required motor torque and speed at the motor shaft (Section 3.2). The motor design (Section 3.3) follows the motor requirements. The drive system design and resulting specifications for the power inverter and power semiconductors are presented next (Section 3.4). An overall description of the drive system configuration (Section 3.5) is followed in order by the control electronics design (Section 3.6), power inverter design (Section 3.7) and transistor power module design (Section 3.8). The next two sections involve the controller family expansion by scaling (Section 3.9) and controller family life cycle cost estimates (Section 3.10). The last section concerns the use of the ac controller as an on-board battery charger (Section 3.11).

#### 3.1 PROPULSION SYSTEM REQUIREMENTS REVIEW AND ANALYSIS

As a general requirement, the ac controller is designed for use in urban electric vehicles according to the SAE J227a—Schedule D driving cycle (Figure 3.1-1), including grade climbing and 89 km/h (55 mph) constant-speed operation. The specifications are primarily vehicle performance requirements and must be analyzed and converted into vehicle tractive effort and speed requirements. A general method for performing this analysis and conversion of the performance requirements of an electric vehicle is presented in Appendix A. This method uses the basic principles which characterize all electrical propulsion systems, regardless of the type of traction motor. This method has also been used to evaluate the effects of regenerative braking and to determine the energy required for driving<sup>(1)</sup>. It has evolved from previous work with electrically propelled rail cars<sup>(2)</sup>.



NOTE THE SHAPE OF THE ACCELERATION PORTION OF THE DUTY CYCLE CURVE IS UNDEFINED

Figure 3.1-1 SAE J227a – Schedule D Driving Cycle

The NASA drive system specifications are presented in two parts. The first is entitled “Tentative Motor Specifications” (Table 3.1-1). The second part of the specification shows the power and speed requirements for the ac motor to meet the SAE J227a—Schedule D driving cycle (Figure 3.1-2). This cycle is based on a vehicle gross weight of 1633 kg (3600 lb) and allows a two-speed transmission. In addition, a practical electric vehicle must satisfy performance requirements in excess of the J227a-D duty cycle in order to merge with traffic, start on a steep grade, pull out of a pothole, and pass. Additional specifications have been added to the NASA specifications to account for these requirements. A summary of specifications is shown in Table 3.1-2. The additional specifications define the maximum desired vehicle performance. Several of these will occur only once or twice per battery charge. The NASA specifications define the basic thermal ratings and performance. These performance requirements are analyzed in detail in Appendix A and the results of this analysis are shown in Figure 3.1-3. This figure is a vehicle specification of tractive effort versus vehicle speed at the vehicle wheels.

**Table 3.1-1**

**TENTATIVE MOTOR SPECIFICATIONS**

Frame Size	NEMA 215TD (aluminum frame) or equivalent
Type	Three-phase, squirrel cage, induction
Horsepower	10 hp, nominal at 60 Hz, 1800 rpm
Voltage Rating	17.5/35 volts RMS at 60 Hz (double windings for series or parallel connected operation)
Frequency	60 Hz, nominal
Speed	Nominal 1800 rpm at 60 Hz
Speed Range	0 to 8000 rpm as per Figure 3.1-2
Horsepower Range	As per Figure 3.1-2
Insulation	Class F
Duty	Continuous driving cycle SAE J227a, Schedule D, (2 hours)
	Constant 72 km/h (45 mph) vehicle speed (3 hours)
	Constant 89 km/h (55 mph) vehicle speed (2 1/2 hours)
	Constant 48 km/h (30 mph), 10% grade (1 minute)
Cooling	Forced air with external blower
Blower Rating	12 VDC, 120 W, 250 CFM thermostatically controlled

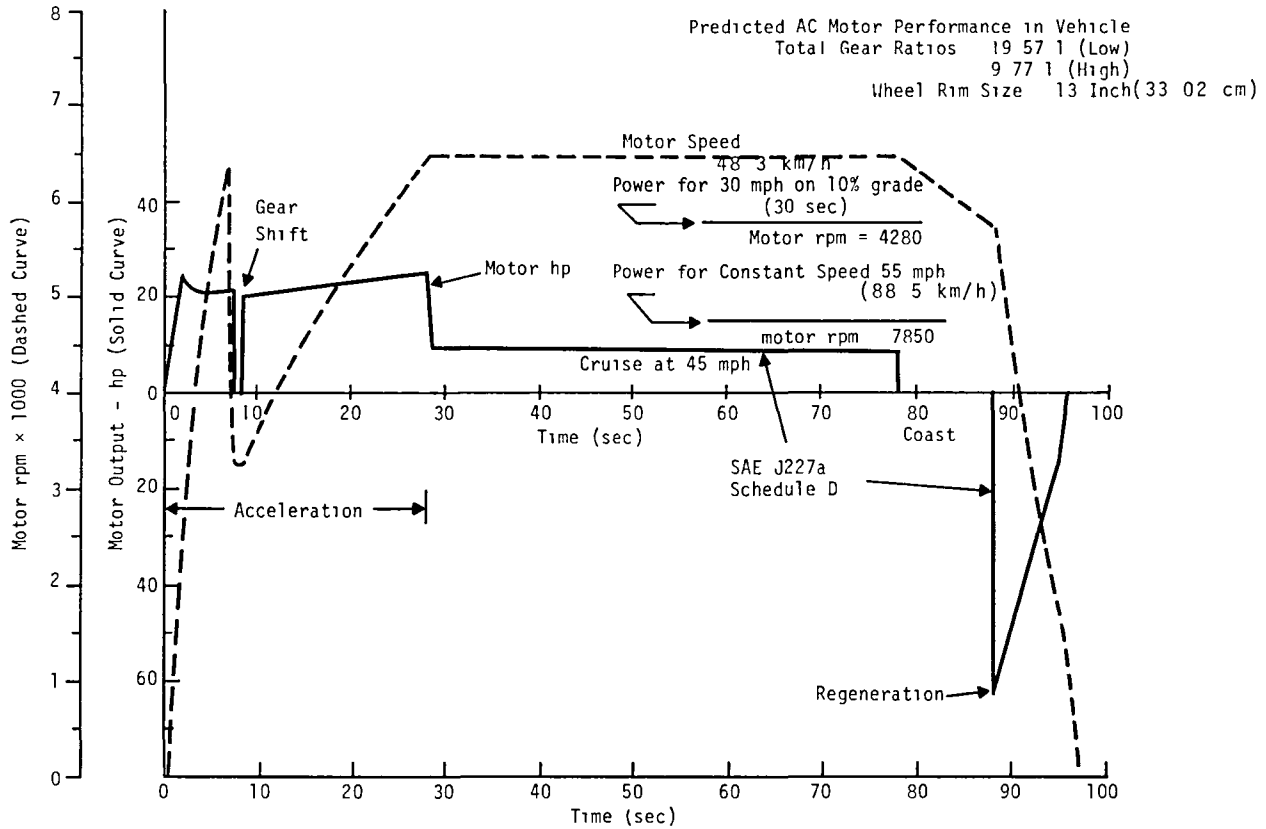


**Figure 3.1-2 NASA Driving Cycle Requirement**

**Table 3.1-2**

**SUMMARY VEHICLE PERFORMANCE REQUIREMENTS**

- 1 Continuous operation on SAE J227a-Schedule D driving cycle
- 2 Constant speed at 72 km/h (45 mph) (3 hours)
- 3 Constant speed at 89 km/h (55 mph) (2 1/2 hours)
- 4 Constant speed at 48 km/h (30 mph) up a 10% grade (one minute)
- 5 Initial acceleration sufficient to start on an 18% grade
- 6 Acceleration from 0 to 48 km/h (30 mph) in 9 seconds
- 7 Merging acceleration of 40 km/h (25 mph) to 89 km/h (55 mph) in 18 seconds
- 8 Minimum balancing speed of 97 km/h (60 mph) for passing

*Note Assume gross vehicle weight of 1633 kg (3600 lb)*

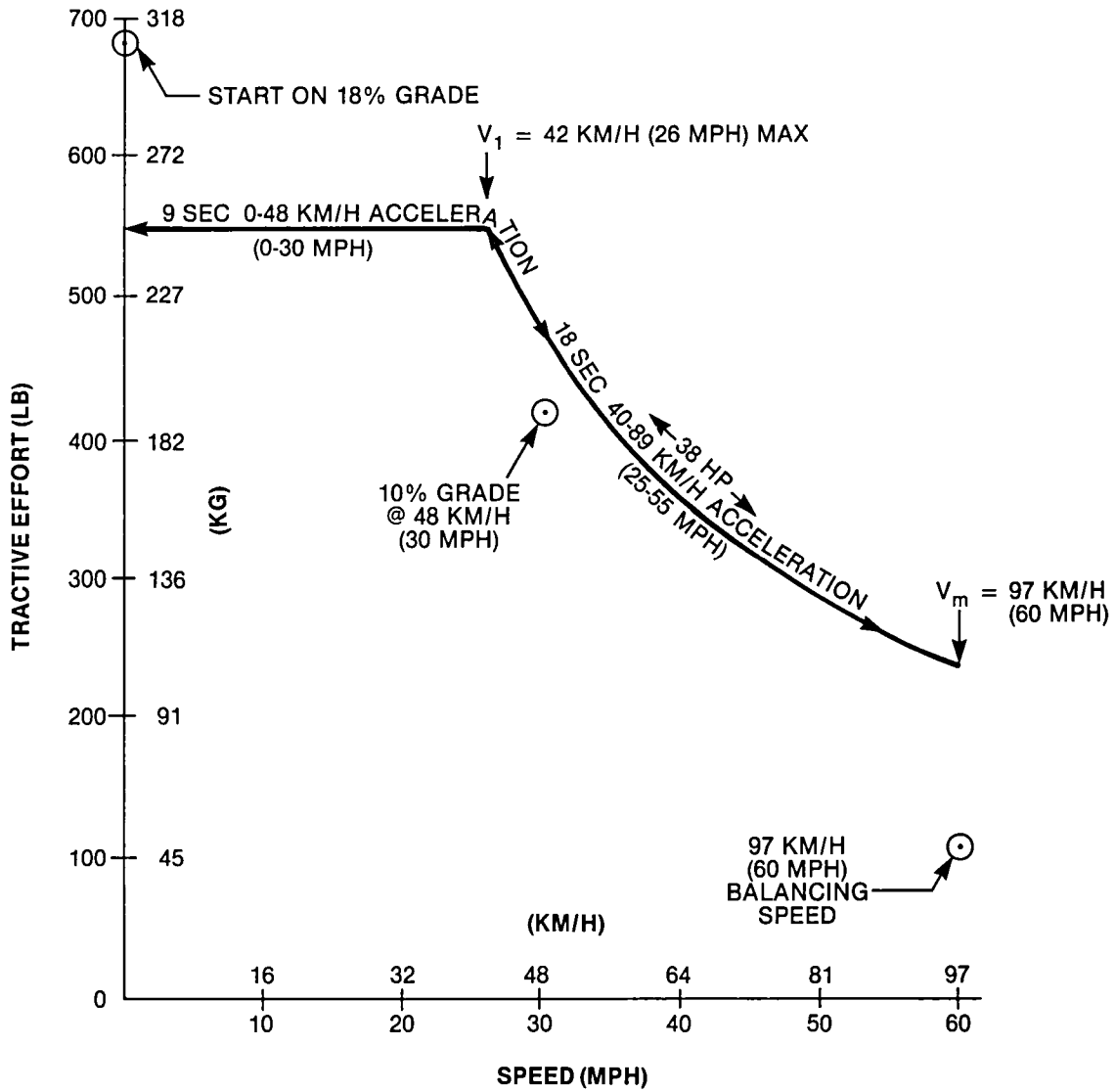


Figure 3.1-3 Summary Vehicle Specification

### 3.2 MOTOR REQUIREMENTS REVIEW AND ANALYSIS

After a review of induction motor characteristics, this section takes the vehicle tractive effort and speed requirements at the vehicle wheels and translates them into the required motor torque and speed at the motor shaft.

#### 3.2.1 Induction Motor Characteristics

AC drives in electric vehicles are considered in order to gain the advantages of low cost, low weight, high reliability, and high efficiency of the induction motor compared with the conventional chopper/dc motor drive system. An induction motor will be smaller than a dc motor (even a synchronous motor) of the same speed and rating (Figure 3.2.1-1). These advantages are gained at the cost of inverter weight, losses, expense, and control complexity. The ac drive itself is justified only if the weight of the drive system can be reduced and its cycle efficiency increased without significantly increasing costs. This can be achieved with a lightweight, high-speed, high-efficiency induction motor in a system where the inverter design, the control strategy, and the motor design have been carefully coordinated from the start. The effect of motor design and/or selection on overall system performance, weight, and cost is too often neglected or minimized. In fact, improper selection, design, or coordination with the power conditioner can result in excessive weight or cost and poor efficiency.<sup>(1,2)</sup>

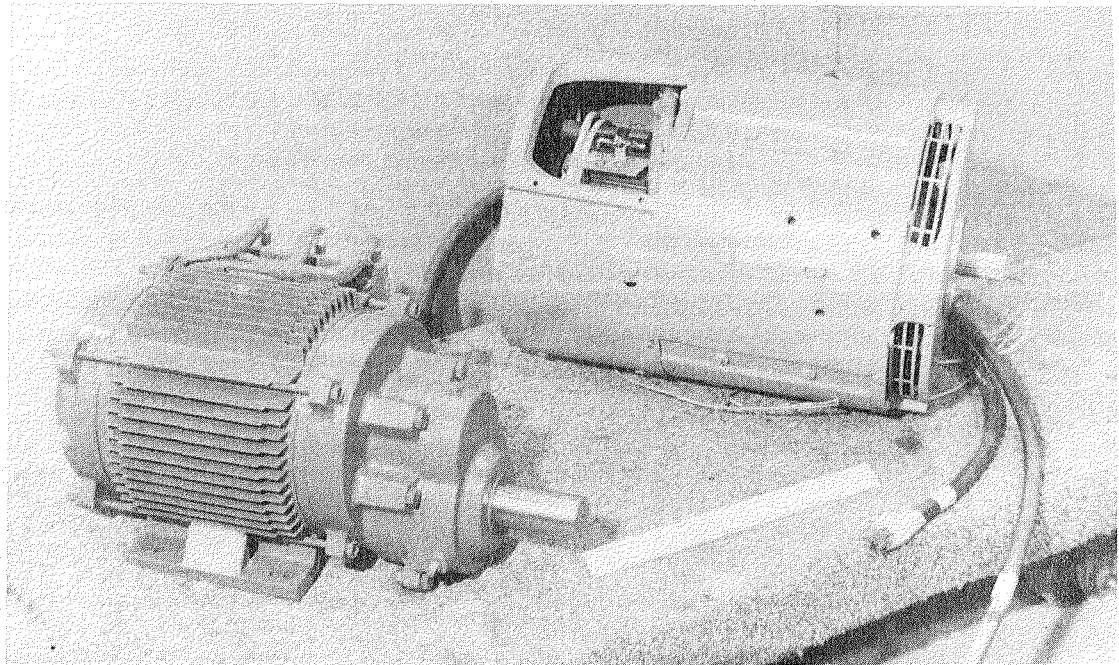


**Figure 3.2.1-1 A Comparison of the Induction Motor with the Standard DC Drive Motor**

*Note: The induction motor is less than half the weight of the dc motor and is higher in efficiency.*

A typical torque (or tractive effort) versus speed requirement for an electric vehicle (Figure 3.2.1-2) usually requires the motor to deliver constant power over a speed range of 2 to 1 or 3 to 1 to provide acceleration for high-speed merging. The speed to which constant torque is held is selected to meet an initial acceleration time requirement without exceeding the power required for merging. Typically, there is a high-speed cruise (level and grade) which

usually requires less torque than the merge. These conditions on the motoring performance typically will yield a motor also capable of full regenerative braking without increasing the size of the motor or inverter.

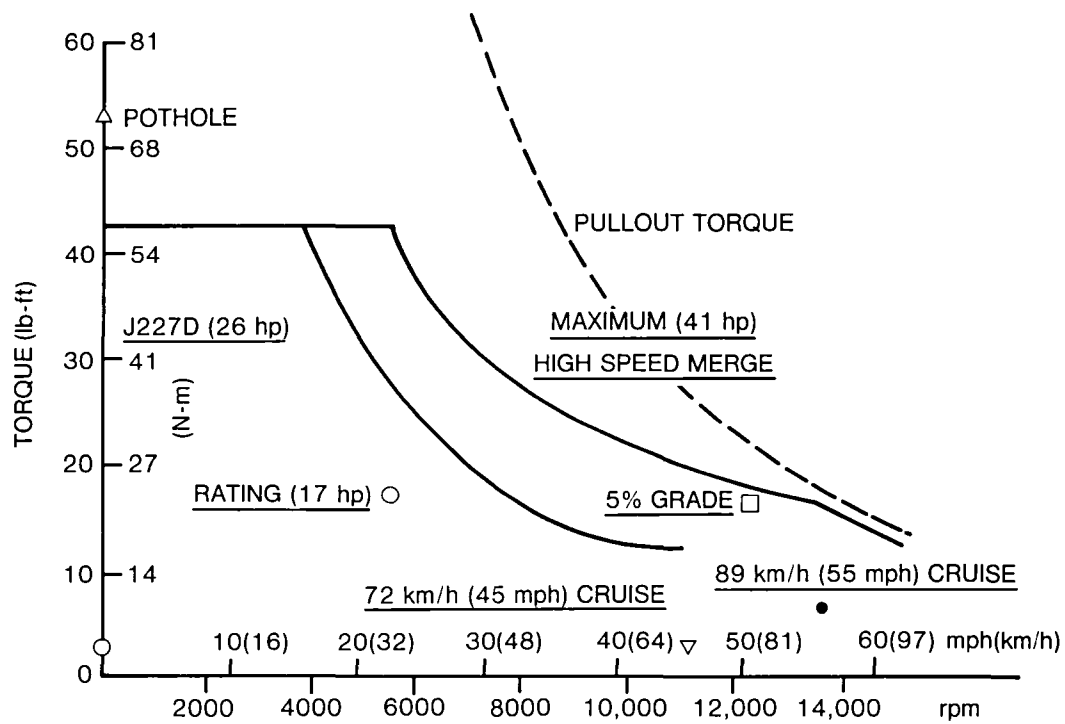


**Figure 3.2.1-2 Typical High-Speed Motor Torque Requirements**

The size and weight of the motor are proportional to the rated torque for continuous duty that must be delivered at the shaft. The rated torque for continuous duty is determined by (1) the maximum speed, (2) the maximum speed at which constant power must be delivered (for merge), and (3) the thermal duty. Therefore, an increase in speed (within the mechanical stress, bearing life, and converter frequency limits) will reduce the size of the motor. The steady-state temperature rise due to losses averaged over the driving cycle determines the rms stator current density allowable, which in turn determines the required air gap area. The influence of the constant power range is illustrated in Figure 3.2.1-2 by the dashed line, which represents the locus of pullout torque at constant voltage. Thus, the maximum speed at which full power must be delivered determines the pullout torque rating of the motor at the voltage corner point where the motor is at full flux. The induction motor is well suited for high-speed operation because of the inherent simplicity and ruggedness of the squirrel cage rotor. Squirrel cage induction motors have been run at 30,000 rpm. A squirrel cage induction motor/inverter drive system for an electric vehicle at 12,000 rpm has been successfully demonstrated.<sup>(3)</sup> Operation at about 15,000 rpm on an electric vehicle drive is within the state of the art of materials, bearings, gears, and electronics.

A motor designed for traction applications (ac or dc) can achieve a 2 to 1 or 3 to 1 constant power speed range at constant voltage without any significant increase in size. The inverter size is determined primarily by the motor current required, which can be minimized by designing the system to deliver the maximum power required by the application at the maximum inverter ac voltage output.

The zero and low-speed torque may be increased with a gearshift, thus reducing the inverter current required, but if the inverter is sized by other considerations (as it usually is), there is no advantage. Even where there is an advantage, studies have shown that the weight-saving in the inverter and motor is largely negated by the added weight of the gears.<sup>(7)</sup> Efficiency suffers because of the gear loss, especially at high speeds, where lubricant pumping accounts for a significant portion of the loss.

With proper design, the efficiency of the induction motor will be higher than a dc motor while meeting the same performance requirements, as it must in order to compensate for the inverter efficiency and motor harmonic losses. A properly designed high-speed induction motor will exhibit an almost constant, high efficiency over a wide speed range by keeping the magnetic,  $I^2R$ , and mechanical losses in balance, as they can be with proper machine design, control strategy, and inverter design. To attain the highest efficiency in the motor, it is desirable to optimize the design at lower values of current and flux density, use lower resistance materials for the rotor bars, and build with thinner laminations than normal. Suitable materials are commercially available for this type of design.

### 3.2.2 Motor Tractive Effort and Speed Requirement

The summary vehicle specification in Section 3.1 is the vehicle tractive effort and speed requirement at the vehicle wheels. In order to establish the motor specifications, it is necessary to translate this requirement from the vehicle wheels to the motor shaft. This involves including the rotary inertia effects of the drive which must be delivered by the drive system, but do not appear at the wheels. This effect is discussed in Appendix A. Using those equations, the results show that the drive system horsepower increases to 41 hp and the maximum corner point speed reduces to 40 km/h (25 mph). The 10% gradability, initial acceleration, and balancing speed specifications are unchanged.

The 40-89 km/h (25-55 mph) acceleration requirement establishes the drive horsepower rating of 41 hp (Figure 3.2.2-1). This sizes the power inverter and motor. The 10% gradability is inherently met if this acceleration is met (Figure 3.2.2-1). In fact, the actual performance would allow a 10% grade to be traversed at up to 58 km/h (36 mph), or a 13% grade could be climbed at 48 km/h (30 mph).

The 0-48 km/h (0-30 mph) acceleration requirement establishes the maximum corner point vehicle speed of 40 km/h (25 mph). The tractive effort at 40 km/h (25 mph) available from 41 hp is 279 kg (615 lb). This is the constant tractive effort available from zero speed to the corner point. The initial acceleration requires 309 kg (681 lb) of tractive effort at zero speed. If the motoring corner point is reduced to 35 km/h (22 mph), the tractive effort available from 41 hp is 317 kg (698 lb). This allows the initial acceleration to be inherently met and the 0-48 km/h (0-30 mph) acceleration will be slightly better than 9 seconds. This is accomplished at the expense of a wider speed range for constant horsepower from the motor, but not sufficient to increase the motor size. Furthermore, this higher starting torque can be delivered without a higher current. The initial acceleration and 35 km/h (22 mph) corner point,  $V_1$ , are shown in Figure 3.2.2-1.

If a constant horsepower speed range of 2.5 is selected, then  $V_2 = 86$  km/h (55 mph). This means the 97 km/h (60 mph) balancing speed must be met with the drive operating in Region III, where the acceleration drops off as the reciprocal of speed squared. This point is easily met, as shown in Figure 3.2.2-1.

The 72 and 86 km/h (45 and 55 mph) cruise requirements are also shown in Figure 3.2.2-1. They are found by using the methods discussed in Appendix A.

The regenerative braking effort curves are shown in Figure 3 2 2-1 The variation in ac current as a function of battery charge, with the resultant variation in braking effort, is also shown The braking effort curves are a derivative of the motoring case and thus show the braking capability of the drive relative to the designed motoring capability

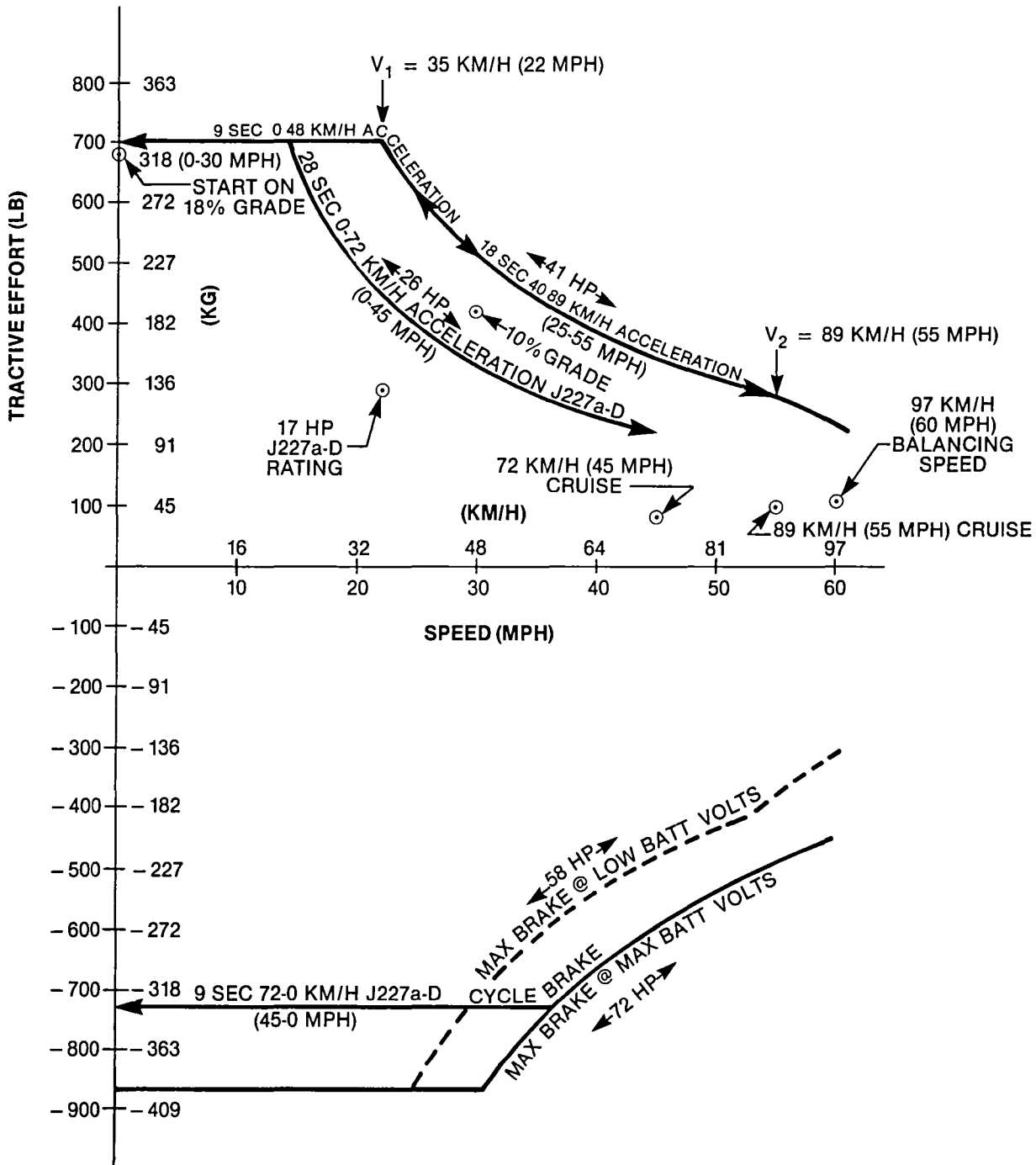


Figure 3.2.2-1 Motor Tractive Effort and Speed Requirement

### 3.2.3 Motor Torque and Speed Requirement

In order to establish the final motor specification, it is necessary to determine the motor speed as related to vehicle speed. The motor is to be operated at about 15,000 rpm maximum. The integral gear box on the motor used to make the traction motor compatible with standard automotive axle gearing is 2.923 to 1. Thus, 97 km/h (60 mph) which is a gear box speed of 5000 rpm results in a motor speed of 14,615 rpm. Figure 3.2.3-1 shows the motor tractive effort-speed requirements of Figure 3.2.2-1 converted to a motor torque-speed curve, assuming a gear box efficiency of 95%.

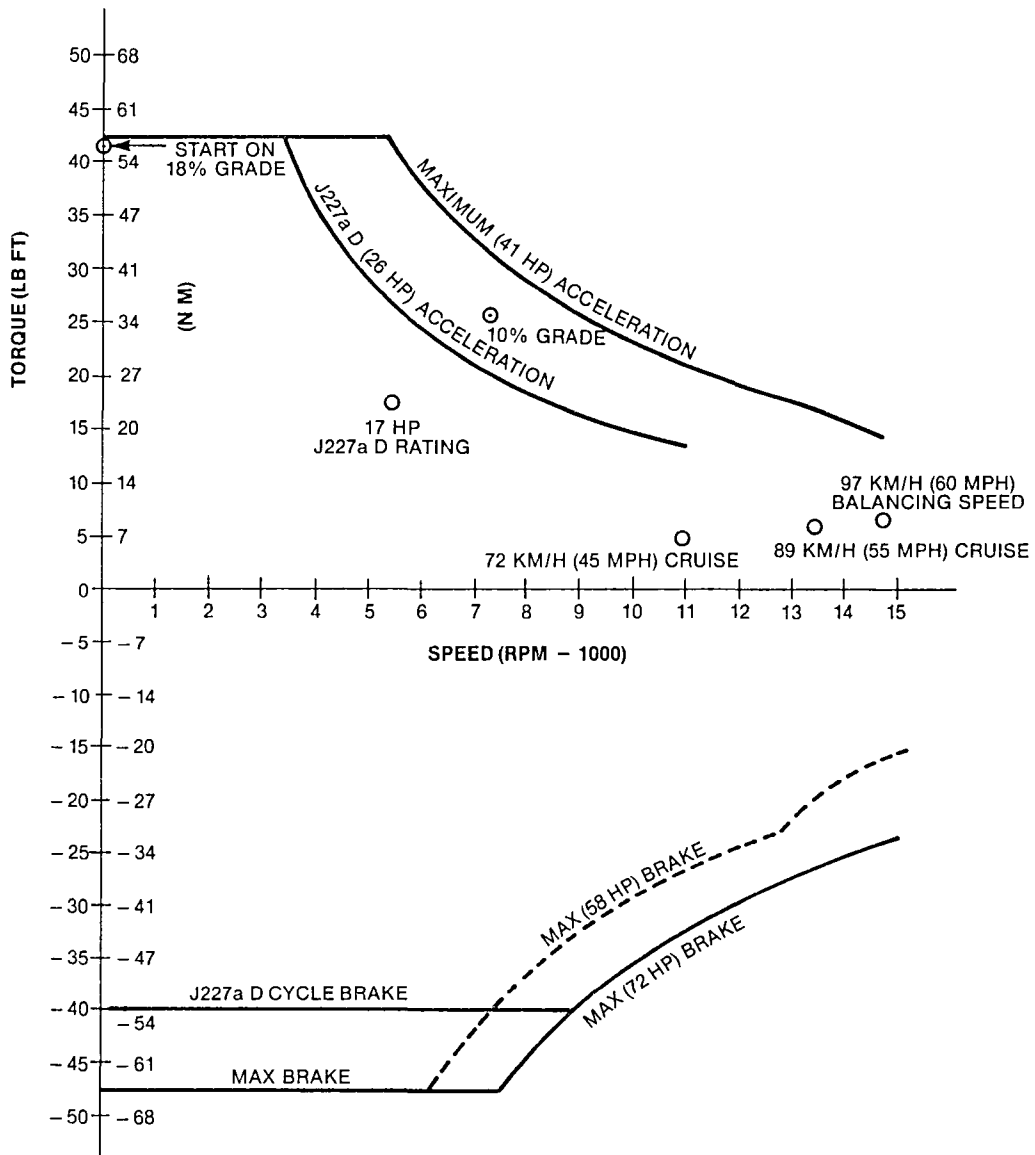


Figure 3.2.3-1 Motor Torque and Speed Requirement

The peak power and torque requirements to meet the J227a-Schedule D driving cycle are somewhat less severe than the maximum peak values, but must be met with a reduced battery voltage due to driving with a nearly discharged battery. When operating on the J227a-Schedule D duty cycle, the vehicle must operate for a period of time longer than the motor thermal time constant, thus, this operation will define the continuous thermal rating of the motor. The maximum performance requirements are for short-time overloads of the traction motor and thus will not significantly affect the steady state rating. However, the motor must have enough peak torque capability to produce the desired performance. The maximum performance is with a fully charged battery. Full regenerative braking is available and desired for the J227a-Schedule D duty cycle. Some of the conditions will occur only once or twice per battery charge.

### 3.2.4 Equivalent Motor Rating

In order to calculate the ac motor current for thermal rating purposes, a schedule of voltage as a function of speed is required. This schedule and the resulting ac motor currents are described in detail in Section 3.4. Considering the J227a-D cycle, using this voltage and the required torque, the ac motor current can be calculated for the required duty cycle. The results are shown in Figure 3.2.4-1. The rms value of the ac motor current over the total time of 122 seconds yields an equivalent power rating of 17 hp at 35 km/h (22 mph). The motor was built using a standard 180 frame, which is smaller than the NASA-specified 215 frame. The motor weight is about 45 kg (100 lb).

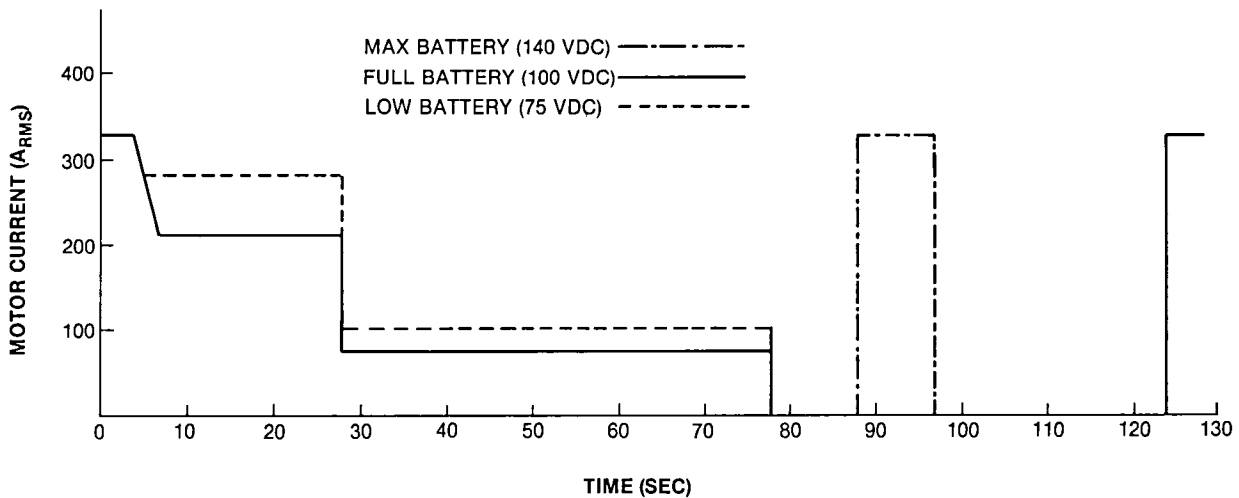


Figure 3.2.4-1 AC Motor Current for J227a-Schedule D Duty Cycle

### 3.3 MOTOR DESIGN

The GE-optimized motor is designed to operate as a vehicle traction motor with a pulse width modulated inverter as a power source. The motor is designed to maximize drive train efficiency, minimize inverter size, eliminate excess gearing, and to be producible by automated manufacturing processes. To further this aim, a standard 180 motor frame and a conventional integral gear box are used to make the traction motor easily usable with standard automotive axle gearing. This section describes the motor design.

#### 3.3.1 Motor Description

The design of a motor for use with an inverter power supply must take into account the presence of time harmonics in the voltage and current.<sup>(4,5)</sup> In some cases, it is possible to design the motor and inverter so that the harmonics will produce useful torque resulting in increased efficiency and lower weight.<sup>(6)</sup> Usually, however, the thermal capability of the motor must be increased to accommodate harmonic losses. Double-cage rotors are not needed; coffin-shaped bars are preferred for an inverter-powered motor. Other factors entering into the motor design include: end winding vibration due to harmonics, forces developed as a result of inverter shoot-through, torque pulsations, and voltage "pileup" due to high  $dV/dt$ .

The motor is shown in a disassembled view in Figure 3.3.1-1. It is a four-pole design and has a maximum frequency given by:

$$f = \frac{np}{60} \text{ Hz}$$

where

$n$  = the speed in rpm (14,615)

$p$  = the number of pole pairs (2)

Therefore,  $f = 487$  Hz.

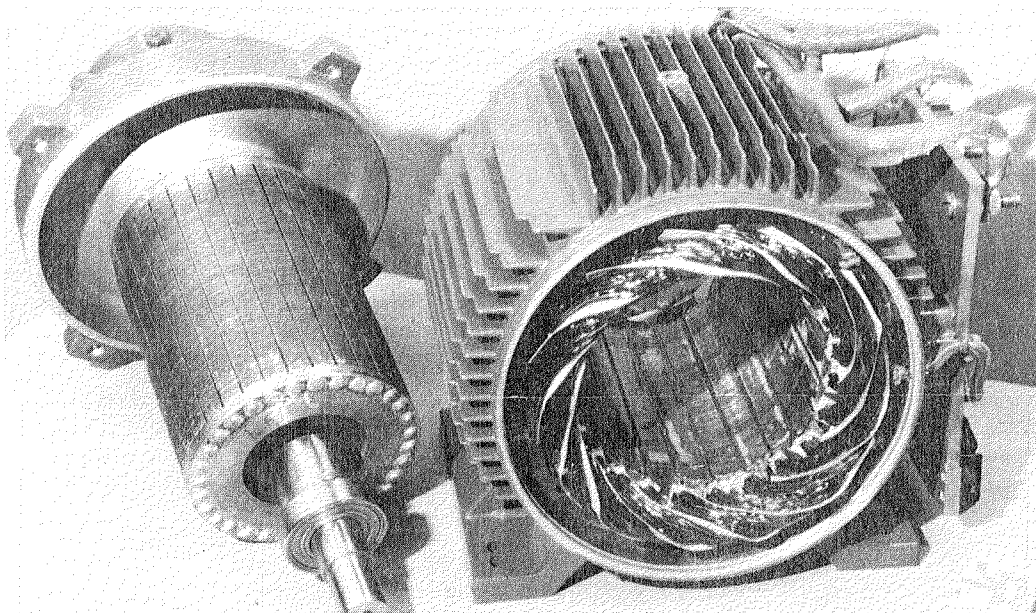


**Figure 3.3.1-1 The Optimized Induction Motor Disassembled**

The double-cage rotors often supplied on standard induction motors in this size range are not required since starting will not be done on a fixed frequency line. Indeed, the exotic and multitudinous varieties of double cages, saturable shunts, and rotor bar shapes that are supplied in the standard inventories will lead to increased harmonic losses in most cases. The GE optimized motor uses coffin-shaped rotor bars, that is, the teeth have parallel sides and the bars are wider at the top than at the bottom. This achieves two objectives for increased efficiency: 1) the maximum conductor area in the rotor to reduce rotor loss, and 2) the rotor bar is as wide as possible in the region where harmonic currents are concentrated to reduce harmonic losses. In addition, since starting torque in the conventional sense for a standard motor is not required with the inverter drive, the rotor bars are high-conductivity copper.

In combination with the large conductor area, a very low rotor resistance for the fundamental is achieved in the GE optimized motor. The torque speed characteristic is, as a result, very steep and operating slips are very low, hence, rotor slip loss is reduced to a minimum. The motor appears to operate almost as a synchronous motor.

The stator copper is also maximized to reduce losses. A special lamination with large slots is used. A commercial motor design seeks to minimize the amount of copper in comparison to iron in order to reduce material costs. The amount of copper in the slot is maximized by using a tightly packed winding, thinly coated insulation, and a single, rather than a dual, winding. Class H materials are used for the turn, ground, and phase insulation in the stator. The overall temperature rating is Class F due to the impregnation material.

A crucial and difficult item is the material and integrity of the laminations. In a commercial offering, the stator lamination material is most often a low carbon steel of 0.064 cm (0.025-inch) thickness. This is adequate for most applications where efficiency is not paramount. In motors where high efficiency is demanded or where a serious steady-state overheating problem has been encountered, a 2.6% silicon steel of 0.048 cm (0.019 inch) will often be used. Sometimes laminations as thin as 0.036 cm (0.014 inch) (at a premium price) may be used. The GE optimized motor utilizes a high-quality 3.25% silicon non-oriented steel 0.018 cm (0.007-inch) thick. The high silicon content reduces hysteresis loss and increases the resistivity which, in conjunction with the small thickness, reduces eddy current loss. Reduction of eddy current losses are relatively more important in a variable speed drive since they vary as frequency squared, whereas, hysteresis loss varies directly with frequency. High-frequency inverter harmonics also must be considered. Hence, it is desirable to use the thinnest lamination consistent with low hysteresis loss and economics. It is possible to further reduce the core loss in the GE optimized motor by using a more expensive nickel-based alloy or by reducing flux density (and increasing the weight). The flux density selected is less than that used in commercial offerings but still higher than the ideal in order to stay within the 180 frame size. At the selected flux density, the efficiency is, however, satisfactorily high over the speed range. The stator and rotor punchings of the GE optimized motor are shown in Figure 3.3.2-2. They were made by an etching process.

Since the laminations are very thin, conventional varnish coatings would be unacceptably thick, leading to a very low stacking factor, hence, a very thin (less than  $10^{-4}$  cm) glassy coat was utilized. An added benefit is a much higher temperature and dielectric capability. This coating had to be applied to the bulk material which in turn required extensive development of a special etching process. Normal commercial machine practice is to utilize the natural oxide coat.

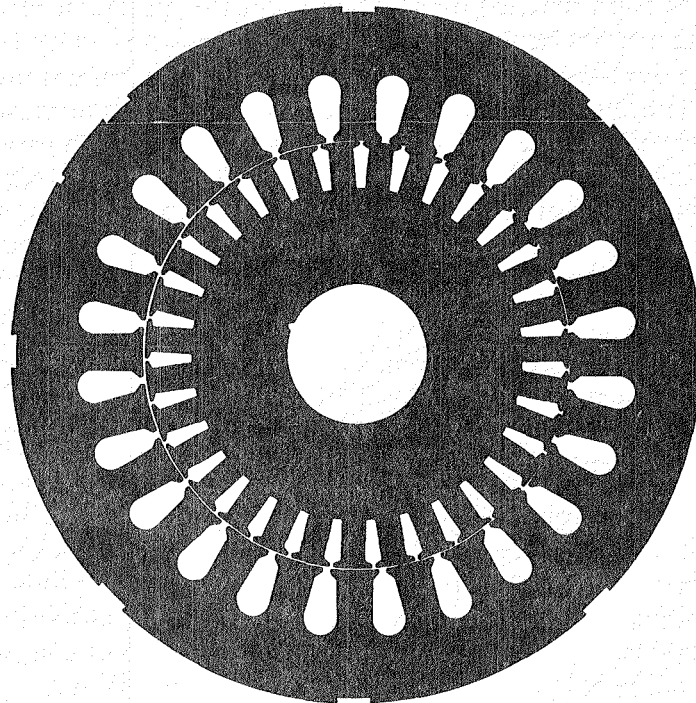


**Figure 3.3.1-2 The Stator and Rotor Punchings of the GE Optimized Motor**

*Note: The coffin shape of the rotor bar area.*

In conventional machines, the rotor laminations are often made very thick and from the cheapest available materials since the bulk of the rotor iron is excited at very low (slip) frequency. However, a significant source of loss in the rotor is due to slot and mmf fluctuations at the rotor surface, which may be of relatively high frequency. Inverter harmonics will also cause high frequencies in the rotor. In order to reduce these losses, the rotor is made from the same material as the stator. This did not materially increase cost since the etching process developed allowed the rotor to be fabricated at the same time as the stator in the stator bore region, out of material that would be scrap in the normal production process.

The end windings of an inverter driven motor should be braced better than a conventional motor to withstand high-frequency excitations due to inverter harmonics. More importantly, the motor will be subjected to inverter “shoot-throughs” and “crowbars,” which can result in extremely high forces in the end windings, as well as in the shaft.

To reduce fabrication cost and time, the GE optimized motor utilizes a standard aluminum 180 frame and end bell. A special end bell with integral gear box is used to reduce the speed from 14,615 rpm to 5000 rpm to interface the standard applications. The layout of the motor and gearbox is shown to scale on drawing ESD-196 (Figure 3.3.1-3). The principal dimensions of the motor outline and interface are also shown. The drive end bearing is lubricated from the gear box. However, as shown on the drawing, an end bell with a grease lubricated bearing may be used to provide a 15,000 rpm interface.

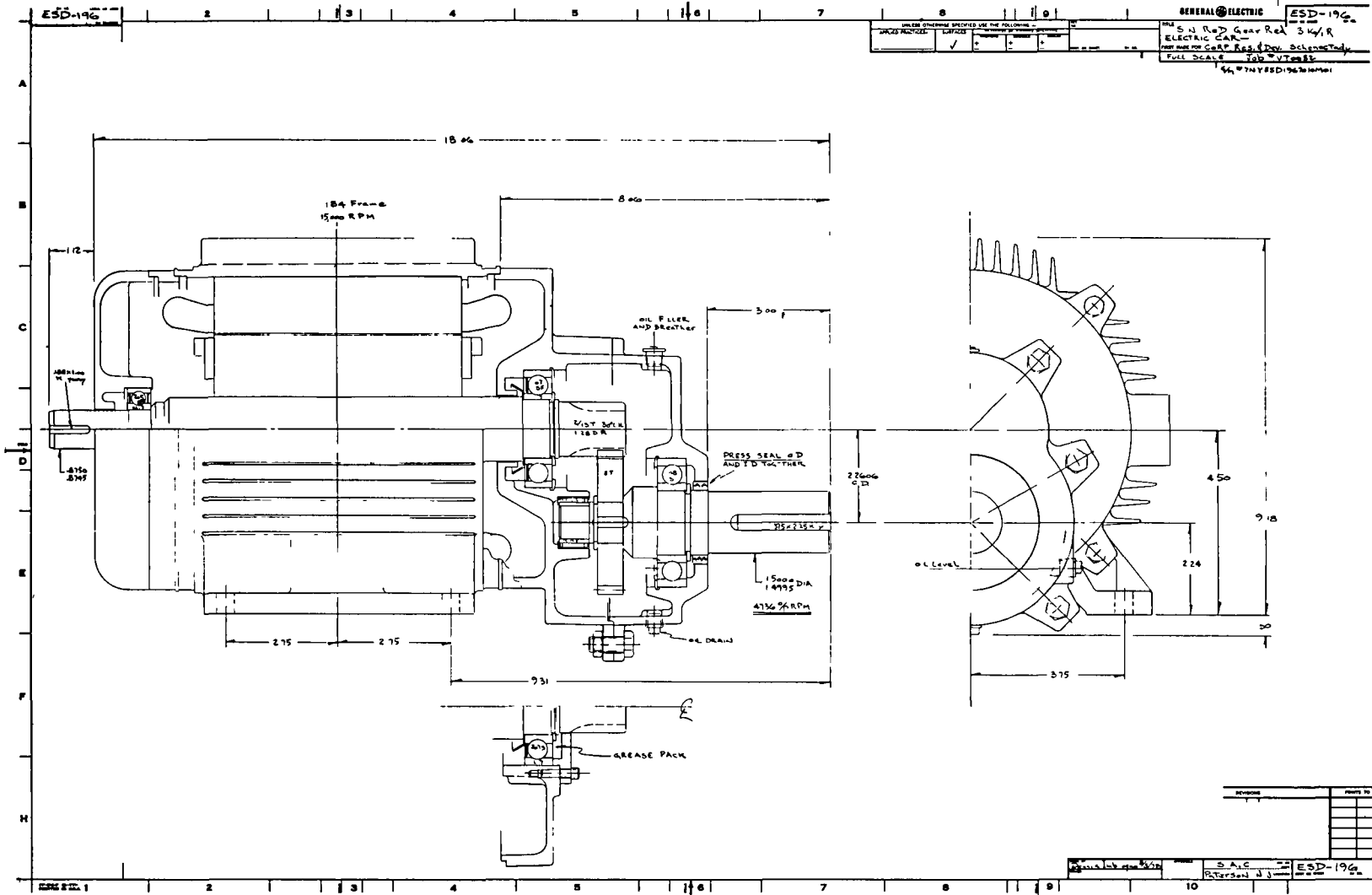


Figure 3.3.1-3 GE Optimized Motor and Gear Box Layout

### 3.3.2 Advantages of the GE Optimized Motor

Advantages accrue in all areas of the electric vehicle and its drive system if a motor and power conditioner are designed together both for a best match to each other and to the application at hand. Other considerations may influence the degree of matching and optimization that can be done, such as the needs of automated mass production or interchangeability of components among vehicles of differing size and/or mission. Such compromises will always result in reduced performance and increased costs for moderate production quantities, although economies of scale and standardization may reduce costs in very large production quantities.

In this case, it is desirable to optimize the system as far as possible. There are a number of advantages to using the GE optimized motor rather than a standard line starting induction motor.

- The inverter kVA rating is reduced by 15% to 30%, which results in as much as a 2-to-1 difference in inverter size and cost. This is due to the motor being designed for an inverter power source, with an optimized motor-inverter voltage and current schedule, and reduced motor harmonic loss,  $I^2R$  loss and magnetic loss.
- The gearshift and clutch mechanism with its associated reliability and loss problems are eliminated.
- The motor size is small and utilizes a 180 frame.
- The motor efficiency is maximized.
- Inverter efficiency will be higher due to the restriction of the PWM mode to about one-third of the speed range.

### 3.4 SYSTEM DESIGN AND CONTROLLER REQUIREMENTS

The system design directly relates the motor characteristics to the inverter design. This section shows the motor performance and describes the effect of the motor on the inverter design. The results are a set of inverter specifications, including system voltage, and a set of power semiconductor specifications. The use of a multiple speed transmission is not required.

The basic factors to be considered in the system design are

1. Battery system voltage
2. Motoring corner point speed
3. Use of a shifting transmission
4. Motor pull-out slip
5. Motor voltage and current schedules

#### 3.4.1 System Voltage

The battery system voltage choice is based on vehicle arguments and transistor voltage capability. From previous work on a dc drive system of basically the same vehicular performance requirements, a 108 volt battery voltage was chosen<sup>(8)</sup>. The GE power Darlington transistors (CRD-3 chip) used in that program were capable of switching about 220 volts (the breakdown voltage was 300 volts). Power zener diodes were needed to clip the overshoot voltage to that level. The improved version (ZJ504) is capable of switching about 300 volts. With the expected overshoot voltages during transistor switching, a transistor voltage requirement of twice the maximum battery voltage is mandatory. The use of a 108 volt battery (18, 6-volt units) will give a maximum dc voltage of about 140 volts during regenerative braking. Thus, the 108 volt nominal battery is about the maximum system voltage that can be used due to the expected voltage transients of up to about 300 volts on the transistors.

#### 3.4.2 Motoring Corner Point Speed

The motoring corner point is chosen so that a shifting transmission is unnecessary. In order to achieve this objective, the starting torque must not require a higher motor current than the full-power, high-speed motoring current. A corner point (maximum speed at which constant torque is possible) of 35 km/h (22 mph) at maximum battery charge will satisfy this requirement. The motor torque capability must also be sufficient to allow two other conditions to be met. The first is that constant maximum power be available to 89 km/h (55 mph) at full battery voltage. The second is that the J227a-D power be carried to 72 km/h (45 mph) at low battery voltage.

#### 3.4.3 Motor Voltage and Current Schedules

The motor voltage and current schedules, along with the corner point speed, optimize the size of the inverter and motor and eliminate the need for a shifting transmission. The schedules are shown in Figure 3.4.3-1 for a nominal dc battery system voltage of 108 volts. The motor voltage is pulse-width-modulated to increase linearly up to the maximum square wave motor voltage, where it becomes constant over the remainder of the speed range. The motor voltage schedule variation with battery voltage is apparent in Figure 3.4.3-1, with the maximum square wave motor voltage increasing from 59 to 109 volts rms as the battery ranges from 75 to 140 volts dc. The voltages shown are line-to-line fundamental rms voltage.

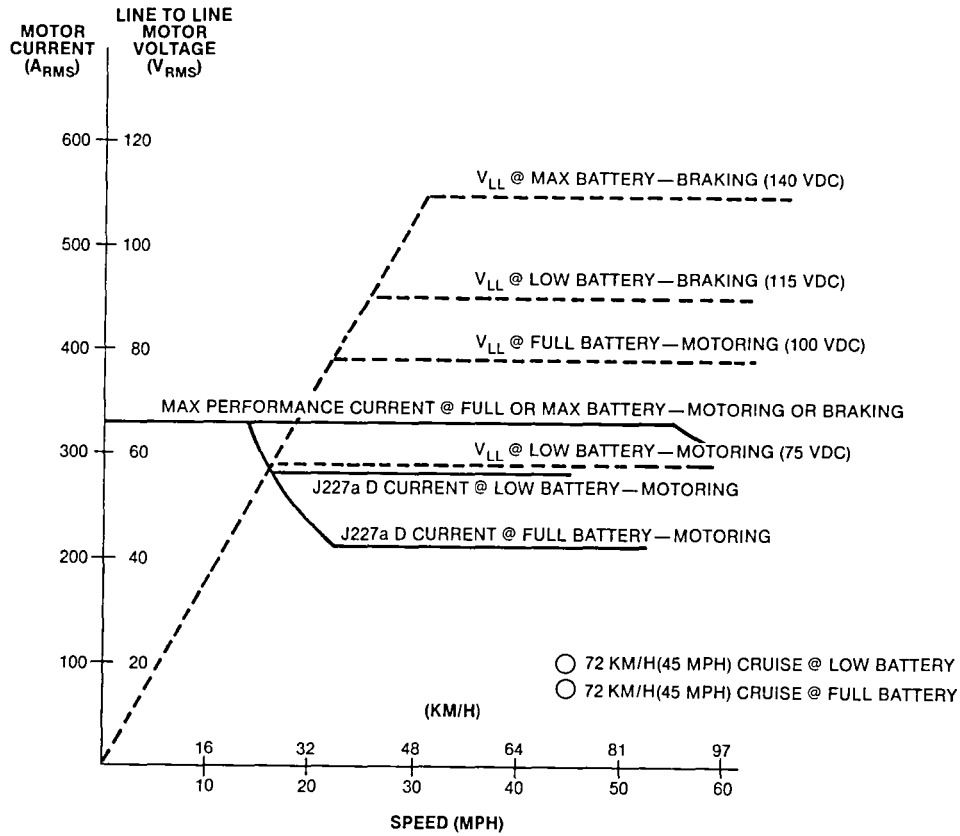


Figure 3.4.3-1 Motor Voltage and Current Schedules

The fundamental rms ac motor current can be calculated for motoring operation from the following equation

$$I_{ac} = \frac{P_o}{0.78 E_B \sqrt{3} \eta_M \eta_G PF}$$

where,

$P_o$  = drive system output power in watts

$E_B$  = battery voltage in volts

$\eta_M$  = motor efficiency (0.90)

$\eta_G$  = gear efficiency (0.95)

$PF$  = motor power factor (0.80)

This equation assumes some values for efficiency and power factor, and is valid for a motor square wave voltage waveform. The current schedules are also shown in Figure 3.4.3-1. In the motoring maximum performance case, the motor current is 330 amps rms, based on the required 41 hp at full battery (100 VDC). This motor current is, then, the current available for the regenerative braking maximum performance case. For the motoring portion of the J227a-D duty cycle requirement, the motor current starts at 330 amps rms and drops off to 280 and 210 amps rms for low battery (75 VDC) and full battery (100 VDC) respectively, based on the required 26 hp.

These motor voltage and current schedules result in the motor performance as required in Figures 3 2 2-1 and 3 2 3-1. In the motoring maximum performance case at full battery, the motor current is held constant while the motor voltage increases linearly up to the motoring corner point speed of 35 Km/h (22 mph). In this case, the corner point occurs when the motor voltage reaches the maximum square wave value. Thus, the motor is operated at constant volts/hertz up to the motoring corner point speed and the motor torque is constant. Thereafter, the motor current and voltage are both constant and the motor operates at a constant horsepower limit. In the motoring portion of the J227a-D duty cycle case, the motor current is held constant while the motor voltage increases linearly up to the motoring corner point speed of 23 Km/h (14 mph). This again results in a constant motor torque output. In this case, the motoring corner point speed is set by the reduced torque requirement, rather than the motor reaching maximum square wave value. Thereafter, a constant horsepower is desired, so the motor current is allowed to drop off as the motor voltage continues to rise linearly up to the square wave value at 26 Km/h (16.5 mph) or 35 Km/h (22 mph), depending on the battery voltage. After this speed, the motor voltage and current are both constant, as before. In regenerative braking maximum performance, the corner point moves up to 50 Km/h (31 mph) and the current is held constant, similar to the motoring performance.

The inverter is not required to operate in the pulse-width modulation mode over the high-speed portion of the speed range, thus considerably reducing the inverter losses and increasing system efficiency. The proper choice of the motor voltage schedule affects both inverter size and motor size. In addition, the system efficiency is increased by a suitable choice of motor voltage schedule.

### 3.4.4 Motor Performance

Figure 3 4 4-1 shows the detailed values of ac current (sine wave rms value) for the voltage schedules shown in Figure 3 4 3-1. The J227a-D low battery voltage curve shows that the

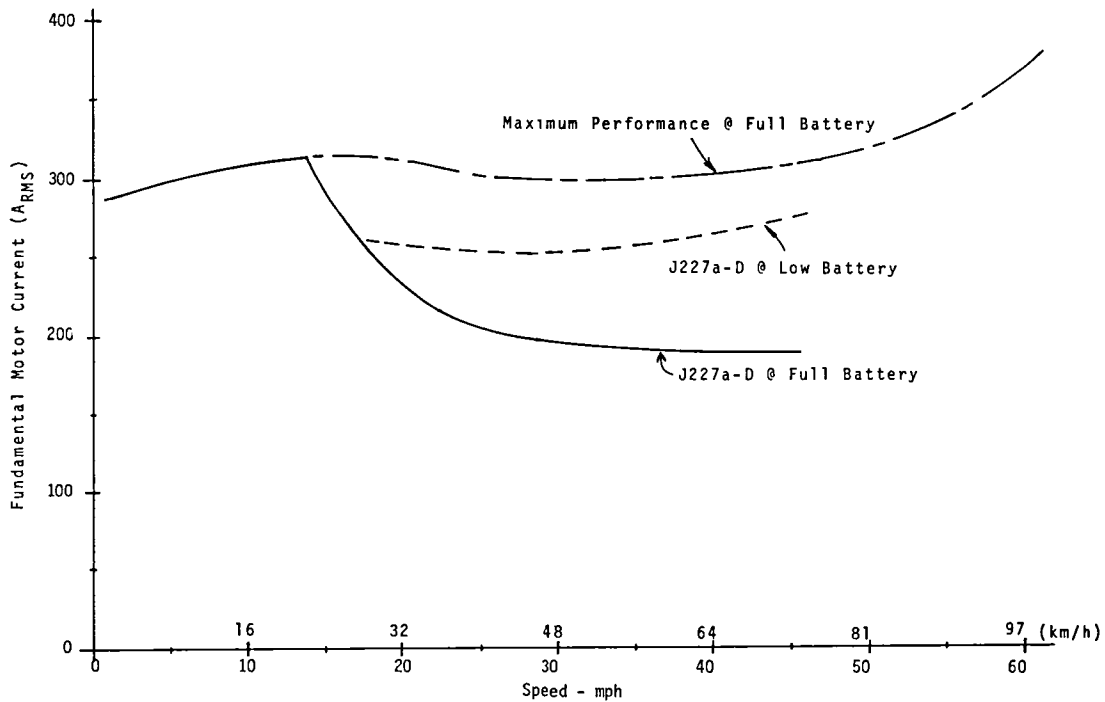


Figure 3.4.4-1 AC Motor Current

current required is a lower value than the maximum performance curve current. Thus, the drive will actually be able to deliver the required J227a-D performance with a battery which is more than 80% discharged since still more current can be delivered. The current increase at high speed on the maximum performance curve is due to operation very near to pull-out motor slip. At lower speeds, there will be a significant percentage of harmonic current which will add to the fundamental component of current shown in Figure 3.4.4-1. At higher speeds, the harmonic currents will be reduced due to the higher frequency, thus, there will be more useable fundamental frequency inverter current capacity available to maintain output power.

Note that the maximum inverter current requirement occurs at speeds over 40 km/h (25 mph). At these speeds, vehicle performance is limited by the peak power capacity of the inverter. Use of a shifting transmission will not reduce the requirement for the high-speed current. At low speeds, as long as the motor can deliver the required starting torque without a higher current, a shifting transmission is not required or desirable.

Figure 3.4.4-2 shows the induction motor efficiency under the various required operating conditions. A gear efficiency of 95% is assumed in these figures. Harmonic loss is not taken into account. Note that the efficiency as a function of speed and battery voltage is relatively constant at a high level. Proper design optimization for variable speed and tradeoff between magnetic losses,  $I^2R$  losses, and windage losses are used to obtain this desirable characteristic.

Figure 3.4.4-3 shows the variation of motor slip frequency and the ac line frequency as a function of speed and loading. Figure 3.4.4-4 shows the motor power input, and loss as a function of speed. The battery current is derived from the power input and is shown in Figure 3.4.4-5. Again, harmonics are not taken into account. The inverter efficiency is assumed to be 92%. The motor is self-ventilated.

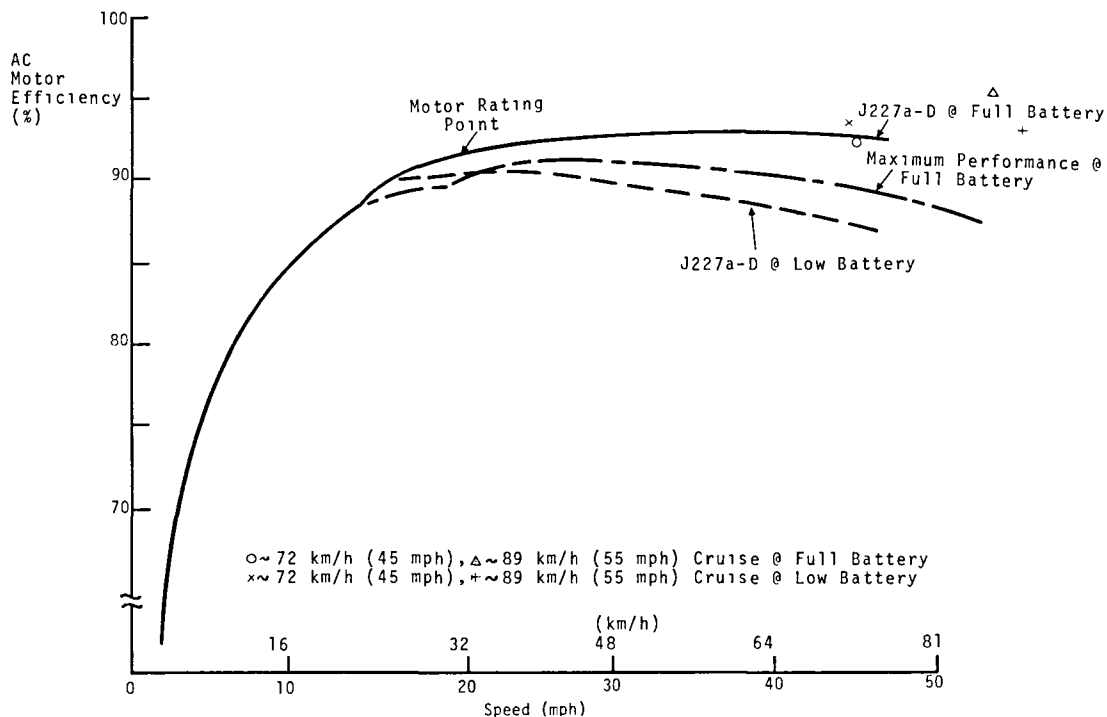
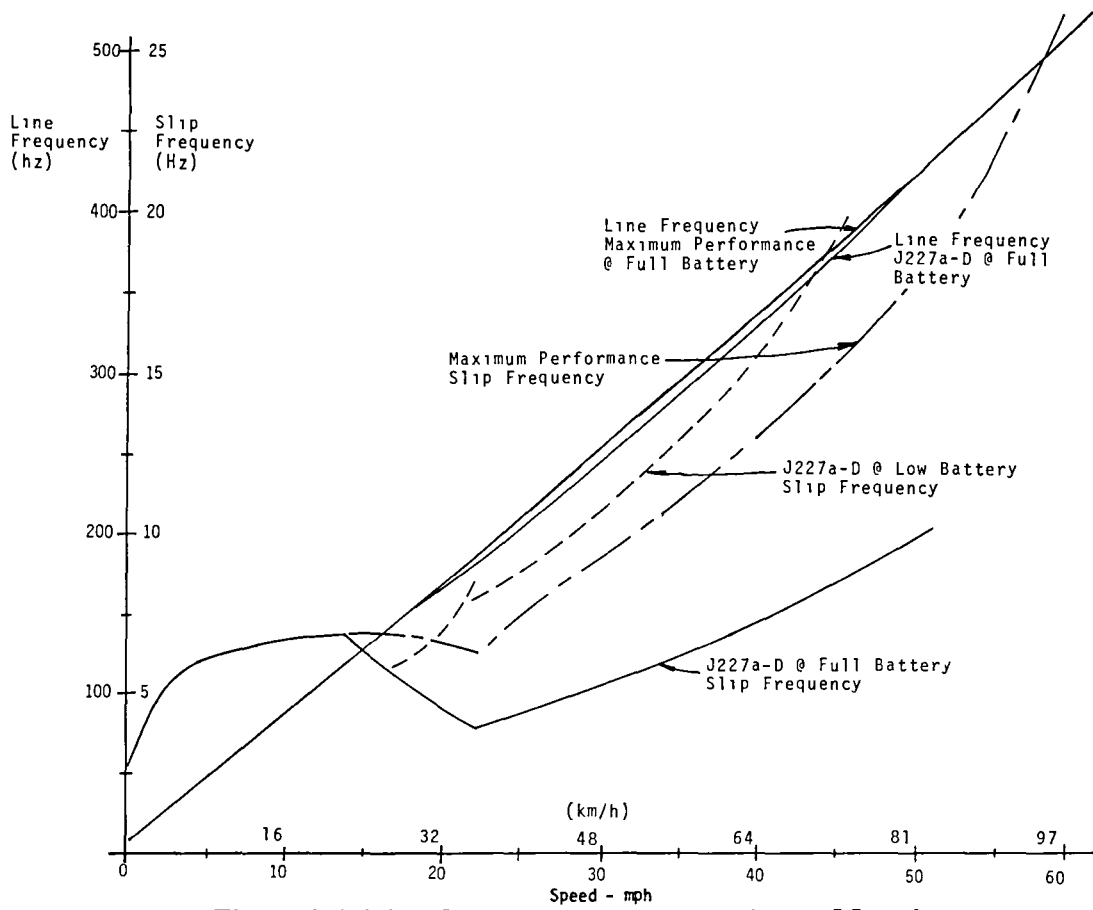
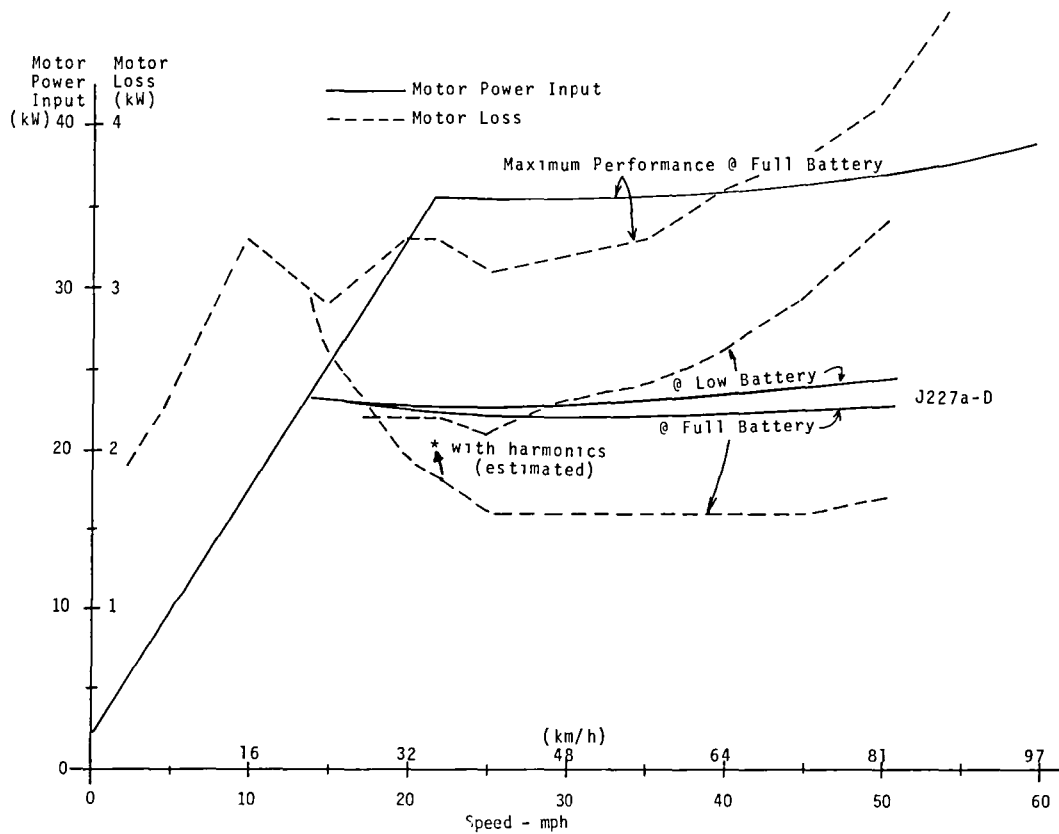


Figure 3.4.4-2 Motor Sine Wave Efficiency – Motoring



**Figure 3.4.4-3 Line and Slip Frequencies - Motoring**



**Figure 3.4.4-4 Motor Power Input and Loss - Motoring**

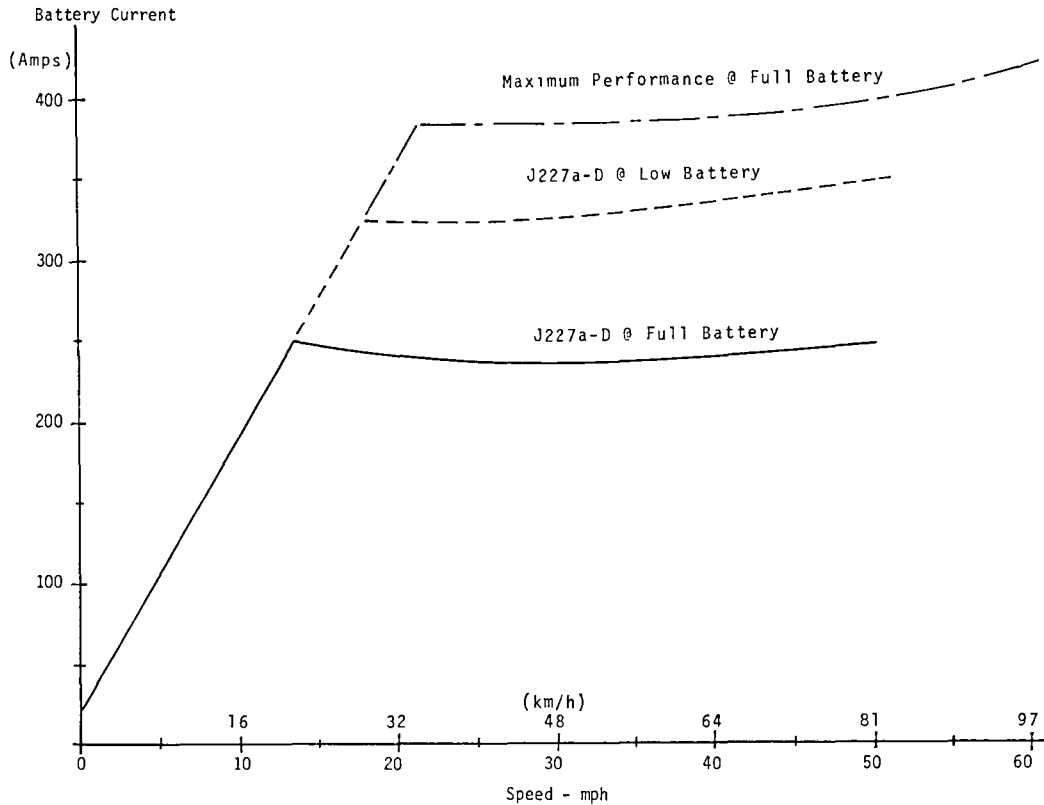


**Figure 3.4.4-5 Battery Current – Motoring**

### 3.4.5 Effects of Pulse Width Modulation (PWM)

The primary effect of using inverter waveforms rather than sine waves to excite the motor is to increase both motor loss and the peak value of ac line current. An analysis is done to assess the effect of using both pulse width modulation and square wave excitation.

The type of pulse width modulation employed for the analysis is generated by comparing the desired output sine wave to a triangle reference wave which is of a higher frequency<sup>(9)</sup>. If the ratio of the triangle reference wave frequency to the output sine wave frequency is high enough, then this analysis is a good approximation of the actual PWM method used in the controller<sup>(10,11)</sup>. Figure 3 4 5-1 shows an example of the method of producing the sine wave type of PWM, with the same definitions as shown in Figure 3 4 5-3. Figure 3 4 5-2 shows an example of the method of producing the current-controlled type of PWM (see Section 3 5)

Above the corner point speed, the inverter control must eliminate all pulse width modulation and produce the well-known six-step square wave in order to produce the maximum output voltage and hence maximum power of which the drive is capable. Six-step square wave operation is illustrated in Figure 3 4 5-3. Below the corner point speed, the current-controlled PWM scheme chops the available dc voltage to reduce the voltage to the motor.

The use of this type of waveform causes currents to flow in the motor at frequencies higher than the desired fundamental output frequency. The inverter must be capable of supplying the extra current required. Also, the extra currents will cause additional losses in the motor, primarily in the rotor bars which tend to exhibit a considerable skin effect at these higher frequencies. The GE optimized motor is designed to minimize this extra loss. Figure 3.4.5-4 shows the calculated motor current waveform for the maximum torque case at

80% of the corner point speed (136 Hz) and full battery voltage. The fundamental torque producing component of ac current is 328 amps rms and the peak current that the inverter must commute is 592 amps. The chopping frequency is twelve times the fundamental frequency of 136 Hz. Figure 3.4.5-5 shows a sample print out from the harmonic analysis program showing some of the details available. Note at the bottom of the print-out the two efficiency figures and the harmonic loss. The efficiency loss is 1.4% and the harmonic loss is 0.44 kW. Figure 3.4.5-6 shows the effect of increasing the chopping frequency to eighteen times the fundamental. The current begins to more closely approximate a sine wave and the harmonic losses decrease to 0.34 kW. This demonstrates the convergence of the current waveshape of the sine wave PWM analysis at high chopping ratios with the current waveshape of the current-controlled PWM technique. The motor current for the six-step square wave operation of the inverter at the corner point speed of 180 Hz is shown in Figure 3.4.5-7. The results of this analysis indicate that choosing a maximum chopping frequency of 3000 Hz will keep the peak currents to less than 600 amps and reduce the harmonic efficiency loss to under 1%. Motor currents and voltages under actual operation are shown in Sections 4.6 and 4.7.

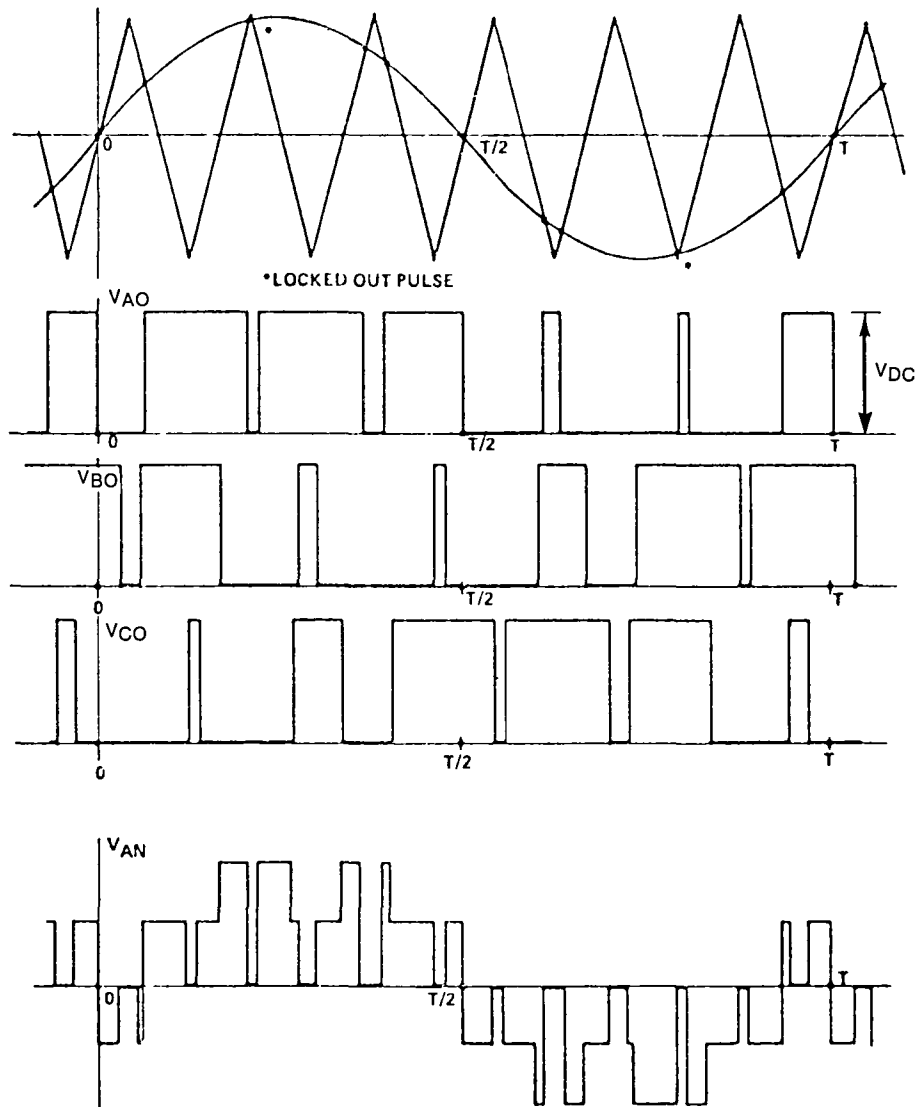
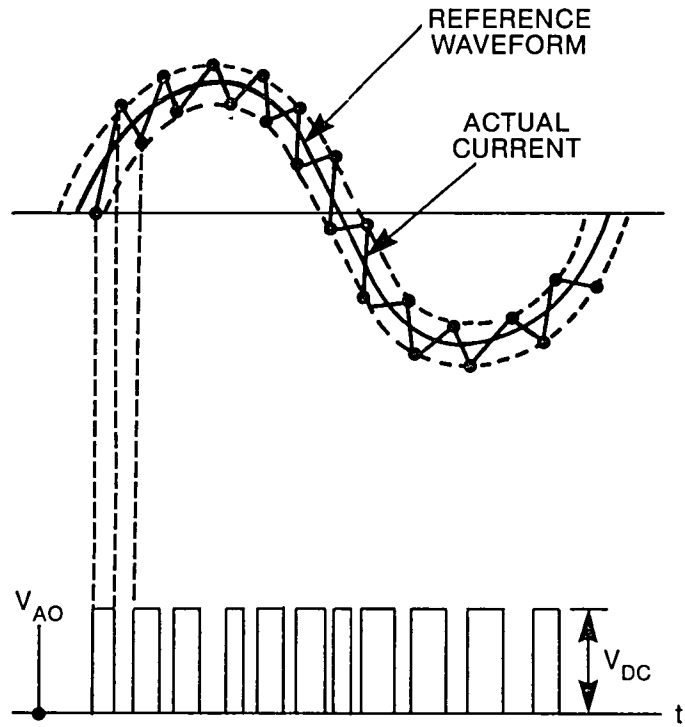
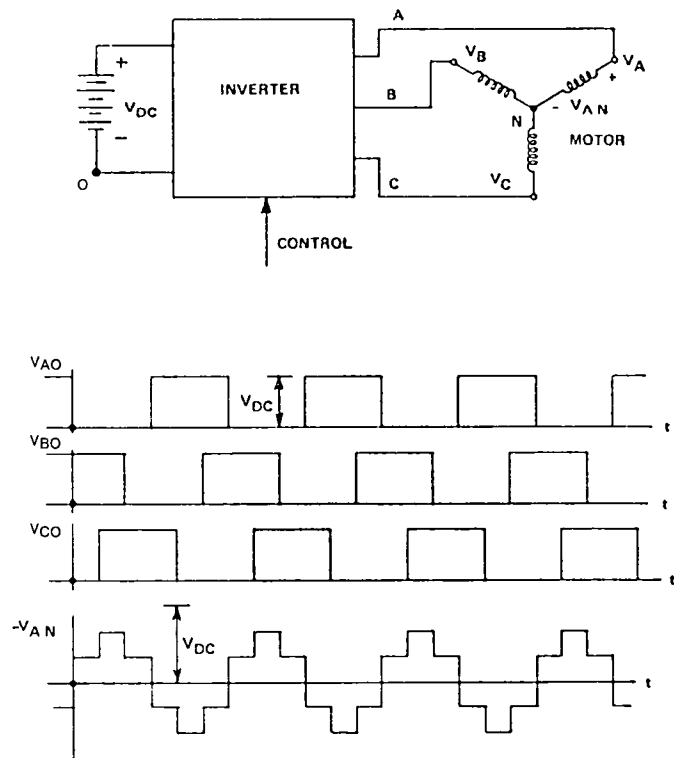


Figure 3.4.5-1 Generation of Sine Wave PWM



**Figure 3.4.5-2 Generation of Current-Controlled PWM**



**Figure 3.4.5-3 Generation of Six Step Square Wave**

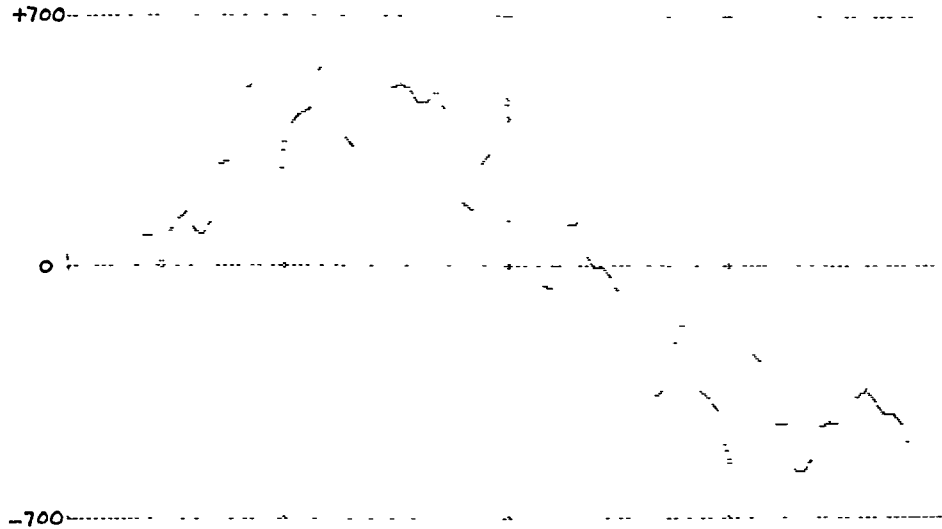


**Figure 3.4.5-4 AC Motor Current for 12X PWM**

```

COMPUTE-HARMONICS

COMPUTE LOSSES + TORQUES

VDC= 108
PHASES= 3

DEEP BAR ROTOR EFFECT
CORE LOSS INCLUDED

HO          SO          FO          VO          W6          F2
18          .0123598      180         45          .03         136.

BAR WIDTHS
B8= .099    B9= .187

MOTOR PARAMETERS
R1          R2          LT          D1          R3          F2
2.96000E-03 1.44000E-03 .02075      .43         2.46000E-06 4

K          I1          FF          I^2*R STAT    I^2*R ROT    CORE
1          AMPS      .8451      WATTS        WATTS        WATT
          464

FILE FOR CURRENT DK:IMHA7

HARMS      81          157          205
TOTALS     1038       519          733

I RMS TOT= 342
I RMS HAR= 96
I RMS FUN= 328
V RMS FUN= 36

HARM      AMFL      SENSE      INFUT      TOT LOSS      EFFI
1          .4768      1          30.3       1.85          .935
50         -5.60000E-03 -1         30.54      2.29          .925
HARMONIC LOSS= .44 KW

```

**Figure 3.4.5-5 Harmonic Results for 12X PWM**

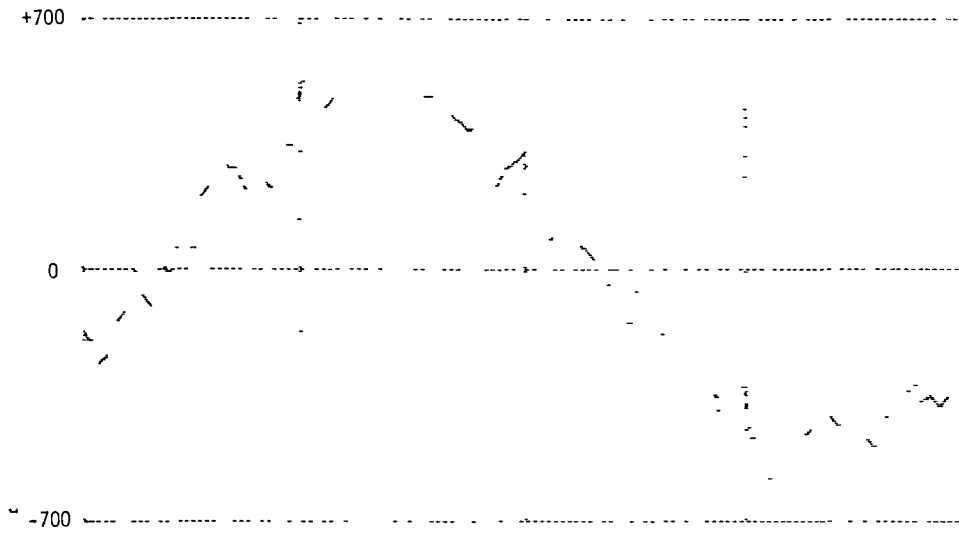


**Figure 3.4.5-6 AC Motor Current for 18X PWM**

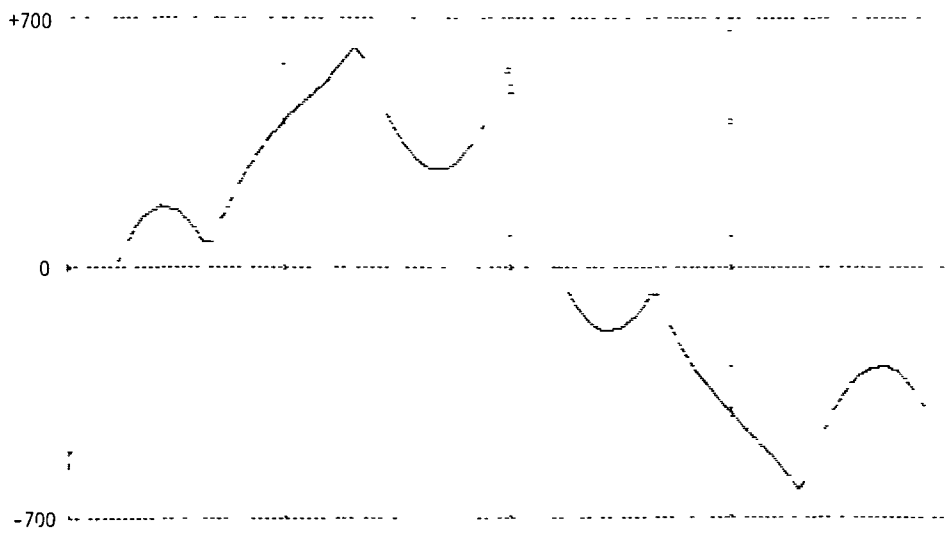
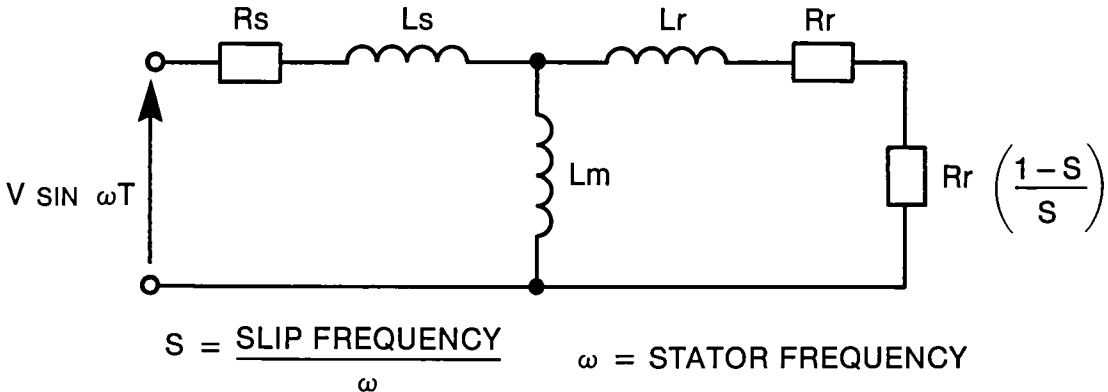


**Figure 3.4.5-7 AC Motor Current for Square Wave**

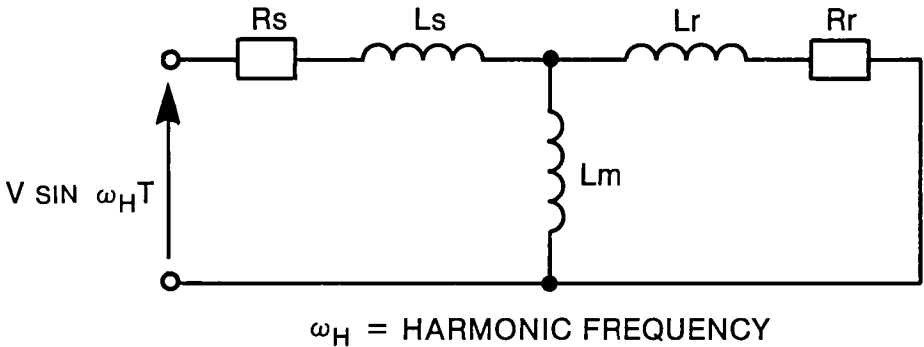
**3.4.6 Motor Leakage Reactance and Harmonics**

The induction motor equivalent circuit for the fundamental frequency is shown in Figure 3 4.6-1a. Considering the harmonics, the rotor resistance at the fundamental frequency appears as a short circuit, thus only the leakage inductance and motor resistance are in the circuit to limit the harmonic currents (Figure 3.4 6-1b) The values for the motor parameters of Figure 3.4.6-1 are

- $R_S = 0.00298 \Omega$
- $R_R = 0.00145 \Omega$
- $L_M = 0.00024 \text{ H}$
- $L_S = 0.00001269 \text{ H}$
- $L_R = 0.00001015 \text{ H}$
- $P = 4 \text{ poles}$



**(A) FUNDAMENTAL FREQUENCY EQUIVALENT CIRCUIT**



**(B) HARMONIC FREQUENCY EQUIVALENT CIRCUIT**

**Figure 3.4.6-1 Induction Motor Equivalent Circuits**

The harmonic losses can be calculated from the following equations

$$I_h = \frac{V_h}{(R_S + R_R) + j\omega_h (L_S + L_R)} \approx \frac{V_h}{j\omega_h (L_S + L_R)}$$

$$P = \sum_{h=2}^{\infty} \left[ \frac{V_h}{\omega_h (L_S + L_R)} \right]^2 (R_S + R_R)$$

where,

$V_h$  = harmonic voltage

$I_h$  = harmonic current

$\omega_h$  = harmonic frequency

The GE optimized motor is designed to supply constant torque with constant flux up to the corner point and constant power to near maximum speed with constant voltage applied. The leakage inductance is maximized consistent with the constant power requirements<sup>(1)</sup>. Maximizing the leakage inductance minimizes the harmonic currents, but limits the pull-out torque and thus the maximum speed for constant power output at constant applied voltage. The leakage inductance is important also in the operation of the current-controlled PWM technique<sup>(11)</sup>. The maximum leakage inductance is given by<sup>(2)</sup>

$$L_T \leq \frac{0.0410 E_B^2}{P_o f_2}$$

where,

$L_T$  = leakage inductance in henries

$E_B$  = battery voltage in volts

$P_o$  = drive system output power in watts

$V_2$  = speed at end of constant power region in mph

$f_2$  = motor frequency at  $V_2$  in hertz

### 3.4.7 Controller and Power Module Requirements

The controller requirements are extracted from this system design and are shown in Table 3.4.7-1. Since the power semiconductors in the inverter have a very short (1 second) thermal time constant, they are sized for the peak inverter currents. The thermal rating of the inverter must be larger than the J227a-D duty cycle rating, so it can handle the peak loads. Its thermal time constant (several minutes) is faster than the motor time constant, and of the order of the duration of the peak loads. Therefore, the inverter is thermally designed to operate nearly continuously at the peak loading requirements.

**Table 3.4.7-1**

**CONTROLLER SPECIFICATIONS**

DC Input Voltage	75-150 Volts
DC Input Current	400 Amps
AC Output Voltage	109 Volts rms
AC Output Current	330 Amps rms
Peak Current	600 Amps
Maximum Chopping Frequency	3000 Hz
Fundamental Frequency, Chopping	0-180 Hz
Fundamental Frequency, Square Wave	180-500 Hz
Maximum Output Power	35.8 Kilowatts

The unique design approach by GE is to build each of the six inverter semiconductor switch positions using a semiconductor power module (reference Section 3.8). Each power module is a combination of four power Darlington transistors in parallel and two fast recovery diodes in anti-parallel. The controller specifications result in a set of power module specifications as shown in Table 3.4.7-2.

**Table 3.4.7-2**

**POWER MODULE SPECIFICATION**

Peak Current	650 Amps
Peak Switch on Voltage	150 Volts
Peak Switch-off Voltage	300 Volts
Chopping Frequency, maximum	3000 Hz
Fundamental Frequency, Chopping	0-180 Hz
Fundamental Frequency Square Wave	180-500 Hz
Thermal Rating Required	
• Usable with 0.1 to 0.15 °C/W Heatsink	
• Ambient Temperature Range of -30 °C to 50 °C	
Inverse Diode of same current rating with a compatible recovery characteristic required for full regeneration	
Gain at 600 A collector current for power Darlington transistors	300

### 3.5 DRIVE SYSTEM DESCRIPTION

This section presents an overall description of the actual drive system configuration chosen to implement the required drive system specifications outlined in the previous four sections (3.1-3.4). The following three sections (3.6-3.8) discuss the detailed design of the drive system electrical components: the control electronics, power inverter and transistor power module. The motor design was discussed in Section 3.3. The overall system configuration, including the power inverter, battery, control electronics and ac motor is shown in Figure 3.5-1.

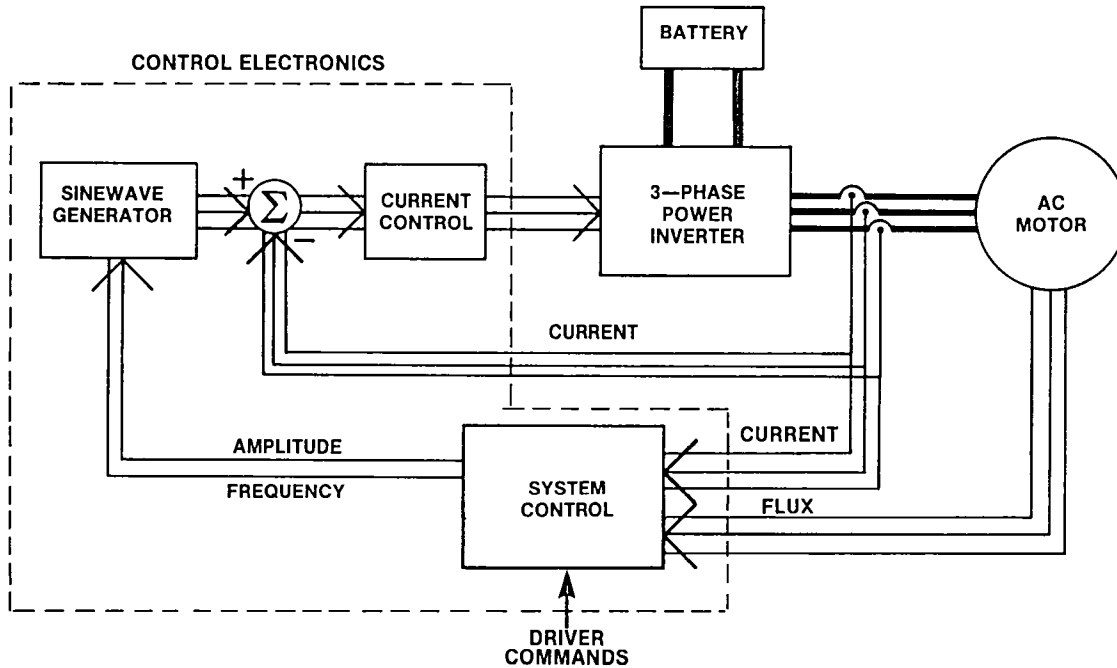


Figure 3.5-1 Simplified System Block Diagram

#### 3.5.1 Control Strategy

The desired motor operating conditions are shown in Figure 3.5.1-1. This figure shows torque, motor voltage, and slip frequency as a function of speed.<sup>(14)</sup> The motoring torque curve consists of three major portions: a constant torque section to speed  $V_1$ , a constant horsepower section from  $V_1$  to  $V_2$ , and a motoring portion at reduced flux from  $V_2$  to the maximum speed. The torque-limited section corresponds to the maximum capacity of the inverter to supply motor current and full motor flux level. The constant horsepower section corresponds to the field weakening mode of operation of a dc motor, and arises from the limitation of maximum voltage available from the inverter in motoring. The section of the motor curve from  $V_2$  to maximum speed corresponds to operation of the motor at breakdown torque with the maximum available voltage from the inverter. Thus, the torque is inversely proportional to speed squared. In general, this section of the curve corresponds to the torque characteristic of a series dc motor, although the curve for a dc motor falls below this curve because of the main field magnetic circuit saturation.

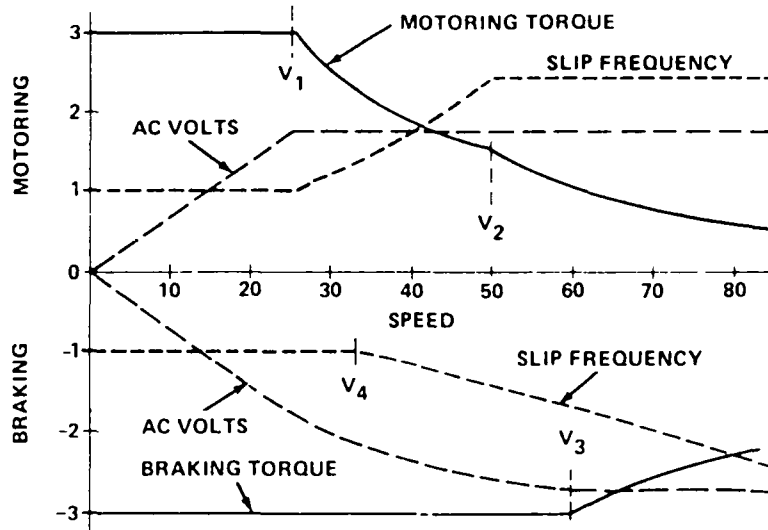


Figure 3.5.1-1 Motor Operating Conditions

The braking torque curve has two sections. The first section is a constant deceleration rate in the speed range from zero to  $V_3$ . The second is the constant power taper, which is the most practical characteristic for a power-limited drive system.

From Figure 3.5.1-1, it is apparent that the motor control can be divided into three modes of operation. Mode I, for a speed of zero to  $V_1$  in which slip frequency is held constant while the motor terminal voltage increases linearly with speed, Mode II, for a speed between  $V_1$  and  $V_2$  in which voltage is held constant with slip frequency increasing with speed; and Mode III, for a speed  $V_2$  to maximum speed for which both voltage and slip frequency are constant. Analogous modes also exist in the braking operation, with the transition between Modes I and II at speed  $V_4$ .

Figure 3.5.1-2 shows the variation of motor flux level with speed when, in the PWM mode of operation (Mode I), the level of flux is regulated to a desired value. The level of flux in the motor is chosen so that it is always regulated at the maximum value. This minimizes the time the inverter is pulse-width modulating, and maintains operation of the inverter at the minimum frequency possible. Thus modulation to any desired torque level within the limiting values shown is accomplished by control of the motor frequency. However, some variation of flux level is permitted in order to reduce light load losses at high speed. In order to operate at any instant in any mode, it is desired to devise a torque and power regulator that will transition smoothly between voltage control and frequency control. Figure 3.5.1-2 indicates only maximum motor and braking performance; however, steady-state operation at any value between these limits must be achievable.

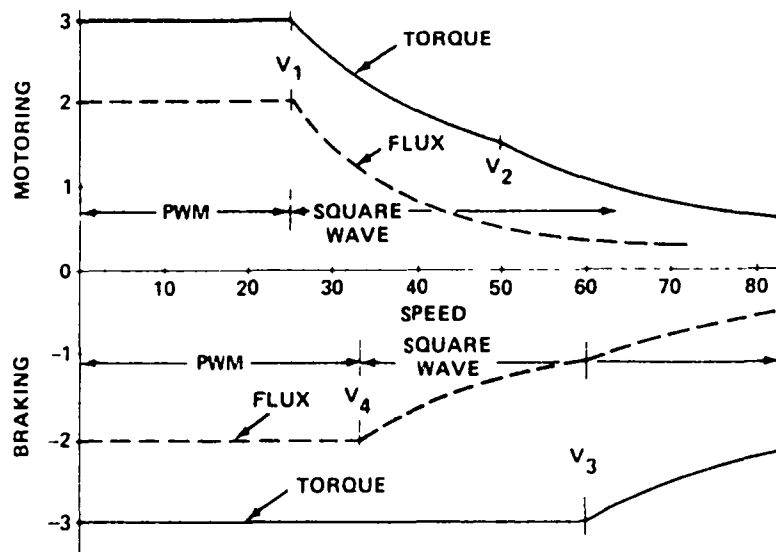


Figure 3.5.1-2 Relative Torque and Flux

### 3.5.2 Current-Controlled PWM

In order to implement the control strategy described in Section 3.5.1 and because the power inverter will operate from a nominally fixed dc source voltage, a PWM method to vary the motor voltage must be chosen. There are a number of PWM methods which could be used<sup>(9,18,19,20)</sup>

One method presently in wide use dates back to the original paper of Schonung and Stemmler<sup>(18)</sup> Figure 3.4.5-1 is an illustration of the method of generating the inverter switching waveforms and the resultant output voltage waveform across the motor line to neutral connection. This voltage waveform causes motor current ripple which adds to the motor losses and requires extra inverter current handling capability. In addition, because the waveform is a voltage waveform, a small imbalance in the motor voltage, due to the small motor stator resistance, can cause a relatively large current imbalance in the motor current. An imbalance in phase voltages will translate to a motor frequency ripple in the dc link, and since the motor frequency varies from 0 to 500 Hz, any resonances in the dc link filter tend to be excited. In addition, it is possible to generate dc currents in the motor which will cause extra heating in the motor and torque ripple in the motor output.

All of these PWM methods<sup>(9,18,19,20)</sup> have in common two disadvantages. The first, discussed above, that these methods are voltage control systems, the second, that a special transition mode of operation involving the synchronization of the reference waveform with the desired output waveform is required. The requirements that the waveforms have very little imbalance and a very small dc offset impose a requirement for a high degree of precision on the waveform generation. This means that the control electronics must precisely generate a waveform with a fairly smooth sinusoidal output. The second problem arises when an inverter output voltage greater than about 80% of maximum is required, as at high speed. For

maximum output voltage (V line to neutral =  $0.45 \times E_B$ , the inverter must operate in the square wave mode without notches in the output waveform. Normally a transition mode of PWM is used that synchronizes the chopping reference waveform to the output frequency waveform, which is a difficult task <sup>(9,19,20)</sup>

An improved PWM method has been devised to eliminate these two problems, while adding significant new advantages <sup>(10,11)</sup>. The PWM method is called current-controlled PWM because it generates the inverter switching times based on controlling the motor current. The inverter switching is controlled adaptively so that the actual motor current follows a reference sine wave within a hysteresis band. Figure 3.5.2-1 is an illustration of the method of generating the inverter switching and the resultant voltage waveform across the inverter output referenced to minus dc battery. The closed loop system control provides a current amplitude and fundamental motor frequency (not switching frequency) to a sine wave generator (Figure 3.5-1). A more detailed current-controlled PWM block diagram is shown in Figure 3.5.2-2. A reference sine wave at the desired frequency and current amplitude is generated and compared with the actual motor current. If the motor current is greater than the

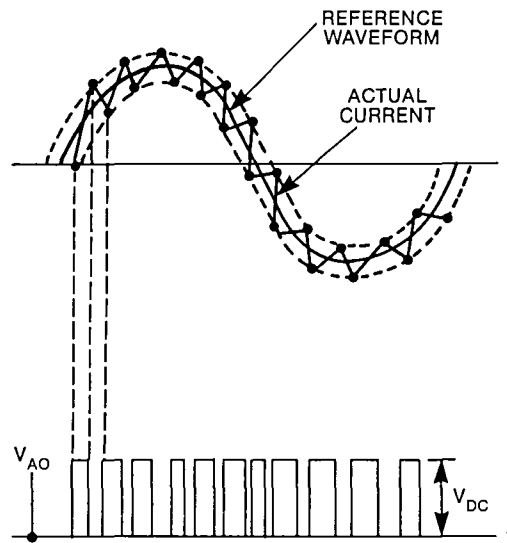


**Figure 3.5.2-1 Generation of Current-Controlled PWM**

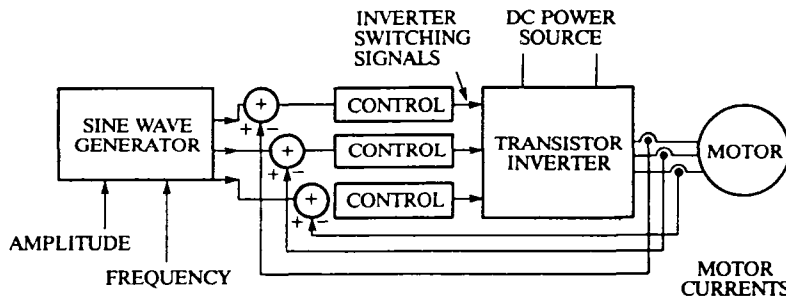


**Figure 3.5.2-2 Current-Controlled PWM Block Diagram**

reference, the inverter switches to decrease the current and vice versa. The frequency of the inverter chopping can be controlled by introducing a small amount of hysteresis into the comparison so that, in effect, the amount of current ripple is regulated, as shown in Figure 3.5.2-1. There is an independent current control on each inverter output phase. Figure 3.5.2-3 shows the current control circuit, including the hysteresis and a 25  $\mu$ sec time lockout on the inverter switching frequency because the transistors need a finite time to turn on or off.

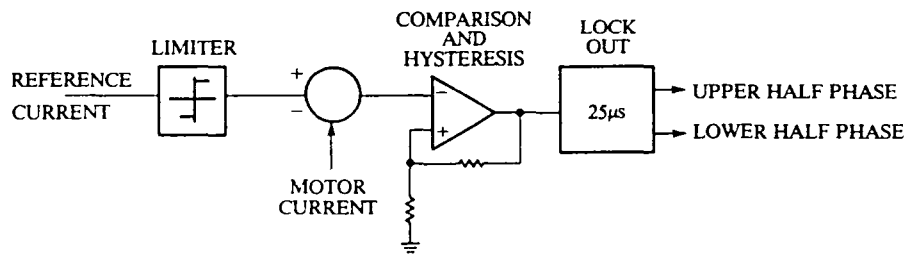


Figure 3.5.2-3 Current Control Circuit for One Phase

The current-controlled PWM method has several advantages. It does not require the high degree of precision in the waveform generation, as do the voltage PWM methods. It does not require a special transition mode from PWM to square wave, because the current control adaptively decreases the inverter switching until square wave operation is achieved. This method produces the maximum possible torque in the motor for the minimum ac peak current. The peak transistor current is also minimized. The motor loss is minimized with better sinusoidal waveforms during PWM operation. Lastly, the drive is inherently more rugged with instantaneous control of the current at all times, instead of an independent current limit that may be too slow to prevent transistor failures during overloads. The motor current in PWM motoring is shown in Figure 4.6-1 and a motor voltage in PWM motoring is shown in Figure 4.7-1. Other waveforms are also shown in Sections 4.6 and 4.7.

### 3.5.3 System Control

The current control method of controlling inverter current causes the transistor inverter to become the same as a current inverter, with all the inherent advantages, stability, and problems of the current inverter at low speeds in the PWM mode. However, at high speed, the system can operate without PWM and thus has the control characteristics of a voltage inverter and does not suffer the inherent frequency limits of the current inverter. Therefore, the system is able to operate over a wide speed range. As the motor speed increases, the output voltage of the inverter will increase as necessary to maintain the motor current. Eventually, the maximum output voltage capability of the inverter will be achieved. The result is a relatively smooth transition from PWM to square wave operation of the inverter, as far as amplitude of the current and voltage is concerned. A problem arises because at low speeds before the transition, the reference wave represents motor current which in an induction motor may lag the voltage by about 30° at full load to 90° at no load. After the transition, the reference represents motor voltage. Thus, as pulses are dropped (chops in the ac output waveform eliminated), jumps in the phase of the reference are required to eliminate torque transients. In addition, some sort of stabilizing control is required for low speed current inverter operation which should ideally be compatible with the voltage inverter operation at high speed.

Some known methods of controlling current inverters for motor stability include some form of slip frequency control combined with current regulation when induction motors are used, <sup>(21,22)</sup> or the well-known shaft position sensing when synchronous motors are used. Both these methods are difficult to use to handle the transition from current-controlled PWM to voltage control. An alternative stabilizing control, suitable for both current and voltage control, is a method of motor electrical angle control applicable to both synchronous and induction motors <sup>(10,23)</sup>. This control method measures and regulates a modified angle between the motor's rotor flux vector and the stator (inverter) current vector <sup>(23)</sup>.

Shown in Figure 3.5.3-1 is an example relating several motor angles to the motor slip frequency and torque for constant air gap flux operation <sup>(23)</sup>. The actual motor angle  $\sin\theta_{sm}$  is not monotonic, which would be undesirable for use as a feedback quantity, and the angle including the rotor leakage flux  $\sin\theta_{sr}$  has low gain for high slips so regulation would be poor. A modified angle  $(\sin\theta)_{eq}$  is developed <sup>(23)</sup> which is actually used in the control system. This control method stabilizes the drive system in current inverter operation (current-controlled PWM) and allows for a feedback-controlled transition between current control and voltage control (square wave operation). The sine wave reference generator (Figure 3.5-1) phase angle will be varied as pulses are dropped to maintain the desired motor operation.

Obtaining the motor angle  $(\sin\theta)_{eq}$  involves measuring the stator currents and the air gap flux as vectors. The air gap flux could be calculated from the terminal voltage but this is not adequate at low frequency due to the voltage drop across the stator resistance. Direct measurement using air gap flux sensing coils wound around the stator teeth is the preferred method and is used for the actual system <sup>(17)</sup>. The method of making and inserting the sensing coils without disturbing the main motor winding was developed by General Electric. <sup>(16)</sup>

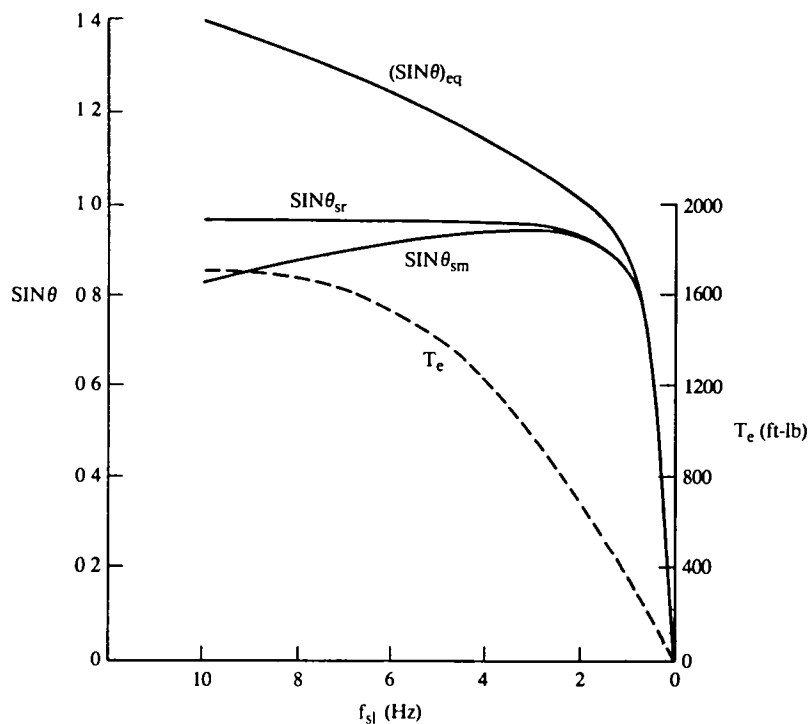


Figure 3.5.3-1 Induction Motor Angle and Torque as Function of Slip Frequency

Shown in Figure 3 5 3-2 is a vector diagram of the stator voltage, stator current, and air gap flux linkage. This diagram defines the relationship of these quantities to each other along with a definition of the machine torque angle.

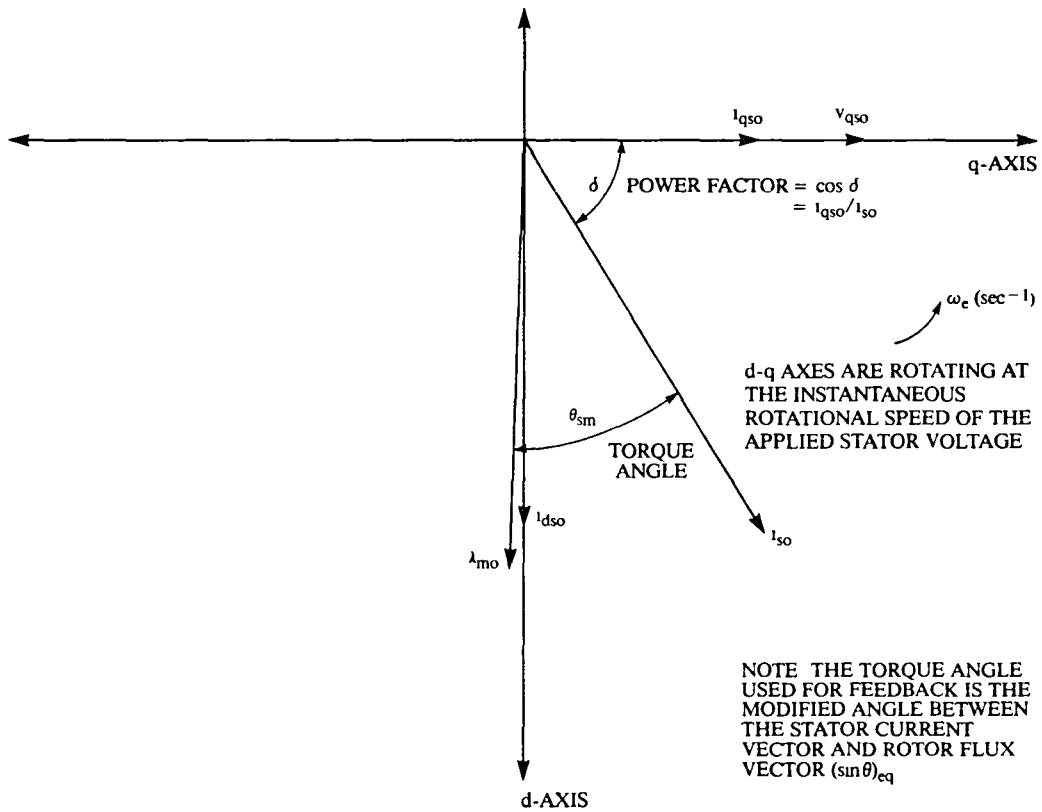


Figure 3.5.3-2 Vector Diagram of Motor Operation

A block diagram of the feedback signal processing of the motor current, flux, torque, angle and real component of stator current is shown in Figure 3 5 3-3. The inputs to the circuit are  $V_{ma}$ ,  $V_{mb}$ ,  $V_{mc}$ , the air gap voltages, and  $i_{as}$ ,  $i_{bs}$ ,  $i_{cs}$  the motor currents. The circuit performs an integration of the air gap voltages to obtain flux  $\psi_{ma}$ ,  $\psi_{mb}$ ,  $\psi_{mc}$ . The a d-q axis multiplication<sup>(14)</sup> (see Appendix B) is performed to calculate electronic torque. A refinement to a torque controller concept is to divide the electronic torque by the magnitude of flux with a small correction for the magnitude of the stator current, yielding the real component of stator current. This is the actual feedback signal, rather than torque, used in the outer loop of the control. Further division of the real component of stator current by the magnitude of current yields the desired control angle  $(\sin \theta)_{eq}$ . These inputs and the angle are satisfactory for complete control of the drive system, but do not allow for an easily generated driver command signal. The addition of two outer control loops (Figure 3 5 3-4), flux and real current, solve this problem. Both of these feedback signals are available as by-products of the motor angle sensing circuits. Use of these signals eliminates the need for a tachometer. Figure 3 5 3-4 shows the addition of the angle control inner loop and the flux and real current outer loops, along with the feedback signal processing, to the current-controlled PWM block diagram.

One of the outer loops chosen is a real current regulator operating through the inverter frequency input because real current control can be maintained in square wave operation and

PWM operation, since frequency is a variable in both regions of operation but voltage amplitude is not. In PWM operation it is desirable to regulate the air gap flux at all speeds so the other outer loop is a flux regulator operating through the inverter current amplitude input.

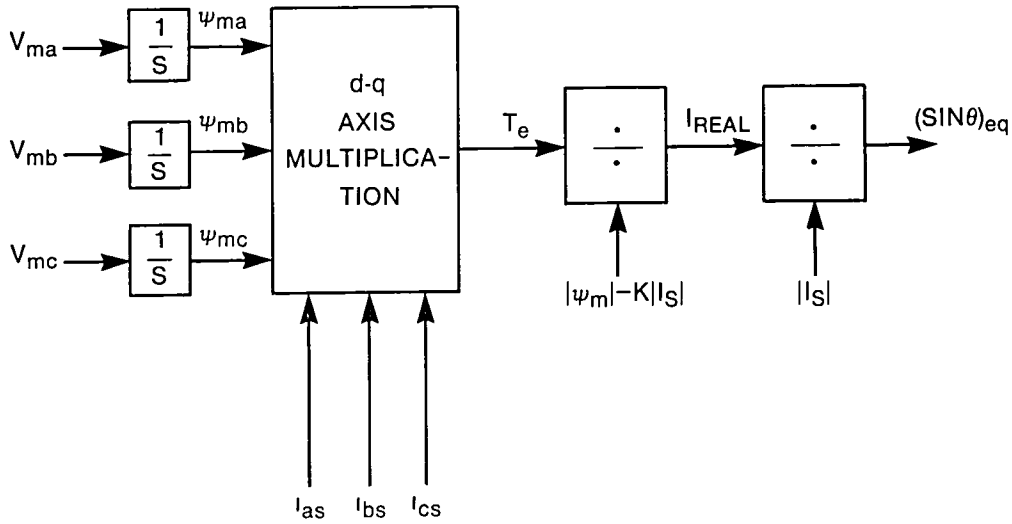


Figure 3.5.3-3 Feedback Signal Processing

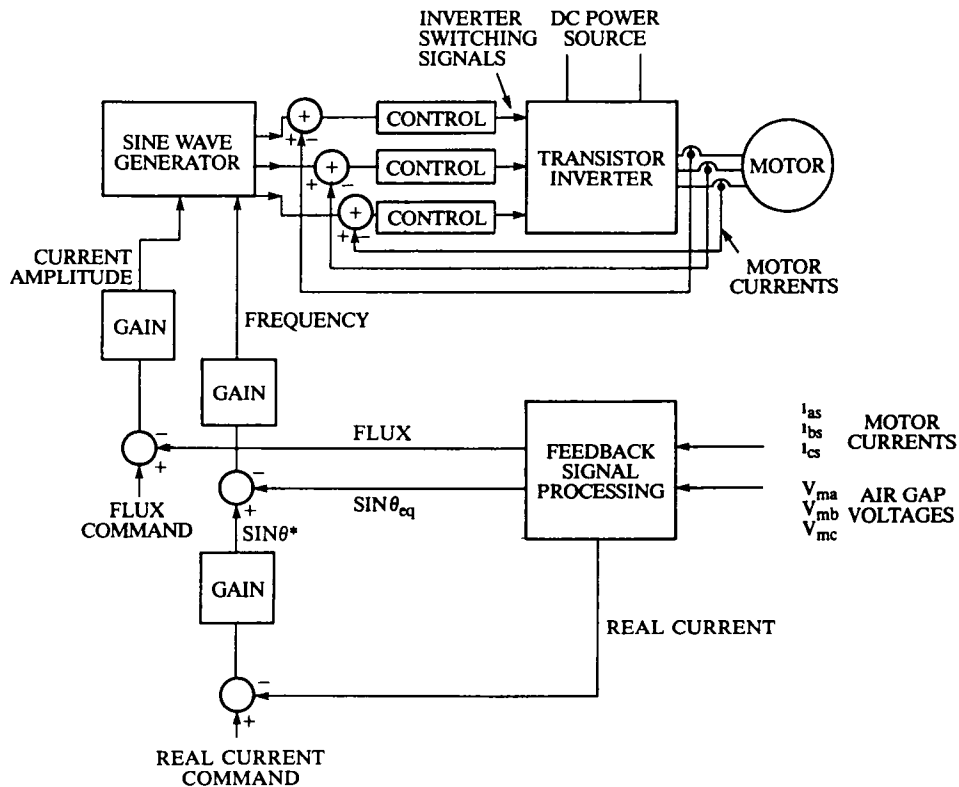


Figure 3.5.3-4 Overall Drive System Block Diagram

### 3.5.4 Power Inverter

The three-phase power inverter of Figure 3 5-1 is the well-known three-phase bridge connection with feedback diodes and uses power transistors, as shown in Figure 3 5 4-1. Each of the six transistor-diode switches is a power module containing a combination of power Darlington transistors and antiparallel fast recovery diodes capable of switching 600 amps at up to 300 volts. In each power module there are four power Darlington transistors in parallel, each rated at 200 amps and 450 volt breakdown, and two diodes in parallel, each rated at 250 amps and 600 volt breakdown. A dc filter capacitor bank is connected across the dc input to the inverter. Each power module is driven by a separate base drive circuit with its own isolated power supply. A snubber is placed across each power module to maintain the instantaneous current and voltage switching locus within the ratings of the power Darlington transistors. The inverter is modularized into six identical half-phase modules built up on heatsink material, which is forced air cooled.

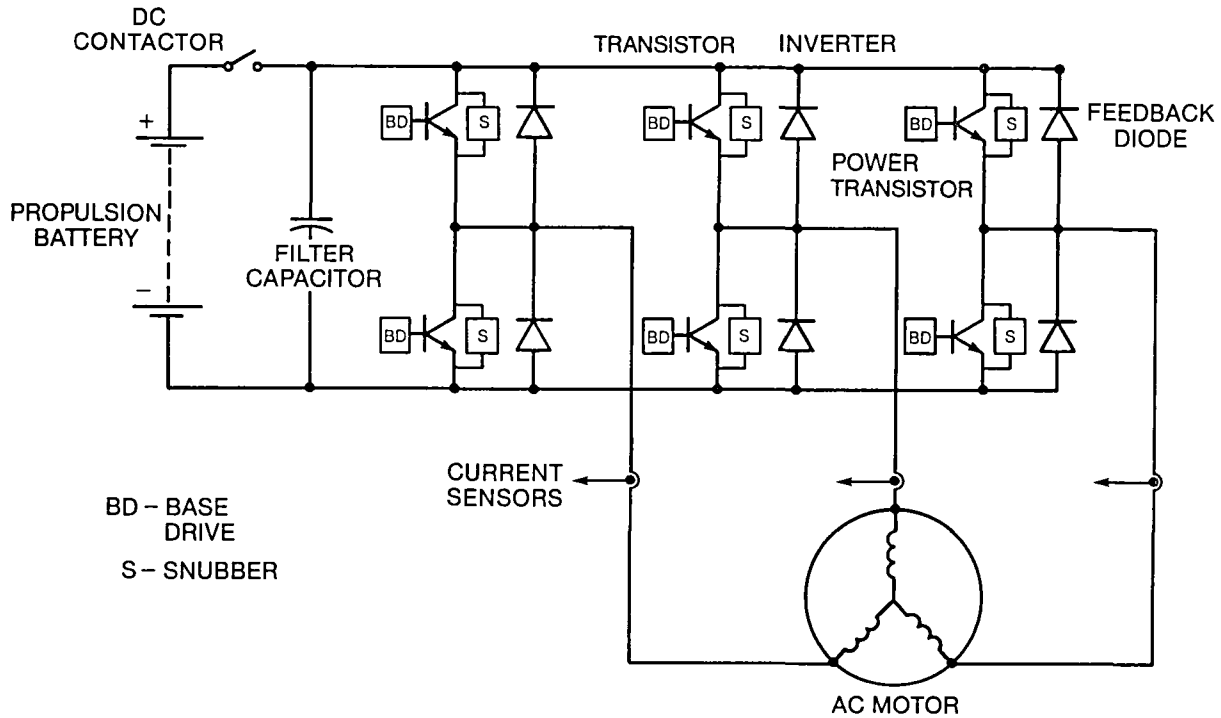


Figure 3.5.4-1 Inverter Power Circuit

### 3.6 CONTROL ELECTRONICS

The control electronics hardware is shown in Figure 3.6-1. The card cage is a  $43.8 \times 36.8 \times 19.1$  cm ( $17.3 \times 14.5 \times 7.5$  in) enclosure weighing 6.4 kg (14.2 lb). There are eight control cards. Note the external connections to the motor and power inverter. Note also the driver command module next to the card cage.

The overall drive system block diagram of Figure 3.5 3-4 is expanded in detail and the eight control cards with their functions are blocked out in Figure 3 6-2. A detailed description of operation for each control card is given in Appendix B. The individual control card drawings are in Appendix D.

This section presents the functional design and operation of the control electronics for the ac controller. This description is more detailed than that presented in Section 3 5.3, but not as detailed as the individual control card descriptions in Appendix B. The signal conventions used when discussing signals on the control cards are defined in Section 7. The following sections refer to the control function block diagram shown in Figure 3 6-3. The control electronics schematic (EP7644 MCEA) in Appendix D may also be useful in reference to the following discussion.

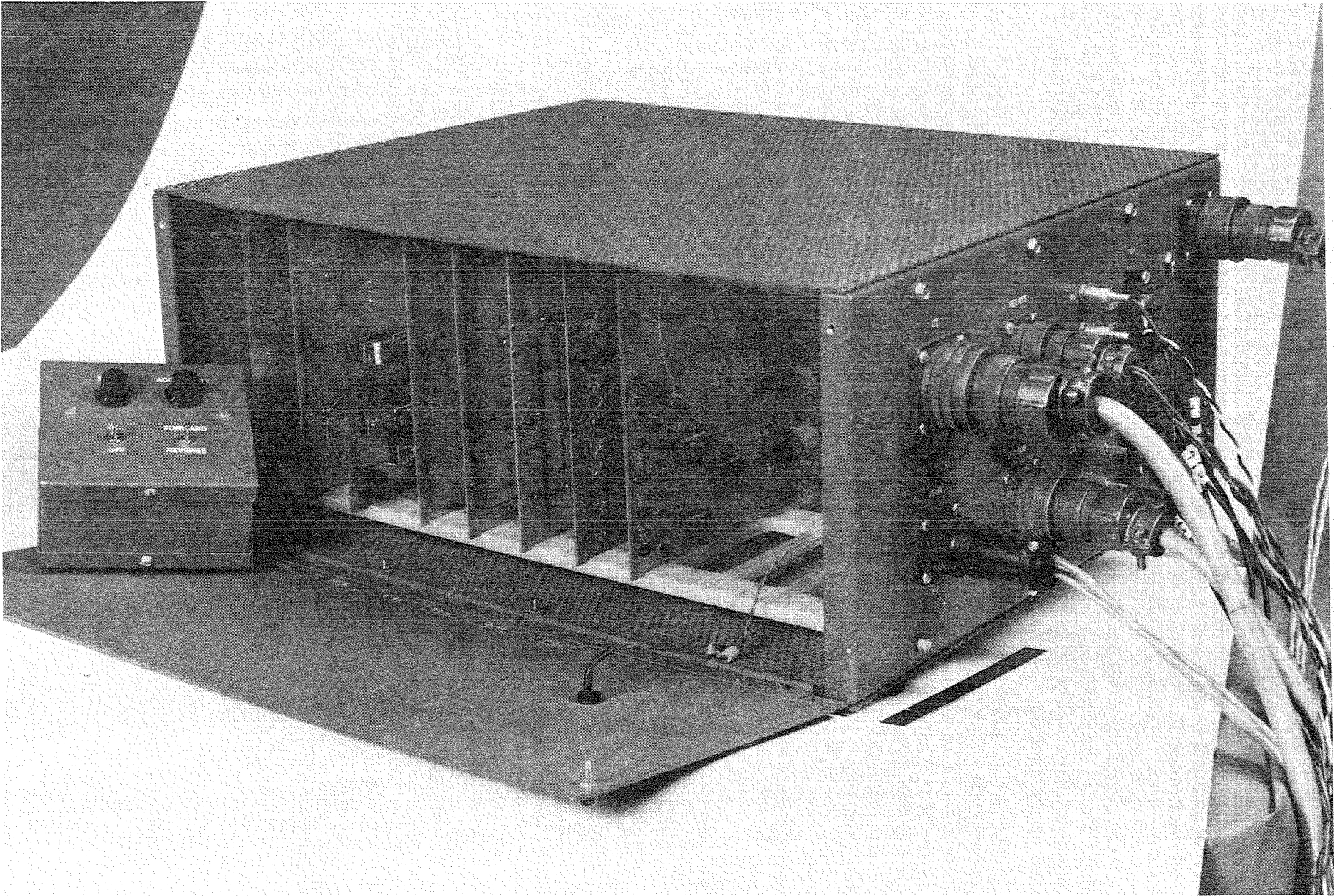


**Figure 3.6-1. Control Electronics Assembly and Driver Command Module**

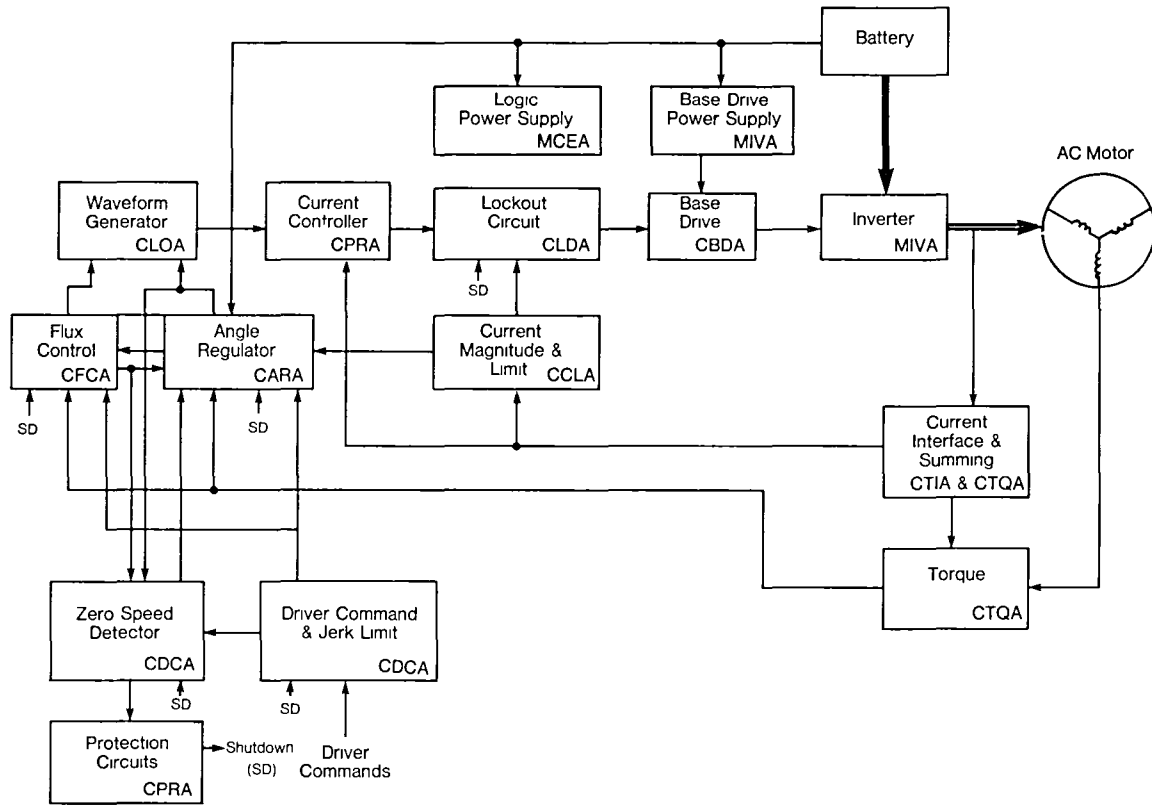


**Figure 3.6-2 Control Circuit Card Block Diagram**

*Note: The letters in the blocks refer to the last four letters of the individual control card drawings in Appendix D.*

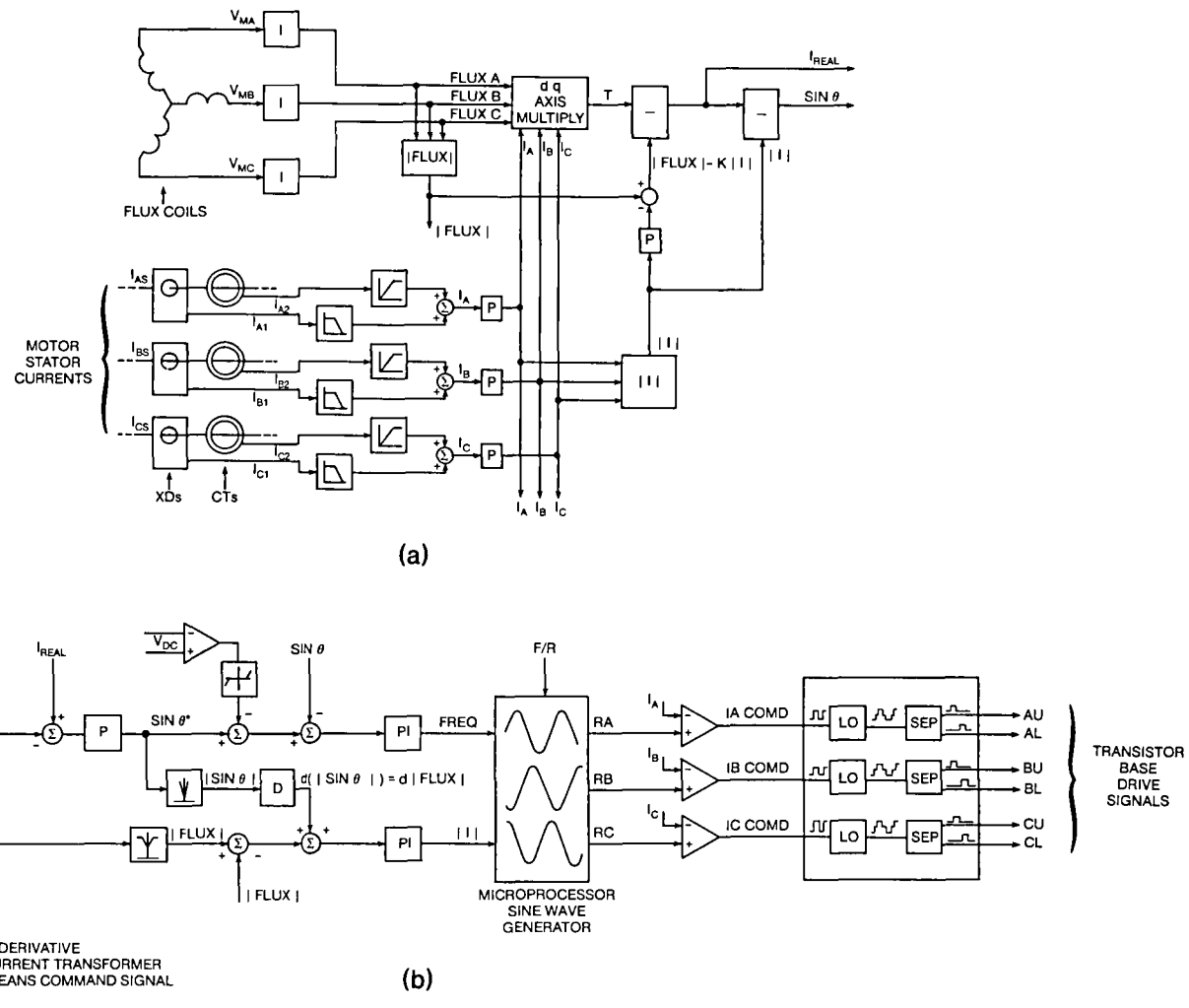


**Figure 3.6-3 Control Function Block Diagram**  
**a. Feedback Signal Processing Block Diagram**  
**b. Closed Loop Controls Block Diagram**

### 3.6.1 Current Control Loop

The current control loop compares the actual three-phase motor currents (IA, IB, IC) to a three-phase sine wave reference (RA, RB, RC) to produce the phase switching commands (IA COMD, IB COMD, IC COMD) which determine when to switch the power transistor modules (reference Figure 3 6-3b). Instantaneous current limit is inherent in this technique since the actual current is always being controlled directly.

The motor current feedback signals enter the control electronics at two points (reference Figure 3 6-3a). The outputs of the Hall-effect current transducers (XD's) are brought in through connector P3 to the transducer interface card (EP7644CTIA), which also provides the calibrated bias currents to the transducers. The outputs of this card (IA1, IB1, IC1), are negative in sign and scaled to 100 amps/volt. The outputs of the current transformers (CT's) enter the control electronics through connector P11, and then to the torque card (EP7644CTQA) where they are scaled to 80 amps/volt (IA2, IB2, IC2). The current transducers have limited high frequency response and are low-pass filtered (below 400 Hz) and re-scaled to 80 amps/volt on the torque card to provide the dc component of the current. The current transformer signals are high-pass filtered (above 400 Hz), and provide the principal component of the current feedback. The two sets of signals are summed on the torque card to generate composite motor current feedback signals (IA, IB, IC), and are available at test points on the edge of the torque card.

The phase current reference waveforms (RA, RB, RC) are filtered on the protection card (EP7644CPRA) and compared to the current feedback signals (IA, IB, IC) to generate the phase current command signals (IA COMD, IB COMD, IC COMD) as shown in Figure 3 6-3b. These are passed to the lockout card (EP7644CLOA) where a lockout function is applied to force a period of time between one power module's turn off and the complementary power module's turn on. This prevents overlap of the power modules' conduction times to prevent a "shoot-thru", a condition which would occur if a continuous path existed through both power modules in the same phase causing a high-fault current which would destroy the two power modules involved. IA COMD, IB COMD, and IC COMD are then split into upper and lower power module drive commands (AU, AL, BU, BL, CU, CL) which are sent to the base driver modules (EP7644MBDA) in the power inverter assembly through coaxial cables. The base driver modules are optically coupled at the input and are designed to source base current to the power modules when current is flowing at the input and to sink base current from the power modules when input current is not flowing. The current sink mode of operation is intended to sweep out stored charge from the base junctions of the power modules for fast turn off.

The phase current reference waveforms (Figure 3 6-3b) are three sinusoidal waveforms separated by 120 electrical degrees whose amplitude is controlled by  $|I|^*$  and whose frequency is controlled by  $FREQ^*$  and are produced by the reference generator portion of the lockout card (EP7644CLOA). The reference generator consists primarily of a microprocessor, three digital-to-analog (D/A) converters, and a voltage-to-frequency (V/F) converter. The microprocessor computes the relative amplitudes of the three waveforms at a single point in the period and sends the results to three D/A converters where they are multiplied by  $|I|^*$  (the amplitude control signal) to set the peak amplitude of the waveforms.  $FREQ^*$  (the frequency control signal) is converted by the V/F converter to a pulse train whose frequency is proportional to the desired frequency of the waveforms. This pulse train clocks the reference generator, causing it to compute successive sets of values of the waveforms. The result is three sinusoidal waveforms with discrete "staircase" values which then must be filtered as discussed in the previous paragraph.

The amplitude and frequency of the reference current waveforms are controlled by the two inputs ( $I^*$  and  $FREQ^*$ ) to the reference generator, which are determined by the outer loop controls of the ac controller

### 3.6.2 Outer Loop Controls

#### 3.6.2.1 Flux regulator

The flux regulator controls the flux in the motor by varying the amplitude of the reference generator using  $|I^*$  as shown in Figure 3 6-3b This controls both the imaginary component of current which generates flux and the real component which generates torque, as shown in Figure 3 6 2 1-1 Since the angle regulator controls the real component of current ( $I_{REAL}$ ) by varying the slip angle  $\theta$  (to be discussed in a later section), the flux regulator is required to compensate for changes in the imaginary component of current caused by the angle regulator and vice versa To avoid unstable interaction, the flux control loop is a much slower loop

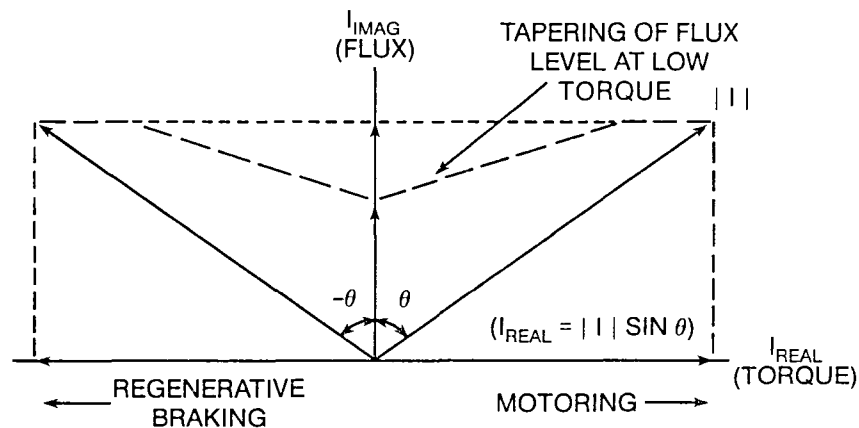
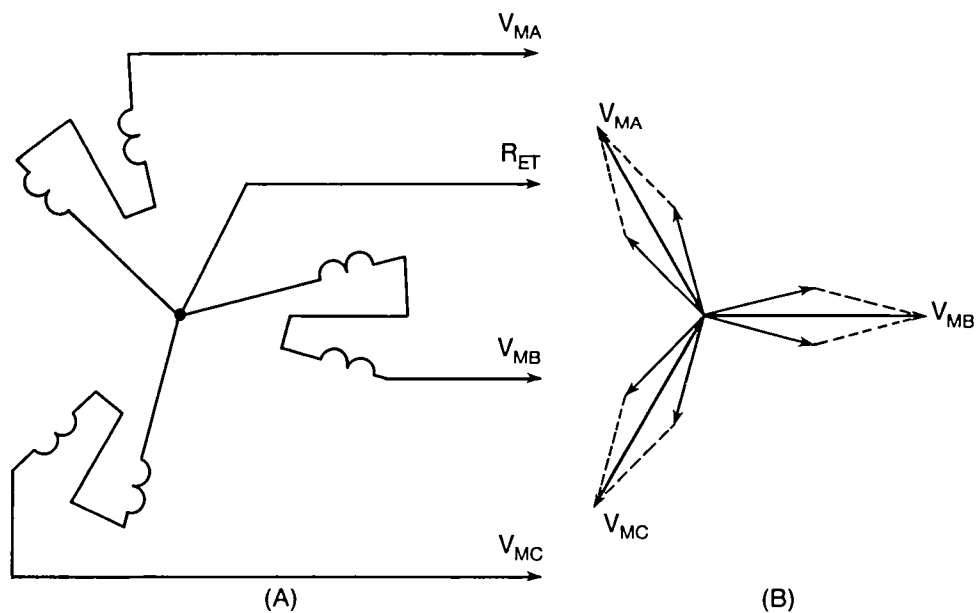


Figure 3.6.2.1-1 Imaginary and Real Components of Current

The air gap flux in the motor is sensed by three pairs of windings, two windings per phase. Since there are no motor pole faces directly in phase with the current, the nearest pole faces are 15 degrees early and 15 degrees late. Therefore, there is one coil on each pole face and the two are connected in series (Figure 3 6 2 1-2a), yielding a vector summation of the two signals (Figure 3 6 2 1-2b) which is in phase with the current. The flux coil voltage signals (VMA, VMB, VMC) are integrated to obtain the flux signals (FLUXA, FLUXB, FLUXC) as shown in Figure 3 6-3a. These are then rectified and summed to obtain  $|FLUX|$ . The command for the flux regulator ( $|FLUX|^*$ ) is obtained from a function generator which sets a minimum value when no torque is being requested (Figure 3 6 2 1-1 and Figure 3 6-3b). Additional flux is commanded at higher torque and is obtained by increasing  $|I^*$  proportionately until maximum flux is commanded. A limit function is applied to  $|I^*$  so that the controller cannot command more than the maximum current that the power modules can handle.

An additional input to the flux regulator senses any abrupt increase in commanded torque and quickly boosts  $|I^*$  via a derivative of  $\sin\theta^*$  until the flux regulator, which has an inherently slow response, can catch up (Figure 3 6-3b). This will be discussed further in the section concerning the real current regulator.



**Figure 3.6.2.1-2 Flux Coil Configuration**

**a. Flux Coil Connections**

**b. Flux Coil Vector Diagram**

### 3.6.2.2 Angle regulator

The main loop for controlling motor torque is the angle regulator. This regulator controls the frequency of the applied stator current waveforms by way of the frequency control input to the reference generator (FREQ\*). If the frequency of the stator current waveforms is equal to the rotating frequency of the motor, no current is induced in the rotor, i.e., an alternating current of zero frequency and zero amplitude (zero slip). The rotor impedance becomes resistive in nature since the reactive component is zero. Therefore, there will be zero angle between the rotor current phasor and the rotor voltage phasor. This angle is the slip angle and determines the torque of the motor. As slip increases, i.e., the difference between the applied stator frequency and the rotating frequency, the frequency of the rotor current increases. This produces an angle between the rotor current phasor and the rotor voltage phasor which increases with increasing slip due to the rotor's reactive impedance causing increasing torque. An applied frequency greater than rotating frequency will produce a positive or accelerating torque. Conversely, an applied frequency less than rotating frequency will produce a negative or braking torque. The angle regulator, therefore, controls the slip angle by increasing or decreasing frequency as required by its inputs, angle command ( $\text{SIN } \theta^*$ ), and angle feedback ( $\text{SIN } \theta$ ), as shown in Figure 3-6-3b.

### 3.6.2.3 Real current regulator

At the zero slip condition, the stator current lies essentially along the imaginary axis since the impedance of the stator is nearly pure reactance and no current is flowing by mutual inductance to the rotor. The stator current phasor will therefore lag the stator voltage phasor by 90 degrees and will generate motor flux only.

The real current regulator controls the real axis component of the stator current (Figure 3-6-2-1-1), which is the component which generates torque. The imaginary axis component of the stator current is the component which generates flux. When no torque is being

generated, the stator current phasor lies along the imaginary axis, generating only flux, and the real axis component is zero. When torque is required, the command appears as a request for the real component of stator current ( $I_{REAL}^*$ ) as shown in Figure 3.6.3b. A positive value of  $I_{REAL}^*$  will cause a positive value of the real current regulator output ( $SIN \theta^*$ ) in order to command a positive torque angle. This, in turn, will cause an increase in frequency through the angle regulator to create the positive torque angle. As the angle increases, the flux regulator must respond with an increase in total current ( $|I|^*$ ) in order to regulate the motor flux. Since the flux regulator cannot quickly respond with an increase in total current, the flux in the motor will tend to decrease momentarily. This is compensated by using the derivative of  $SIN \theta^*$  to boost  $|I|^*$  until the flux regulator can catch up, as discussed earlier.

As speed increases, the motor will require more output voltage to generate a given flux level. When the inverter can no longer increase the output voltage, having reached the full square wave voltage, the flux regulator will lose control and the flux will begin to fall off. The angle regulator will respond with an increase in angle to regulate the real component of current ( $I_{REAL}$ ), as shown in Figure 3.6.2.3-1. This automatically creates a transition from the constant torque region of operation to the constant horsepower region.

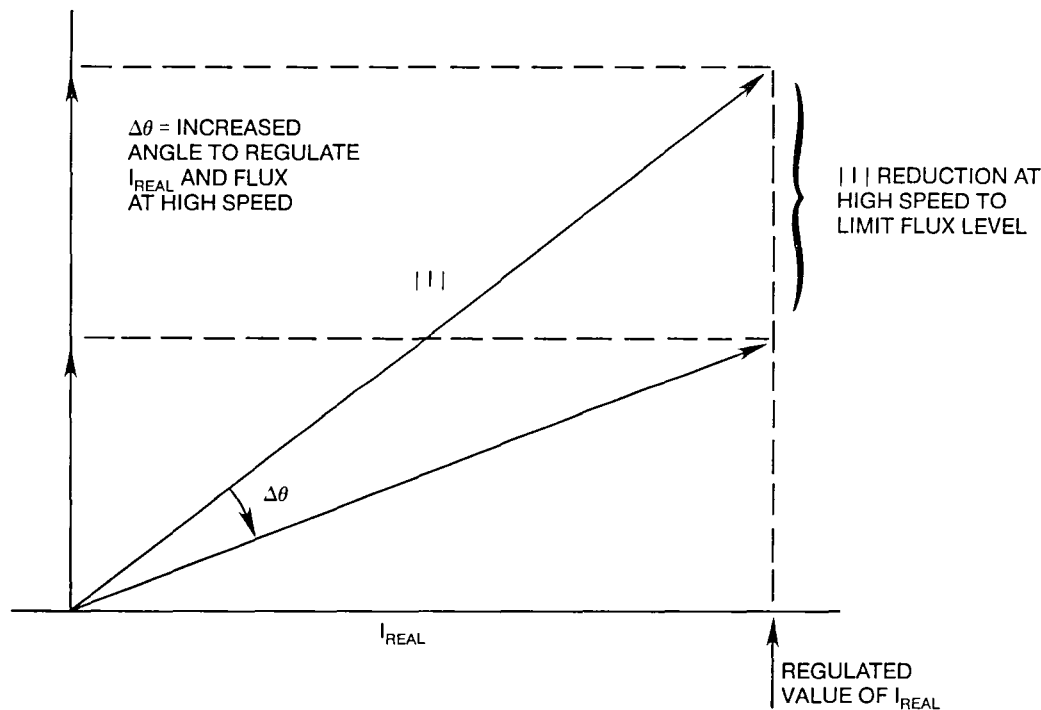


Figure 3.6.2.3-1 Regulation of Real Component of Current

### 3.6.3 Motor Reversing

To change the direction of rotation of an induction motor, the phase sequence of the power applied to the motor must be reversed. For operation from a fixed power system, this is accomplished by switching two of the motor's power leads by means of a contactor. When operating from an inverter such as used on this drive, the reversal can come from the inverter itself by reversing the phase sequence of the transistor firing. This is easily accomplished by means of the sine wave reference generator (Figure 3.6.3b).

The microprocessor is programmed to accept a direction sense signal and will produce the reverse phase sequence when commanded. The output frequency can be programmed to zero with a phase sequence of A,B,C, and can be restarted having the opposite sequence of A,C,B. This reversal is sent to the transistor base drive circuits causing the inverter to change phase sequence and reversing the motor direction. Thus, motor reversing is incorporated in the basic design.

Additional controls need to be added to ensure the proper conditions prior to allowing reverse mode from a vehicle safety standpoint. Also, an upper limit on the maximum speed in reverse, e.g., 24 km/h (15 mph), is desirable from a vehicle safety consideration.

The drive itself can be protected from adverse operation by applying a maximum rate-of-change limit to the sine wave reference generator, coupled with a current limit (power) to modify the control for cases of descending grades and similar situations.

#### **3.6.4 Other Functions**

There are many other necessary functions built into the control electronics. The conventional driver commands of accelerator and brake pedals, direction selection, and ignition switch must all be simulated. A jerk limit function operates on the accelerator and brake commands to slow down their rate-of-change. A system of shutdown and reset signals to appropriate control cards is necessary for the initial startup, protection during operation, and shutdown of the drive system. The drive system also monitors several other conditions as part of its protection system: logic power supply voltage, logic card interlock, power module heatsink overtemperature, dc overvoltage and dc undervoltage, and others. All of these other functions are discussed in detail in the individual control card description of operation (Appendix B).

#### **3.6.5 Control Performance**

The transfer functions of the three loops, angle, flux and torque, are shown in Section 4.3. They show the magnitude and phase response of the loop versus frequency.

The flux level for the motor and the flux versus torque function (Figures 3.6-3b and 3.6.2.1-1) must be determined. The flux level is determined and the control cards calibrated as shown in Section 4.4. The flux-torque function block is programmed according to the results presented in Section 4.5. This flux program results in an optimized motor efficiency, because flux is reduced at low torque levels to better balance the motor magnetic and  $I^2R$  loss. The waveform of the air gap voltage is shown in Figures 4.7-2 and 4.7-5.

The calculations of  $I_{REAL}$  and  $\sin\theta$  from the feedback signals and the d-q axis calculation of torque are shown in Section 4.9. Also presented in Section 4.9 are the relationships of various control signals to torque.

The performance of the complete drive system is illustrated in Sections 4.9 and 4.12. These are torque-speed and strip chart recording presentations of the system operation, respectively. The drive system performance recordings (Section 4.12) show the measured torque and speed, along with several control signals of interest.

### 3.7 POWER INVERTER

The power inverter hardware is shown in Figure 3 7-1 with the protective cover installed, and in Figure 3 7-2 without the cover. This engineering model power inverter is 97 cm (38 in) × 66 cm (26 in) × 20 cm (8 in) and weighs 59 kg (130 lb). There are six identical half-phase modules, which are described in Section 3 7 2. Note the dc filter capacitor bank down the middle of the inverter. The hall effect current transducers, current transformers, and line fuses for each output phase are visible in the foreground of Figure 3 7-2. The blowers for cooling the half-phase module heatsinks are on the right end of the inverter.

The power inverter circuit is shown in simplified form in Figure 3 7-3 and in full detail in drawing EP7644MIVA (Appendix D).

The power inverter has three major technical functions:

- Interface between the storage battery and induction motor during normal operation during both motoring and regenerative braking
- Provide the capability of controlling the developed motor torque (both motoring and regenerative braking) by adjusting the applied motor current, voltage, and frequency
- Provide the capability to protect itself against abnormal conditions such as overloads, short circuits, temperature extremes, and reversed battery connections

#### 3.7.1 Power Circuit

The power circuit configuration is the well-known three-phase bridge connection<sup>(29)</sup>. Three-phase ac power is supplied to the ac motor. Each phase of the inverter acts as a single pole double throw switch connected to either the positive or common side of the dc bus. The switches are bilateral—they can carry current in both directions, using the transistor for forward current and the antiparallel feedback diode for reverse current. The diodes carry the power factor related motor current as well as the bulk of the regeneration current. Due to the motor lagging power factor, the bilateral switches must be capable of forced commutation.

The pulse-width-modulated (PWM) approach was chosen for the motor voltage control because:

- The electric vehicle drive has a fixed dc bus voltage established by the battery and is well suited for PWM
- Other approaches using a regulated dc bus with an input converter have more power level semiconductors, require an inductor/capacitor dc filter, and regeneration is difficult
- The regeneration with PWM is inherent and only a small dc capacitor filter is needed
- The power switches are utilized for inversion and voltage control, increasing their contributed value
- No large, heavy inductors are required, as in some current-source approaches
- The generation of complex PWM waveforms is easily accomplished with microelectronic controls

The choice of transistors over thyristors was made because:

- The transistors obviate the need for costly and heavy thyristor commutation circuits that are needed for forced commutation

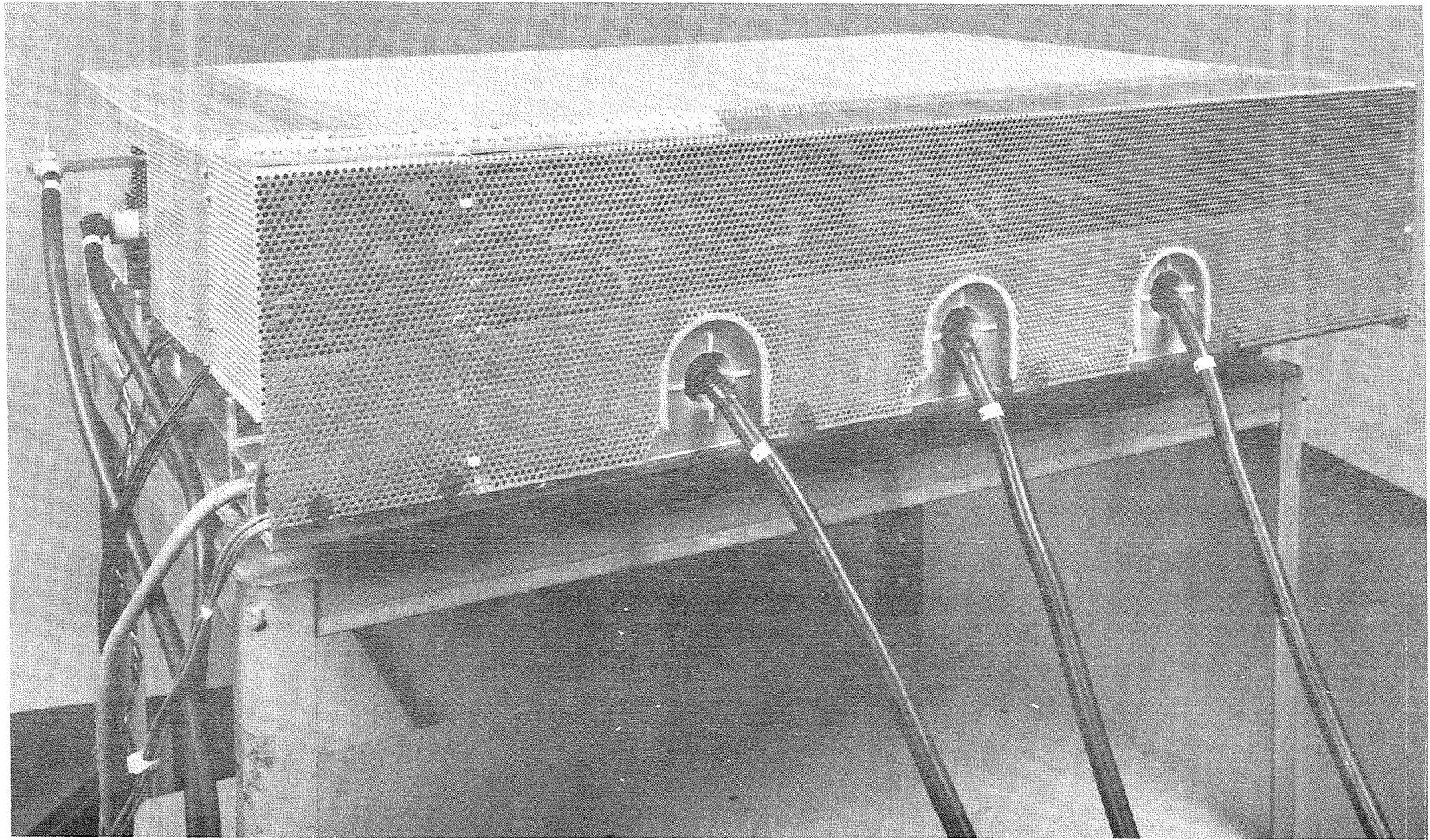
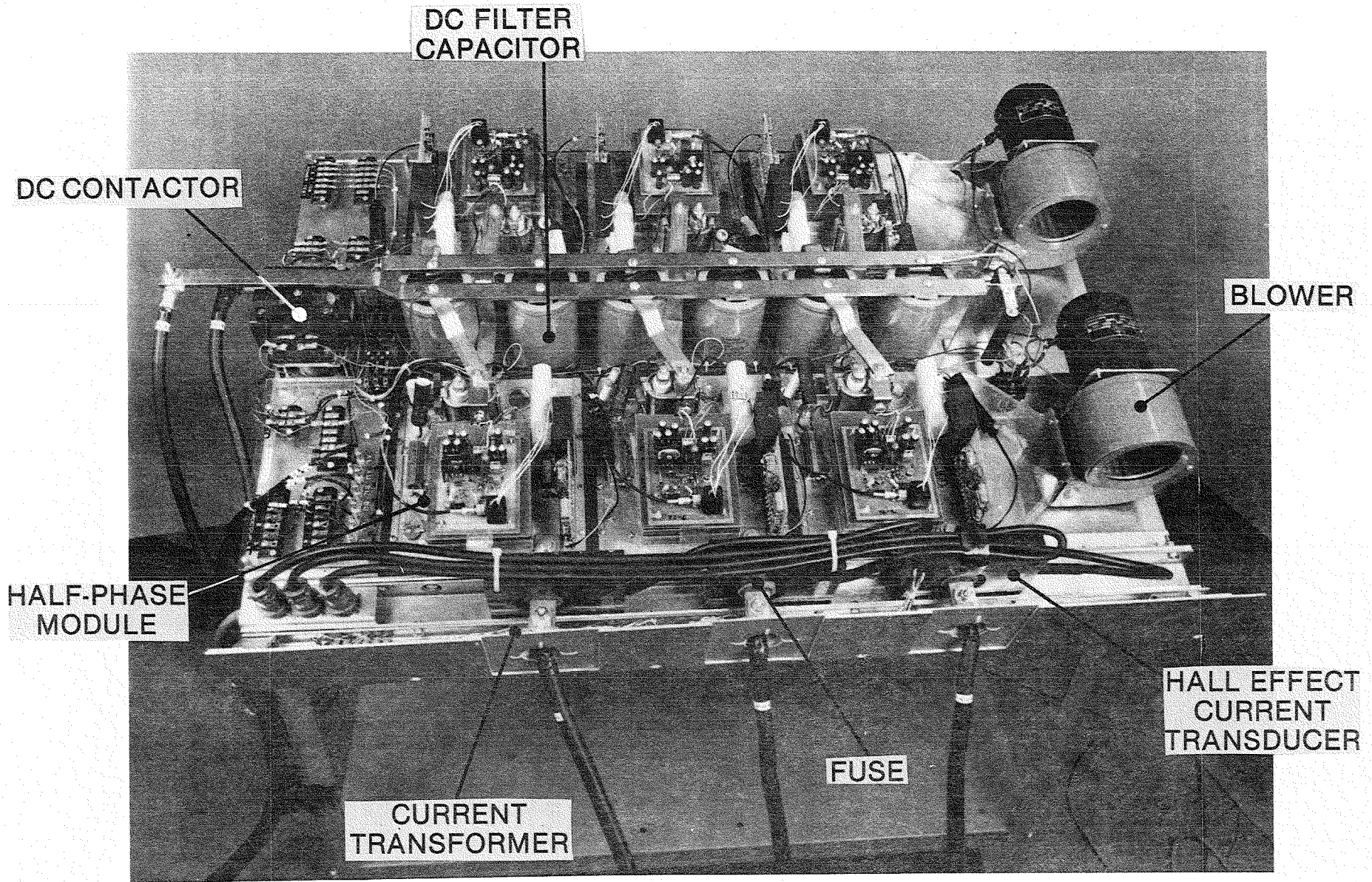


**Figure 3.7-1 Power Inverter with Cover Installed**



52

Figure 3.7-2 Power Inverter Without Cover

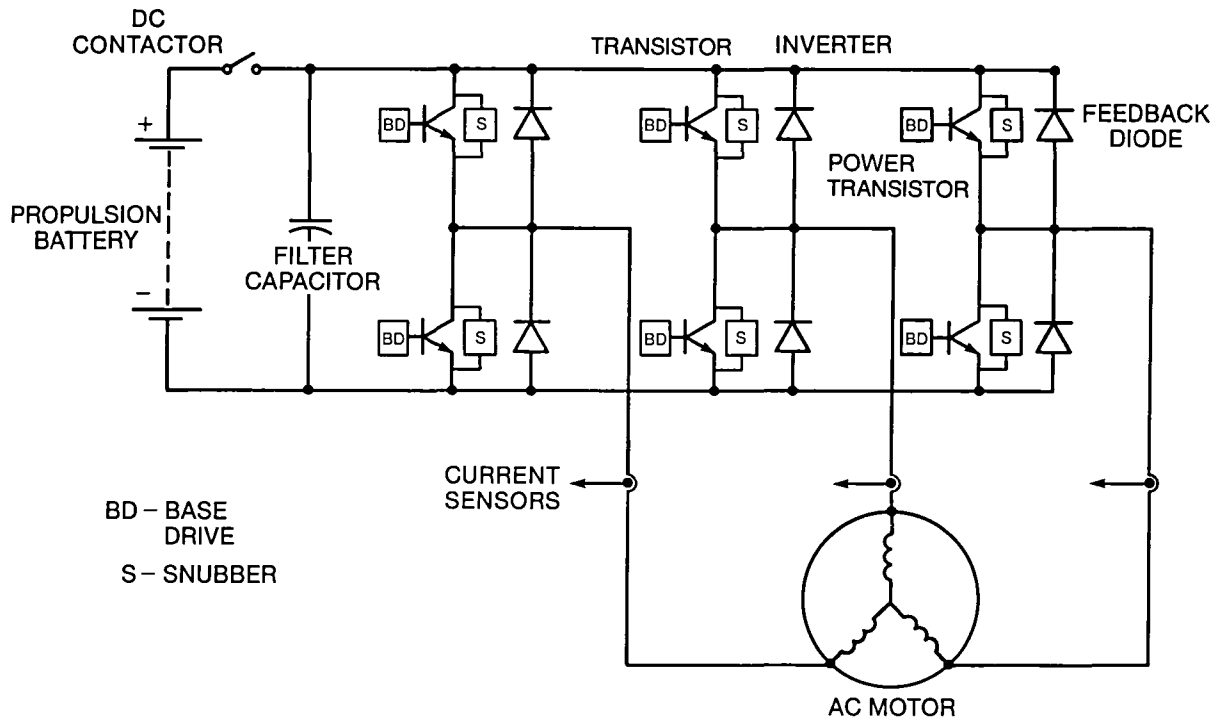


**Figure 3.7-3 Inverter Power Circuit**

- The present power Darlington transistors are evolving rapidly with availability improving, ratings increasing, prices reducing, etc. As these devices begin to mature, it is beneficial to gain experience with their application.
- Transistors have the speed of switching required to implement the current-controlled PWM method for reducing the motor harmonic losses. They have a 5 to 10 times advantage in commutation time over thyristors.

The dc filter capacitor bank across the input of the inverter (Figure 3.7-3) serves to filter the dc input voltage and provide a low impedance path for the high-frequency currents generated by the inverter during PWM switching. The filter is precharged through a 25 ohm resistor and relay (K3) before the dc contactor (K1) is closed. This prevents a large inrush current into the discharged capacitors, which would blow the dc fuse.

Abnormal modes of operation (e.g., overcurrents) are sensed by current sensors and compared with the reference signal. If the current exceeds the reference, the power transistors are then switched to reduce the current. This instantaneous current limit is inherent to the current-controlled PWM. Overtemperature is sensed with heat sink temperature sensors, if the heat sink temperature exceeds a safe value, the controller is shut down. Connection of the battery in the incorrect polarity will result in conduction through the reverse diodes and will blow the fuse in the dc link. Contactors are provided in the dc link for safety isolation from the battery. The inverter terminals are identified and test points for diagnostics are made available.

### 3.7.2 Inverter Switching Frequency

A problem that must be faced is the maximum operating frequency of the inverter, which is determined by the current-controlled PWM chopping at low speeds. The inverter switching losses are proportional to frequency and must be controlled, thus the chopping frequency should, on the average, be limited. The rate of change of current and thus the chopping frequency is automatically controlled by the comparator hysteresis, the motor stator plus rotor leakage inductance, and the dc link voltage by the equation

$$\frac{di}{dt} \approx \frac{E_B - E_m \sin \omega t}{L_{eq}}$$

which, however, applies only approximately since the motor leakage inductance is a function of frequency and the voltage is actually the dc link voltage minus the motor back emf

With the three-phase inverter shown in Figure 3 7-3 and three-wire wye motor, there is no neutral connection. Thus, the operation of the inverter is constrained because the sum of the three line currents must be zero at all instants,

$$i_a + i_b + i_c \equiv 0$$

The current in any one phase is completely determined by controlling the currents in the other two phases, rendering one phase of a current controller redundant. The switches of one phase cannot, however, be removed and the circuit simplified because the conventional three phase configuration is more efficient under square wave operation at high speed.

When the three phase inverter circuit of Figure 3 7-3 without a neutral connection is controlled by three identical current controllers, it can be expected that the inherent redundancy should affect the operation in some manner that preserves symmetry between the phases. This is seen in the waveforms obtained from the actual drive system in Section 4 6. The actual current chopping in Figure 4 6-1 is observed to diminish to very low frequency twice per cycle on each phase for a period of about 60°. The current for this phase is being maintained within the hysteresis band by the chopping on the other two phases. Thus, the average chopping frequency is lower than expected. The portion of the losses that depend on the current are significantly less when the power factor is near unity, because the peak current will occur in the vicinity of the peak counter emf with which the period of low chopping frequency coincides. The frequency spectrum (Figure 4 6-2) of this current shows the chopping frequency is spread over a range of 500 to 4500 Hz. Figure 4 6-5 is the motor current waveform during PWM operation in regeneration. The chopping is nearly uniform over the cycle, unlike motoring, because the counter emf is low. The frequency spectrum (Figure 4 6-6) shows a nearly constant 4.3 kHz chopping frequency. These chopping frequencies are slightly higher than the design specifications, but are acceptable.

### 3.7.3 Inverter Packaging

The basic inverter packaging block is the half-phase module shown in Figure 3 7 3-1 and drawing EP7644MPHA (Appendix D). This module contains the power module, snubber, base drive, base drive power supply, overtemperature sensor, and thermocouple (under the power module, part of the test instrumentation). All of these devices are mounted on a length of heatsink extrusion material. The three modules common to the upper dc rail are one half of the inverter and share the same blower, while the other three form the other half and share the other blower. The blowers operate from the main dc bus.

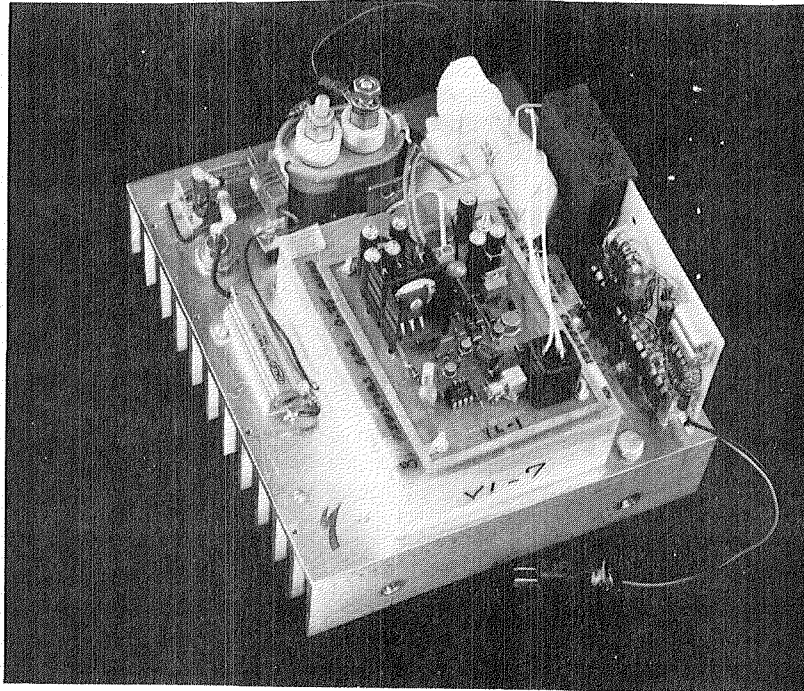


**Figure 3.7.3-1 Half-Phase Module**

The inverter is cooled with forced air and is specified to operate in a 239 K (−30 °F) to 322 K (+120 °F) ambient. The approximate air flow required can be calculated from the equation:

$$F = \frac{1.76 P}{T_{out} - T_{in}}$$

where,

$F$  = air volume flow in ft<sup>3</sup>/min

$P$  = heat load in watts

$T_{out}$  = Exhaust temperature in K

$T_{in}$  = Inlet temperature in K

At full power (41 hp) the 7080 l<sup>3</sup>/min (250 ft<sup>3</sup>/min) blowers will hold about a 25 K rise on the heatsinks.

The entire inverter is covered by an aluminum mesh cover. This provides personnel safety, yet adequate convection cooling. The half-phase modules are insulated from the inverter aluminum chassis. All other components are mounted to this chassis. The current transducers and transformers are contained in their own assemblies and are bolted to the inverter chassis.

#### **3.7.4 Power Darlington Transistor Base Drive**

Both bases, B1 and B2, of the power Darlington transistor are driven. B1 is the base of the npn driver transistor and B2 is the base of the npn output transistor. Figure 3.7.4-1

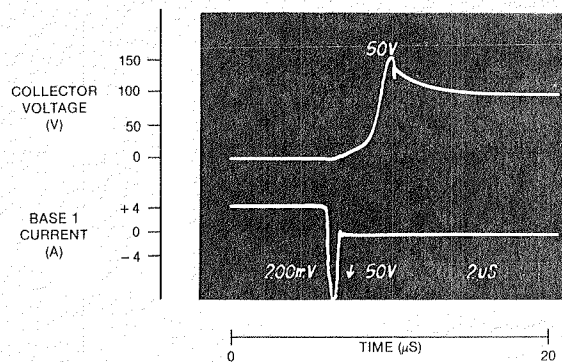


**Figure 3.7.4-1 Power Darlington Turn-off Without Reverse Base 2 Drive**

shows the collector to emitter voltage and the base 1 current of a single Darlington transistor switching off about 100 amps, with a 10 amp reverse base 1 drive and without any reverse base 2 drive. Note the initial slow rise of collector voltage as the device turns off and the relatively long storage time (from the base 1 current reversal to the steep rise of collector voltage). Figure 3.7.4-2 shows the result of applying a reverse base 2 current of about 1.5 amps to the same device, base 1 drive and switching conditions. The reverse base 2 drive is achieved by adding an external diode and resistor between base 2 and base 1. The base drive current in Figure 3.7.4-2 shows the sum of the two base currents. Note the initial slow rise of collector voltage is shortened and the storage time is reduced, thus reducing the transistor switching loss. These tests were done on an early version of the ZJ504 Darlington transistor, but are representative of the effect of driving both B1 and B2.

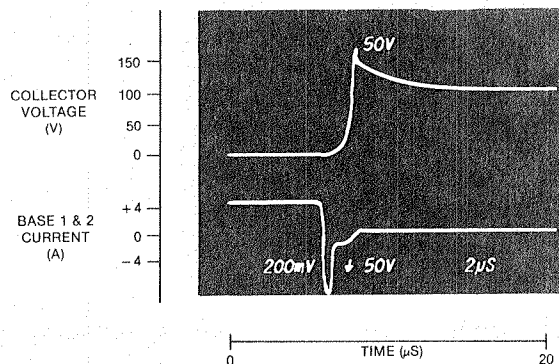


**Figure 3.7.4-2 Power Darlington Turn-off with Reverse Base 2 Drive**

The base drive circuit for a power module is shown in drawing EP7644CBDA (Appendix D) and the half-phase module circuit is shown in drawing EP7644MPHA (Appendix D). The power module base drive circuit design is based on driving both base 1 and 2, as discussed above, with a total forward (positive) base current into the power module of 4 amps peak and a total reverse (negative) current of 5 amps peak. This is based on the gain characteristic of the ZJ504 Darlington transistor, the base drive power supply requirements and the desired turn-off switching time. The diode and resistor between B1 and B2 are shown in drawing EP7644CBDA. There are four Darlington transistors in parallel in each

power module. A 0.5-ohm resistor is in series with base 1 for each Darlington transistor in the power module, to assist in the sharing of the base current (EP7644MPHA). A blocking diode is in series with each base 2, which allows a reverse base 2 drive but isolates base 2 during a Darlington transistor fault. This is discussed further in Section 3.8.6. Each power module base drive circuit has its own isolated base drive power supply which operates from the 12-volt auxiliary power.

The total base drive current for a power module under actual square wave operation is shown in Figures 4.8-3, 4.8-4 and 4.8-5. These figures show one cycle of the base drive, the turn-on and turn-off, respectively. In this case, the total base drive current levels are about 4 amps forward and 4 amps reverse. The current level is somewhat dependent on individual Darlington transistor characteristics and the characteristics of the output transistors in the base drive circuit.

### 3.7.5 Power Darlington Transistor Snubber

The snubbing for the power Darlington transistors (Figure 3.7.5-1) is composed of two circuits: a resistor-capacitor snubber circuit in parallel with the power module and a parasitic, but intentionally placed, snubber inductance in series with the power module. The snubber circuit is effective during the turn-off of the Darlington transistors and the snubber inductance is effective during the turn-on of the Darlington transistors, as described below. The two snubbers actually operate on the parallel combination of the four power Darlington transistors, i.e. the power module. The four Darlington transistors are matched (see Section 3.8.6) so that each one is operated safely when the set is protected by the snubbers. The dc filter capacitor bank provides a low impedance path (much lower than the power cables and battery) for the high-frequency currents generated during switching.

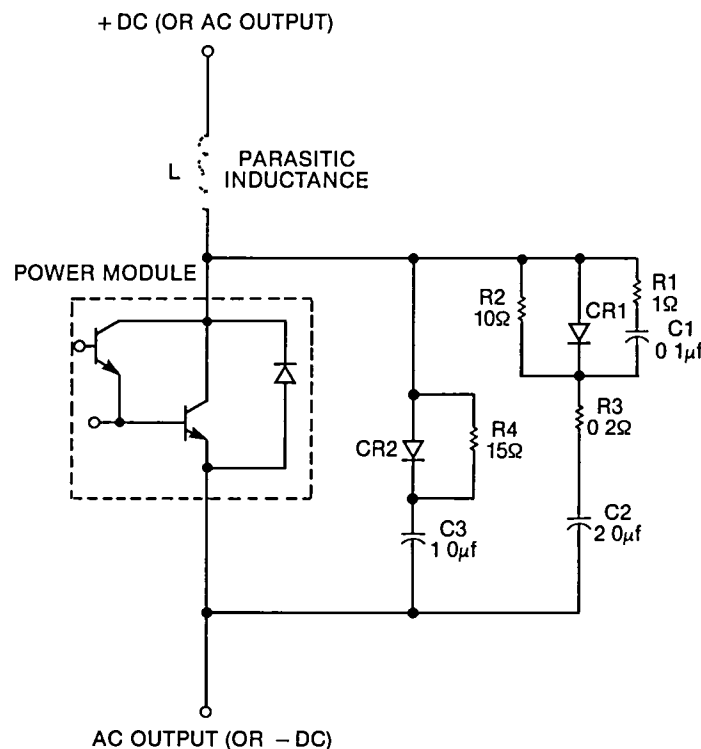
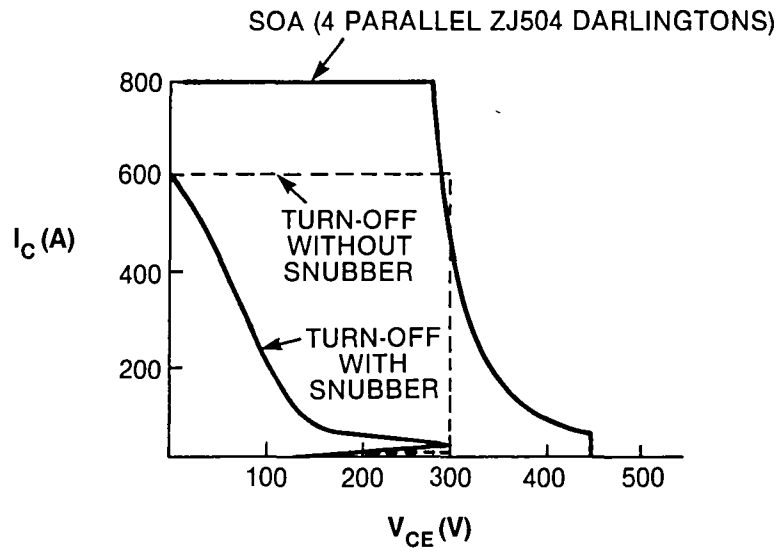


Figure 3.7.5-1 Power Darlington Transistor Snubber

The small parasitic inductances (approximately  $0.25 \mu\text{H}$ ) in series with the power modules (Figure 3.7.5-1) are obtained by the routing of the bus bars between the input capacitor bank and the half-phase modules, and between the upper and lower half-phase modules in each phase. These inductances are required during turn-on to limit the power module transistor current to a safe value. There are several currents which flow through the transistors during turn-on, with an inductive load: the load current, the snubber capacitor discharge current, the opposite snubber capacitor charging current and the recovery current of the opposite feedback diode. With an inductive load (such as a motor), the turn-on switching of the transistor transfers the load current from the opposite feedback diode in the same phase of the inverter to the on-coming transistor. The inductance limits the rate-of-change of current ( $di/dt$ ) during this transfer which prevents an excessively large recovery current in the opposite feedback diode. The inductance also interacts with the capacitance of the opposite snubber to limit the peak magnitude of its charging current. Lastly, the inductance reduces the transistor turn-on switching loss, because as soon as the transistor starts to conduct current the dc bus voltage appears across the inductances, allowing the voltage across the transistor to fall from the dc bus voltage to its low on-state voltage. This loss is, however, only moved from the transistor to the snubber, not eliminated completely.

The snubber circuit is required because transistors have safe-operating-area (SOA) limitations during turn-off to avoid catastrophic second breakdown failure. The SOA (Figure 3.7.5-2) is a locus of points of maximum permissible simultaneous occurrence of collector current and collector-emitter voltage. With an inductive load (such as a motor), the turn-off switching of the transistor transfers the load current from the transistor to the opposite on-coming feedback diode in the same phase of the inverter. Without a snubber, as the transistor turns off, the collector-emitter voltage rises from its low on-state voltage up to the dc bus voltage, while still conducting the load current. Then, the transistor current falls and the opposite diode can begin to conduct load current. This simultaneous locus of current and voltage must be within the transistor SOA (Figure 3.7.5-2). Unfortunately, the two snubber inductances in the inverter phase now generate an overshoot voltage above the dc bus voltage, which appears across the transistor during the transistor current fall time ( $V_{pk} = 2L di/dt$ ). This overshoot can be as high as 150 volts above the maximum 140 volt dc bus (Figure 3.7.5-2). The action of the snubber circuit is to alter this locus of current and voltage to a safe condition within the SOA (Figure 3.7.5-2) and provide margin for paralleling. With a snubber, as the transistor turns off and the collector-emitter voltage begins to rise, the snubber capacitance begins to charge. The charging current is current diverted from the transistor and eventually all the load current is in the snubber, charging the snubber capacitance to the dc bus voltage. At this point the on-coming opposite feedback diode can begin conduction and the current transfers from the snubber to the diode based on the interaction of the snubber inductances and the snubber capacitors. The choice of snubber capacitance limits the peak overshoot voltage.<sup>(24)</sup> Therefore, the snubber displaces the transistor current and voltage so they are within the SOA (Figure 3.7.5-2). The snubber circuit also reduces the transistor turn-off switching loss, because as the collector-emitter voltage rises the collector current is falling instead of remaining constant. The loss is, however, only moved from the transistor to the snubber, not eliminated completely.

The snubbers, as can be seen for the above discussion, depend a great deal on the parasitic inductances of the layout of the inverter power circuit and of the snubber circuit itself. The final snubber design and component values were selected after experimentation, using the actual inverter package layout. A two-stage snubber is used (Figure 3.7.5-1). The first stage is the C3 capacitor and the second is the R3-C2 resistor-capacitor. The stages are polar-



**Figure 3.7.5-2 Power Darlington Transistor Turn-off Safe-Operating-Area (SOA) and Switching Locus**

ized with a diode (CR1,CR2) so that large resistors (R2,R4) are in series with the capacitors to reduce the peak currents when they discharge during turn-on. The second stage diode is also snubbed (R1,C1). The turn-off waveforms under actual operation for the collector-emitter voltage and collector current of a power module are seen in Figures 4.8-1 and 4.8-2, respectively. The first-stage snubber is tightly coupled to the power module and, in the first few microseconds, controls the reapplied voltage. This initial control of the rate of reapplied voltage ( $dv/dt$ ) prevents the high gain Darlington transistors from turning on again. The second stage, less tightly coupled due to the component physical sizes, then comes into action to continue control of the reapplied  $dv/dt$  and peak voltage. The transient at 4 microseconds (Figure 4.8-1) is the CR2 diode recovery and the transient at 5 microseconds is the CR1 diode recovery. The CR1 diode is itself snubbed so that its snap off recovery does not turn on the high gain Darlington transistor.

### 3.7.6 Power Inverter Performance

The ac output current and voltage waveforms during actual operation are presented and discussed in Sections 4.6 and 4.7, respectively. Examples of waveforms during all modes of operation (PWM motoring, square wave motoring, PWM regenerative braking and square wave regenerative braking) are given. The separation of the sources of losses in the ac controller (control electronics and power inverter) is discussed in Section 4.10. The ac controller losses and efficiency, over the torque and speed range of the drive system, are mapped in Section 4.11.

### 3.8 TRANSISTOR POWER MODULES

#### 3.8.1 Available Transistors

The power transistors chosen for these modules were General Electric monolithic power Darlington transistors with 450 V, 200 A ratings. This choice was made on the basis of the successful usage of an earlier design chip in an electric vehicle drive with operation in a dc chopper (ETV-1) <sup>(8)</sup>. The ETV-1 program used the CRD-3 chip. This program used the ZJ504 chip with a breakdown of 450 volts versus the earlier 300 volts, a lower current density, and the second base was made available. There was also better current distribution due to a revised layout of the output stage transistors. These transistors could be paralleled to provide the necessary current for each phase of this inverter, after initial testing as individual partially packaged devices to allow for matching of transistor parameters, such as forward voltage drop and gain. The parallel General Electric Darlington transistors had significantly higher current handling capability and current gain than the only other suitable candidate transistors (from Power Tech), with faster switching speed and a potential for lower production cost. Actually, the Power Tech transistors could not be operated at their rated current at kilohertz frequencies because they were slow in turn off and, hence, dissipated excessive power in switching operation.

#### 3.8.2 Power Darlington Chip

The transistor (Figure 3.8.2-1) is a two-stage Darlington, monolithically integrated on a 1.27 cm × 1.91 cm (0.50 inch × 0.75 inch) chip available from the General Electric Semiconductor Products Department in Auburn, NY. This top view shows the driver transistor as the dark area along the center line of the chip, the base 1 input as the white square, the base 2 input as the white rectangle, and the six symmetrically located output transistor interdigitated emitter areas.

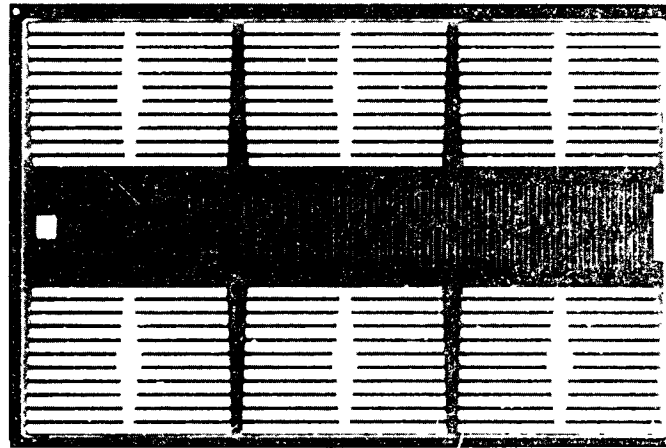
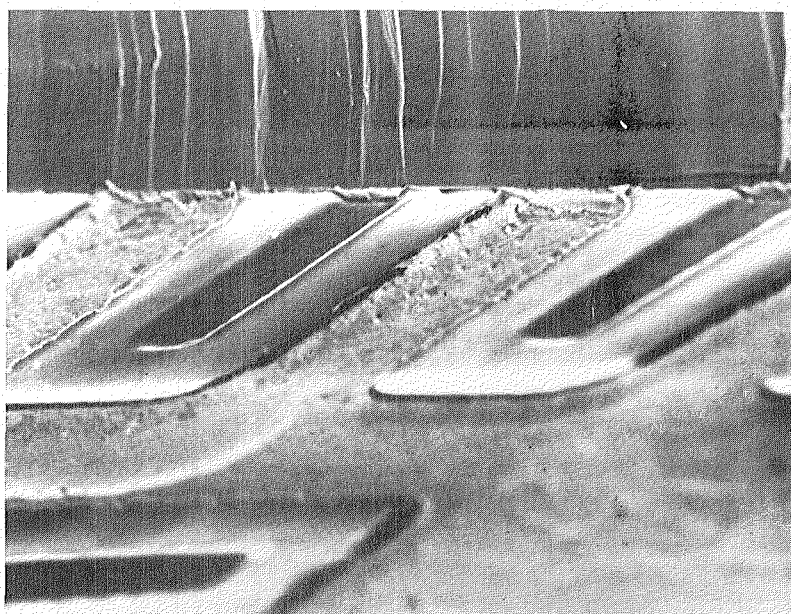


Figure 3.8.2-1 Top View of ZJ504 Darlington Transistor Chip

*Note: White areas are solder bumped emitter areas of the six output transistors. Smaller white square is base 1 input, larger white rectangle is base 2 input. Driver transistor is dark area along the center line of the chip.*

The base and emitter electrodes on the silicon surface have a highly interdigitated pattern, with the output emitter electrodes covered with a multilayer metal interconnection system culminating in Pb-Sn solder bumps built up over the aluminum contact metallization. An insulating film of a proprietary polyimide copolymer is applied and patterned like a photoresist to protect, passivate, and insulate the base metal from being shorted to the emitter metal. Thus, the polyimide copolymer film serves as a solder mask, defining areas of the chip which are to be solder bumped (the output emitter and two base contacts). It also serves as a dielectric layer protecting the interdigitated base fingers of the output transistors to permit the attachment of an electrode to the entire solder-bumped surface of the emitter. A low electrical and thermal conduction path is thereby provided to the output emitter side of the transistor, particularly important in ensuring that all six of the output transistors share current equally. The more common aluminum wire metallization would require careful attention to wire position and length to area consuming pads to provide that the parallel output transistors have the equal lead resistance important for high current sharing. Figure 3.8.2-2 shows a scanning electron micrograph of a section of the solder-bumped Darlington chip.

The back side of this Darlington transistor chip is made with a solderable metallization of Cr/Ni/Ag for the collector contact. The collector itself has a multiple epitaxial structure to give an optimized trade-off of forward drop, gain, reverse breakdown, and safe operating area of the transistor.



**Figure 3.8.2-2** Scanning Electron Micrograph of Darlington Chip

*Note: Aluminum emitter stripes and polyimide copolymer over the base metal stripes.*

### 3.8.3 Power Darlington Subscrete®

The Darlington transistor chips were fabricated in Subscrete form, providing a rugged, low-stress, high-thermal dissipation package, which allows for low duty cycle electrical testing for transistor matching. Figure 3.8.3-1 is a photo with two views of the Subscrete structure.

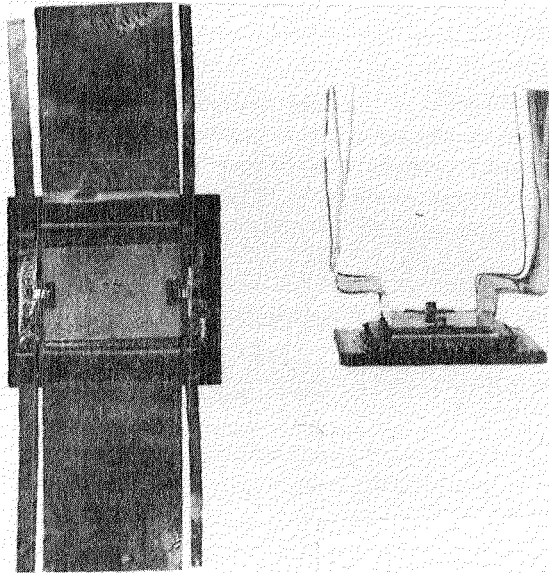


**Figure 3.8.3-1 Top and Side Views of the Darlington Transistor in Subscrete Form**

***Note: Outside narrow copper strips connect with soldered tabs to Base 1 and Base 2. Wide copper strip solders via a Mo plate to solder bumped emitter regions. Collector is soldered to structured copper on a copper plate.***

On the top side of the transistor chip, the soldered-bumped emitter area is bonded with an Indalloy 151 solder (92.5 Pb, 5 Sn, 2.5 Ag) to a 508-micron (20 mil) thick molybdenum sheet with cutouts for the two base contacts. Molybdenum closely matches the expansion coefficient of silicon. In turn, the molybdenum sheet is soldered to a 127-micron (5-mil) copper sheet to provide expanded emitter contacts. The copper sheet has side lanes which serve as base leads, connected by short copper tabs (Figure 3.8.3-1).

The collector side is soldered to a 1524-micron (60 mil) thick structured copper layer bonded on a 1600-micron (63 mil) copper base. This proprietary structured copper layer consists of a multitude of parallel 254-micron (10-mil) copper wires pressed together and bonded on one end to a 25.4-micron (1-mil) copper sheet and on the other end to the 1600-micron (63-mil) copper base. The packing density of the copper wire is about 90%, so the structured copper has this fraction of the electrical and thermal conduction of a solid piece of copper. Copper foil of any appreciable thickness cannot be soldered directly as a contact to large silicon areas because, with thermal cycling, the large thermal expansion mismatch of copper and silicon ( $17$  vs  $3 \times 10^6$  per K as expansion coefficients) would cause cracks either at the copper-silicon interface or in the silicon itself. Within the structured copper layer, the individual wires are free to move independently as the temperature changes. As a result, the mismatch stress is largely absorbed by small distortions in the wires and little stress is transmitted to the silicon.

® Registered trademark of the General Electric Company

With the usage of two proprietary techniques — structured copper, and chip polyimide copolymer passivation and isolation — and solder bumping on the chip with a molybdenum stress relief plate, the Subscrite package has the following desirable features

- Rugged structure
- Compact and low profile
- Excellent thermal dissipation
- All soldered joints
- Low stress structure to withstand thermal cycling
- Testable to full current ratings at low duty cycle for precise matching of gain

### 3.8.4 Thermal Resistance and Thermal Cycling

The thermal dissipation of the Subscrite is a critical consideration for high-power inverter operation, particularly because many transistors must be in parallel and near-equal currents are necessary to share the electrical and thermal loads within each module. The Subscrite is soldered to a copper heat spreader, which in turn is fastened by screws to a heat sink common to all of the Subscrites in a half-phase module. An analysis has been made of the heat flow under device operation from the transistor chip through the structured copper, copper plate, copper heat spreader, and into the heat sink. The results of this analysis are shown in Table 3.8.4-1, with the active output emitter area of the transistor chip taken as 1.4 cm<sup>2</sup> (0.22 in<sup>2</sup>) or about 60% of the total chip area, and the solder layer represented by Pb

**Table 3.8.4-1**  
**THERMAL RESISTANCE**  
**(Junction to Sink)**

Material	L Thickness cm	A Area cm <sup>2</sup>	$\sigma$ Conductivity watt/cm K	$R_{\theta} = L/A\sigma$ Resistance K/watt
Si	0.028	1.4	1.2	0.017
Pb	0.0025	1.4	0.34	0.005
Structured Cu	0.15	1.4	3.4	0.031
Cu	0.16	1.4	3.7	0.031
Pb	0.0025	1.6	0.34	0.004
Cu heat spreader	0.48	14.6	3.7	0.05-0.12
Thermal grease	0.0025-0.006	14.6	0.007	————— 0.14-0.20

A graph which relates the thermal resistance (junction to sink) to the area of the copper heat spreader is given as Figure 3.8 4-1. For this graph, the thickness of the thermal grease layer was taken as 0.0028 cm, or just over 1 mil. It is clear that increasing the heat spreader beyond the chosen area of 15 cm<sup>2</sup> does not yield any real reduction in the overall thermal resistance.

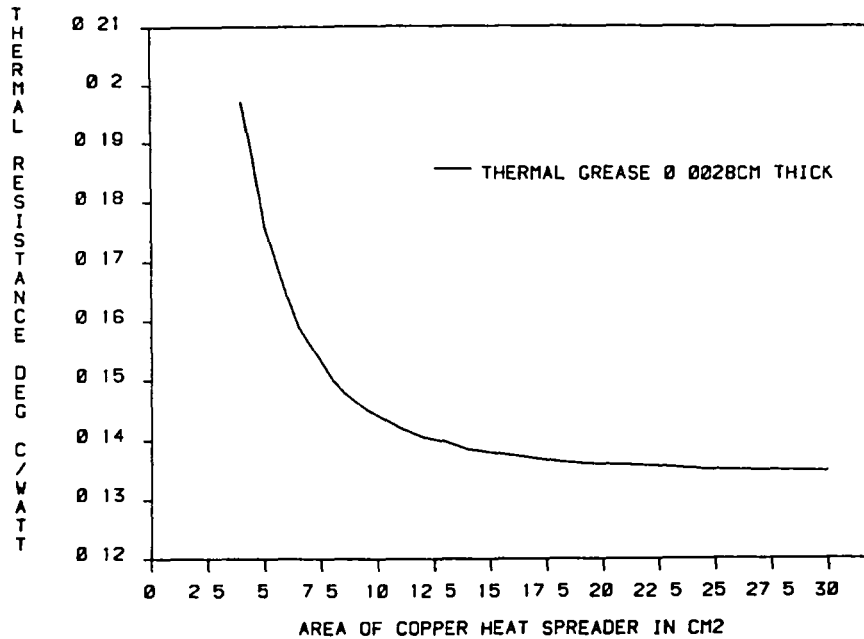
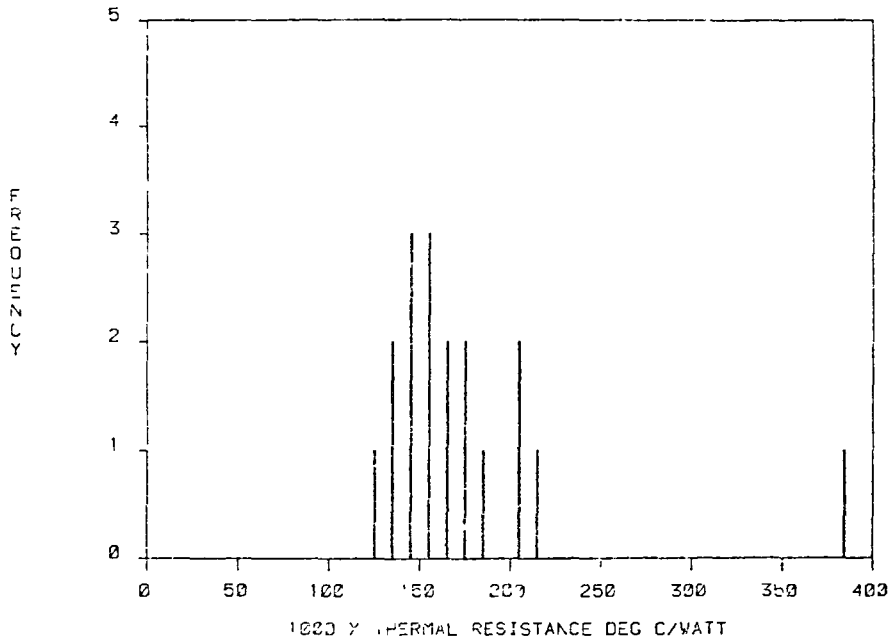


Figure 3.8.4-1 Thermal Resistance of Darlington Substrate

The major uncertainty is in the calculation of the loss through the heat spreader and thermal grease to the heat sink (assumed to remain at a fixed temperature). The analysis considered the direct thermal resistance due to heat conduction from the bottom of the active chip area through all the layers, in parallel with this, a spreading resistance, due to heat conduction, out radially in the heat spreader and then through the poorly conducting thermal grease (Wakefield Engineering, Inc Type 120 Thermal Joint Compound). The thickness of this grease layer is difficult to determine and to reproduce.

Thus, experimental measurements on a large number of Substrates soldered to heat spreaders and then attached to a heat sink show some spread in  $R_{\theta}$  values, as indicated in Figure 3.8.4-2. These data were derived from measuring the shift in emitter-base voltage (calibrated against temperature) after heat pulses of about ten seconds were applied by operation of the transistor. Presumably, the one very high  $R_{\theta}$  value represents a case of poor solder attachment with significant area voids or cracks to greatly increase the thermal resistance of the solder layers. Such a Substrate was rejected for usage.

The reliability of the mounted Substrate was checked by thermal cycling between 223 K (−50 °C) and 398 K (125 °C), a half hour at each temperature. Through 50 such cycles, no change was measurable in the thermal resistance, a far more sensitive indicator of device degradation than the electrical parameters, such as forward voltage drop, gain, or reverse breakdown.



**Figure 3.8.4-2 Experimental Measurements of Substrate Thermal Resistance**

**Note:** 18 Substrates mounted with thermal grease on a heat sink. Heat spreader area is 14.6 cm<sup>2</sup>. Calculated thermal resistance is 0.17 ± 0.03 K/watt.

### 3.8.5 Electrical Performance

The reverse breakdown of the ZJ504 Substrates chosen for module fabrication was at least 450 volts at 0.5 mA. A typical dc common emitter gain ( $h_{FE}$ ) dependence on collector current is plotted in Figure 3.8.5-1 for three different temperatures. Note the gain reduction at higher temperatures for higher collector currents. The transistors were matched using the collector-emitter voltage  $V_{CE}$  for a base current of 2 A and an emitter current of either 140 A or 160 A. The  $V_{CE}$  characteristic was read from a curve tracer display under low duty cycle with the transistor mounted on a hot plate held at 398 K (125 °C). This higher temperature rather than room temperature was used for matching because of the gain falloff with temperature and desire to match at the more critical junction temperature. Values of  $V_{CE}$  at 140 A in one batch of 20, for example, varied from 0.88 volt to 1.20 volts, but three groups of four transistors could be chosen to match within 0.04 volt. The reverse breakdown  $V_{CEO}$  (base open) for an emitter current of 0.5 mA varied from 450 to 700 volts.

CURRENT GAIN HFE OF DARLINGTON TRANSISTORS  
AT THREE TEMPERATURES, VCE=2 0V, PA18-20-2 TRANSISTOR

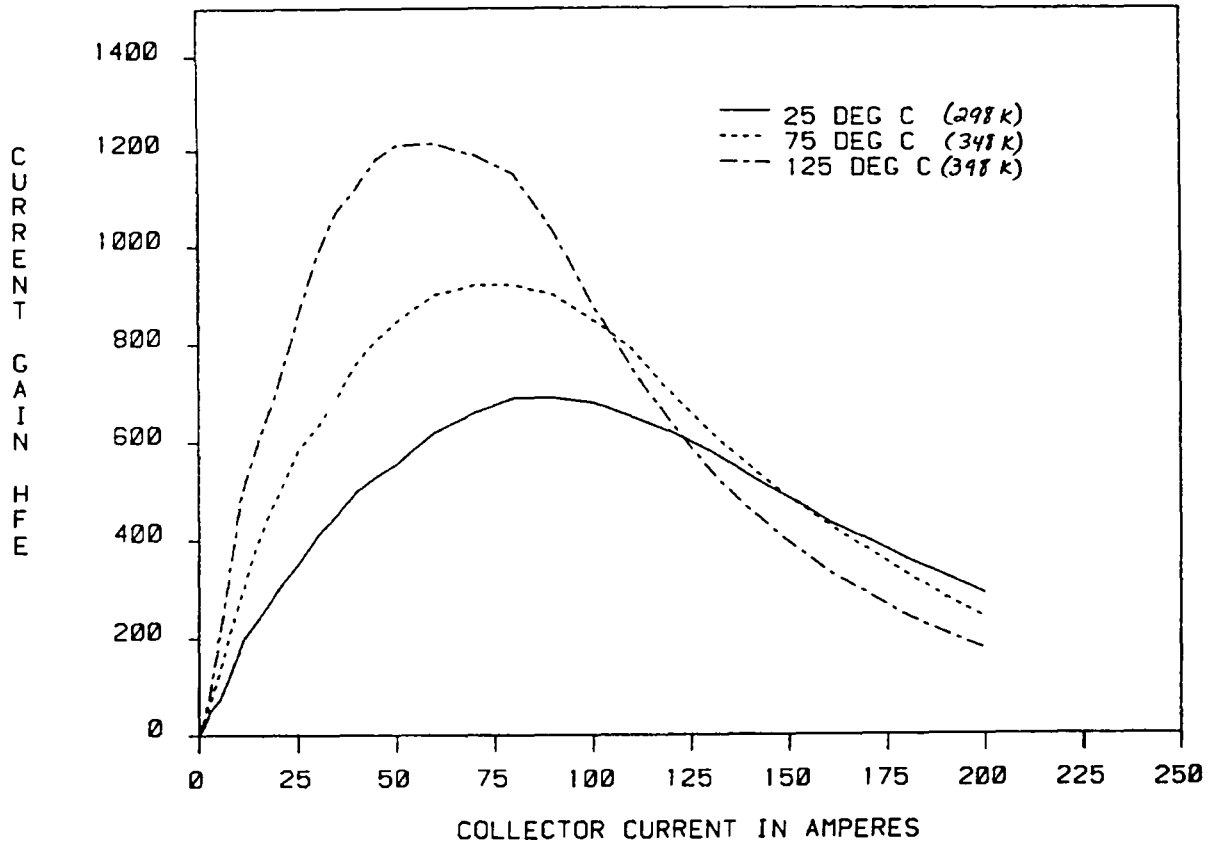


Figure 3.8.5-1 Gain Characteristic of ZJ504 Darlington Transistor

### 3.8.6 Power Module

The maximum current through one power module of the three-phase inverter circuit is 600 A. While individually mounted ZJ504 transistors could be operated at well over 200 A and three transistors could, in principle, supply 600 A, it was desirable to parallel four transistors to provide some safety margin for current sharing among the transistors. Furthermore, with four transistors there was better thermal dissipation to limit the junction temperature under the most demanding conditions of power delivery.

Four matched Subscreses soldered to copper heat spreaders of dimensions 3.175 cm × 4.763 cm (1.25-inch × 1.875-inch) were mounted on a common nickel-plated heat sink to form the transistor portion of a power module. The individual Subscreses were bolted down to the heat sink with thermal grease under each Subscrete to improve the heat flow. Figure 3.8.6-1 is a photo of the power module, with the Darlington chip and Subscrete in the foreground, while Figure 3.8.6-2 shows the open power module. In addition to the four Darlington transistor Subscreses, the module also has two diodes in parallel in an anti-parallel configuration to the four parallel transistors. These diodes are fast recovery diodes which allow a path for reactive and regenerative currents, while preventing reverse current and voltage of the transistors and the resulting inverted mode operation. The diodes used in these power modules were International Rectifier type 251 UL diodes with 0.2 microsecond turn-off, obtained in chip form with a molybdenum backing plate. These diodes were mounted on

the same size heat spreader as the transistors and were similarly screwed down to the heat sink plate with thermal grease between the spreader and sink. The pair of diodes for individual power modules were matched for forward voltage drop at 200 A at room temperatures;  $V_F$  varied from 1.02 to 1.12 volts in a large batch, and could be selected to match to 0.02 volt forward drop.

A further area inside the power module was taken for an A-114D blocking diode in each Base 2 lead to the Darlington transistor and for a 0.5 ohm non-inductive resistor in each Base 1 lead (EP7644 MPHA). The purpose of the blocking diodes was to isolate the transistors because it was found that a catastrophic breakdown in one of the transistors allowed high voltage to be applied across the Base 2 leads of the remaining three transistors. The Base 1 series resistors provided some measure of base drive equality for the four transistors in the power module, and limited the base drive to 2 A for any one transistor.

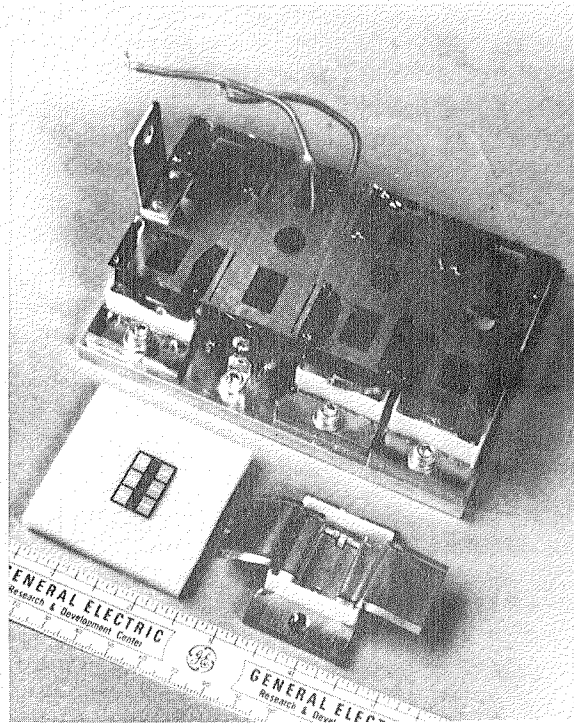


**Figure 3.8.6-1 Power Module with Darlington Chip and Subcrate in the Foreground**

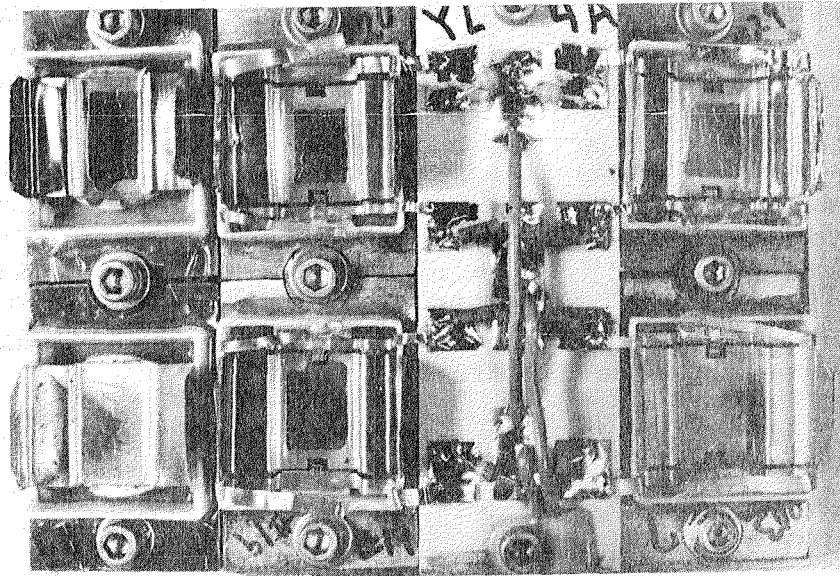


**Figure 3.8.6-2 Open Power Module**

*Note: Top view of an assembled power module with four Darlingtons Subscrites and two fast recovery diode Subscrites (left side), all on copper heat spreaders and mounted down to a common 9.75 cm × 13.03 cm (3.84 inch × 5.13 inch) copper heat sink. Base 1 leads have 0.5 ohm resistors, Base 2 leads have blocking diodes in the third section above.*

### 3.8.7 Half-Phase Module Testing

In order to test the capabilities of the completed half-phase modules (including power module, base drive, and snubber) separately, before combining six such modules to form a three-phase inverter, the circuit configuration shown in Figure 3.8.7-1 was used. A schematic diagram for each half-phase module is shown in EP7644 MPHA.

A typical turn-off switching event is shown in Figure 3.8.7-2. Here the emitter (or load) current was set to 120 A. About four microseconds after the base drive voltages were reversed, the load current started to fall off, with a drop to zero in about three microseconds. The actual shape and duration of the current fall-off was a function of the snubber circuitry and temperature as well as the transistor construction itself. The voltage overshoot in this particular circuit was up to 180 volts, whereas the power supply was about 90 volts; the overshoot, an  $L di/dt$  effect, is strongly affected by the circuit layout and the snubber circuitry and must be limited to avoid transistor second breakdown and destruction. Half-phase modules were tested to 600 A with a 100 volt power supply; a fair percentage of initial power modules were destroyed until problems, such as poor transistor collector contacts, diode breakdown, and snubber component selection, were solved. Once such problems were isolated, identified, and solved, the yield of tested and acceptable transistor chips into final matched Subscrites in power modules was very good and reproducible.

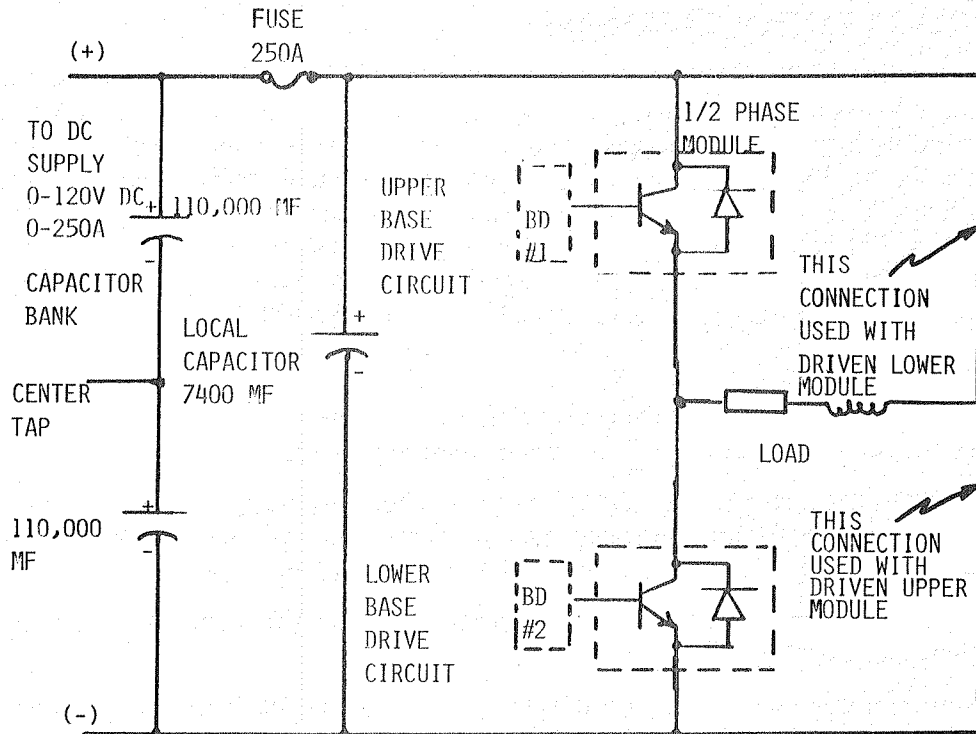


**Figure 3.8.7-1 Test Circuit for Half-Phase Module**

*Note: Circuit configuration for testing completed half-phase module in a switching mode. Base drive circuit per drawing EP7644CBDA; Half-phase module circuit per drawing EP7644MPHA; Opposite module transistor held in turned off condition; Opposite diode used as flyback diode.*

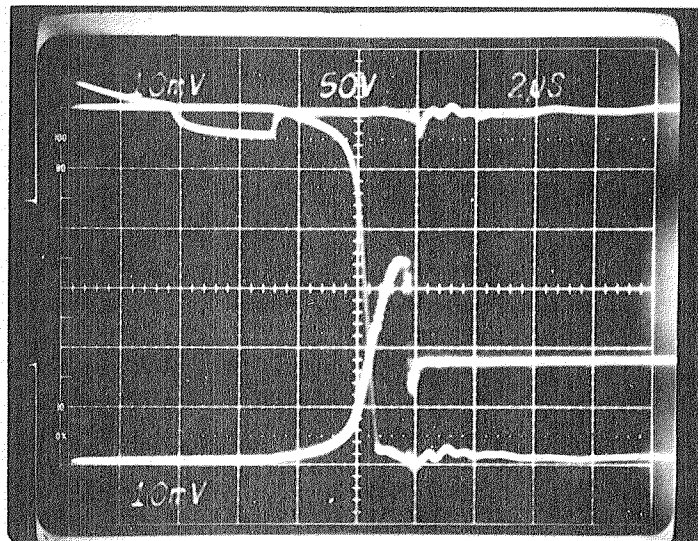


**Figure 3.8.7-2 Typical Turn-Off Waveforms for a Power Module**

*Note: Operation of power module at turn-off of the quad of transistors.  $I_E = I_{LOAD} = 120 A$  (20 A/div),  $V_{CE(peak)} = 180 V$  (50V/div). Base voltage reversal is 4 microseconds from left (time 2 microseconds/div).*

### 3.9 CONTROLLER FAMILY EXPANSION

A specific objective of the contract was to develop preliminary designs and design guidelines to expand the existing 20 hp 108-volt controller to cover a wide range of motor horsepower ratings and battery system voltages. The motor horsepower range specified is for vehicles requiring a 10, 20, 30, 40, or 50 hp motor. The battery system voltage range for each of the motors is from  $96 \pm 12$  volts to  $270 \pm 30$  volts. Specific nominal battery system voltage values of 84 volts, 108 volts, 150 volts, and 300 volts have been chosen for evaluation. The larger motors are intended to be applicable to heavier passenger vehicles, delivery vans, and trucks for urban service in accordance with the J227a – Schedule D driving cycle.

#### 3.9.1 Assumptions

In order to make such a series of designs, numerous assumptions are necessary to define the framework for the system designs. The major assumptions are outlined below.

- 1) All system designs are based on the existing laboratory design 20 hp, 108-volt battery system. No attempt has been made to cost-reduce this basic design as would be desirable before committing to a prototype production design.
- 2) All system designs are based on power and/or voltage ratios from the existing design, i.e., a scaling approach is used.
- 3) No attempt was made to ensure that the vehicles using different drive motors would meet any specific duty or driving cycle.
- 4) The “Tractive Effort vs Speed” curve for all drives maintained the same speeds for transition of operating modes of the inverter.
- 5) All system partitioning is based on state-of-the-art technology, although some product design work may be necessary to achieve requested component ratings.

Examination of the controller for the range of motor horsepower and battery system voltage levels reveals that the system can be divided into two major portions: the power circuit, and the sensing and control circuits. The power circuit components will vary for each and every power and voltage level. In contrast, the control circuit will remain fixed and one set of circuit components can be used for any system. The controller family designs reflect this division of the system.

#### 3.9.2 Input Capacitor Scaling

##### 3.9.2.1 Summary

Because the input capacitor bank is a large part of the controller in volume and cost, it is always called upon to do more than the technology allows. As of this study, the availability of high-voltage capacitors required for application in the 300-volt system does not exist. An extrapolation of those capacitors used in the low-voltage systems will be made.

Table 3.9.2.1-1 gives the required ratings of the capacitor bank. The total capacitance, voltage rating, and total ripple current required are scaled from the base values. Table 3.9.2.1-2 lists hand chosen values of capacitance which satisfy or exceed the minimum capacitance and ripple current ratings required for the system. The values do not represent commercially available values, but are interpolations based on commercially available capacitors offered, from stock, by Cornell-Dubilier Electric Corporation.<sup>(13)</sup> Also listed is the interpolated capacitor volume. Because the capacitor technology is changing and custom packaging has not been considered, the volume estimates of Table 3.9.2.1-2 can vary 10-20%.

**Table 3.9.2.1-1  
REQUIRED CAPACITOR RATINGS**

BAT. V		10 HF	20 HF	30 HF	40 HF	50 HF
84V	C= (UF)	34692	73355.9	110094	146792	182170
	I RIFFLE	88.6371	177.274	265.911	354.549	443.186
	V RATING	155.556	155.556	155.556	155.556	155.556
108V	C= (UF)	22200	44400	66600	88200	111000
	I RIFFLE	66.64	137.28	206.82	275.76	344.7
	V RATING	200	200	200	200	200
150V	C= (UF)	11508.5	23017	34525.4	46033.9	57542.4
	I RIFFLE	49.6368	99.2736	148.91	198.547	248.184
	V RATING	277.778	277.778	277.778	277.778	277.778
300V	C= (UF)	2877.12	5754.24	8631.36	11508.5	14385.6
	I RIFFLE	24.8184	49.6368	74.4552	99.2736	124.092
	V RATING	555.556	555.556	555.556	555.556	555.556

**Table 3.9.2.1-2  
CAPACITOR SELECTIONS**

Bat V		10 HP	20HP	30HP	40HP	50HP
84V	C = (UF)	36 7E3	73 4E3	113E3	160E3	210E3
	I RIPPLE	106	186	266	354	443
	V RATED	156	156	156	156	156
	VOL (IN)	182	352	530	737	953
108V	C = (UF)	22 2E3	45 0E3	74 2E3	105E3	138E3
	I RIPPLE	76 8	139	207	276	345
	V RATED	200	200	200	200	200
	VOL (IN)	175	338	537	741	955
150V	C = (UF)	11.5E3	24 9E3	40 9E3	58 2E3	76 4E3
	I RIPPLE	52 5	99 2	149	198	248
	V RATED	278	278	278	278	278
	VOL (IN)	125	251	392	538	688
300V	C = (UF)	2 9E3	5 8E3	8 6E3	11 6E3	14 4E3
	I RIPPLE	25 1	49 6	74.5	99 4	124.2
	V RATED	556	556	556	556	556
	VOL (IN)	125	222	308	394	472

The base values for the 20 hp, 108 volt system are

$$C = 44400 \mu\text{F}$$

$$V = 200 \text{ V}$$

$$I = 138 \text{ A (RMS Ripple)}$$

### 3.9.2.2 Assumptions

- 1 There is no change in frequency or ripple current wave shape characteristic to effect capacitance rating
- 2 The input capacitor supplies amounts of energy which are proportional to the system energy for any horsepower rating

### 3.9.2.3 Calculations

For constant supply voltage and varying horsepower, the energy stored by the capacitor bank varies proportionally. Since voltage remains fixed, the capacitance varies proportionally. Thus,

$$C = (\text{HP}/\text{HP}_b) C_b$$

$$I = (\text{HP}/\text{HP}_b) I_b \text{ (Ripple current)}$$

Where,

$$C = \text{desired capacitance value}$$

$$C_b = \text{base value of capacitance for 20 hp, 108 V system (44400 } \mu\text{F)}$$

$$\text{HP} = \text{desired horsepower rating}$$

$$\text{HP}_b = \text{base value of horsepower (20 hp)}$$

$$I = \text{desired ripple current rating}$$

$$I_b = \text{base value of ripple current (138 A, RMS)}$$

Maintaining horsepower constant and varying supply voltage will vary the capacitance value as the inverse square. Ripple current will vary as the inverse. Thus,

$$C = (E_b/E)^2 C_b$$

$$V = (E/E_b) V_b$$

$$I = (E_b/E) I_b \text{ (RMS ripple)}$$

Where,  $E$  = desired supply voltage

$$E_b = \text{base value of supply (108 v)}$$

$$V = \text{desired capacitor module voltage rating}$$

$$V_b = \text{base value of voltage rating (200 V)}$$

The interpolated capacitor bank volume for the 156-volt rated capacitor is calculated by:<sup>(13)</sup>

$$\text{Vol} = (0.00782 C^{0.948}) \times 6$$

Where,

$C$  = one-sixth the selected capacitance value

The 200 volt rated capacitor volume is calculated by <sup>(13)</sup>

$$\text{Vol} = (0.01444 C^{0.927}) \times 6$$

The 278 volt rated capacitor volume is calculated by <sup>(13)</sup>

$$\text{Vol} = (0.0234 C^{0.899}) \times 6$$

The 556-volt rated capacitor volume is calculated by <sup>(13)</sup>

$$\text{Vol} = (0.1237 C^{0.8293}) \times 6$$

### 3.9.3 Motor Parameter Scaling

#### 3.9.3.1 Summary

The conventional model for an induction motor is shown in Figure 3.4.6-1b. The 20-horsepower design values for a 108-volt battery are

$$R_S = R_1 = 0.00298 \text{ ohms}$$

$$R_R = R_2 = 0.00145 \text{ ohms}$$

$$L = L_1 = 0.01269 \text{ mH}$$

$$L_R = L_2 = 0.01015 \text{ mH}$$

$$L_M = L_3 = 0.24 \text{ mH}$$

The motor parameters are scaled to higher and lower horsepower and power source voltage values to complete a matrix table. The resistances and inductances scale inversely proportional to horsepower rating. The inductances scale proportional to power supply voltage and resistances scale by the square of the voltage ratio. The resulting values are shown in Table 3.9.3.1-1.

#### 3.9.3.2 Assumptions

- 1 The wire gauge was assumed to be of non-standard size, if necessary
- 2 Corona effects on stator winding conductors was assumed not to change
- 3 No interwinding capacitance was assumed
- 4 No other second order effects were considered

#### 3.9.3.3 Calculations

The equations for computing the values of Table 3.9.3.1-1 are derived in two steps. Parameters are scaled with a constant power supply voltage and variable horsepower, then with variable power supply voltage and constant horsepower. For either procedure, the volts per turn and current density within the stator winding conductors remains constant.

When the horsepower is varied and supply voltage remains constant, the volts per turn remain constant, however, windings must be paralleled to maintain the current density per conductor and provide the needed flux. Thus,

**Table 3.9.3.1-1**  
**SCALED MOTOR PARAMETERS**

BAT. V		10 HP	20 HP	30 HP	40 HP	50 HP
84V	R1=	3.60543E-03	1.80277E-03	1.20181E-03	9.01358E-04	7.21086E
	R2=	1.75432E-03	8.77160E-04	5.84774E-04	4.38580E-04	3.50864E-04
	L1=	1.97400E-05	9.87000E-06	6.58000E-06	4.93500E-06	3.94800E-06
	L2=	1.57889E-05	7.89444E-06	5.26296E-06	3.94722E-06	3.15778E-06
	L3=	3.73333E-04	1.86667E-04	1.24444E-04	9.33333E-05	7.46667E-05
108V	R1=	5.96000E-03	2.98000E-03	1.98667E-03	1.49000E-03	1.19700E-03
	R2=	2.90000E-03	1.45000E-03	9.66667E-04	7.25000E-04	5.80000E-04
	L1=	2.53800E-05	1.26900E-05	8.46000E-06	6.34500E-06	5.07000E-06
	L2=	2.03000E-05	1.01500E-05	6.76667E-06	5.07500E-06	4.06000E-06
	L3=	4.80000E-04	2.40000E-04	1.60000E-04	1.20000E-04	9.60000E-05
150V	R1=	.0114969	5.74846E-03	3.83230E-03	2.87423E-03	2.29938E-03
	R2=	5.59414E-03	2.79707E-03	1.86471E-03	1.39853E-03	1.11033E-03
	L1=	3.52500E-05	1.76250E-05	1.17500E-05	8.81250E-06	7.05000E-06
	L2=	2.81944E-05	1.40972E-05	9.39815E-06	7.04861E-06	5.63889E-06
	L3=	6.66667E-04	3.33333E-04	2.22222E-04	1.66667E-04	1.33333E-04
300V	R1=	.0459877	.0229938	.0153292	.0114969	9.19753E-03
	R2=	.0223765	.0111883	7.45835E-03	5.59414E-03	4.47531E-03
	L1=	7.05000E-05	3.52500E-05	2.35000E-05	1.76250E-05	1.41000E-05
	L2=	5.63889E-05	2.81944E-05	1.67963E-05	1.40972E-05	1.12778E-05
	L3=	1.33333E-03	6.66667E-04	4.44444E-04	3.33333E-04	2.66667E-04

$$L = (HP_b/HP) L_b$$

$$R = (HP_b/HP) R_b$$

Where,

HP = Desired horsepower rating

HP<sub>b</sub> = Base value of horsepower (20 hp)

L<sub>b</sub> = Base value of inductance (for 20 hp)

R<sub>b</sub> = Base value of resistance (for 20 hp)

When the supply voltage varies and horsepower is constant, the number of turns must vary for constant volts per turn and the stator conductor's cross-sectional area varies for constant current density. Thus,

$$L = (E/E_b) L_b$$

$$R = (E/E_b) (E/E_b) R_b$$

Where,

E = desired power supply voltage rating

E<sub>b</sub> = base value of source voltage (108 V)

The combined equations that are used to scale each resistance and inductance of the model for the 20 hp, 108 V system are

$$L = (HP_b/HP) (E/E_b) L_b$$

$$R = (HP_b/HP) (E/E_b)^2 R_b$$

### 3.9.4 Power Module Scaling

#### 3.9.4.1 Summary

The parameters for the present 20 hp, 108 V propulsion system power module are given in Table 3 4 7-2. The parameters of interest are:

Peak Module Current	650 A
Peak Switch-off Voltage	300 V
Gain (at $I_C = 600$ A)	300

The parameters for module specification are peak current ( $I_C$ ), peak voltage (at switch-off,  $V_C$ ), gain (expressed as values of base current,  $I_B$  and collector current,  $I_C$ ). Also silicon chip area values are derived from data of an existing equivalent bipolar transistor and are supplied only for reference purposes

The parameter values are calculated for 10, 20, 30, 40, and 50 horsepower drives with power supply voltages of 84, 108, 150 and 300 volts. The currents and silicon area scale directly with horsepower rating while the voltage and gain remains constant. For variations of supply voltage the current ratings scale inversely while voltage ratings scale directly to the variation. The area, however, scales at a constant amps per volt, which is dependent on the device process. The resulting power module parameters are listed in Table 3 9 4 1-1

**Table 3.9.4.1-1**  
**SCALED POWER MODULE PARAMETER**

VAT. V		10 HF	20 HF	30 HF	40 HF	50 HF
84V	IC=	417.857	835.714	1253.57	1671.43	2089.29
	VC=	233.333	233.333	233.333	233.333	233.333
	IB=	1.28571	2.57143	3.85714	5.14286	6.42857
	@ IC=	385.714	771.429	1157.14	1542.86	1928.57
	AREA=	.41026	.82052	1.23079	1.64104	2.0513
108V	IC=	325	650	975	1300	1625
	VC=	300	300	300	300	300
	IB=	1	2	3	4	5
	@ IC=	300	600	900	1200	1500
	AREA=	.39	.78	1.17	1.56	1.95
150V	IC=	234	468	702	936	1170
	VC=	416.667	416.667	416.667	416.667	416.667
	IB=	.72	1.44	2.16	2.88	3.6
	@ IC=	216	432	648	864	1080
	AREA=	.459491	.918982	1.37847	1.83796	2.29745
300V	IC=	117	234	351	468	585
	VC=	833.333	833.333	833.333	833.333	833.333
	IB=	.36	.72	1.08	1.44	1.8
	@ IC=	108	216	324	432	540
	AREA=	.415658	.831316	1.24697	1.66263	2.07829

### 3.9.4.2 Assumptions

- 1 Changes in peak switch-off voltage are due solely to variations of power supply voltage rating. No effect from changes of inductance of interconnect leads is assumed.
- 2 Silicon area calculations use two bipolar transistor types, one under development, the other commercially available, as bases for calculation.
- 3 The switching speed of the module remains constant for any rating.
- 4 Thermal specifications remain the same.
- 5 The characteristic shape of the tractive effort versus speed curves remains the same and the corner speed does not change.

### 3.9.4.3 Calculations

The equations for computing the values of Table 3.9.4.1-1 were derived in two steps. Parameters were scaled with constant supply voltage and variable horsepower then with variable supply and constant horsepower. For either procedure the parameter values are dependent on the system variation, not the device.

For constant supply voltage and variable horsepower, the current for the system and hence, for the module scales proportionally. Thus,

$$I_C = (HP/HP_b) I_{Cb}$$

$$I_B = (HP/HP_b) I_{Bb}$$

Where,

$$I_C = \text{Module current at desired horsepower}$$

$$I_B = \text{Gate current (transistor base current) at the desired horsepower}$$

$$I_{Cb} = \text{Base value of module current (650 A)}$$

$$I_{Bb} = \text{Base value of gate current (2 A, } I_C = 600 \text{ A)}$$

For constant horsepower and variable supply voltage the current for the system varies inversely as the supply voltage. Thus,

$$I_C = (E_b/E) I_{Cb}$$

$$I_B = (E_b/E) I_{Bb}$$

$$V_C = (E/E_b) V_{Cb}$$

Where,

$$E = \text{desired supply voltage rating}$$

$$E_b = \text{base value of supply (108 V)}$$

$$V_C = \text{desired peak switch-off voltage}$$

$$V_{Cb} = \text{base value of switch-off voltage (300 V)}$$

The silicon AREA contained in the module is a direct measure of the cost. For constant supply voltage the silicon area increases proportionally as the horsepower to maintain a constant current density. This is conceptually equal to paralleling the internal transistor chips. Thus,

$$\text{AREA} = (\text{HP}/\text{HP}_b) \text{ AREA}_b$$

Where,

AREA = desired silicon area of power module (equivalent)

AREA<sub>b</sub> = base value of AREA As an example for this study AREA<sub>b</sub>  
 (< 600 V) = 0.4" × 0.6", AREA<sub>b</sub> (> 600 V) = 0.5" × 0.7"

Computing silicon area with constant horsepower, but varying supply voltage is complex and depends on the module process and fabrication. Through consultation with the Discrete Semiconductor Device Center, Semiconductor Products Department, General Electric Company, voltage versus current ratings for the commercially available D67DV bipolar single transistor chip and another developmental chip device were obtained. This information is shown in Figure 3.9.4.3-1. The amps per volt ratio of the D67DV is 0.666 amps per volt and the developmental Darlington transistor chip is 0.278 amps per volt.

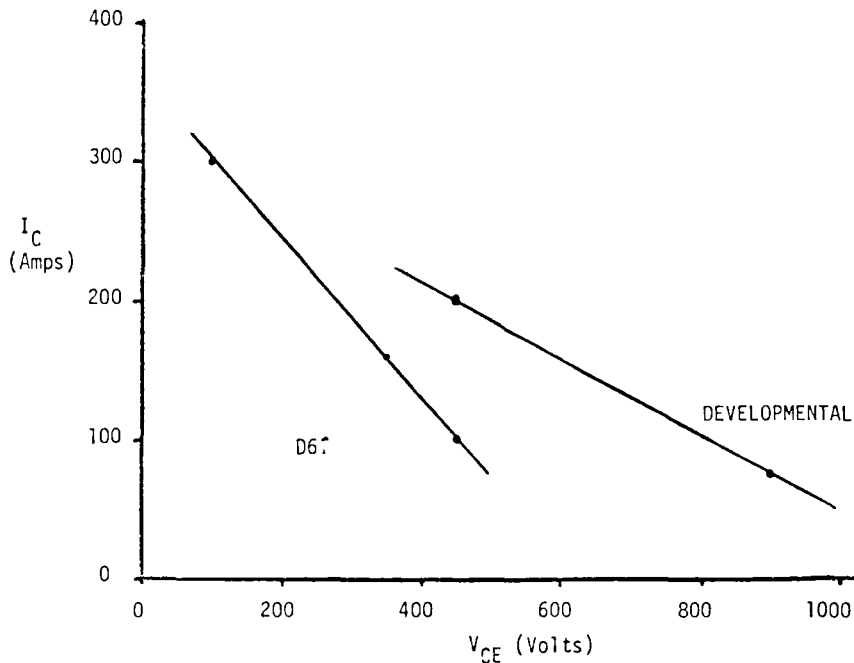


Figure 3.9.4.3-1 GE Devices Area

With constant horsepower rating of the system, as the supply voltage is varied the amount of current required to be controlled is inversely proportional. This conceptually would vary the silicon area of the device by paralleling more or fewer chips. However, by varying the voltage value applied to the paralleled chips, each chip's current capability is varied by the I<sub>C</sub> versus V<sub>CE</sub> characteristic. Thus, the required silicon area may be doubled because of increased current demand, but the overall area must be decreased slightly because the chips' rated current density will increase with decreased voltage rating. For constant horsepower and varying supply voltage

$$\text{AREA} = \left( \frac{(E/E_b)^{-1} I_{Cb}}{M(E/E_b) V_{Cb} + I_1} \right) \text{ AREA}_b$$

Where,

$M$  = amps per volt ratio of the current vs voltage rating characteristics for the chip device being considered

$I_1$  = The artificial current value of the characteristic rating curve for a supposed zero voltage applied (vertical axis intercept of the curve)

The fundamental derivation of the current versus voltage ratings curve maintains a constant device gain when operated within the ratings

The final area equation for varying horsepower rating and voltage is:

$$\text{AREA} = (\text{HP}/\text{HP}_b) \left( \frac{(E/E_b)^{-1} I_{Cb}}{M(E/E_b) V_{Cb} + I_1} \right) \text{AREA}_b$$

### 3.9.5 Power Module Snubber Scaling

#### 3.9.5.1 Summary

The actual values for the resistive and capacitive components, scaled for different horsepowers and supply voltages, are not presented due to the complexity of the circuit and dependence on waveshape characteristics. However, the equations for calculating the Thevenin equivalent resistance and capacitance are given

#### 3.9.5.2 Assumptions

- 1 The amount of overshoot voltage seen across the power module is directly proportional to the supply voltage and is unaffected by current, to a first order approximation
- 2 Interconnect inductances remain constant
- 3 The characteristic waveshape of the energy which the snubber is absorbing changes only in magnitude, not time (The time interval of snubber operation remains constant.)
- 4 The possible resonance of the motor winding inductance and capacitance is a second order effect not needing consideration.

#### 3.9.5.3 Calculations

The equations for scaling the snubber are derived from the conceptual realization of Thevenin resistances and capacitances. The circuit in Figure 3.9.5.3-1 shows the contributing components

For constant supply voltage and variable horsepower, the overshoot voltage must be maintained constant by the snubber. This ensures the power module voltage rating remains constant. At the first instant of time of snubber operation, the overshoot voltage is applied directly across the equivalent snubber resistance and its magnitude is determined by the current and this resistance. Thus, the peak voltage is:

$$V = I R_s$$

Where,

$V$  = Peak overshoot voltage

$I$  = Peak motor current occurring with  $V_p$

$R_s$  = Equivalent snubber resistance

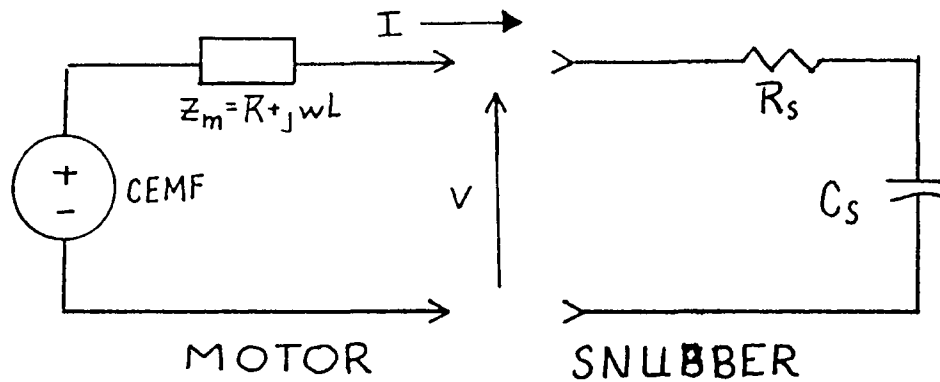


Figure 3.9.5.3-1 Snubber Equivalent Circuit

Since the peak voltage must remain constant and the current varies directly as horsepower, the resistance varies inversely with horsepower. Thus,

$$I = (HP/HP_b) I_b$$

$$V = (HP/HP_b) I_b (HP_b/HP) R_{sb}$$

$$R_s = (HP_b/HP) R_{sb}$$

Where,

HP = Desired horsepower rating

HP<sub>b</sub> = Base value of horsepower

R<sub>sb</sub> = Equivalent Thevenin resistance at 20 hp rating

Because it is assumed that the response time of the snubber network and characteristic waveshape remains constant for any horsepower rating, the equivalent snubber capacitor scales directly with horsepower. Thus,

$$t = R_s C_s = (HP_b/HP) R_{sb} C_s$$

$$C_s = (HP/HP_b) C_{sb}$$

Where,

t = Response time

C<sub>s</sub> = Equivalent Thevenin capacitance desired

C<sub>sb</sub> = Base value of equivalent capacitance at 20 hp rating

The power of the snubber scales proportionally with horsepower because the peak overshoot voltage remains constant, the characteristic waveshape remains constant and the current scales directly with horsepower. Thus,

$$P = I V = (HP/HP_b) I_b V$$

$$P = (HP/HP_b) P_b$$

Where,

P = Snubber dissipation at desired rating

P<sub>b</sub> = Base value of power dissipation at the 20 hp rating

For constant horsepower and varying supply voltage, the overshoot voltage varies directly as supply voltage and the current varies inversely. This can be seen, again, by the Thevenin approach. The current from the motor (and power switches) varies inversely as the supply voltage to maintain constant system ( $P = P_b$ ). Thus,

$$I = (E_b/E) I_b$$

Where,

$$E = \text{desired supply voltage}$$

$$E_b = \text{base value of supply voltage (108 V)}$$

Because the overshoot energy is due primarily to motor inductance as a generating source, the overshoot voltage varies directly as supply voltage. Thus,

$$V = L (dI/dt)$$

$$L = (E/E_b)^2 L d[(E_b/E) I]/dt$$

$$V = (E/E_b) V_b$$

Where,

$$L = \text{motor inductance}$$

$$t = \text{constant time interval}$$

Using the above information and basing the calculations on the same assumptions and time periods as our previous calculations, the equivalent snubber resistance can be computed as

$$V = I R_s$$

$$(E/E_b) V_b = (E_b/E) I_b R_s$$

$$V_b = I_b (E_b/E)^2 R_s$$

Therefore,

$$R_s = (E/E_b)^2 R_{sb}$$

As assumed before, the time response of the network remains constant. The equivalent capacitance is

$$t = R_s C_s$$

$$C_s = (E_b/E)^2 C_{sb}$$

In summary, the equations which express power consumption and the variation of the equivalent Thevenin resistances and capacitances of the snubber network are

$$R_s = (HP_b/HP) (E/E_b)^2 R_{sb}$$

$$C_s = (HP/HP_b) (E_b/E)^2 C_{sb}$$

$$P = (HP/HP_b) P_b$$

### 3.9.6 Base Drive Scaling

#### 3.9.6.1 Summary

The approach taken is to determine the characteristics of the present circuit (reference drawing EP7644CBDA in Appendix D) and scale them accordingly. For reasons of simplicity,

it would be highly desirable to maintain a common circuit and adjust components and cooling to cover the range. This is done and recommendations for the two main drive transistors are summarized in Table 3.9.6.1-1. The other base drive circuit components remain basically the same.

**Table 3.9.6.1-1  
BASE DRIVE TRANSISTORS**

Nominal Battery Voltage	Transistor	Motor Horsepower				
		10	20	30	40	50
84	Q4	2N5991	2N6338	2N6338	MJ10020	MJ10020
	Q7	D45H11	D45H11	2N6285	2N6285	2N6285
108	Q4	2N5991	2N5991	2N6338	2N6338	MJ10020
	Q7	D45H11	D45H11	D45H11	2N6285	2N6285
150	Q4	D42C5	2N5991	2N5991	2N6338	2N6338
	Q7	D43C5	D45H11	D45H11	2N6285	2N6285
300	Q4	D42C5	D42C5	2N5991	2N5991	2N5991
	Q7	D43C5	D43C5	D45H11	D45H11	D45H11

### 3.9.6.2 Calculations

The pertinent 20 hp 108-volt power module specifications are

DC Voltage	150 V (Braking)
Peak Current	650 A
Peak Switch-off Volts	300 V
Gain at $I_c = 600$ A	300

The gain of 300 is typical at room temperature. The base drive must supply more current than this gain would indicate to account for minimum gain transistors, temperature variations, and sharing among the individual paralleled Darlington transistors in the power module. The present base drive circuit supplies 4 amps of positive current from Q4 and sinks 5 amps of negative current with Q7.

The design value of peak motor current for the 20 hp 108-volt system is 650 amps. This current scales inversely with battery voltage and directly with horsepower. The peak motor currents are shown in Table 3.9.6.2-1.

The required base drive currents, both positive and negative, are scaled from the peak motor currents, assuming constant gain for the power module. The matrix of base drive currents are shown in Table 3.9.6.2-2.

The matrix of base drive currents can be supplied by selecting the proper base drive circuit output transistors. The other portions of the base drive circuit can remain basically the same. The number of different output transistors is limited to only a few, if similar base drive currents are lumped together. This is shown by separating the base drive current matrix in Table 3.9.6.2-2 into three areas.

**Table 3.9.6.2-1**  
**PEAK MOTOR CURRENTS (Amps)**

Nominal Battery Voltage	Motor Horsepower				
	10	20	30	40	50
84	413	825	1238	1650	2062
108	325	650	975	1300	1625
150	234	468	702	936	1170
300	117	234	351	468	585

**Table 3.9.6.2-2**  
**BASE DRIVE CURRENTS (Amps)**

Nominal Battery Voltage	Transistor	Motor Horsepower				
		10	20	30	40	50
84	Q4	2.54	5.08	7.62	10.15	12.69
	Q7	3.17	6.35	9.52	12.69	15.86
108	Q4	2.00	4.00	6.00	8.00	10.00
	Q7	2.50	5.00	7.50	10.00	12.50
150	Q4	1.44	2.88	4.32	5.76	7.20
	Q7	1.80	3.60	5.40	7.20	9.00
300	Q4	0.72	1.44	2.16	2.88	3.60
	Q7	0.90	1.80	2.70	3.60	4.50

} Area 3

{ Area 1
{ Area 2

The present design is capable of meeting the current requirements in Area 2. This was determined after examining the gain and other characteristics of the 2N5991 and D45H11 transistors. These are npn and pnp transistors, respectively, for Q4 and Q7. Area 1 can be served with lower current-rated transistors. The characteristics of the D42C5 and D43C5 are a good choice for Q4 and Q7, respectively. Both of these are shown in Table 3.9.6.1-1.

The considerations in Area 3 are more complex. The 2N6338 npn transistor has a sufficient current rating for currents of 8 amps or less, but the MJ10020 must be used for currents above 8 amps. These choices for Q4 are shown in Table 3.9.6.1-1. The D45H11 pnp transistor can be used up to about 8 amps and the 2N6338 is a good choice above 8 amps. These choices for Q7 are also shown in Table 3.9.6.1-1.

### 3.9.7 Base Drive Power Supply Scaling

#### 3.9.7.1 Summary

The approach taken is to determine the power supply ratings of the present circuit (reference drawing EP7644CBDA in Appendix D) and scale them accordingly. The power supply volume and size, based on the required rating, can be determined from available switching power supplies. The base drive power supply weight and volume for the matrix of controller designs is shown in Table 3.9.7.1-1. One such supply is needed for each one of six power modules.

**Table 3.9.7.1-1**  
**BASE DRIVE POWER SUPPLY**  
**WEIGHT AND VOLUME**  
**(lb and in<sup>3</sup>)**

Nominal Battery Voltage		Motor Horsepower				
		10	20	30	40	50
84	Vol	50	50*	50 <sup>Δ</sup>	100*	100 <sup>Δ</sup>
	Wt	1	1.5	1.5	3.0	3.0
108	Vol	30*	30 <sup>Δ</sup>	30 <sup>Δ</sup>	50 <sup>Δ</sup>	100*
	Wt	1	1	1	1.5	3.0
150	Vol	30	30*	30 <sup>Δ</sup>	30 <sup>Δ</sup>	50 <sup>Δ</sup>
	Wt	1	1	1	1	1.5
300	Vol	20	20*	20*	20 <sup>Δ</sup>	20 <sup>Δ</sup>
	Wt	1	1	1	1	1

\*Larger heat sinks

<sup>Δ</sup>Forced convection

**(kg and cm<sup>3</sup>)**

Nominal Battery Voltage		Motor Horsepower				
		10	20	30	40	50
84	Vol	127	127*	127 <sup>Δ</sup>	254*	254 <sup>Δ</sup>
	Wt	0.5	0.7	0.7	1.4	1.4
108	Vol	76*	76 <sup>Δ</sup>	76 <sup>Δ</sup>	127 <sup>Δ</sup>	254*
	Wt	0.5	0.5	0.5	0.7	1.4
150	Vol	76	76*	76 <sup>Δ</sup>	76 <sup>Δ</sup>	127 <sup>Δ</sup>
	Wt	0.5	0.5	0.5	0.5	0.7
300	Vol.	51	51*	51*	51 <sup>Δ</sup>	51 <sup>Δ</sup>
	Wt	0.5	0.5	0.5	0.5	0.5

\*Larger heat sinks

<sup>Δ</sup>Forced convection

### 3.9.7.2 Calculations

An independent study has been made of commercially available switching power supplies. The results are made available here in terms of size and weight as shown in Figures 3 9 7 2-1 and 3 9 7 2-2.

The present supply is a 10-volt nonregulated center tapped bridge output. The positive output is 2.5 amps average at +5 volts and the negative output is 0.5 amps average at -5 volts. Based on reliability, manufacturing experience and volume sensitive prices, the approach chosen is to have one base drive power supply for each base drive circuit for each power module in the inverter. The base drive power supply wattage rating can be scaled in the same way the base drive currents are scaled in Section 3.9.6. The resulting power supply rating matrix is shown in Table 3 9 7 2-1.

Again, it is prudent to satisfy the many power supply requirements with only a few designs. A basic power supply can be chosen and its rating increased with larger heatsinks and forced cooling until the next design is needed. The Darlington transistors for the drive at the higher horsepower/lower battery voltage ratings may need a one- or two-volt higher power supply than the high-voltage high horsepower. Based on this and the required wattage ratings, the volume and weight in Table 3 9 7 1-1 can be determined from the Figures 3 9 7 2-1 and -2.

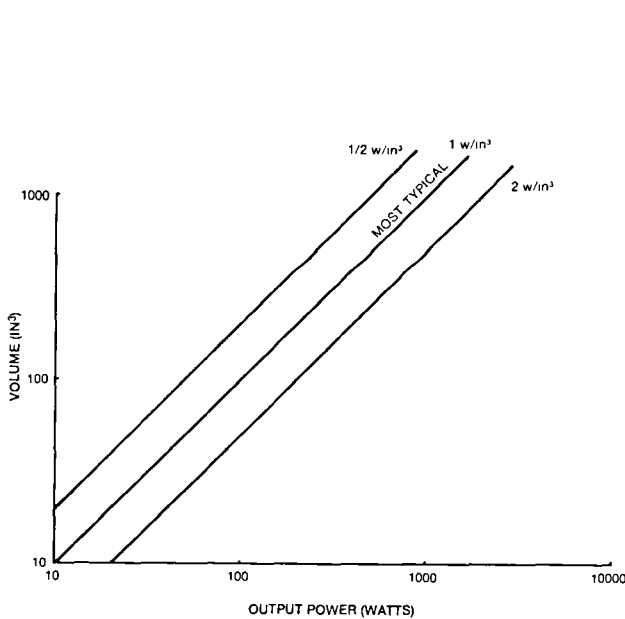


**Figure 3.9.7.2-1 Switching Power Supply Size**

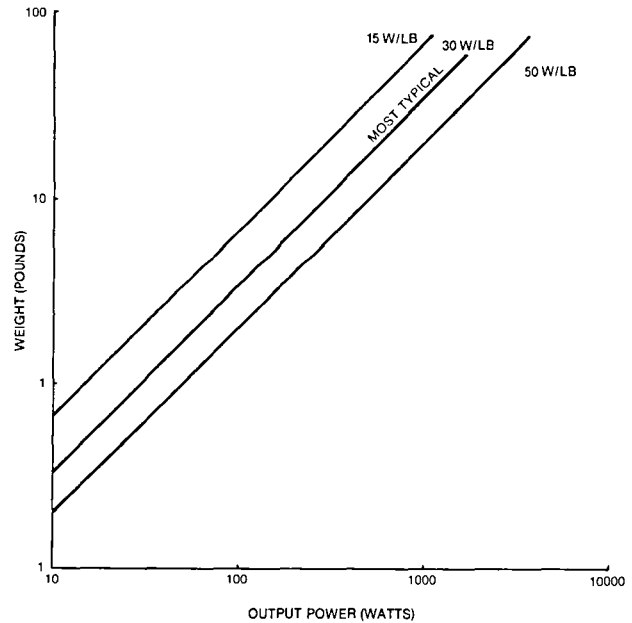


**Figure 3.9.7.2-2 Switching Power Supply Weight**

**Table 3.9.7.2-1**

**BASE DRIVE POWER SUPPLY RATING (WATTS)**

Nominal Battery Voltage	Motor Horsepower				
	10	20	30	40	50
84	25	51	76	102	127
108	20	40	60	80	100
150	15	29	44	58	72
300	10	15	22	29	36

**3.9.8 Control Scaling**

**3.9.8.1 Summary**

The assumption is made that the same blocks will be required for all models. The variations in power handling are accomplished in the interface circuitry. The simplified controller block diagram is shown in Figure 3.9.8.1-1. An analysis of expected maximum system speed requirements indicates that a single microprocessor cannot accomplish the required data handling fast enough. Therefore, a hybrid system of digital, analog, and custom circuits is proposed. The mixture of blocks and their implementation recommended for a production model are

Driver Command and Jerk Limit	— Configurable Controller
Lockout Circuit	— 3 Custom IC's
Waveform Generator	— Microprocessor
Flux Control	— Analog
Angle Regulator	— Analog
Current Magnitude, Limit and Controller	— Analog
Zero Speed Detector and Protection Circuits	— Configurable Controller
Current Interface and Summing, and Torque	— Analog
Logic Power Supply	— Switching power supply

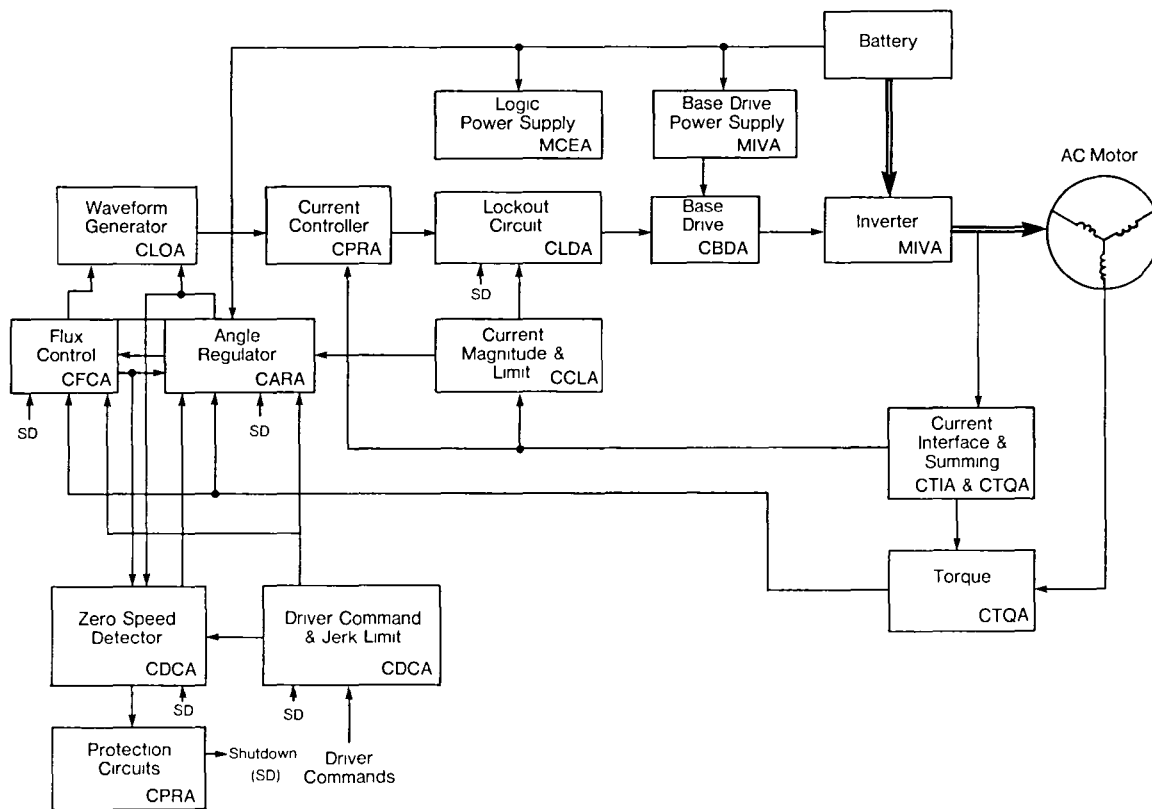


**Figure 3.9.8.1-1 Simplified AC Controller Block Diagram**

### 3.9.8.2 Control timing considerations

The first step in examining the practicality of a microprocessor type of control is to examine the speed with which data needs to be manipulated. This will not be a rigorous analysis, but one to determine feasibility. Assume a maximum chopping frequency of 1320 Hz, which is conservative. A chop may take place because any one of the logic functions shown in Table 3.9.8.2-1 concludes that current should change. In some cases, the input to the block needs also to be manipulated.

If a microprocessor is employed for control, a program outline can be constructed to estimate timing. This outline is shown in Table 3.9.8.2-2.

Given that 1320 Hz represents the maximum rate, this would probably be in a square-wave high-speed mode where some current chopping would be required to current limit. It would probably not be necessary to pulse width modulate the waveforms at this speed, but to merely keep everything under limits. Thus, the timing can be estimated:

$$1 \text{ cycle} = 7.576 \times 10^{-4} \text{ sec}$$

$$1/2 \text{ cycle} = 3.788 \times 10^{-4} \text{ sec}$$

It might be necessary to examine 5 samples per half cycle or 75  $\mu\text{s}$  for each set of comparison sequences. Since this must be done in three phases, this is about 25  $\mu\text{s}$  for each, unless some type of information sharing or averaging is employed. Assume a compromise of 50  $\mu\text{s}$  for each data point manipulation.

**Table 3.9.8.2-1**  
**LOGIC FUNCTION SPEEDS**

Lockout Circuit	(1)
Current limit circuit - current summing	(1)
Protection circuits - zero speed detector	(2)
over temperature	(3)
logic card interlock	(2)
+15 V logic power	(2)
-15 V logic power	(2)
Current controller - waveform generator	(1)
Flux regulator - limiter	(1)
Flux magnitude	(1)
Angle regulator - limiter	(1)
Over/under voltage regulator	(1)
Function desired with limits	(3)
Angle - current magnitude	(1)
flux magnitude	(1)
torque	(1)

**NOTE**

- (1) Judged to be high speed
- (2) Judged to be lower speed
- (3) Judged to be slow speed

**Table 3.9.8.2-2**  
**MICROPROCESSOR PROGRAM OUTLINE**

---

Power up delay
Reset registers
Determine desired function from controls (i e , accelerate, brake, direction)
Branch to proper subroutine
Set registers - flux limit
- angle limit
- sine wave factor
- triangle wave factor
- power contactor logic
Cycling motor phases
Generate waveforms A, B, C phases
Generate switch patterns
Check limits - current
- time
Calculate - torque
- angle
- voltage
Shut down sequences
Coast
Dynamic brake
Mechanical brake
Off

---

The motor time constants should be examined to see if they impose a limit on the control timing. From the motor model in Figure 3.4.6-1b, the shortest time constant is the rotor-stator time constant which is  $5.156 \mu s$ . This is long compared to the minimum time needed at the highest possible motor speed.

Thus, the limiting item is the need for digital manipulation of the variables. For each sample point, a number of logic steps need to be implemented. The terminology for an Intel 8080 microprocessor will be employed only to estimate processor timing, as shown in Table 3.9.8.2-3. Since only about  $50 \mu s$  are available and some housekeeping functions (failure or mode change interrupts) also need to be performed, this analysis shows that the control requires more than one microprocessor.

**Table 3.9.8.2-3**  
**MICROPROCESSOR TIMING**

		<u>Cycles</u>
Load phase current from A/D converter	LDA	13*
Compare register to accumulator	CMP	4
Exit of accumulator > register	JP	10
Load elapsed time	LDA	13
Compare register to accumulator	CMP	4
Exit if accumulator > register	JP	10
		—
		54
		cycle times

\* A-D Conversions Required  
Each cycle =  $2 \mu sec$

These estimates show that a control system sectioned as one microprocessor does not appear to be a good early entry production model control element. The approach taken is to place the functions which must be treated in an approximately continuous manner in analog circuitry with appropriate control by a digital microprocessor. Since under these conditions the processor need only supervise other modules once per half cycle (all three phases) instead of several times per half cycle, the work load of the processor is reduced to performing a switching command about once per  $379/3 \mu s$  at maximum speed.

### **3.9.8.3 Driver command and jerk limit (Drawing EP7644CDCA)**

This could be implemented by a configurable controller as shown in Figure 3.9.8.3-1. This should be a cost effective solution since it requires less silicon area for the stored program than for a hardware implemented logic gate.

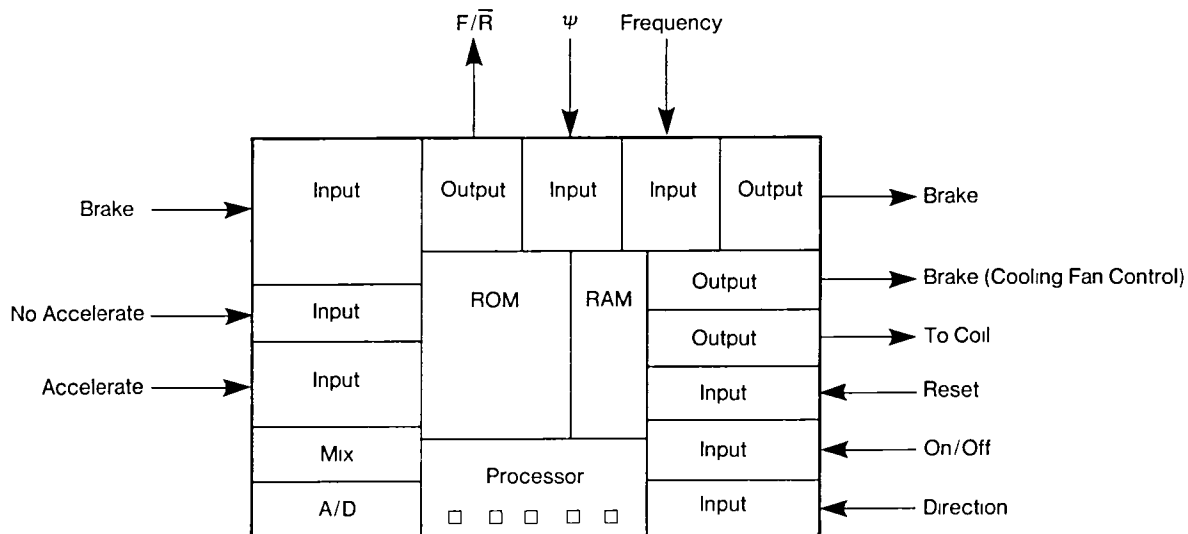


Figure 3.9.8.3-1 Driver Command and Jerk Limit Configurable Controller

#### 3.9.8.4 Lockout and waveform generator (Drawing EP7644CLOA)

It is proposed to make a custom integrated circuit (IC) per phase for the lockout circuit function. The custom IC represents a reasonable cost, yield, volume, and modularity. It needs 7 signal pins plus 3 pins for the power supply. The resistors are not critical and could be placed on the chip or simulated. The functions contained in each custom IC are

- Dual D Flip-Flop (2)
- Exclusive OR
- Monostable Multivibrator
- 2 Input NOR

The waveform generator function is already a microprocessor implementation and should remain so.

#### 3.9.8.5 Flux control (Drawing EP7644CFCA)

The flux regulator needs to be able to react during a half cycle of operation or about every  $379/3 \mu s$ . The flux magnitude function is also performed by this block and may as well be left analog as the rectification would need to be performed ahead of any A/D converter anyway. The composite output signal could be manipulated digitally as there is adequate time, however leaving it an analog signal minimizes A/D conversions.

#### 3.9.8.6 Angle regulator (Drawing EP7644CARA)

The angle regulator needs to be able to react during a half cycle of operation or about every  $379/3 \mu s$ . The inputs to this block are primarily analog as are the outputs, so it is chosen to remain in analog form.

#### 3.9.8.7 Current magnitude, limit, and controller (Drawings EP7644CCLA and EP7644CPRA)

It would be difficult to propose a custom integrated circuit which would have any advantage, except possibly conserving space, compared to the use of low cost commercial integrated circuits. It is recommended to leave this circuit analog, so it operates in real time.

**3.9.8.8 Zero speed detector and protective circuits (Drawings EP7644CDCA and EP7644CPRA)**

This could be implemented by a configurable controller as shown in Figure 3 9 8 8-1

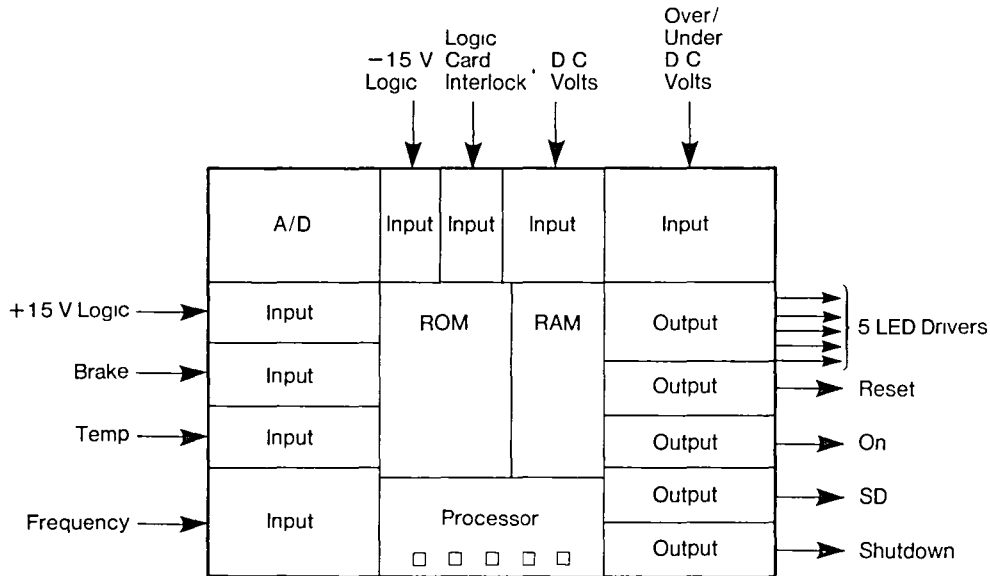


**Figure 3.9.8.8-1 Zero Speed Detector and Protection Circuit Configurable Controller**

**3.9.8.9 Current interface and summing, and torque (Drawings EP7644CTIA and EP7644CTQA)**

These are relatively simple circuits to implement using commercially available integrated circuits. The inputs, both current and voltage, should be normalized by proper scaling so the same modules can be employed over the total range of motor horsepower and battery system voltage. It is recommended these inputs remain analog and function in real time.

**3.9.9 Logic Power Supplies**

As a best engineering judgment, these power supplies should have regulated outputs (+5 V especially) and have good balance between  $\pm 15$  V. The sum of volt amperes (or watts) needed is 10.5, so a 20-watt supply is picked. The size of this supply will be invariant with vehicle size unless an output is employed for lights, horn, and entertainment electronics. The sizing is based on the switching power supply study discussed earlier in Section 3.9.7.2. The detailed logic power estimates are shown in Table 3.9.9-1. Using very conservative design and generous allowances for regulators, the logic power supply should be

- 20-watt capability
- +15 V, -15 V center-tapped
- +5 V regulated
- 655 cm<sup>3</sup> (40 in<sup>3</sup>) in volume (natural convection cooling)
- 0.45 kg (1 lb) weight; 0.59 kg (1.3 lb) if extra enclosure needed

**Table 3.9.9-1**  
**ESTIMATE OF TOTAL LOGIC POWER**

	mA At Voltage			
	<u>+15 V</u>	<u>-15 V</u>	<u>+5 V</u>	
Digital Accelerator and Brake	80			
Driver Command and Jerk Limit Configurable Controller			51	
Flux Regulator and Control	37	36		
Angle Regulator/Over-Under Voltage Regulator	36	36		
Lockout Circuit and Waveform Generator	91	3	151	
Current Controller	22	21	50	
Current Limit and Magnitude	37	36		
Current Summing and Torque	64	64		
Protection Circuits and Zero Speed Detector Configurable Controller			51	
Current Transducer Interface	15	9		
	<u>382</u>	<u>205</u>	<u>303</u>	<b>mA</b>
	6	3	1½	<b>VA</b>

### 3.10 CONTROLLER FAMILY LIFE CYCLE COST ESTIMATES

A specific objective of the contract was to analytically determine life cycle cost estimates of the controller for the 10, 20, 30, 40 and 50 hp controllers designed in the family expansion. The larger motors are intended to be applicable to heavier passenger vehicles, delivery vans and trucks for urban service in accordance with the J227a—Schedule D driving cycle. The controller is divided into two major portions, the power circuit and the sensing and control circuits.

#### 3.10.1 Life Cycle Cost Estimates Summary

The life cycle cost estimates for the family of controllers at the two production levels are shown in terms of present worth (Table 3.10.1-1) and average cost per mile (Table 3.10.1-2). The average costs per kilometer for the base 20 hp, 108-volt system are 3.3¢ per km (5.3¢ per mile) and 2.4¢ per km (3.9¢ per mile) for the 10,000 and 100,000 annual production levels, respectively. The costs are in 1980 dollars.

An objective of this development is a significant reduction in the projected life cycle cost of the ac drive system, as compared to a dc drive system. In order to fully assess this reduction, the two drive systems (motor, controller and control electronics) will be compared. The comparison will be made for the base 20 hp, 108-volt system in 100,000 annual production quantity. The factors used for this comparison are summarized in Table 3.10.1-3.<sup>(1,8)</sup> The economic parameters are the same for both systems and are the same as discussed in Section 3.10.5. The ac system is appreciably lighter, less costly, and more efficient than the dc system. The projected life cycle cost is 3.2¢ per km (5.1¢ per mile) for the ac system versus 3.5¢ per km (5.7¢ per mile) for the dc system. When the fuel costs are calculated on the basis of the total vehicle weights including the difference in drive system weight, the real impact of the system efficiency difference is observed. Improvements in the power Darlington transistors and snubbers will reduce the inverter losses and increase inverter efficiency by 1-2%.

**Table 3.10.1-1  
PRESENT WORTH LIFE CYCLE COST  
ESTIMATE SUMMARY (\$)**

Nominal Battery Voltage	Quantity	Motor Horsepower				
		10	20	30	40	50
84	10K	\$2,773	\$3,595	\$4,421	\$5,544	\$6,461
	100K	2,079	2,647	3,216	4,012	4,669
108	10K	2,655	3,404	4,195	5,116	6,246
	100K	2,003	2,510	3,066	3,713	4,538
150	10K	2,690	3,542	4,396	5,441	6,499
	100K	2,003	2,580	3,154	3,786	4,516
300	10K	2,563	3,307	4,086	4,866	5,696
	100K	1,920	2,416	2,937	3,480	4,066

**Table 3.10.1-2**  
**AVERAGE COST PER MILE LIFE CYCLE COST ESTIMATE SUMMARY**  
**(\$/mile)**

Nominal Battery Voltage	Quantity	Motor Horsepower				
		10	20	30	40	50
84	10K	\$0 043	\$0 056	\$0 069	\$0 086	\$0 100
	100K	0 032	0 041	0 050	0 062	0 072
108	10K	0 041	0 053	0 065	0 079	0 097
	100K	0 031	0 039	0 048	0 058	0 070
150	10K	0 042	0 055	0 068	0 084	0 101
	100K	0 031	0 040	0 049	0 059	0 070
300	10K	0 040	0 051	0 063	0 076	0 088
	100K	0 030	0 037	0 046	0 054	0 063

**Table 3.10.1-3**  
**AC AND DC DRIVE SYSTEM COMPARISON**

Item	AC	DC
Controller Cost	\$1028 00	\$560 00
Controller Weight	59 kg (130 lb)	33kg (73 lb)
Controller Efficiency	92%	94 5%
Control Electronics Cost	\$1145 00	\$1145 00
Control Electronics Weight	72 kg (15 8 lb)	72 kg (15 8 lb)
Motor Cost	213 00	820 00
Motor Weight	45 kg (99 lb)	99 kg (218 lb)
Motor Efficiency	90%	84%
Total System Cost	\$2386 00	\$2525 00
Total System Weight	111 kg (244 lb)	139 kg (307 lb)
Total System Efficiency	82 8%	79 4%
Fuel Cost, Total Vehicle*	\$95 72	\$104 97
Salvage Credit, Total System	\$47 72	\$50 50
Maintenance and Repair Cost, Total System	\$51 00	\$77 00
Present Worth	\$3313 00	\$3678 00
Average Cost Per Mile	\$0 051	\$0 057
Average Cost Per Km	\$0 032	\$0 035

\*Based on a 1633 kg (3600 lb) vehicle for ac system and 1662 kg (3663 lb) vehicle for dc system

### 3.10.2 Description of Life Cycle Cost Analysis

A significant reduction in the projected life cycle cost of the ac drive system, compared with present state of the art approaches, was one of the objectives of this development. Therefore, an underlying concern in design trade-off was consideration of the impact on life cycle cost by design options. Furthermore, this specific study is conducted to evaluate quantitatively the improvements obtained in the selected design. This is accomplished in the following steps:

1. Decide upon assumptions to be used (generic data, discount rate, social costs, fuel cost, inflation, etc )
2. Develop life cycle costing model and procedures
3. Compute life cycle costs for the proposed system as well as a representative baseline system

Modeling assumptions must be made before the life cycle cost model can be developed or adapted. The set of assumptions is listed below:

1. Life cycle costs will be computed over a base period, whose length may be arbitrarily specified but which must be the same for all candidates considered
2. All life cycle costs fall into one of three categories
  - a. The initial or capital cost, which is expended at the start of the base period and thereafter whenever the controller reaches the end of its economic life
  - b. A yearly recurring cost which includes fuel and power, maintenance and repairs, and (possibly) social benefits and costs
  - c. Salvage credit, which is attained at the end of lifetime and is coincident with the capital cost for the replacement controller
3. Inflation affects all costs at the same rate
4. Inflation occurs at a constant rate per annum. It is convenient to assume zero inflation and adjust the discount rate accordingly.
5. The discount rate is applied equally to all cost elements, and the discount rate is constant from year to year
6. When equipment reaches the end of its economic life, it will be replaced by similar equipment, whose cost performance is identical (except for inflation) to those of the equipment being replaced
7. Yearly recurring costs will be approximated by a single payment occurring at midyear. While end-of-year payments are commonly assumed, a midyear representation is more accurate.
8. Capital investment is amortized equally during each year of the equipment's lifetime, regardless of inflation
9. All data are assumed known with certainty, the life cycle cost model will be deterministic rather than stochastic
10. The life cycle costs will be computed over the entire economic life of vehicles, regardless of changes in ownership

The first step in this task will be to review these ten assumptions and decide what revisions, if any, should be made.

A model was developed by adapting existing models for life cycle cost developed by General Electric for transit vehicles<sup>(25,26)</sup>. Two measures of life cycle cost will be available from the model: the "present worth" and the average "cost per mile". Present worth is the amount which would have to be deposited in a bank account, drawing interest at the discount rate, in order to prepay all costs of controller ownership and operation during a defined base period.<sup>(27)</sup> Average cost per mile is the amount, averaged over the defined base period, which would be paid by a vehicle owner who pays all expenses as they occur, including amortization of capital costs with interest at the discount rate. Both present worth and average cost per mile are valid measures of life cycle cost. For a given discount rate and base period, the two measures bear a fixed ratio.

A general expression for present worth,  $P$ , is <sup>(25)</sup>

$$P = \left[ C_0 - S_0 \left( \frac{1+e}{1+r} \right)^L \right] \left[ \frac{1 - \left( \frac{1+e}{1+r} \right)^{[Y/L]L}}{1 - \left( \frac{1+e}{1+r} \right)^L} \right. \\ \left. + \left( \frac{1+e}{1+r} \right)^{[Y/L]L} \frac{1 - (1+r)^{-\text{MOD}_L Y}}{1 - (1+r)^{-L}} \right] \\ + \sqrt{\frac{1+r}{1+e}} \sum_{i=1}^Y R_{0i} \left( \frac{1+e}{1+r} \right)^i$$

where  $[Y/L]$  denotes the largest integer in the quotient  $Y/L$ , and  $\text{MOD}_L Y$  denotes the remainder in that quotient, where

- $C_0$  = Capital cost prior to inflation, \$
- $S_0$  = Salvage credit prior to inflation, \$
- $R_{0i}$  = Recurring cost in year  $i$  prior to inflation, \$
- $e$  = Escalation or inflation rate per annum
- $r$  = Discount rate per annum
- $L$  = Economic lifetime, years
- $Y$  = Base period for present worth analysis, years

For the special case where recurring cost is constant from year to year and where inflation is zero, this simplifies to

$$P = \left[ C_0 - S_0 (1+r)^{-L} \right] \frac{1 - (1+r)^{-Y}}{1 - (1+r)^{-L}} + R_0 \sqrt{1+r} \frac{1 - (1+r)^{-Y}}{r}$$

While an economy without inflation appears unattainable, a reasonable assumption is to adjust the discount rate to include the effects of inflation. This simplified equation has an interesting property: the base period  $Y$  appears only in the factor  $[1 - (1+r)^{-Y}]$ , which may be factored out of both terms in  $P$ . Thus the base period has only the effect of changing  $P$  by the same multiplier for any set of costs, choice of base period  $Y$  will not impact the comparison between two competing controllers. This is true only when recurring costs are constant ( $R_{0i}=R_0$ ) and inflation is zero ( $e = 0$ )

While use of present worth is a common criterion for life cycle cost, a more meaningful measure for vehicles is “average cost per mile,” which is the average cost paid by a vehicle owner who pays all expenses as they occur, including amortization of capital costs<sup>(28)</sup> A relation is developed between present worth,  $P$ , and average cost per mile,  $\bar{m}$ , which is<sup>(25)</sup>

$$\bar{m} = \frac{P}{Y \sum_{t=1} M_t (1+r)^{-(t-1/2)}}$$

where

$M_t$  = miles of use during year  $t$ , miles

When mileage per year is constant, this conversion simplifies to<sup>(25)</sup>

$$\bar{m} = \frac{P}{M} \frac{r}{\sqrt{1+r} [1 - (1+r)^{-Y}]}$$

where

$M$  = miles of use during any year, miles

Note that the same factor including the base period  $Y$  is in the numerator of  $P$  and the denominator of  $\bar{m}$ , so that it cancels out of the equation

A list of required data is essential in order that other inputs for life cycle costing can be prepared. A list of required data is as follows:

1. Elements of capital cost
  - a. Controller cost in production quantities
  - b. Salvage credit
2. Elements of recurring cost
  - a. Fuel and power for the specified mission, including taxes, based on the weight of the controller
  - b. Maintenance and repair costs
3. Economic and utilization parameters
  - a. Discount rate
  - b. Inflation rate
  - c. Life of vehicle (mission dependent)
  - d. Miles per year
4. Social benefits and costs
  - a. Benefit of reduction in air pollution
  - b. Benefit of noise reduction
  - c. Strategic benefit of petroleum conservation

Assumptions on generic data includes such factors as the discount rate, inflation rates, and fuel cost per gallon. It is convenient to assume zero inflation (constant dollars), with a compensated discount rate which represents the difference between the actual discount rate and the general inflation rate. All costs are in 1980 dollars.

Social costs and benefits comprise a special area of generic data. A rationale for establishing social costs associated with urban transit vehicles are air pollution, noise, delays, and visual intrusion <sup>(26)</sup>. Much of this rationale is directly applicable to passenger vehicles, however, its effects are not included in this study.

### 3.10.3 Elements of Capital Cost

#### 3.10.3.1 Power circuit cost estimate summary

The power circuit components evaluated for the various motor power and battery voltage levels are

- Input filter capacitor
- Transistor-diode power module
- Power module snubber
- Transistor base drive and power supply

The details of the cost analysis for each of the above components is given in Appendix E of this report. The cost estimate results are shown in Tables 3.10.3.1-1 and 3.10.3.1-2 and include miscellaneous component costs and assembly costs. Suitable devices are not currently available for the input filter capacitor required for the 300-volt system. Aluminum electrolytic capacitors, as used in the basic design with adequate voltage and ripple current ratings for the 300-volt system, are not currently manufactured. Rather than switch to a different capacitor type, having higher cost and weight, values for the 300-volt system are extrapolated from the lower voltage cases. A product development effort is needed for this voltage range, or a system redesign that will allow a larger ripple current.

**Table 3.10.3.1-1**  
**POWER CIRCUIT COST ESTIMATES**  
**FOR 10,000 VEHICLES/YEAR**

Nominal Battery Voltage	Motor Horsepower				
	10	20	30	40	50
84	\$1022	\$1758	\$2474	\$3457	\$4181
108	904	1567	2248	3028	3966
150	941	1709	2453	3359	4226
300	819	1480	2152	2792	3431

**Table 3.10.3.1-2**  
**POWER CIRCUIT COST ESTIMATES**  
**FOR 100,000 VEHICLES/YEAR**

Nominal Battery Voltage	Motor Horsepower				
	10	20	30	40	50
84	\$684	\$1165	\$1620	\$2274	\$2737
108	609	1028	1472	1976	2606
150	610	1100	1564	2053	2589
300	533	944	1356	1757	2149

Transistor power modules of the type required for this inverter do not exist as commercial items. It is felt that these modules can be designed and manufactured with reasonable yields and it is on this basis that the power module costing is based.

**3.10.3.2 Control circuit cost estimate summary**

In contrast to the power circuit, the control circuit is common for all power and voltage ranges. In order to keep costs per unit as low as possible, the costing is based on the use of microprocessor control technology. The existing laboratory controller is partitioned such that only high speed portions of the inverter control are performed with analog control components, the balance being handled with a microprocessor or a digital system.

The particular microprocessor implementation chosen is known as a "configurable controller." This is a new concept wherein the microprocessor and the necessary support devices (such as I/O ports, connectors, timers) are interconnected at the mask level to form a new mask for a specialized chip having the same performance as the host devices. The concept of the programmable controller is to take advantage of the standardized existing chips yet yielding many of the benefits of a custom chip, i.e., fewer devices, fewer circuit board connections, and lower costs.

The details of the cost analysis for each of the control functions is given in Appendix E of this report. The results of the cost estimates of any horsepower and system voltage are shown in Table 3.10.3.2-1. These costs also include the logic power supply.

**Table 3.10.3.2-1**  
**CONTROL COST ESTIMATES**

10,000 units/year	\$1507
100,000 units/year	\$1145

**3.10.3.3 Controller cost estimate summary**

The cost estimates for the controller are the sum of the values shown in Tables 3.10.3.1-1 and 3.10.3.2-1 or Tables 3.10.3.1-2 and 3.10.3.2-1 for either 10,000 or 100,000 units per year, respectively. This is shown in Tables 3.10.3.3-1 and 3.10.3.3-2. The cost estimates given are for the controller only and do not include the drive motor, the battery, or other power and control devices that may be necessary for the vehicle from an operations or safety consideration. The cost estimates also do not include any software costs, since this is considered as a one-time development cost.

**Table 3.10.3.3-1  
TOTAL CONTROLLER COST ESTIMATES  
FOR 10,000 UNITS/YEAR**

Nominal Battery Voltage	Motor Horsepower				
	10	20	30	40	50
84	\$2529	\$3265	\$3981	\$4964	\$5688
108	2411	3074	3755	4535	5474
150	2448	3216	3960	4866	5733
300	2326	2987	3659	4299	4938

**Table 3.10.3.3-2  
TOTAL CONTROLLER COST ESTIMATES  
FOR 100,000 UNITS/YEAR**

Nominal Battery Voltage	Motor Horsepower				
	10	20	30	40	50
84	\$1830	\$2310	\$2766	\$3420	\$3882
108	1754	2173	2617	3121	3752
150	1756	2246	2709	3198	3734
300	1678	2089	2501	2902	3295

### 3.10.3.4 Salvage Credit

Salvage credit is similar to capital cost and is discounted through the controller economic life. A salvage credit of 2% of the capital cost is assumed representative of the type of materials and assemblies in the controller.

### 3.10.4 Elements of Recurring Cost

#### 3.10.4.1 Maintenance and repair costs

The costs for repairs and maintenance are expected to be lower for an electric drive system than for an internal combustion engine (ICE) system. The cost estimates presented here are based on previous life cycle cost studies<sup>(25,26)</sup>. Of course, these costs are only for the controller portion and are not constant with system horsepower as shown in Table 3.10.4.1-1. The costs are independent of system voltage, however.

**Table 3.10.4.1-1  
ANNUAL MAINTENANCE AND  
REPAIR COSTS (\$)**

Motor Horsepower				
10	20	30	40	50
\$38	\$51	\$68	\$90	\$120

#### 3.10.4.2 Controller weight

In order to find the fuel cost attributable to the controller hardware weight, the weights of the family of controllers must be estimated. The weight of inverter equipment used as a motor drive has been found to follow the form in this equation:

$$W = a (HP \times SR)^{.6} \text{ lb}$$

where,

$W$  = controller weight in lb

HP = controller horsepower in the constant hp region

SR = constant horsepower speed range ratio

$a$  = 13.2 at 84 VDC

$a$  = 12.4 at 108 VDC

$a$  = 11.1 at 150 VDC

$a$  = 6.4 at 300 VDC

The weight of the control electronics is estimated as shown in Table 3.10.4.2-1. It is the same for the family of controllers. The combined weights of the controllers and control electronics is shown in Table 3.10.4.2-2.

**Table 3.10.4.2-1**  
**ESTIMATED CONTROL ELECTRONICS WEIGHT**

Control Function		Weight (lb)	Weight (kg)
Driver Command and Jerk Limit	(CDCA)	0 40	0 18
Lockout and Waveform Generator	(CLOA)	0 40	0 18
Flux Control	(CFCA)	0 25	0 11
Angle Regulator	(CARA)	0 30	0 14
Zero Speed & Protection Circuits	(CDCA) (CPRA)	0 30	0 14
Current Limit	(CCLA)	0 25	0 11
Torque	(CTQA)	0 30	0 14
Current Transducers	(CTIA)	6 00	2 72
Logic Power Supply		<u>1 00</u>	<u>0 45</u>
		9 20	4 17
Enclosure		4 60	2 09
Interconnect Wiring		<u>2 00</u>	<u>91</u>
		15 80 lb	7 17

**Table 3.10.4.2-2**  
**ESTIMATED AC CONTROLLER WEIGHTS**

Nominal Battery Voltage	Motor Horsepower									
	10		20		30		40		50	
	(lb)	(kg)	(lb)	(kg)	(lb)	(kg)	(lb)	(kg)	(lb)	(kg)
84	107	49	154	70	192	87	225	102	255	116
108	101	46	145	66	181	82	212	96	240	109
150	92	42	132	60	164	74	192	87	217	99
300	60	27	83	38	101	46	117	53	132	60

### **3.10.5 Economic Parameters**

The discount rate, or the time value of money to the controller owner, is assumed to be 10% <sup>(25,26)</sup> This includes the effects of inflation. The economic lifetime is 10 years at 6,093 km (10,000 miles) per year, which coincides with the required 100,000 J227a-D cycle life <sup>(26)</sup> The base period for the present worth analysis is arbitrarily chosen to also be 10 years, recalling that this changes the present worth by a constant and does not appear in the average cost per mile.

### 3.11 BATTERY CHARGER

The ac controller could be further integrated into the powertrain for an electric vehicle and be more useful by providing the additional feature of on-board battery charging. The requirements for incorporating this function are examined and a boost chopper design approach is presented.

#### 3.11.1 On-Board Battery Charging

An important item, often overlooked in electric vehicle studies, is that of the battery charger. Two primary options exist for recharging the battery: a stationary garage unit or an on-board unit. Both serve the same purpose, namely recharging the battery pack from the ac line.

The on-board unit has the advantage of allowing the electric vehicle the freedom of recharging wherever there is an available power source. The penalty paid for this freedom is the increased vehicle weight due to the added components that must be carried around at all times. Any increase in vehicle weight causes a decrease in the vehicle range for a given battery charge. Hence, the emphasis for the on-board charger is clearly that of low weight, high efficiency, and integration into the existing inverter hardware.

The stationary unit does not have this constraint and it should be designed for the least cost system that meets the charging specifications. Only the on-board charger is examined in this section.

A fundamental safety requirement for the on-board charger is electrical isolation from the power line. This enables the vehicle frame to be grounded, assuring personal safety without regard to the grounding of the power supply. This requires a power transformer to be a part of the charger system, only systems having such an isolation transformer have been considered.

An innovative system has been examined in order to determine its suitability for this application. This system utilizes the main inverter semiconductor components operating as a boost chopper for the power flow control, along with a 60 Hz transformer for voltage matching and electrical isolation. The system has good efficiency, however, more development work would be required to establish the detailed design of this system and its final performance.

#### 3.11.2 Battery Charger Maximum Power Specifications

Work done on the Near Term Electric Vehicle (ETV-1)<sup>(8)</sup> has provided a base for establishing the on-board charger specifications. For a 1430 kg (3150 lb) vehicle with a 277 kg (600 lb) payload, the energies for a full discharge of the batteries 114 km (71 miles) of the J227a-Schedule D cycle are

Battery output	18.6 kWh
Battery efficiency	72%
Battery input	25.9 kWh
Regeneration energy	3.8 kWh
Charger output	22.1 kWh
Charger efficiency	90%
Charger input	24.6 kWh

If the charging is done from a 230-volt line, it is desired that approximately 80% of the recharge be completed in 6 hours, at which time a lower charging rate is begun to avoid excessive gassing and overcharge. This will call for a per hour charging rate (output) of 2.95 kW. For larger vehicles, the charging rate should be increased to maintain the same 80% recharge time. The charging rate requirements for the vehicles considered are shown below.

Motor hp	Assumed Vehicle Weight (kg)	Assumed Vehicle Weight (lb)	Maximum Charging Rate (kW)
10	681	1500	1.5
20	1362	3000	3.0
30	2043	4500	4.5
40	2724	6000	6.0
50	3405	7500	7.5

All systems will operate from 230-volt single phase line.

The charger controls should operate to hold a constant current during the initial charge period. When the cell voltage reaches a limit value, the charge current should be reduced to hold the cell voltage of that value. The limit voltage has been determined to be

$$V_c = (2.92 - 0.004 T) \text{ volts/cell}$$

where  $T$  is cell temperature expressed in °F.

The final charge period should be a low-current equalizing charge of approximately 4 amperes, which is maintained for several hours or until the vehicle is used again.

### 3.11.3 Boost Chopper Approach

A schematic diagram of the ac controller power circuit showing the components added to perform the battery charging is shown in Figure 3.11.3-1. The basic charger system is that of a boost chopper utilizing the inverter power transistor and diode in the power module. An input 60 Hz power transformer is required for electrical isolation and for providing the proper voltage to the boost chopper. Also, two power contactors are utilized: one to disconnect the drive motor during charging, and the other to connect the transformer output to two of the inverter phases. Control for these contactors is from the 12-volt auxiliary battery. When the charger plug is extended, a door switch (or other suitable interlock) energizes contactor DR which removes power from the drive motor. Battery charging can be initiated from a push button which picks up contactor CH connecting the transformer output to the inverter.

The additional logic and control for the power transistors needed to perform the charging function is not shown.

A boost chopper requires that the peak voltage of the chopper input be less than the lowest battery voltage. A fully discharged battery will have a voltage as low as 1.3 volts per cell under load, yet its no-load voltage is approximately 2 volts/cell. Under charging conditions, the voltage will rise above 2 volts/cell.



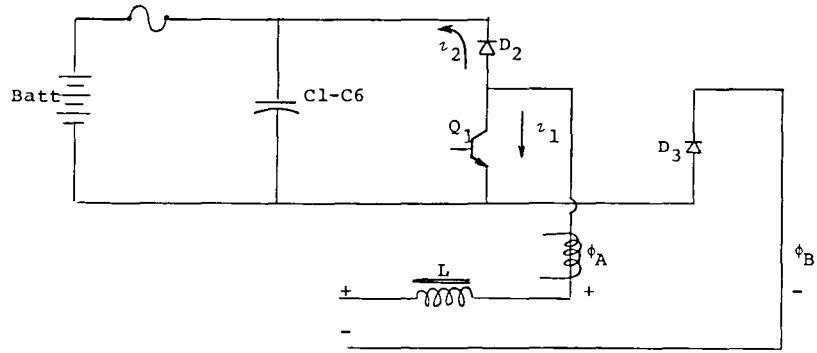


Figure 3.11.4-1 Active Components for Positive Half Cycle

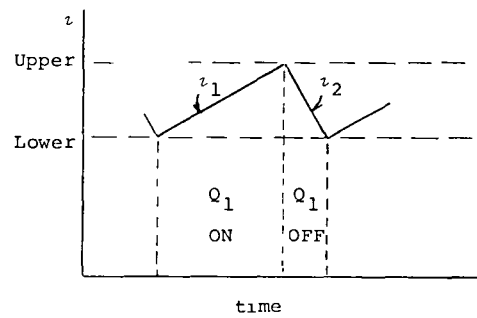


Figure 3.11.4-2 Current Flow for Positive Half Cycle

During the negative half cycle of the line voltage, the active components are as shown in Figure 3.11.4-3. The operation is similar, with transistor  $Q_3$  doing the current chopping and  $i_3$  and  $i_4$  responding in similar fashion to  $i_1$  and  $i_2$ , respectively.

A published analysis of this type of boost charger can be used for evaluating the major items of (12)

- Chopping frequency
- Inductor size
- Efficiency estimates

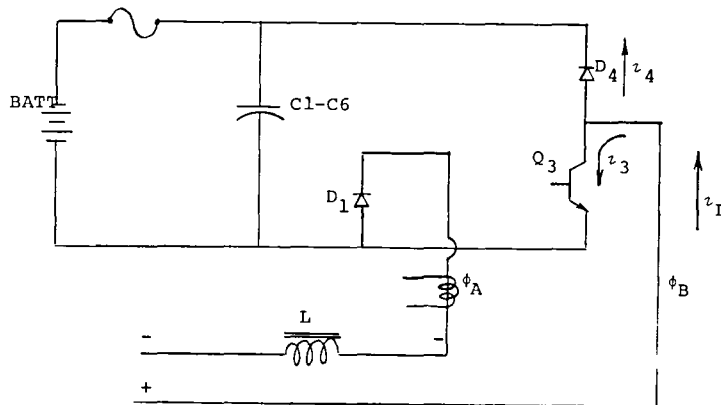


Figure 3.11.4-3 Active Components for Negative Half Cycle

Two forms of current control can be used with this charger, sine wave or constant current. For the sine wave current control, the current over a half cycle of the line voltage is controlled as an approximate sine wave shape (Figure 3.11.4-4a). This is done by using sine waves as the upper and lower current switching levels. The constant current control will maintain an approximately constant average current flow during the half cycle, independent of the applied voltage (Figure 3.11.4-4b). The sine wave control offers many advantages from the standpoint of the ac line, i.e., a reduction of current harmonics and a near-unity power factor. For these reasons, this is the form of control that will be assumed.

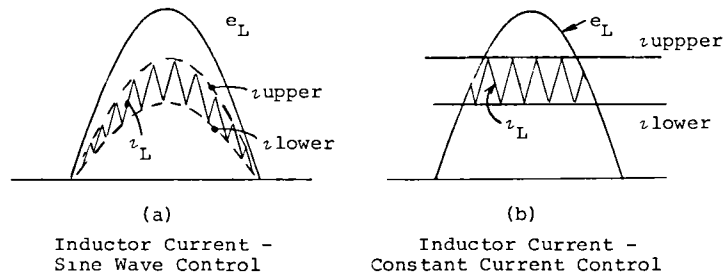


Figure 3.11.4-4 Chopper Current Controls

### 3.11.5 Major Component Sizing

#### 3.11.5.1 Inductor

The desired mode of operation is that of sine wave current control of the inductor current in order to minimize the line harmonics. In order to maximize the power transfer over a given circuit, it is desired that the inductor current be closely in phase with the line voltage. Ideally,

$$i_L(t) \cong kV_2(t)$$

where  $i_L$  = inductor current

$k$  = constant

$V_2$  = transformer secondary voltage

If the inductor is too small, ripple will be excessive for practical chopping frequencies, however, if it is too large, the desired power levels may not be achieved. Bounds on the inductor size and the chopping frequency can be established from the following analysis.

For the maximum power value, the chopping frequency and the inductor should be sized to maintain current flow over the entire half cycle. If,

$$f_c \gg f_l$$

where  $f_c$  = chopping frequency

$f_l$  = line frequency

then we can assume

$V_2$  = constant over chopping cycle

$i_L$  = same value at beginning and end of chopping cycle

During the first portion of the chopping cycle with  $Q_1$  turned on, the current increases at a rate

$$\frac{di_L}{dt} = \frac{V_2}{L_{\min}}$$

During the second portion ( $Q_2$  turned off), the current decreases at a rate

$$\frac{di_L}{dt} = - \frac{V_B - V_2}{L_{\min}}$$

A transistor duty cycle is defined as

$$\eta = \frac{\text{On Time}}{\text{Chopping Period}}$$

For the critical case,  $i_L = 0$  at the start and finish of the chopping period. The maximum current will be

$$(i_L)_{\max} = \frac{V_2 \eta T_c}{L_{\min}}$$

and the average current is

$$i_L = \frac{V_2 \eta T_c}{2 L_{\min}}$$

so that

$$L_{\min} = \frac{\eta T_c}{2} \left( \frac{V_2}{i_L} \right)$$

If the current is controlled sinusoidally, this can be written as

$$L_{\min} = \frac{\eta T_c}{2} \left( \frac{V_{2\text{rms}}^2}{P} \right)$$

where,  $P$  = maximum charging power

$V_{2\text{rms}}$  = secondary volts (rms)

The maximum inductance is determined by the tracking of the current, i.e., the maximum rate of rise of  $i_L$ . If it is arbitrarily stated that tracking should hold for voltages above 0.1  $V_2$ , then the  $di/dt$  relationship with  $Q_1$  ON can be expressed as

$$\omega i_L = \frac{0.1 V_2}{L_{\max}}$$

or

$$L_{\max} = \frac{0.1}{2\pi f_1} \left( \frac{V_{2\text{rms}}^2}{P} \right)$$

With two expressions describing the bounds on  $L$ , the chopping frequency can be obtained

Given that

$$L_{\max} > L_{\min}$$

or

$$\frac{0.1}{2\pi f_l} > \frac{\eta T_c}{2}$$

for  $\eta=1$ , this yields

$$\frac{f_c}{f_l} > 10\pi$$

This indicates that the chopping frequency must be at least 31.4 times the line frequency. For a 60 Hz line, this requires a minimum of 2 kHz chopping frequency.

The maximum inductor size is set by the line conditions of transformer voltage and charging power. The minimum inductor size is set by these same items and the chopping frequency (20 kHz assumed). The inductor sizes for the battery voltage and motor horsepower ranges are shown in Table 3.11.5.1-1.

**Table 3.11.5.1-1**  
**INDUCTOR SIZE RANGES (Min/Max)**

Motor Horsepower	Nominal Battery Voltage			
	84	108	150	300
10	0.049/0.516	0.080/0.842	0.154/1.630	0.614/6.52
20	0.024/0.258	0.040/0.421	0.077/0.815	0.307/3.26
30	0.016/0.172	0.026/0.281	0.051/0.543	0.205/2.17
40	0.012/0.129	0.020/0.210	0.038/0.407	0.154/1.63
50	0.009/0.103	0.016/0.168	0.031/0.326	0.123/1.30

- Note 1. Upper figures are minimum inductance for 20 kHz chopping frequency, lower figures are maximum inductance.  
2. All values in millihenries.

### 3.11.5.2 Transformer

The input transformer is required for voltage matching and electrical isolation of the vehicle components from the power source. It is a 60 Hz unit and its design can be based on conventional practice. Discussion with engineers in General Electric's Specialty Transformer Department resulted in the weight-kVA curve for transformers in this size class (Figure 3.11.5.2-1). This curve is based on the core, coil, and terminal board only, minus any protective case. This curve is used for estimating the weights of the transformers for the various vehicle classes shown below.

Motor Horsepower (hp)	Maximum Charge Rate (kW)	Transformer Weight (kg)	Transformer Weight (lb)
10	1.5	12	27
20	3	20	45
30	4.5	30	66
40	6	40	88
50	7.5	49	109

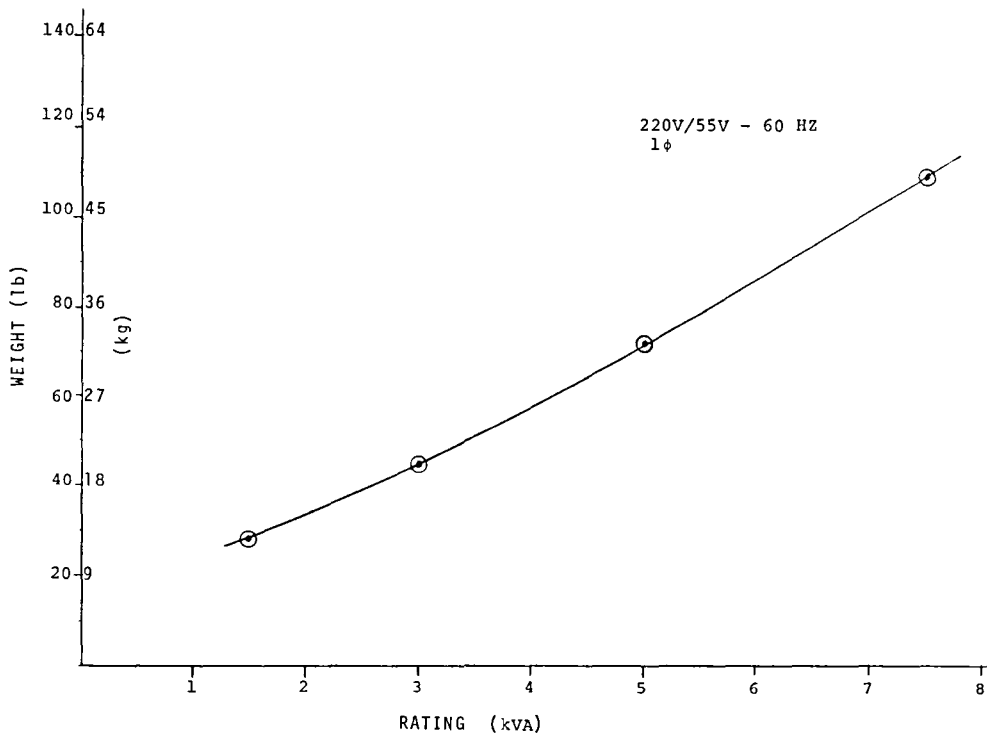


Figure 3.11.5.2-1 Transformer Weight

### 3.11.6 Efficiency Estimates

The major losses in the system can be estimated to give an estimate of the overall charging system efficiency. These losses are

- Transformer — core and copper

- Transistor – switching and voltage drop
- Inductor – core and copper
- Diode – voltage drop
- Control Power – including base drive

### 3.11.6.1 Transformer

Transformers in this size range have efficiencies that typically are in the 97-97.5% range, with the higher efficiency being typical of the higher power ratings. For this study, the transformer loss is assumed to be 3% of rating.

### 3.11.6.2 Transistor switching loss

The ratio of the transistor switching loss to the total power is, assuming a linear switching characteristic, given by<sup>(12)</sup>

$$\frac{P_{sw}}{P_T} = \frac{\sqrt{2}}{\pi} f_c \frac{E_B}{V_{2rms}} (T_R + T_F)$$

- where  $P_{sw}$  = switching loss – watts  
 $P_T$  = total power  
 $f_c$  = chopping frequency  
 $E_B$  = battery voltage  
 $V_{2rms}$  = secondary volts (rms)  
 $T_R$  = rise time  
 $T_F$  = current fall time

Assuming typical values for the rise and fall times of 0.4  $\mu$ s and a chopping frequency of 20 kHz, the power loss can be estimated. Assuming the transformers are sized for the battery as discussed in Section 3.11.3, the ratio of  $E_B/V_{2rms}$  will be approximately 1.56 for all systems. The transistor switching loss will be

$$\frac{P_{sw}}{P_T} = 1.12\%$$

If the recovery effects of the blocking diode ( $D_2$  or  $D_4$ ) in Figure 3.11.3-1 is included, the switching loss is increased approximately 50% or

$$\frac{P_{sw}}{P_T} = 1.68\%$$

### 3.11.6.3 Transistor saturation loss

The power loss in the transistor during the conducting period can be calculated by assuming a fixed saturation voltage and integrating the losses over a half cycle of line current. The ratio of the power loss to the input power is

$$\frac{P_{SAT}}{P_T} = \frac{V_S}{E_B} \left[ \frac{2\sqrt{2}}{\pi} \left( \frac{E_B}{V_{2rms}} \right) - 1 \right]$$

- where  $P_{SAT}$  = Transistor saturation loss in watts  
 $V_S$  = Transistor saturation voltage drop in volts

Referring to Figure 3 11 4-1, it is noted that for the positive half cycle, transistor  $Q_1$  is in series with diode  $D_3$ . The loss calculation should include both voltage drops in  $V_S$ .

Using typical values of 1.5 volts for the transistor and 1.1 volts for the power diode, the saturation loss can be calculated for all the systems. The ratio of  $E_B/V_{2rms}$  is a design parameter and constant for all systems at 1.56. Hence, the saturation loss becomes

Nominal Battery Voltage	Sat. Loss
84	1.25%
108	0.97%
150	0.70%
300	0.35%

#### 3.11.6.4 Blocking diode loss

The blocking diodes  $D_2$  and  $D_3$  (Figure 3 11 4-1) are in series with the battery during the charging current pulse on the positive half cycle of line voltage. The conduction losses in these diodes can be calculated by an estimate of the diode drop

$$\frac{P_D}{P_T} = \frac{V_D}{E_B}$$

where  $P_D$  = power loss in diode

$V_D$  = voltage drop across the diode

Assuming a 1.1-volt drop for each diode, this yields

Nominal Battery Voltage	Diode Losses
84	2.62%
108	2.04%
150	1.47%
300	0.73%

#### 3.11.6.5 Inductor losses

Inductor losses will include the core and copper losses. However, assuming the use of low-loss ferrite cores, the copper loss dominates. For a properly designed inductor, the copper loss should be kept to less than 0.5% of the input power.

#### 3.11.6.6 Control power losses

The control power loss, including the transistor base drive losses, can only be estimated until a complete control is designed. For a properly designed control, the losses should be no more than 0.5% of the rated power.

### 3.11.6.7 Summary losses

Table 3.11.6.7-1 summarizes the losses for this charger. Clearly, the transformer is a major component of loss. The reduction in percentage loss is clearly shown for the higher voltage batteries, which is a direct result of the fixed voltage drop by solid-state devices resulting in a smaller percentage of the total loss.

**Table 3.11.6.7-1**  
**SUMMARY OF CHARGER LOSSES**

	Nominal Battery Voltage			
	84	108	150	300
Transformer Loss	3.0%	3.0%	3.0%	3.0%
Transistor Switching Loss	1.7	1.7	1.7	1.7
Transistor Saturation Loss	1.3	1.0	0.7	0.4
Diode Loss	2.6	2.0	1.5	0.7
Inductor Loss	0.5	0.5	0.5	0.5
Control Power	0.5	0.5	0.5	0.5
Total Losses	9.6%	8.7%	7.9%	6.8%
Rated Efficiency	90.4%	91.3%	92.1%	93.2%

## Section 4

### TEST AND EVALUATION

#### 4.1 TEST PLAN

The tests on the ac controller are of three general types. The first series of tests verifies the operation of the control system, debugs the hardware, and establishes the desirable operating conditions for all combinations of input signal commands. The second series of tests measures the efficiencies of the motor and inverter, the peak ac currents, and the torque output or input as a function of command. The third series of tests establishes the performance of the ac controller under duty cycle conditions and evaluates the effects of regeneration. The system debug continued throughout the tests.

##### 4.1.1 Steady-State Tests

Steady-state tests are used to establish the operating conditions of the motor. The following motor measurements were made:

- Flux level
- Torque per amp
- Efficiency
- Harmonic losses
- Voltage and current waveforms

At up to the full load current operating condition, the operation of the power inverter was tested. Measurements included:

- Transistor voltages and currents
- Base current
- Inverter efficiency
- Heat sink temperature rise
- Sample output voltage and current waveforms

##### 4.1.2 System Cyclic Tests

A series of tests were performed to establish the operation of the ac controller and motor in combination as an electric vehicle drive system. These tests were performed using a flywheel load to simulate the effect of the inertia of (approximately) a 1600 kg (3600 lb) electric vehicle. The tests included overall controller and motor system performance over the speed range of 0 to 97 km/h (0 to 60 mph) in both motoring and braking. Special attention was paid to:

- Starting
- Transition from pulse-width-modulation to square wave
- Braking to a stop

- Maximum vehicle performance
- Performance at reduced load
- Effects of battery voltage change
- Regeneration
- Low and high battery voltage protection

## 4.2 TEST INSTRUMENTATION

Figure 4 2-1 is a block diagram of the ac controller, the associated three-phase induction motor, and various apparatus and instrumentation used in conducting all tests. The power measurements are made across three drive-system boundaries. The basic power measurements are the dc power input to the inverter, the ac power output from the inverter, and the mechanical shaft power output from the ac induction motor with integral gear box. These measurements are all automated under computer control. Additional measurements of low-level electronic control system performance are also made to evaluate control system accuracy and dynamic performance. Figure 4 2-2 is a schematic diagram illustrating the test signal information flow between sensors and the computer system.

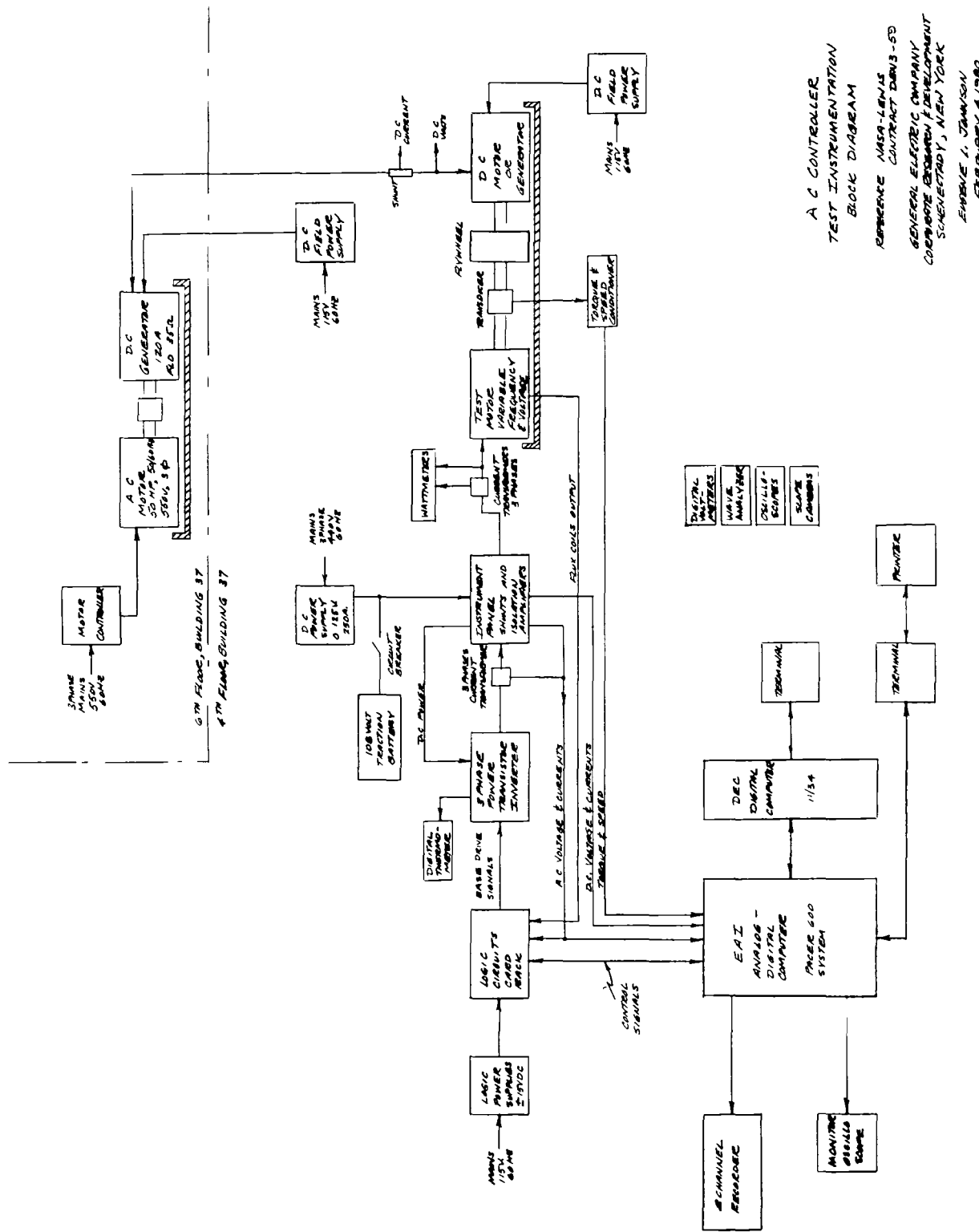
The computer system performs the functions of test data acquisition and data processing. The ac controller logic exists on circuit boards in the associated control electronics assembly, with the vehicle drive functions fed to the computer. A combination of analog and digital techniques are used to acquire and process performance data. This is done using a hybrid computer system.

The block diagram of Figure 4 2-1 shows extra instrumentation such as a wave analyzer and ac wattmeters, which are used to verify the accuracy of the computer controlled instrumentation.

The computer program is an interrupt driven, real time program which can also be used for test control, if desired, by the addition of appropriate software modules. The program consists of a master background program which interfaces with the user and prints a data summary. The routine H CONT is executed by a fixed time interval interrupt every 10 milliseconds. H CONT acquires the real time data and outputs real time diagnostics. The block diagram (Figure 4 2-3) illustrates the analog computer functions for power computation.

Figures 4 2-4, -5, and -6 illustrate the test equipment and lab setup. The motor test stand (Figure 4 2-4) is comprised of the ac controller, three-phase induction motor, the load motor/generator, flywheel, torque/speed sensors, associated instrumentation, and tie-lines to the load motor/generator controls. The instrumentation panel (Figure 4 2-5) contains the electrical shunts and isolation amplifiers used to measure the ac and dc voltages and currents. Also pictured are the three current transformers, which supply ac current signals to the computer instrumentation. A general view of the hybrid computer system lab area is seen in Figure 4 2-6. The hybrid computer and terminal, associated monitor oscilloscope, strip chart recorder, and various instruments are seen in the picture.

It should be noted that the speed measurements in this section always refer to the speed of the motor after the integral gear box reduction of 2.923 to 1.



A C CONTROLLER  
TEST INSTRUMENTATION  
BLOCK DIAGRAM

REFERENCE NASA-LENIS  
CONTRACT DORS-58  
GENERAL ELECTRIC COMPANY  
CORPORATE RESEARCH & DEVELOPMENT  
SCHENECTADY, NEW YORK

ENGINEER I. JOHNSON  
FEBRUARY 4, 1980

Figure 4.2-1 Test Instrumentation Block Diagram

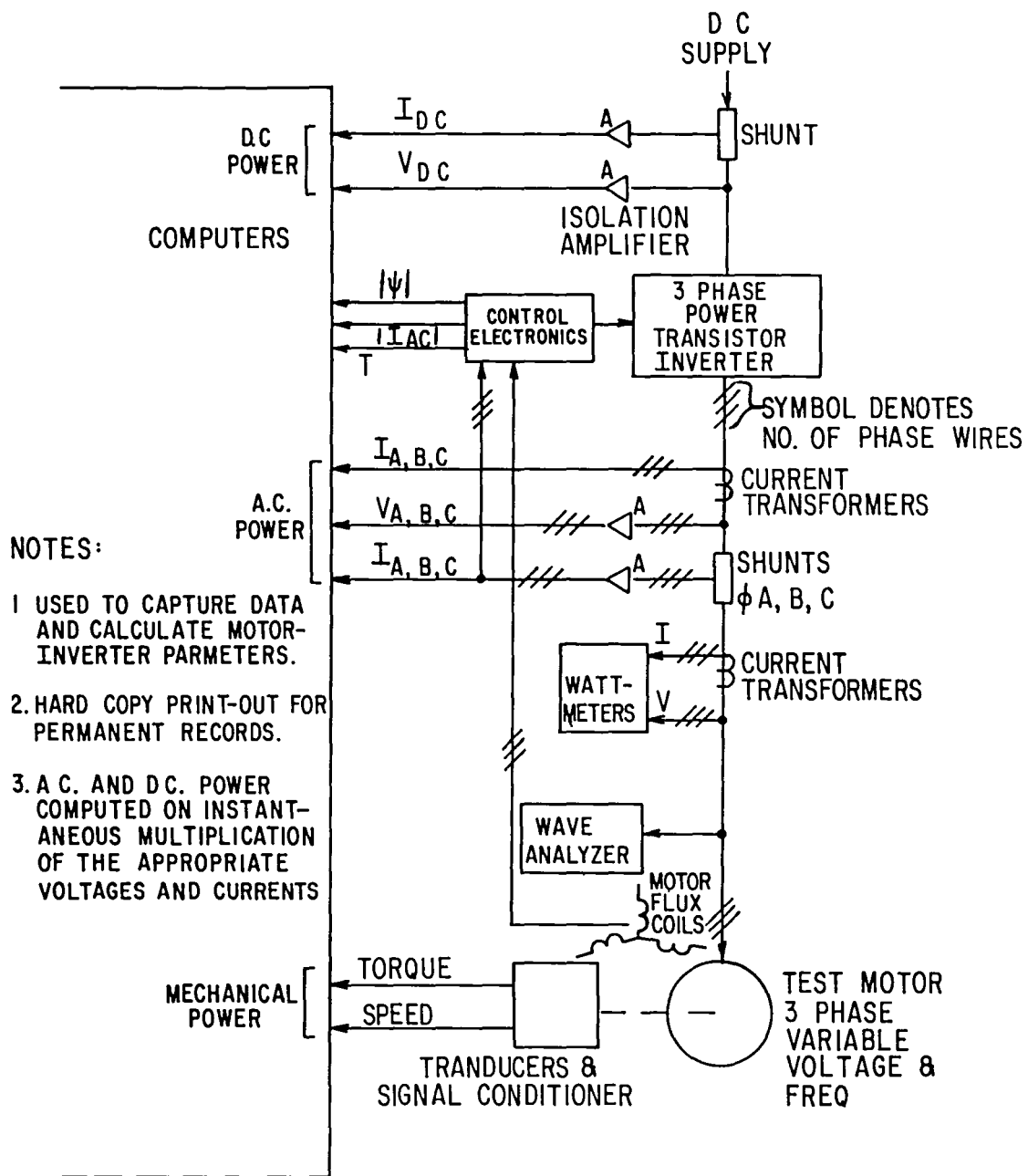
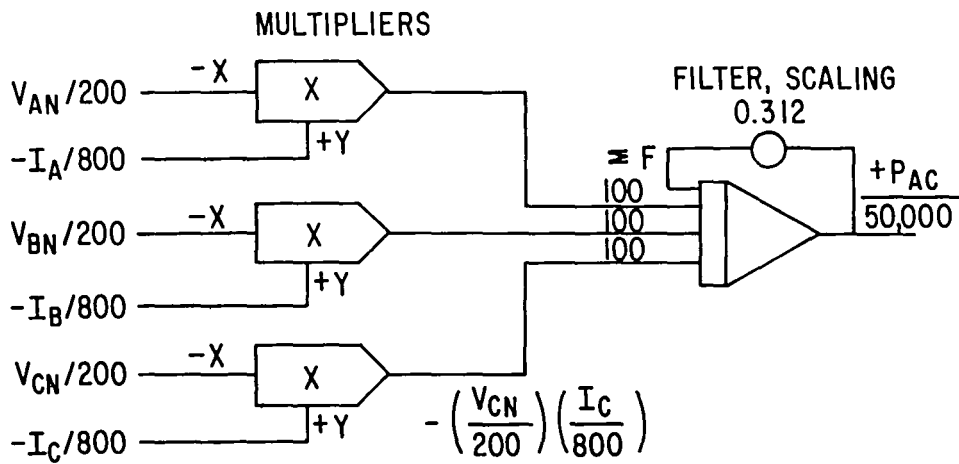


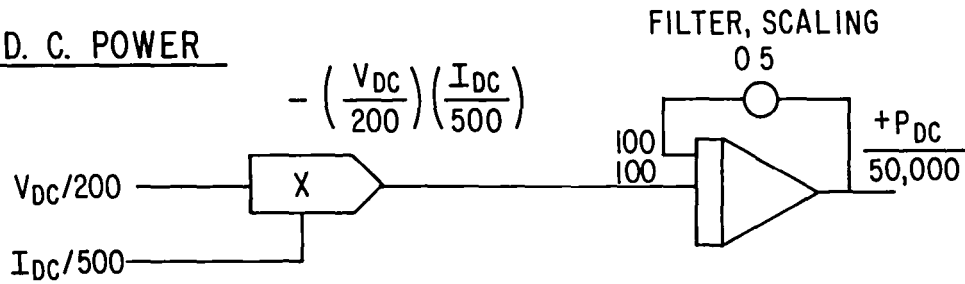
Figure 4.2-2 Test Signal Information Flow

A C. POWER



VOLTAGE FULL SCALE : 200V  
CURRENT FULL SCALE : 800A.

D. C. POWER



VOLTAGE FULL SCALE 200V  
CURRENT FULL SCALE 500A

Figure 4.2-3 Analog Computer Computation Functions

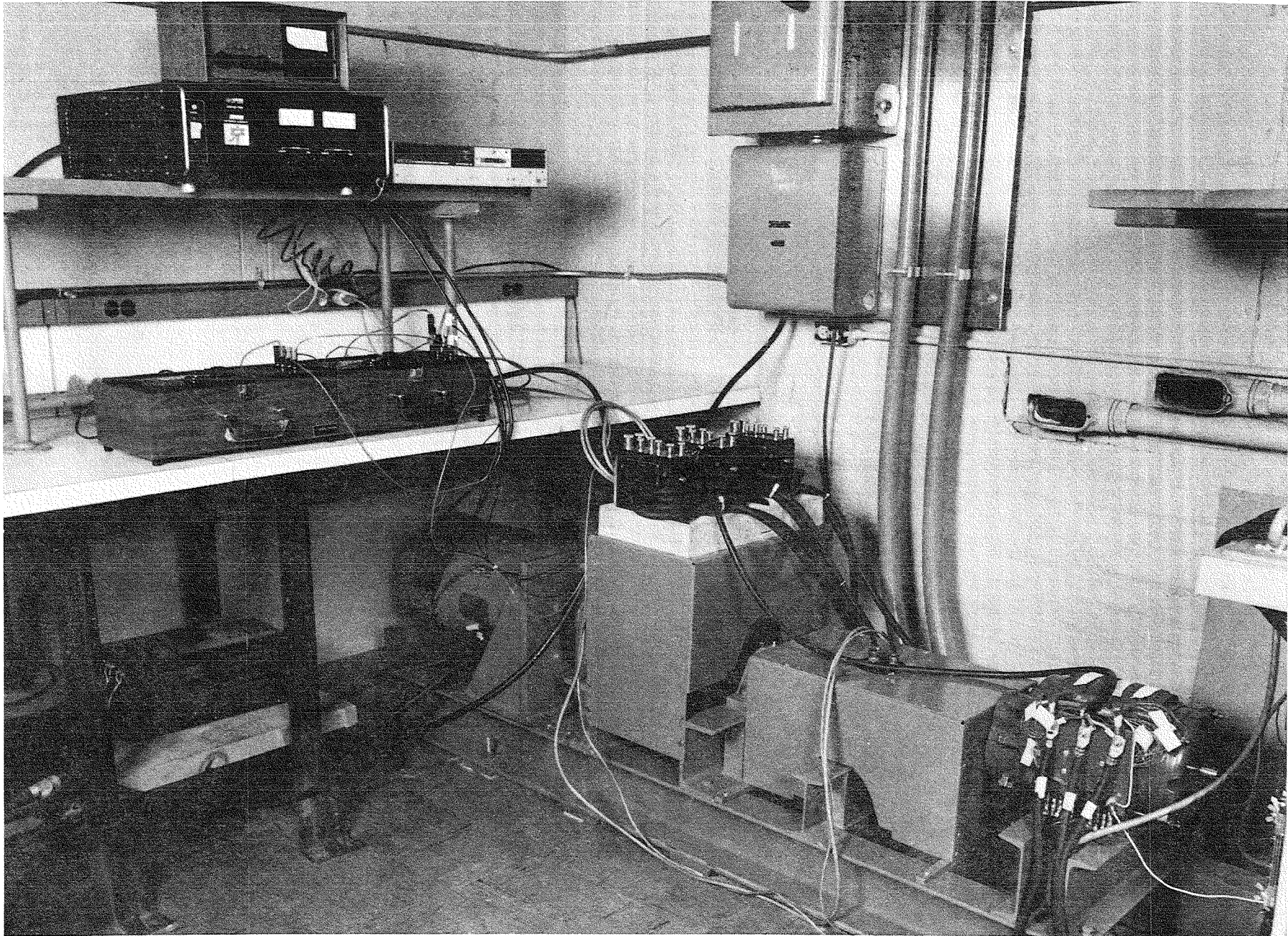


Figure 4.2-4 AC Controller Motor Test Stand

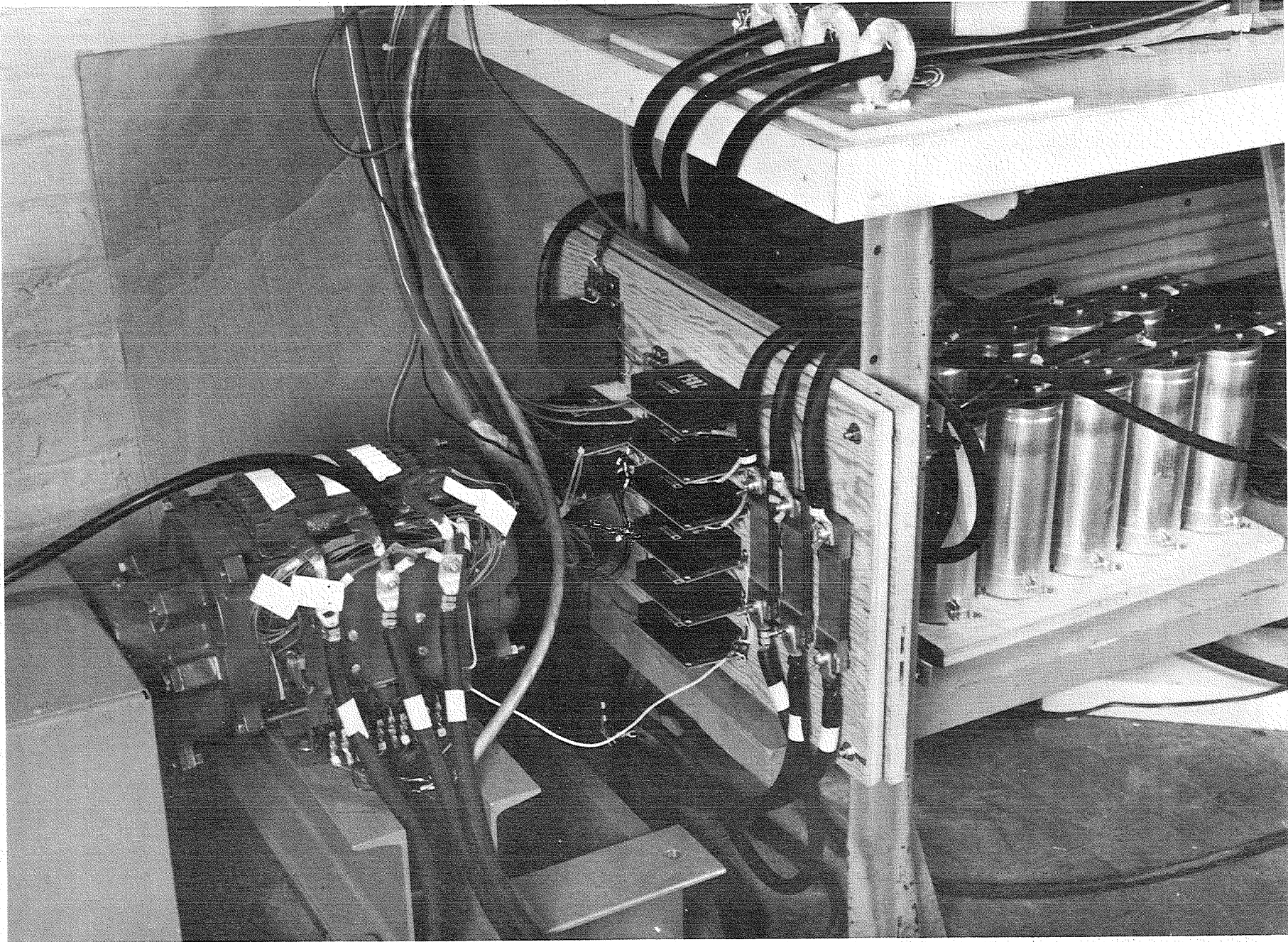


Figure 4.2-5 AC Controller Instrumentation Panel



Figure 4.2-6 Hybrid Computer System

### 4.3 CONTROLLER TRANSFER FUNCTIONS

The overall drive system block diagram is shown in Figure 4 3-1. The system control transfer functions are determined for each one of the three closed loops ( $\sin \theta_{eq}$ , flux and torque) for both modes of controller operation (PWM and square wave). The method for determining the transfer functions is to open the desired loop, remove the gain block, inject a loop output signal and measure the resultant loop input signal, at various frequencies. The angle loop,  $\sin \theta_{eq}$ , is the inner loop and is the most important. Figures 4 3-2 and 4 3-3 show the angle loop transfer function for the PWM and square wave modes, respectively. Figures 4 3-4 and 4 3-5 show the torque loop transfer function for the PWM and square wave modes, respectively. Figures 4 3-6 and 4 3-7 show the flux loop transfer function for the PWM and square wave modes, respectively.

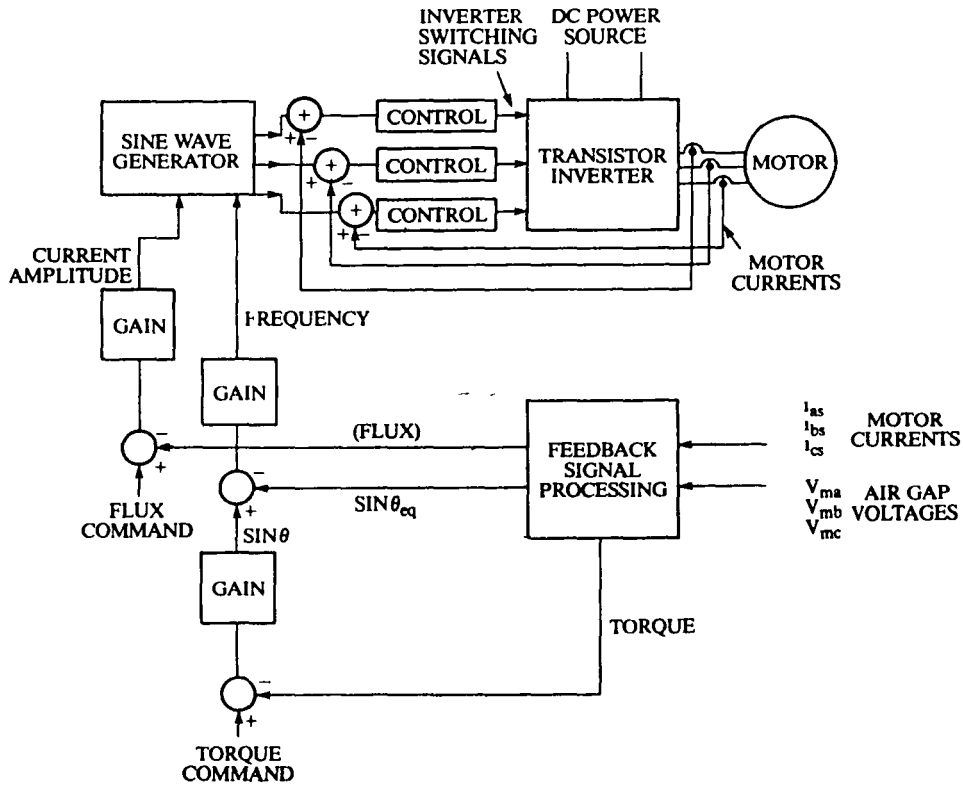
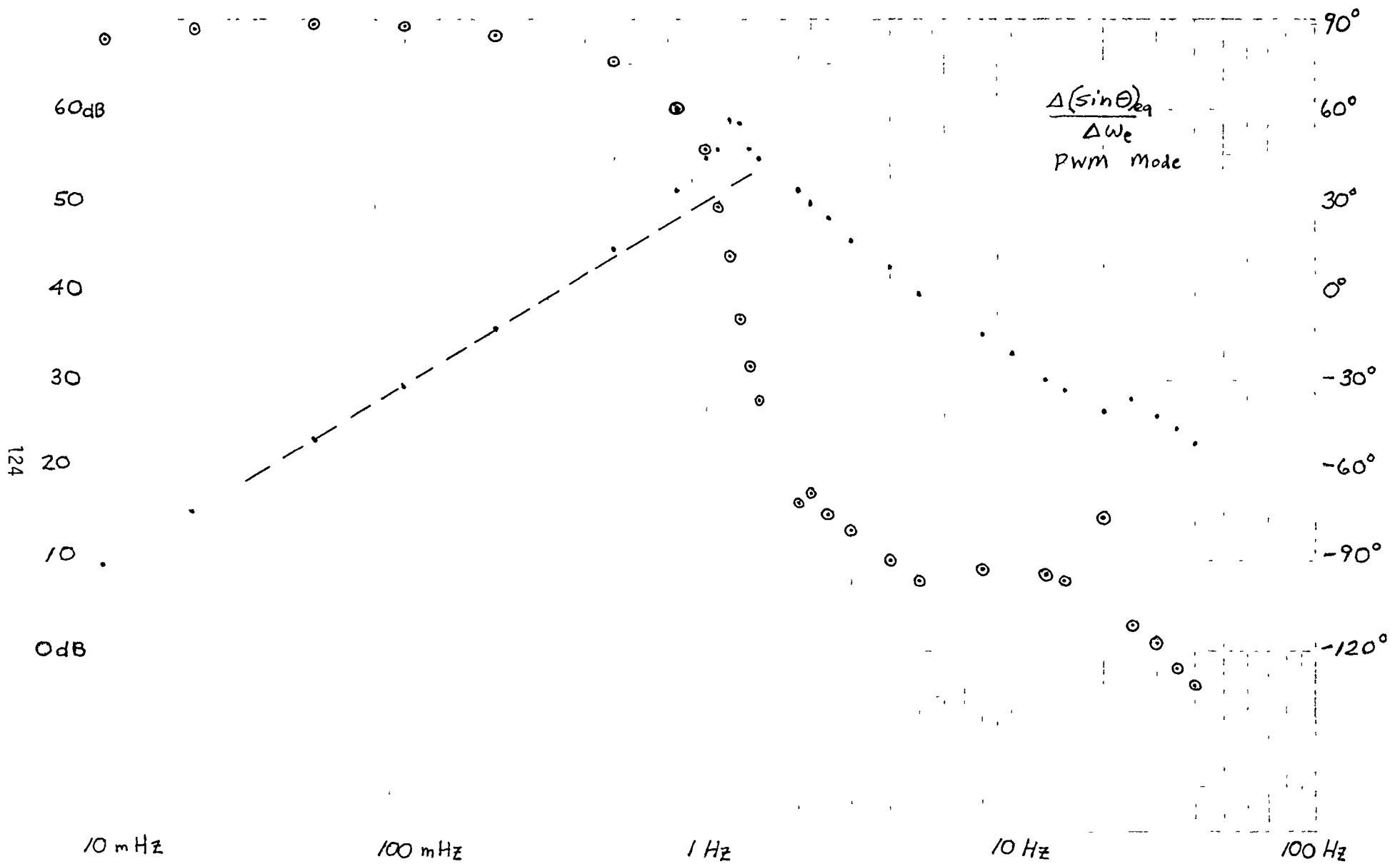
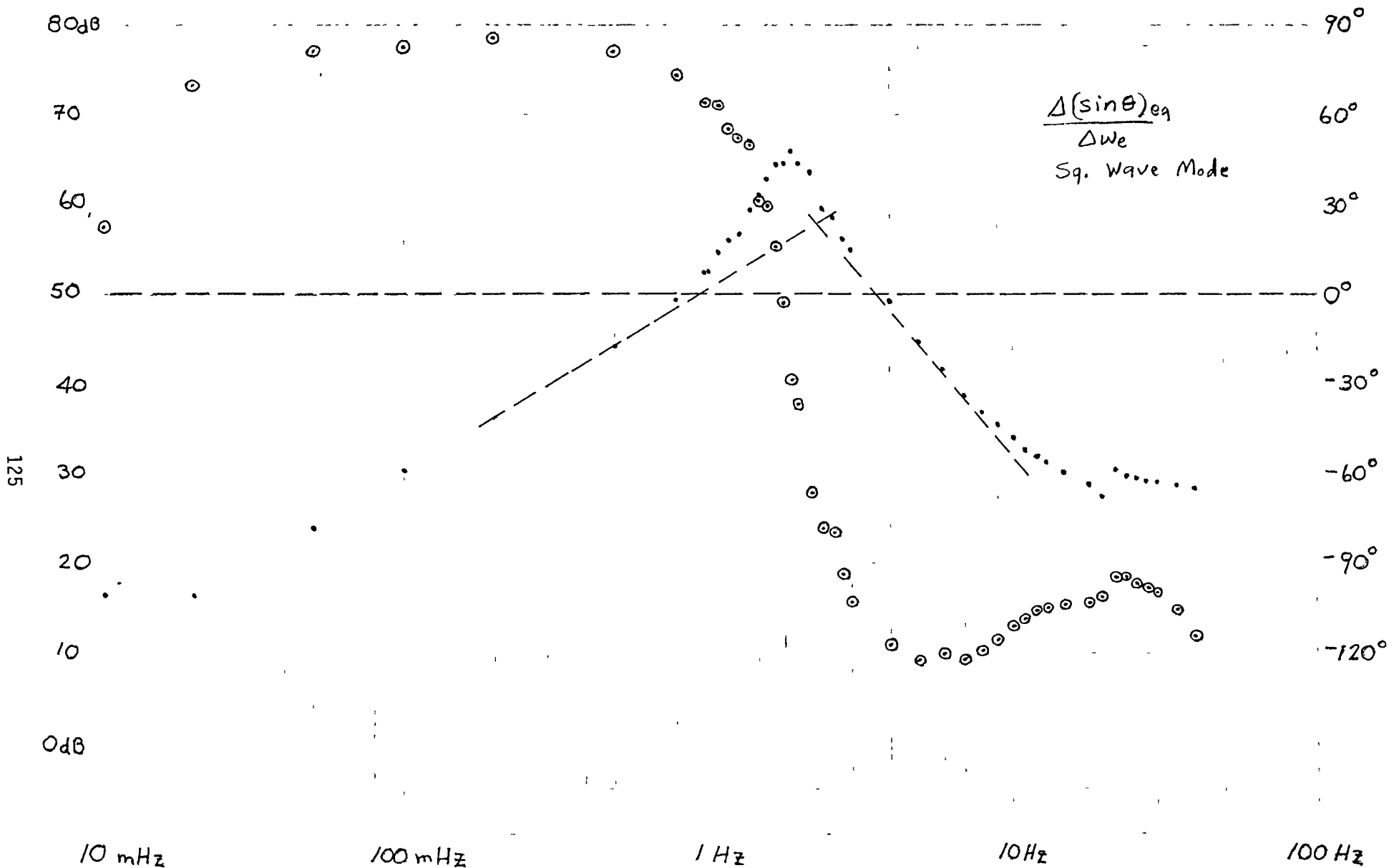


Figure 4.3.1 Overall Drive System Block Diagram



**Figure 4.3-2 Angle Loop Transfer Function in PWM**  
*Note: Magnitude is plotted as points with the scale (vertical) in db, Phase is plotted as circled points with the scale (vertical) in degrees, Frequency is the horizontal scale.*



**Figure 4.3-3** Angle Loop Transfer Function in Square Wave  
*Note: Magnitude is plotted as points with the scale (vertical) in db, Phase is plotted as circled points with the scale (vertical) in degrees, Frequency is the horizontal scale.*

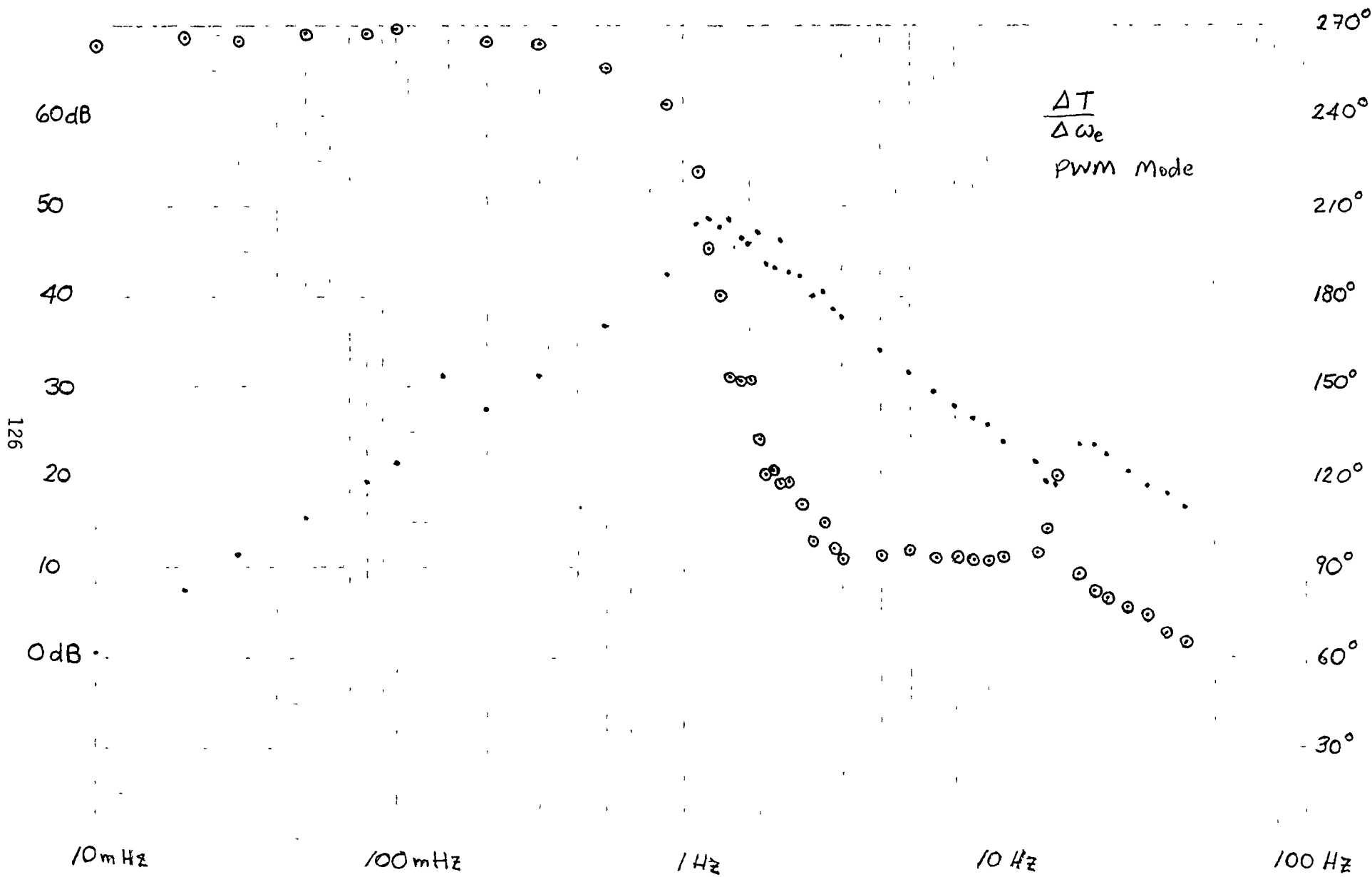


**Figure 4.3-4 Torque Loop Transfer Function in PWM**

*Note: Magnitude is plotted as points with the scale (vertical) in db, Phase is plotted as circled points with the scale (vertical) in degrees, Frequency is the horizontal scale.*



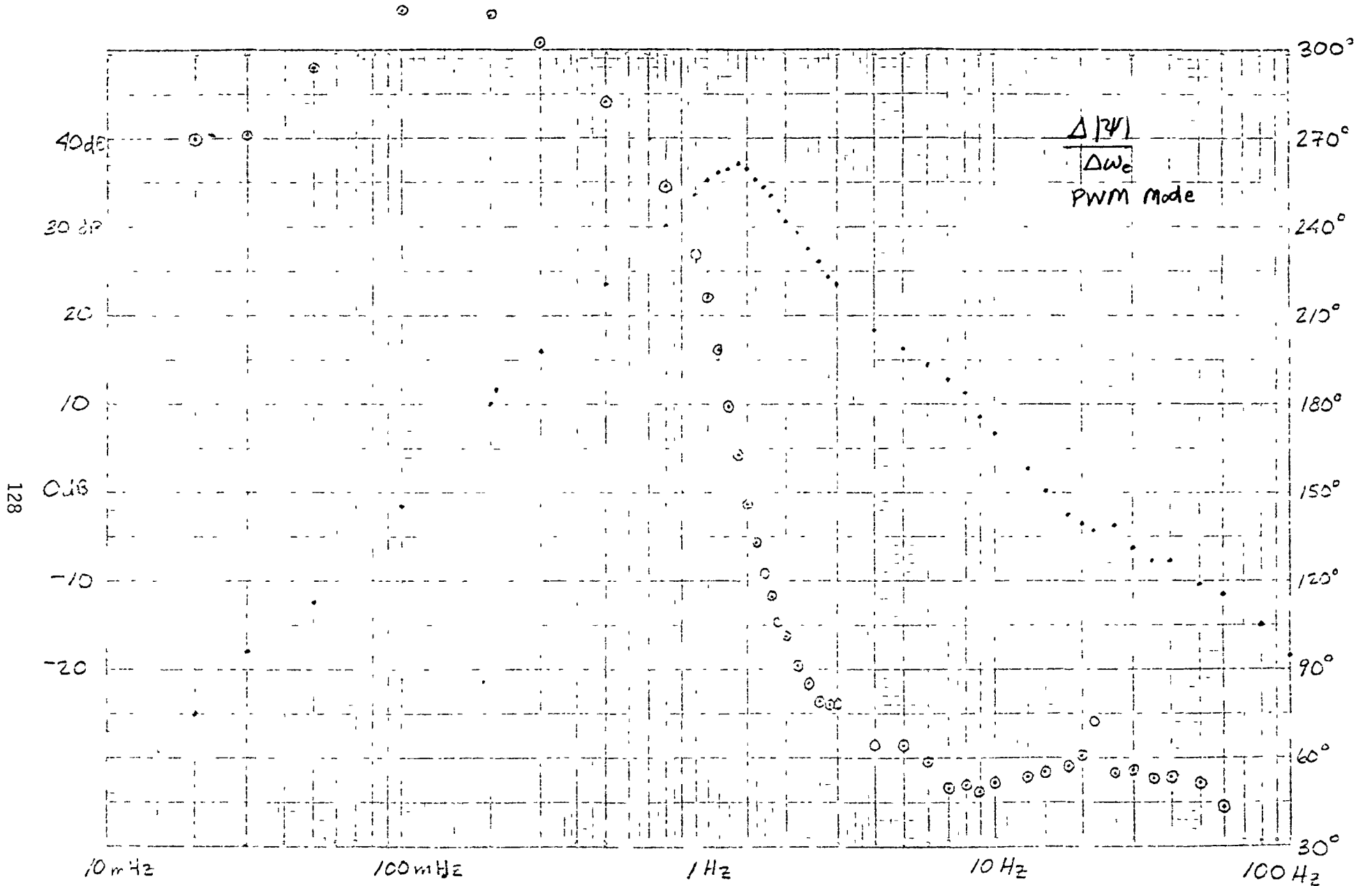


Figure 4.3-6 Flux Loop Transfer Function in PWM

Note: Magnitude is plotted as points with the scale (vertical) in db, Phase is plotted as circled points with the scale (vertical) in degrees, Frequency is the horizontal scale.

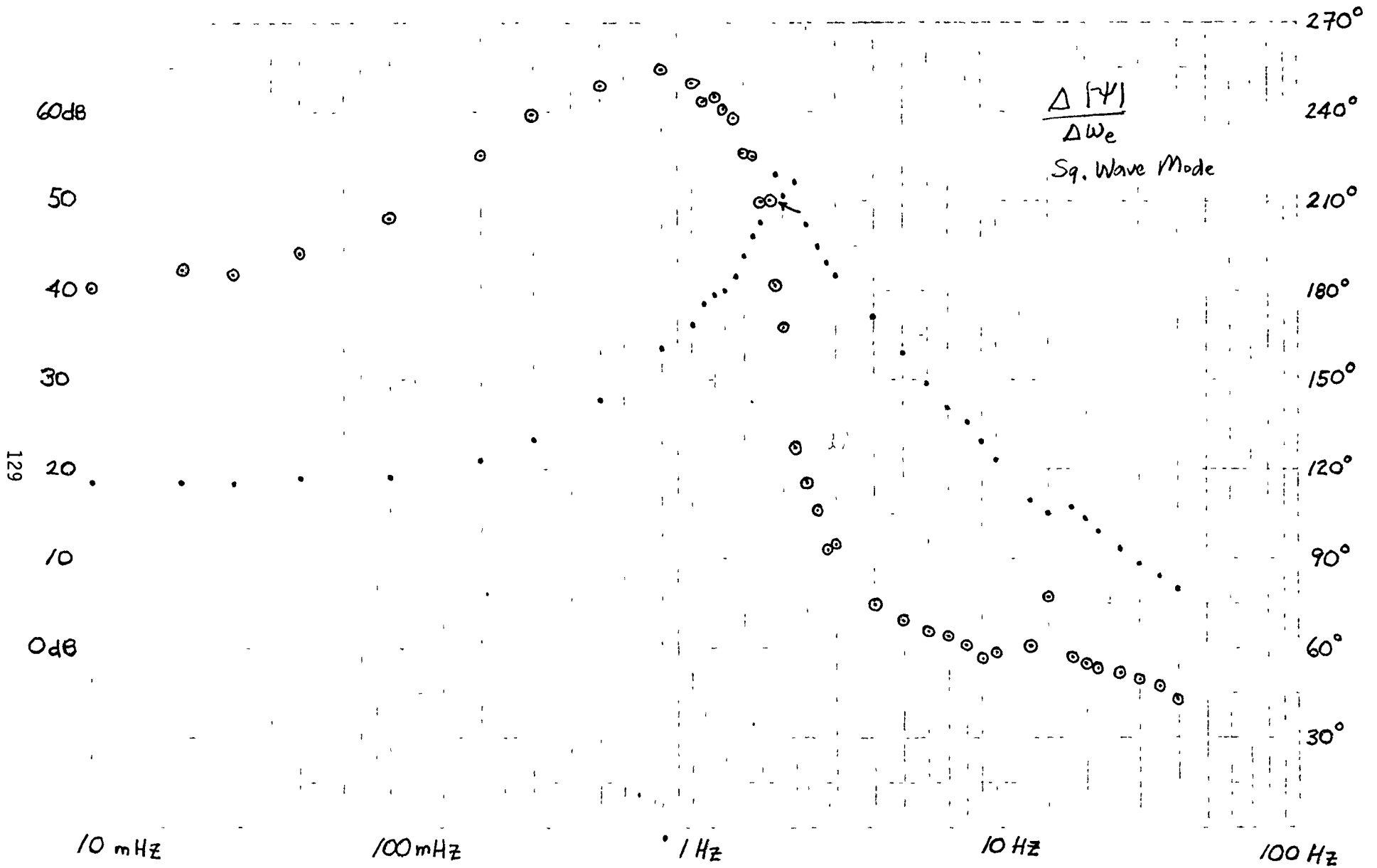
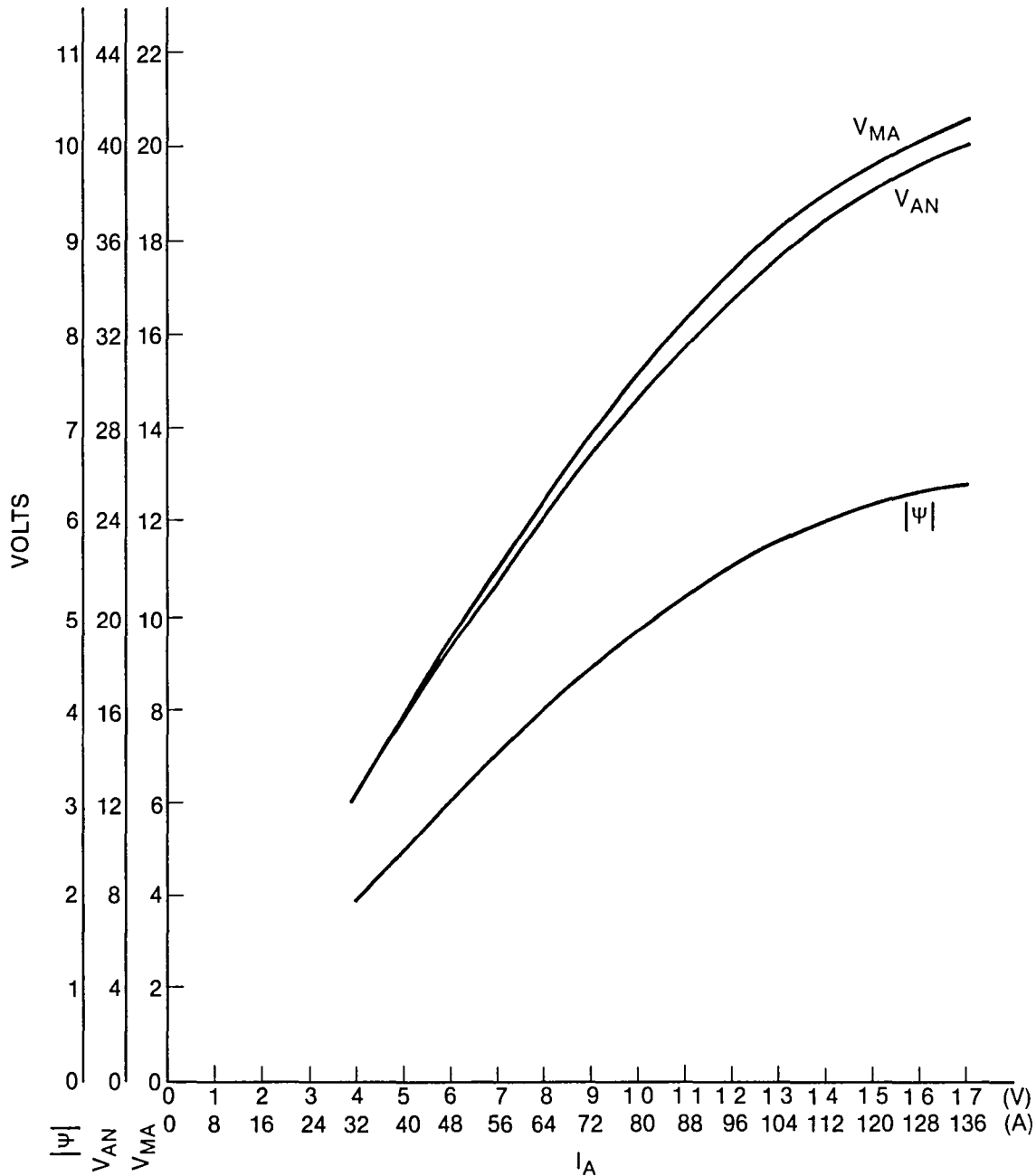


Figure 4.3-7 Flux Loop Transfer Function in Square Wave  
 Note: Magnitude is plotted as points with the scale (vertical) in db, Phase is plotted as circled points with the scale (vertical) in degrees, Frequency is the horizontal scale.

#### 4.4 MOTOR NO-LOAD EXCITATION

A motor excitation test was performed, using the controller as the power source, to determine the motor flux level and calibration. The results are presented in Figure 4.4-1. The conditions are no motor loading, base speed (180 Hz), and square wave mode. The flux magnitude ( $|\text{FLUX}|$ ), fundamental air gap voltage ( $V_{MA}$ ), and fundamental line-to-neutral voltage ( $V_{AN}$ ) were measured as a function of fundamental current ( $I_A$ ). The results indicate good agreement with other no-load sine wave tests, however, saturation is approached more rapidly than predicted.



**Figure 4.4-1 Motor No Load Excitation**  
*Note: Vertical scales are in volts as measured at test points on control cards, Current (horizontal) scales are volts on control card (80 amps/volt) and amps.*

#### 4.5 MOTOR FLUX OPERATING POINT

The GE optimized induction motor is a motor designed to be run with an inverter. The required drive system torque could be met by a variety of motor current and flux operating points (Figure 4.5-1). The controls should call for a flux along the locus of minima (dashed line) in order to reduce inverter peak currents and reduce losses. The flux-torque function block in the control has this characteristic. Figure 4.5-1 was determined by maintaining constant torque and varying flux to find the operating points.

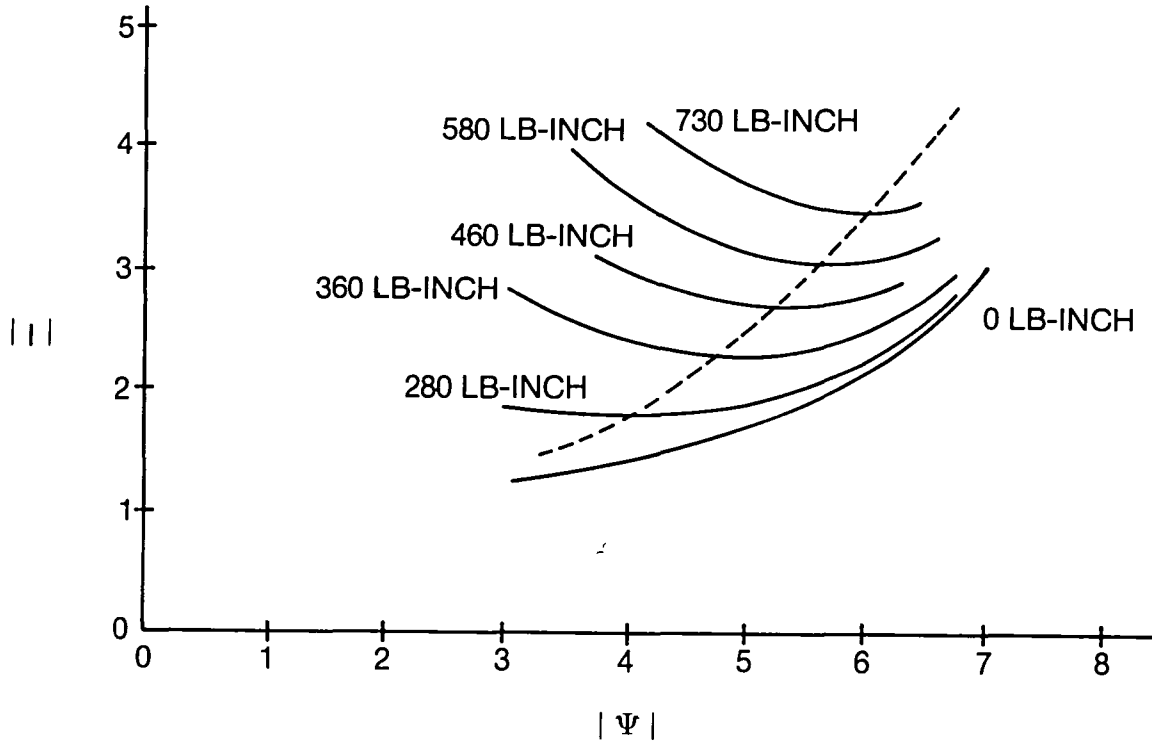


**Figure 4.5-1 Motor Flux Operating Point**  
*Note: Current (vertical) scale is 80 amps/volt, Flux (horizontal) scale is in volts on the control card.*

## 4.6 AC CURRENT WAVEFORMS

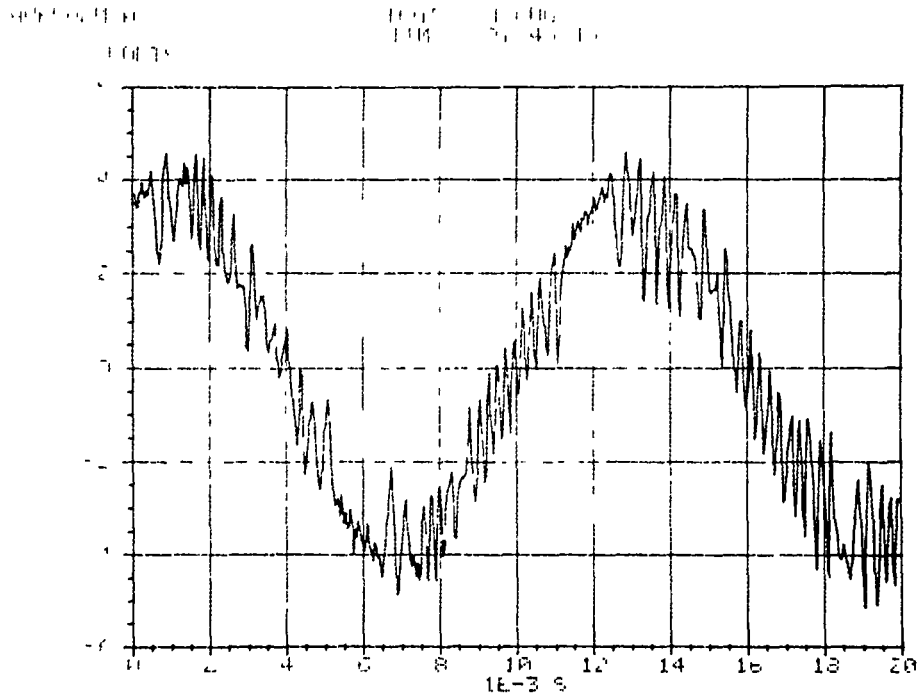
The ac controller with the current-controlled PWM delivers an improved sinusoidally shaped current waveform to the ac motor. The motor current has lower harmonic content than with other PWM techniques, resulting in lower harmonic losses and higher motor efficiency.

Figure 4-6-1 is the motor current waveform during PWM operation in motoring at 105 volts dc, 850 rpm and 87.1 N-m (64.2 lb-ft) of torque. Figure 4-6-2 is the frequency spectrum of this current waveform. The chopping frequency is swept over a frequency range of 500 to 4500 Hz, as discussed in Section 3-7-2. Note the two periods of almost no chopping in Figure 4-6-1, at 6 and 12 milliseconds.

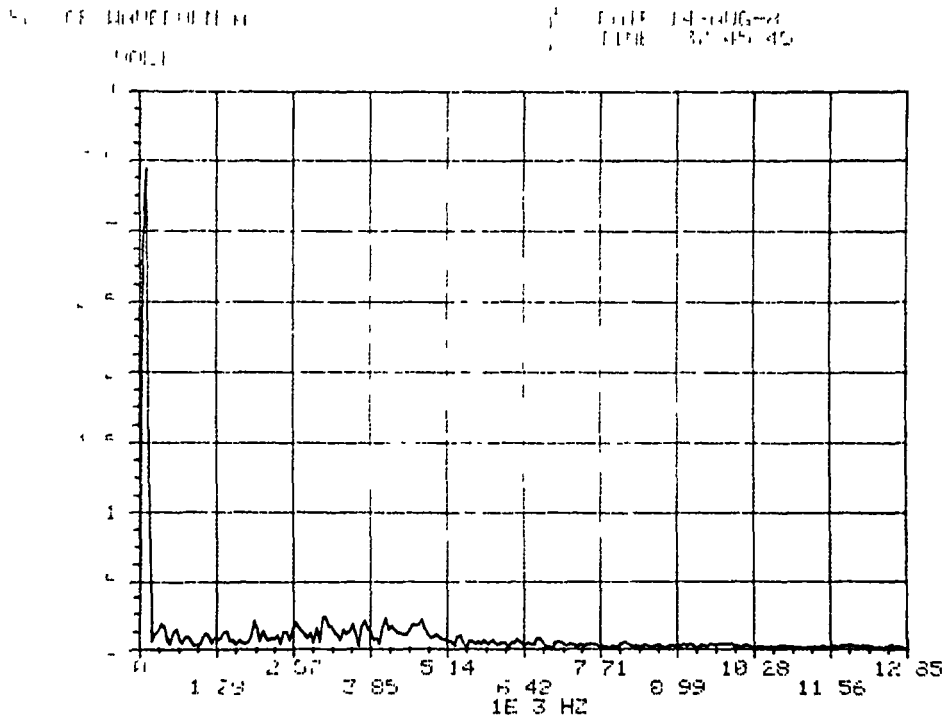
Figure 4-6-3 is the motor current waveform during square wave operation in motoring at 106 volts dc, 3230 rpm and 33.4 N-m (24.6 lb-ft) of torque. Figure 4-6-4 is the frequency spectrum of this current waveform. Note the low order harmonics in this square wave waveform. The fundamental at 3230 rpm is 318 Hz, the 5th harmonic shows up at 1590 Hz and the 7th shows up at 2226 Hz.

Figure 4-6-5 is the motor current waveform during PWM operation in regeneration at 454 rpm and 80.5 N-m (59.4 lb-ft) of torque. The chopping is nearly uniform over the cycle because the emf is low. Figure 4-6-6 is the frequency spectrum of this current waveform. The chopping frequency shows up clearly at about 4.3 kHz.

Figure 4-6-7 is the motor current waveform during square wave operation in regeneration at 3795 rpm and 22.2 N-m (16.8 lb-ft) of torque.



**Figure 4.6-1 Motor Current in PWM Motoring**  
*Note: Current (vertical) scale factor is 80 amps/volt, time (horizontal) scale is in milliseconds.*



**Figure 4.6-2 Frequency Spectrum of PWM Motoring Current**  
*Note: Current (vertical) scale factor is 80 amps/volt, frequency (horizontal) scale is in kilohertz.*

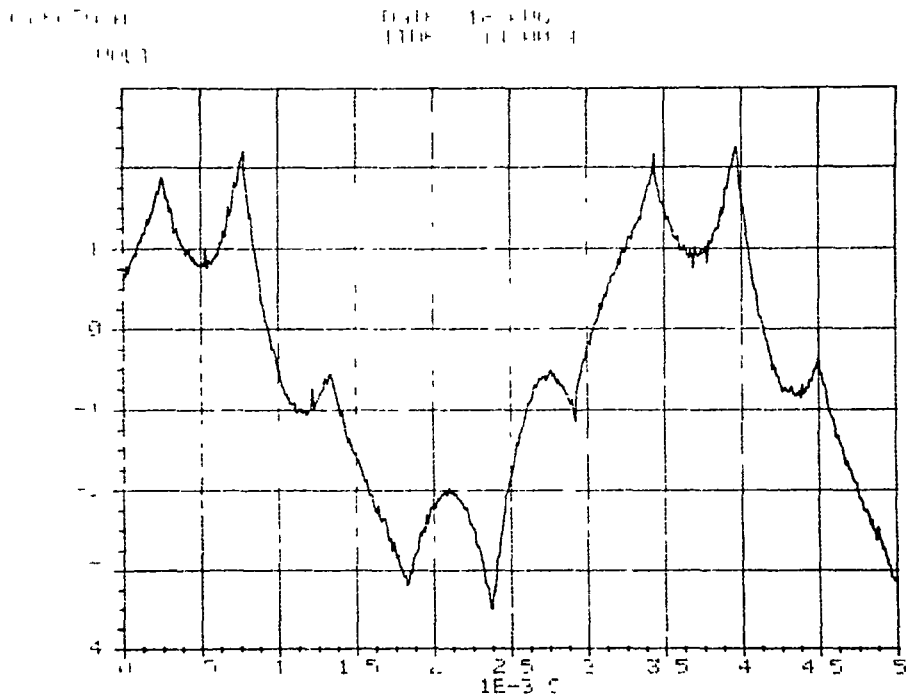


**Figure 4.6-3 Motor Current in Square Wave Motoring**  
*Note: Current (vertical) scale factor is 80 amps/volt, time (horizontal) scale is in milliseconds. Waveform is slightly offset from zero.*

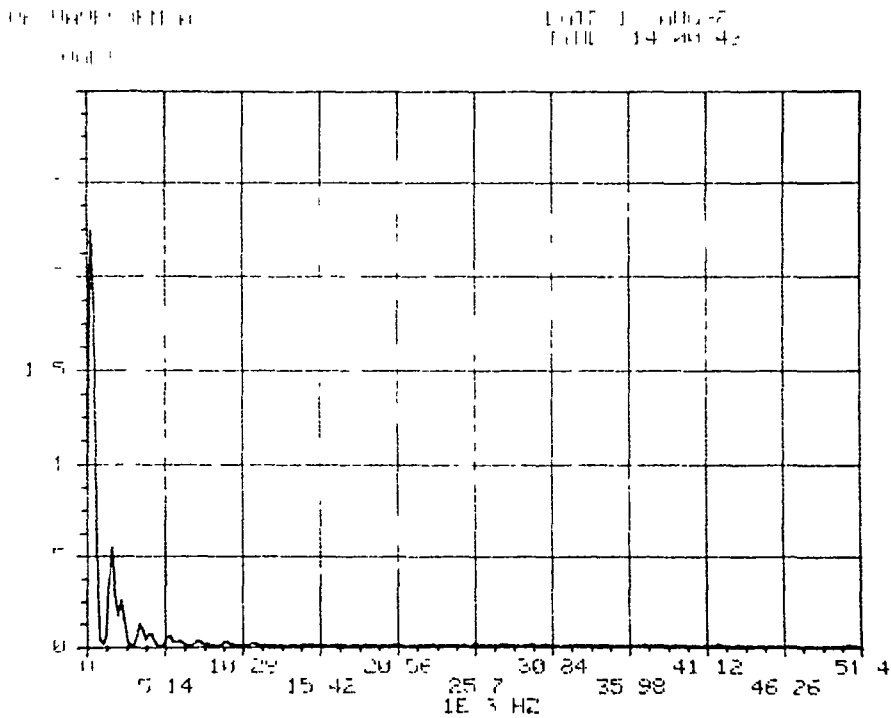


**Figure 4.6-4 Frequency Spectrum of Square Wave Motoring Current**  
*Note: Current (vertical) scale factor is 80 amps/volt, frequency (horizontal) scale is in kilohertz.*

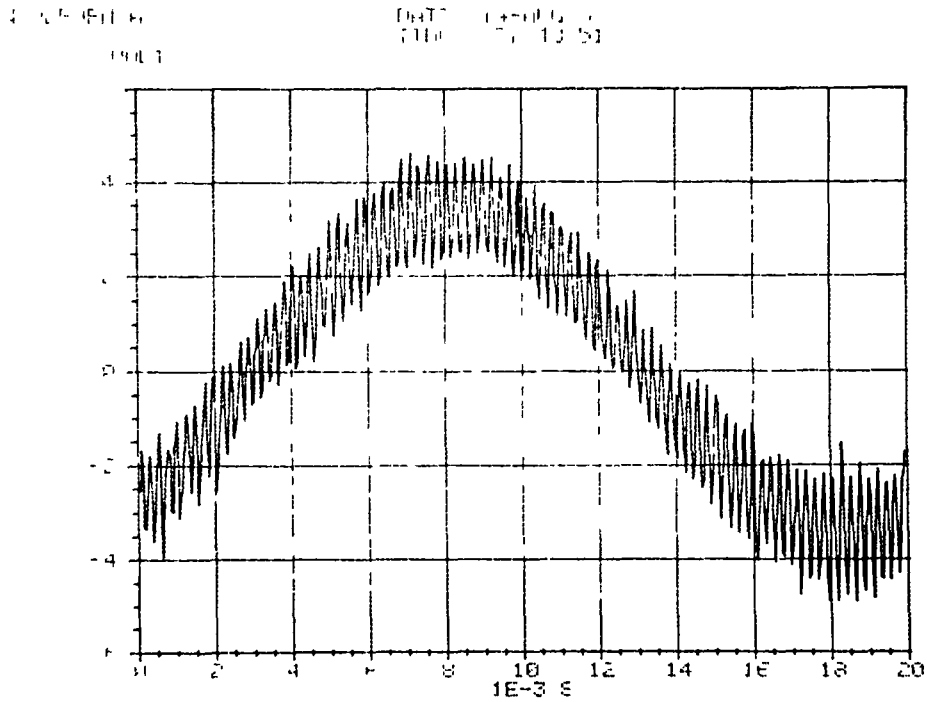


**Figure 4.6-5 Motor Current in PWM Regenerative Braking**  
*Note: Current (vertical) scale factor is 80 amps/volt, time (horizontal) scale is in milliseconds.*

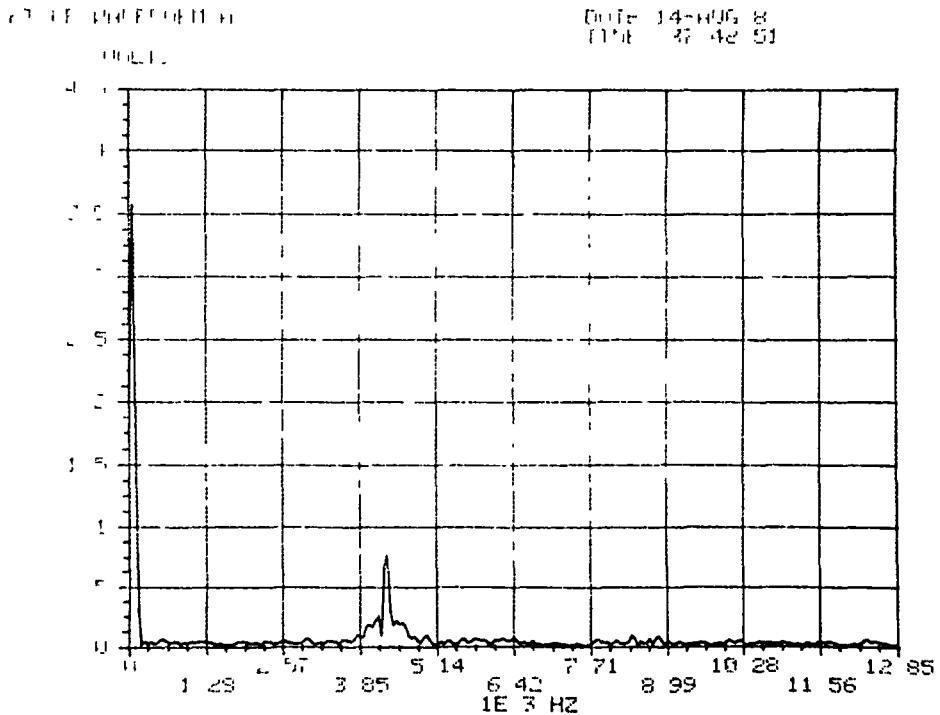


**Figure 4.6-6 Frequency Spectrum of PWM Regenerative Braking Current**  
*Note: Current (vertical) scale factor is 80 amps/volt, frequency (horizontal) scale is in kilohertz.*

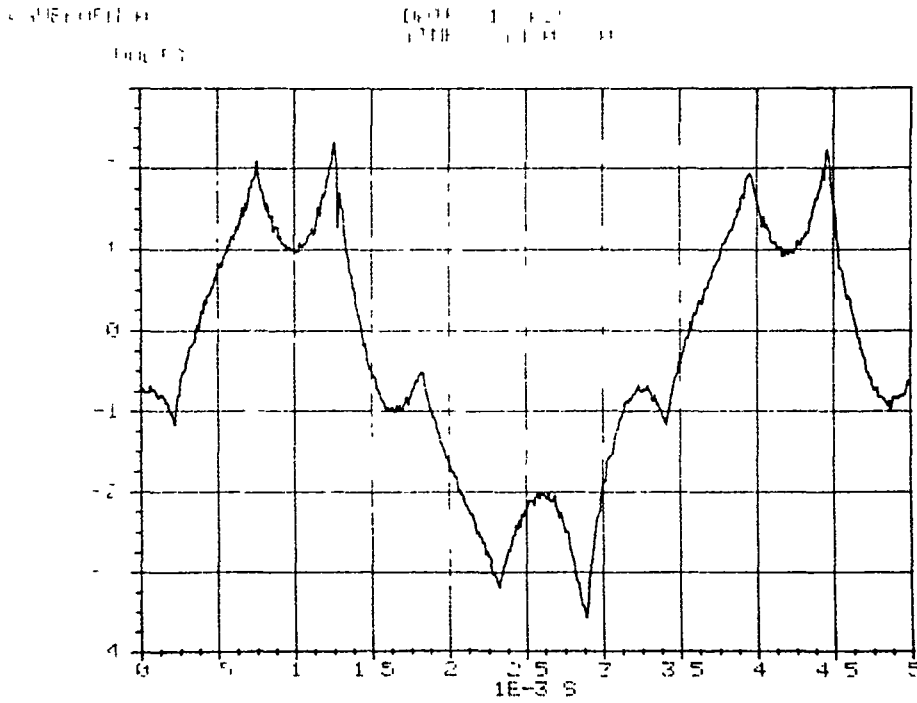


**Figure 4.6-7 Motor Current in Square Wave Regenerative Braking**  
*Note: Current (vertical) scale factor is 80 amps/volt, time (horizontal) scale is in milliseconds.*

### 4.7 AC VOLTAGE WAVEFORMS

The ac voltage waveforms of interest are those in PWM operation, both in motoring and regenerative braking. Figure 4 7-1 is the line-to-neutral motor voltage waveform during PWM operation in motoring at 106 volts dc, 1850 rpm and 66 4 N-m (49 lb-ft) of torque. The motor air gap flux voltage waveform resulting from the integration of the air gap flux sensing coil voltage is shown in Figure 4 7-2. This is the voltage at test point 8 on EP7644CTQA. The corresponding motor current waveform is shown in Figure 4 7-3.

Figure 4 7-4 is the line-to-neutral motor voltage waveform during PWM operation in regenerative braking at 123 volts dc, 1850 rpm, and 55 6 N-m (41 lb-ft) of torque. The resultant air gap flux voltage waveform is shown in Figure 4 7-5 and the corresponding motor current waveform is shown in Figure 4 7-6.

Note the sinusoidal shape of the current and flux voltage, even with the relatively few number of chops in the cycle. The motor voltage has the expected quasi-square wave shape (reference Figure 3 4 5-1) with the notches due to PWM chopping.

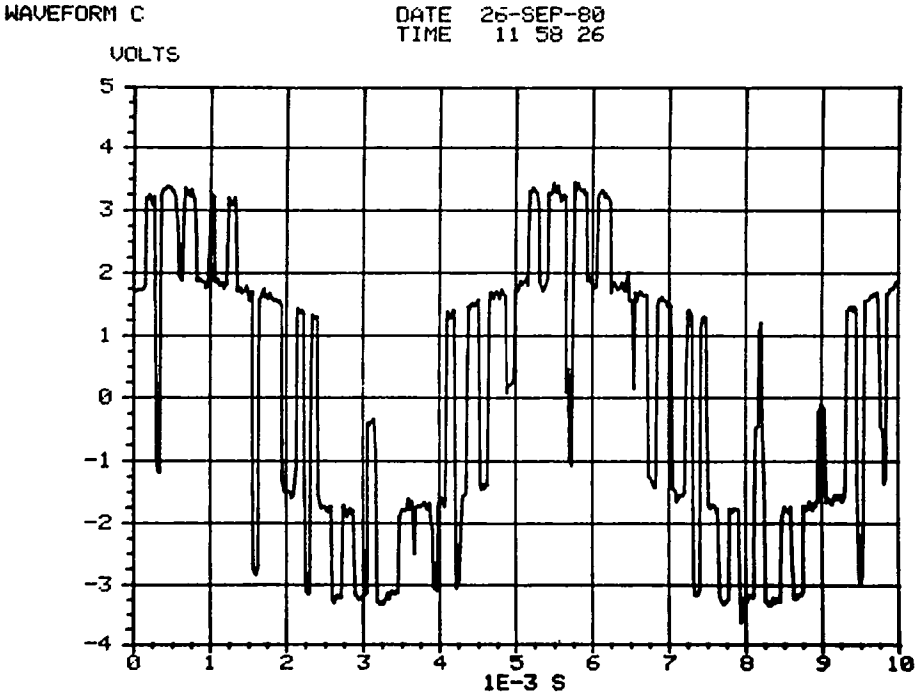


**Figure 4.7-1 Motor Line-to-Neutral Voltage in PWM Motoring**  
*Note: Voltage (vertical) scale factor is 20 volts/volt, time (horizontal) scale is in milliseconds.*

WAVEFORM B

DATE 26-SEP-60  
TIME 11 58 13

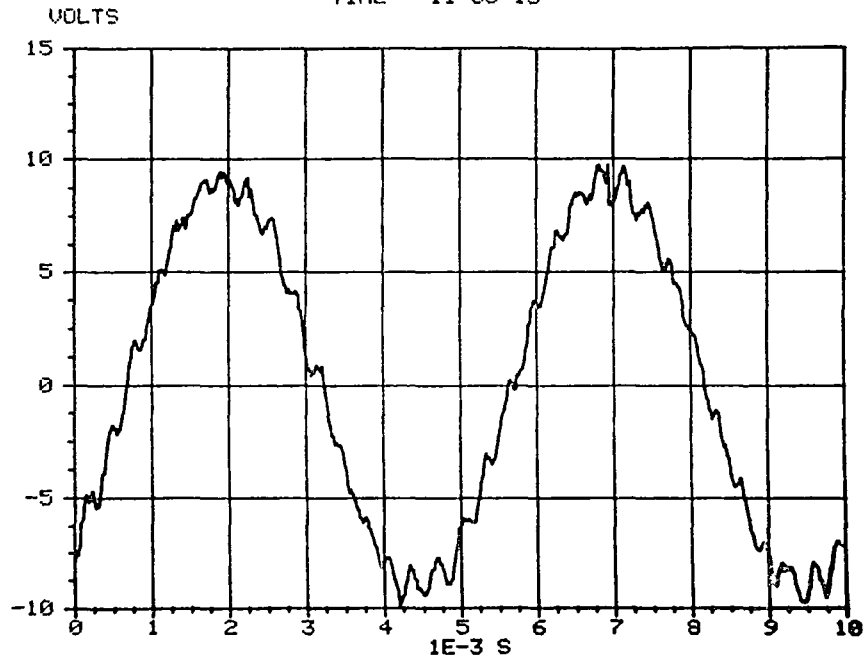


**Figure 4.7-2** Motor Air Gap Flux Voltage in PWM Motoring  
*Note: Voltage (vertical) scale is in volts, time (horizontal) scale is in milliseconds.*

WAVEFORM A

DATE 26-SEP-60  
TIME 11 52 00

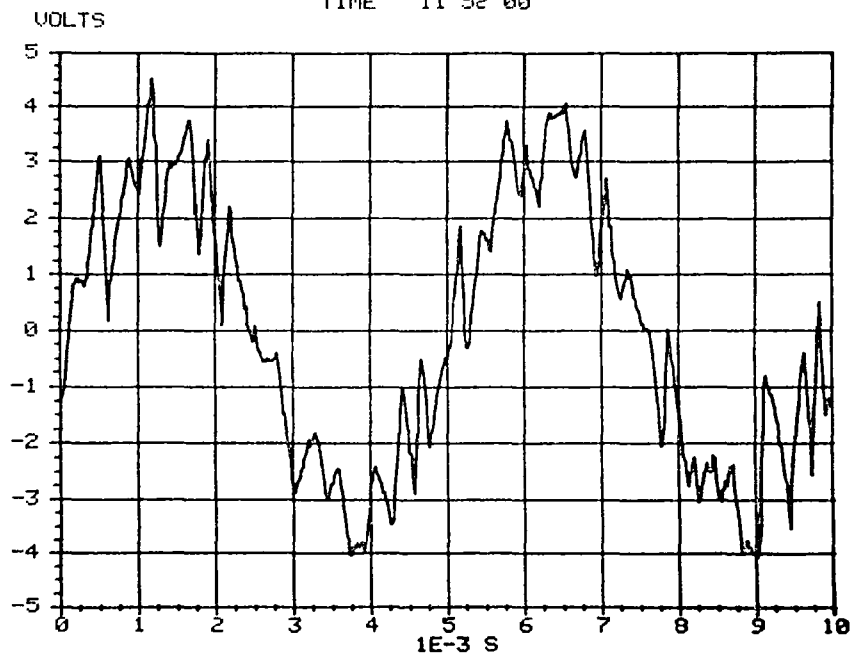


**Figure 4.7-3** Motor Current in PWM Motoring  
*Note: Current (vertical) scale factor is 80 amps/volt, time (horizontal) scale is in milliseconds.*

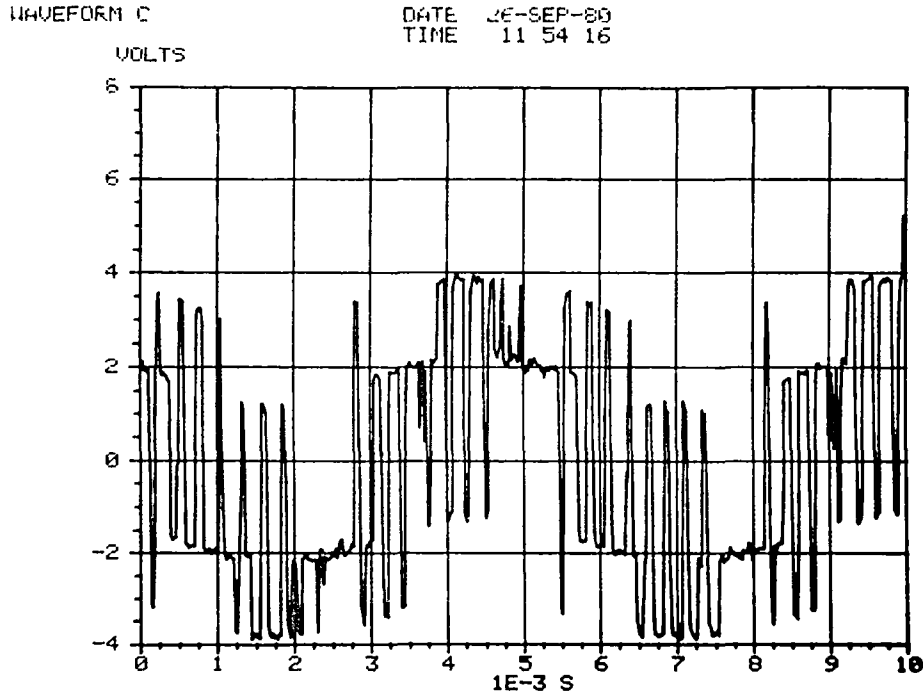


**Figure 4.7-4** Motor Line-to-Neutral Voltage in PWM Regenerative Braking  
*Note: Voltage (vertical) scale factor is 20 volts/volt, time (horizontal) scale is in milliseconds.*

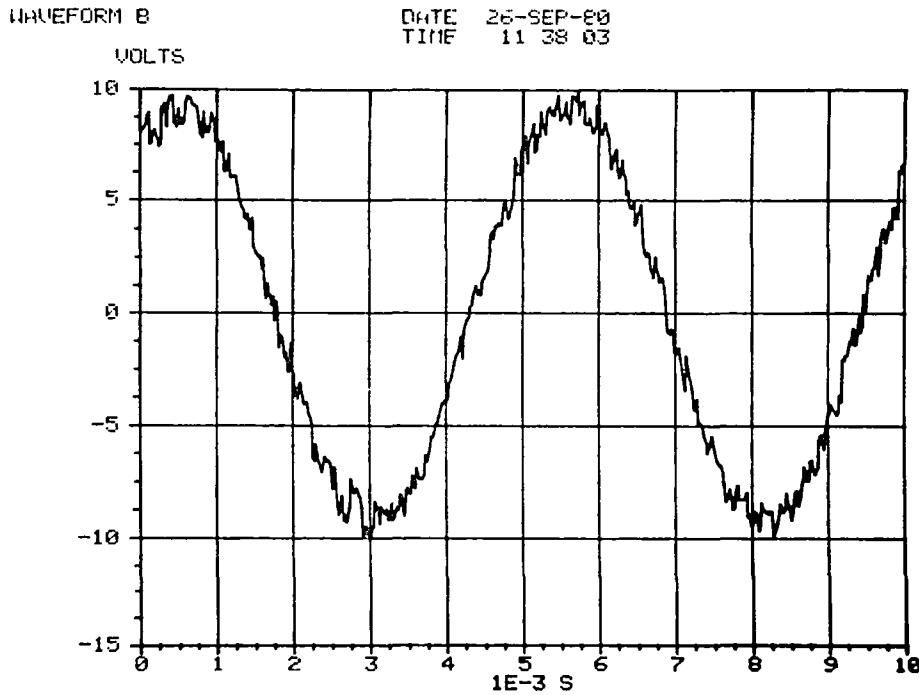


**Figure 4.7-5** Motor Air Gap Flux Voltage in PWM Regenerative Braking  
*Note: Voltage (vertical) scale is in volts, time (horizontal) scale is in milliseconds.*

WAVEFORM A

DATE 26-SEP-80  
TIME 11 37 50

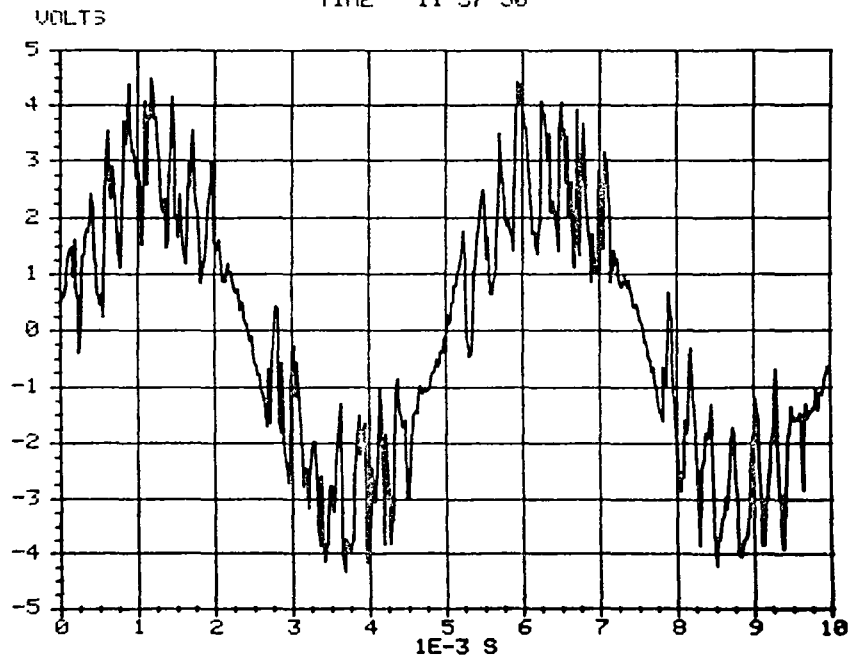


**Figure 4.7-6** Motor Current in PWM Regenerative Braking  
*Note: Current (vertical) scale factor is 80 amps/volt, time (horizontal) scale is in milliseconds.*

## 4.8 POWER MODULE WAVEFORMS

The power module voltage (collector-emitter) and current (total collector) during switching, especially turn-off, are of particular interest. The voltage and current waveforms were taken during PWM motoring operation at 600 amps peak with a 110 volt dc bus. The voltage at the turn-off of 600 amps is shown in Figure 4.8-1. The peak overshoot voltage is 240 volts. The current at turn-off is shown in Figure 4.8-2. The current fall time (90% to 10%) is about 1.5 microseconds.

The power module base drive current for one cycle of square wave motoring operation is shown in Figure 4.8-3. The figure shows both the forward current (between 3 and 4 amps) during the conduction time (0.8 milliseconds) of this half-phase of the inverter and the reverse current spike at turn-off (3.7 amps) to initiate the off time of this half-phase. Figure 4.8-4 is an expanded view of the current at turn-on showing the rise of the base current in about 0.5 microseconds. Figure 4.8-5 is an expanded view of the current at turn-off showing a peak reverse current of 3.9 amps and a total turn-off time (including storage time) of about 4 microseconds (measured from zero crossing to abrupt change in reverse current).

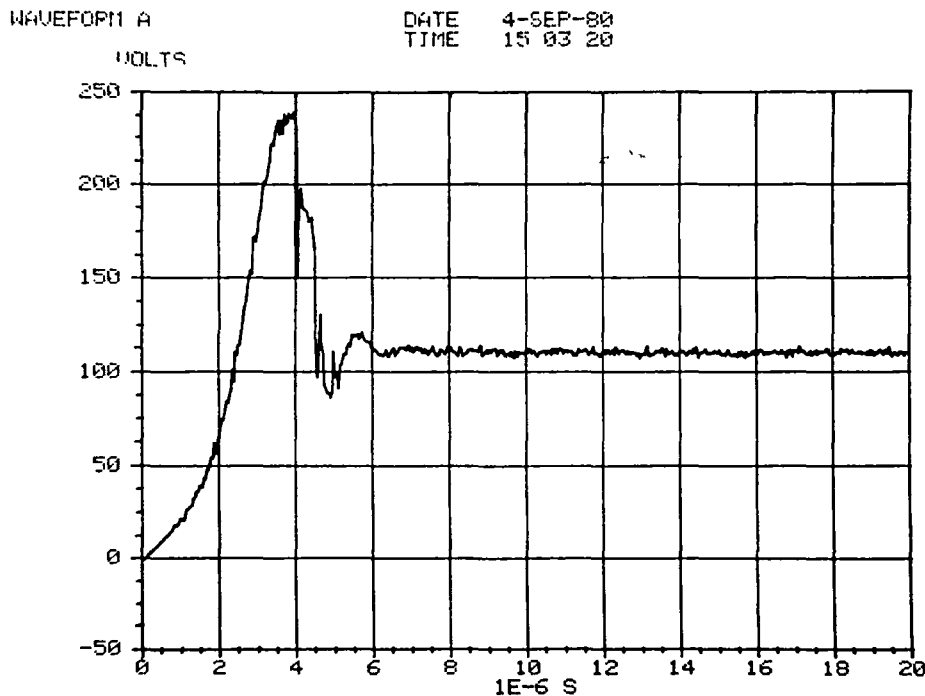


**Figure 4.8-1 Power Module Voltage at Turn-off in PWM Motoring**  
*Note: Voltage (vertical) scale is in volts, time (horizontal) scale is in microseconds.*

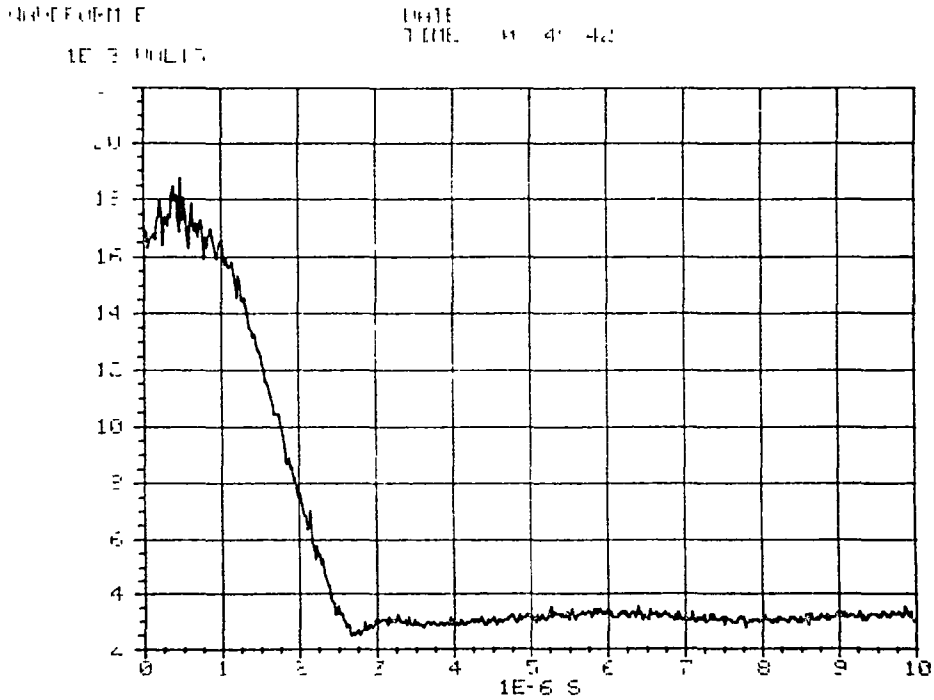


**Figure 4.8-2 Power Module Current at Turn-off in PWM Motoring**  
*Note: Current (vertical) scale factor is 40 amps/millivolt, time (horizontal) scale is in microseconds. Actual zero current is at 3 millivolts in waveform.*

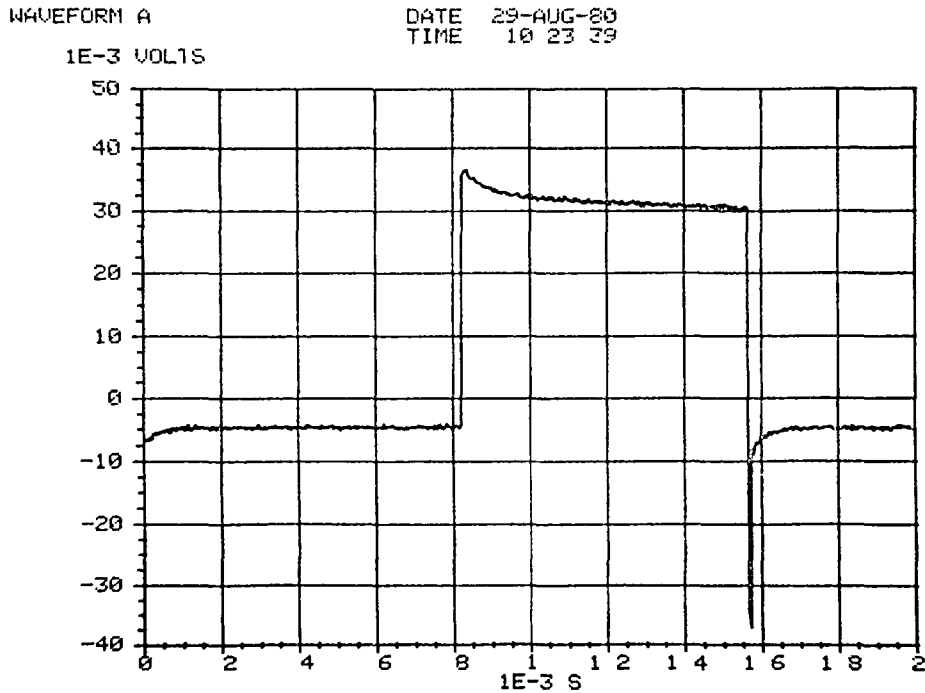


**Figure 4.8-3 Power Module Base Drive Current in Square Wave Motoring**  
*Note: Current (vertical) scale factor is 1 amp/10 millivolts, time (horizontal) scale is in milliseconds.*

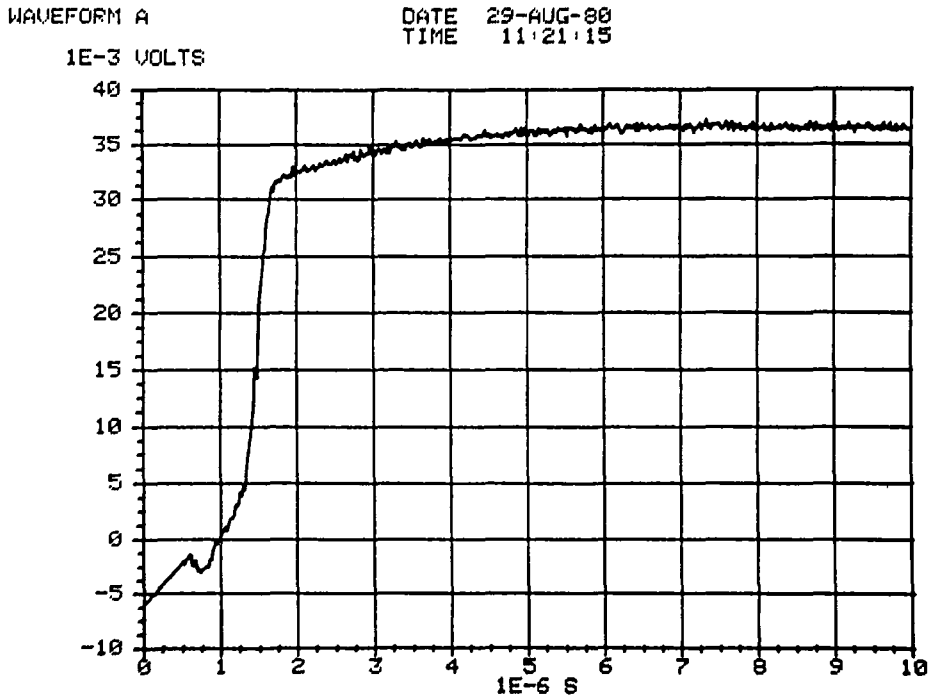


**Figure 4.8-4 Power Module Base Drive Turn-on Current in Square Wave Motoring**  
*Note: Current (vertical) scale factor is 1 amp/10 millivolts, time (horizontal) scale is in microseconds.*

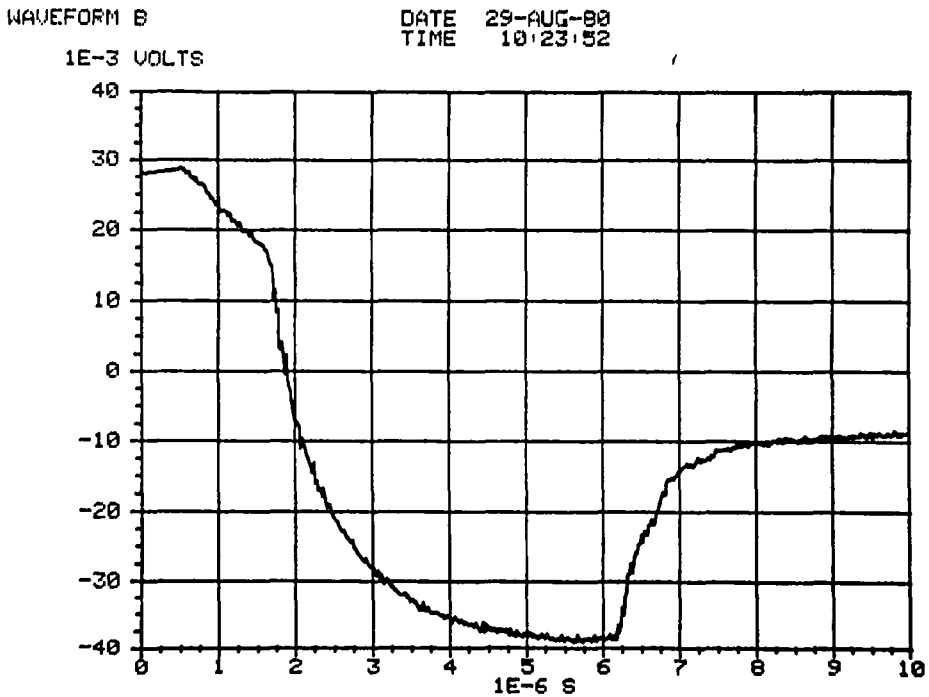


**Figure 4.8-5 Power Module Base Drive Turn-off Current in Square Wave Motoring**  
*Note: Current (vertical) scale factor is 1 amp/10 millivolts, time (horizontal) scale is in microseconds.*

## 4.9 CONTROLLER PERFORMANCE CHARACTERIZATION

The complete ac drive system was loaded with the flywheel and dynamometer as described in Section 4.2. The data acquisition system recorded motor, inverter, and control parameters as illustrated by the sample computer printout (Figure 4.9-1). The data listed under **\*\*Motor\*\*** are measured (or calculated from the measurements) motor values. The data under **\*\*Inverter\*\*** are also measured values. The data under **\*\*\*Controller\*\*\*** are in two groups, the feedback signal data and command signal data. The feedback signals are scaled, except angle which is in control volts. The commands are in control volts, except for frequency

```

***** AC CONTROLLER SUMMARY *****
DATE 24-SEPT-80                FINAL      47

** MOTOR **                    ** INVERTER **

AC PWR      SPEED              AC PWR      EFFICIENCY
WATTS       RPM                WATTS
13903.81    1856.69              13903.81    .92

SHAFT PWR   TORQUE             DC PWR
WATTS       LB/FT                    WATTS
12885.60    48.87                    15000.26

EFFICIENCY  SLIP                 DC CURRENT   DC VOLTAGE
            HZ                    AMPS         VOLTS
.93        18.00                142.70      105.66

*** CONTROLLER ***

"FEEDBACK SIGNALS"           "COMMANDS"

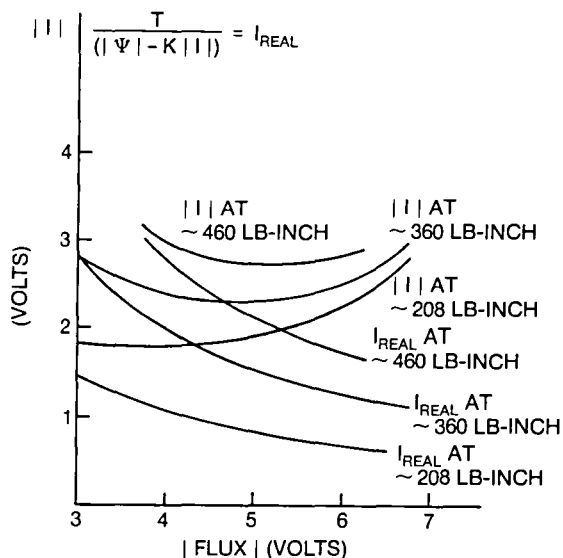
IAC      ANGLE              IAC      ANGLE
AMPS     VOLT                AMPS     VOLT
253.25   2.67                10.00    2.91

FLUX     TORQUE,ELEC.        FLUX     FREQ.
VOLT SEC. LB.FT.           VOLT SEC. HZ.
35.32    48.25                2.43     198.91

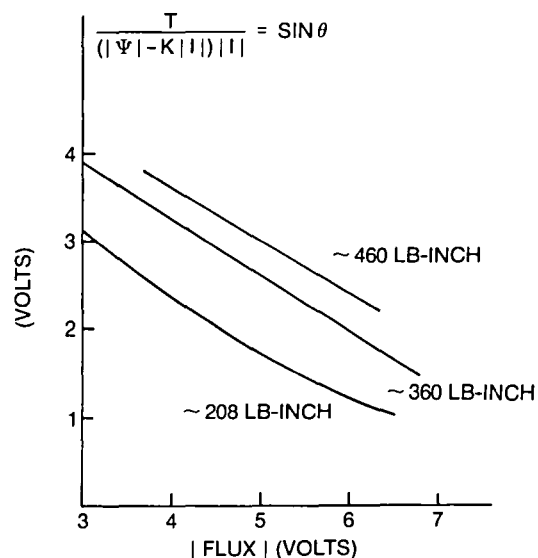
```

Figure 4.9-1 Computer Printout

The calculations of  $I_{REAL}$  and  $SIN\theta$  from the feedback signals and the d-q axis calculation of torque are shown in Figures 4.9-2 and 4.9-3, respectively. These were determined from actual test data by measuring the control voltages and are plotted versus  $|FLUX|$  at constant torque levels. The  $|I|$  is also plotted versus  $|FLUX|$ , similar to Figure 4.5-1. These calculations are shown in Figures 3.5.3-3 and 3.6-3a. The relationships of  $|FLUX|$ ,  $|I|$ ,  $SIN\theta$ , and  $I_{REAL}$  as a function of torque (Figure 4.9-4) were also derived from actual test measurements of the control voltage signals.



**Figure 4.9-2 Real Current Computation**  
*Note: I<sub>REAL</sub> and |I| (vertical) scales are in control volts, |FLUX| (horizontal) scale is in control volts.*



**Figure 4.9-3 Angle Computation**  
*Note: SIN theta (vertical) scale is in control volts, |FLUX| (horizontal) scale is in control volts.*

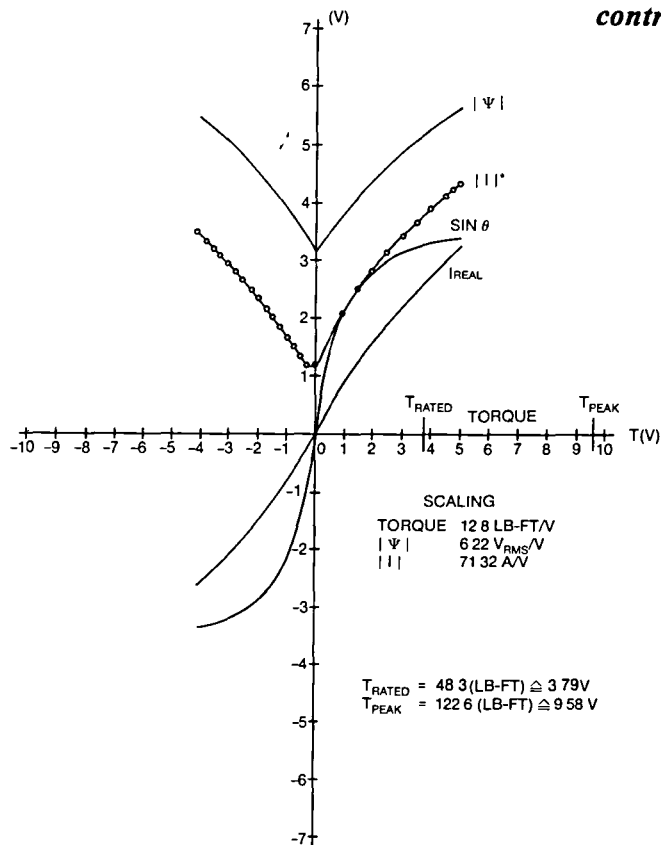


**Figure 4.9-4 Control Functions Related to Torque**

The torque-speed curves of Figure 4.9-5 are plotted from test data, with the motor flux voltage and motor current also shown. The torque and speed are at the gear box shaft after the 2.923:1 reduction. The current is the average of the three-phase full-wave rectified ac motor line current. The flux is scaled from the controlled voltage. Three cases, A, B, and C, are shown for the three different accelerator commands, demonstrating the part-throttle drive system performance. Case B is the J227a-D cycle 26 hp requirement. Case A is a higher power level (about twice-rated torque) and Case C is a lower power level (about half-rated torque). The rated torque at the gear box shaft is 66.0 N-m (48.7 lb-ft) at 1833 rpm, i.e., 17 hp. Case C shows that 37 N-m (27 lb-ft) of torque could maintain up to 3700 rpm, with a current of 180 amps and a flux voltage of 27 volts. In Case B, the 73 N-m (54 lb-ft) of torque is held up to 2500 rpm, with 270 amps and 33 volts flux, the flux then begins to decrease and the output is limited to 26 hp. In Case A, the flux is lower than desired between 1200 and 2500 rpm due to the motor approaching saturation. The torque output follows this flux with a current between 420 and 370 amps. A 35 hp limit is reached at 2700 rpm. The reduction of flux at reduced torque levels by the controls is apparent from this graph (reference Section 3.6.5).

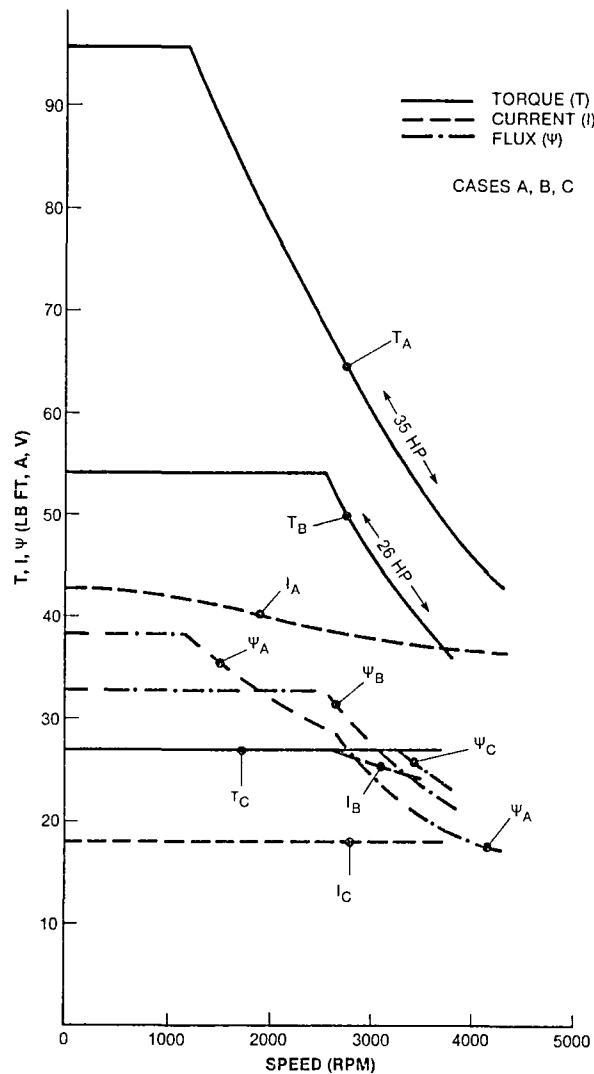


Figure 4.9-5. System Torque-Speed Performance

#### 4.10 CONTROLLER LOSS SEPARATION

The principal individual controller losses were measured or calculated at four operating conditions, for which the total controller, motor, and system parameters were measured with the data acquisition system (Table 4 10-1) The operating conditions were in the PWM and square wave modes in motoring and regenerative braking Note that the measurement with the data acquisition system does not include the 12-volt auxiliary power loss (control electronics and base drives), but does include the blower loss These two losses have almost the same value (Table 4 10-1) Since the blowers were oversized and were included only in regard to the engineering model system, the inclusion of their losses accounts very well for the base drive and control electronics losses

The principal controller losses are listed in Table 4 10-1 The controller losses include some constant losses (independent of power level, etc ) and variable losses The variable losses depend not only on power level, but also on ac motor frequency, chopping (PWM) frequency, dc voltage, and ac current magnitude The behavior of the losses is discussed more fully in Section 4 11 The loss separation results in Table 4 10-1 are in good agreement with the total inverter loss measured by the data acquisition system The small differences between them were included as miscellaneous loss, which were due to conductor loss, fuses, contactor/relay coils, etc The power module switching loss and snubber loss are observed to be higher in PWM than in square wave, due to the high chopping frequency The power module conduction loss depends basically on the ac motor current magnitude The base drive loss is somewhat higher in square wave because the transistors are driven for a complete half-cycle

Referring to the separate losses in Table 4.10-1, a few observations about losses can be made The power module conduction loss could be reduced by raising the battery system voltage to reduce the motor rms current, thus reducing the rms transistor and diode current This would also reduce other current-related losses Faster switching transistors and diodes could reduce the combined snubber and switching losses Transistors with a higher voltage rating (larger SOA) could reduce the size of the snubber capacitors, thus reducing the snubber loss

**Table 4.10-1**  
**SEPARATION OF LOSSES**

<b>Operating Point</b>				
Drive System Mode	Motoring	Motoring	Regen	Regen
Output shaft torque (lb-ft)*	97 02	57 33	-96 19	-53.63
Output shaft speed (rpm)*	1093	3228	1242	4055
Inverter operating mode	PWM	SW	PWM	SW
Inverter output current (A)†	421	379	429	294
Inverter frequency (Hz)	108 99	327 01	119 00	382.08
DC voltage (V)	104 41	102 06	120 20	124 27
DC current (A)	181 38	285 89	-92 71	-214 68
Inverter input power (W)	19019	29196	-15298	-28835
Inverter output power (W)	16377	27315	-11139	-26817
Inverter loss (W)	2642	1881	4159	2018
Inverter efficiency (%)	86 1	93 6	72.8	93.0
<b>Loss Separation</b>				
Blower loss (W)	150	150	264	264
Control electronics loss (W)‡	48	48	48	48
Power modules conduction loss (W)	1560	1340	1610	1090
Power modules switching loss (W)	350	118	960	210
Snubbers loss (W)	480	150	1140	270
Base drivers loss (W)‡	113	185	113	185
Miscellaneous loss (W)	102	123	185	184
Total controller loss (W)	2803	2114	4320	2251

\*At the gear box shaft after the 2 923 1 reduction

†Three-phase full wave rectified ac motor line current

‡Not included in efficiency measurements (data acquisition system)

## 4.11 EFFICIENCY MAPPING

Among the most important series of tests are the watts loss and efficiency mapping of the ac controller and ac drive system (motor and controller). The loss results for the controller motor and drive system in the motoring and regenerative braking modes are presented. The results are in the form of the watts loss versus motor current at various speeds. The motor current is the average of the three-phase full-wave rectified ac line motor current. The speed is at the gear box shaft after the 2.923:1 reduction. The analysis of available test data from the data acquisition system (reference Figure 4.9-1), in terms of loss, results in a qualitative as well as quantitative understanding of the loss mechanisms and trends. The controller loss does not include the 12-volt auxiliary power loss (control electronics and base drives, 161 watts to 233 watts), but does include the blower loss (150 watts in motoring, to 264 watts in regenerative braking). The motor loss includes the gear box loss. The drive system loss includes the controller, motor, and gear box losses. Rated torque at the gear box shaft is 66.0 N-m (48.7 lb-ft) at 1833 rpm, i.e., 17 hp.

The controller, motor, and drive system losses for motoring operation are shown in Figures 4.11-1, -2, and -3, respectively. Depending on the current and speed, the drive system may be operating in the PWM or square wave mode. Below base speed (1833 rpm), the drive operates in PWM regardless of the current, but as the speed increases, the drive transitions to square wave. Because the flux level in the motor is varied as a function of torque, this transition does not occur at the same speed. At low currents, the drive operates in PWM up to relatively high speeds, but at high currents the drive transitions to square wave at base speed. The controller loss (Figure 4.11-1) in PWM decreases with increasing speed (for a constant current) as the controller drops the number of chops, then the loss in square wave increases with increasing speed as the frequency increases. The loss increases with increasing current (for any constant speed). The controller loss has several components: constant loss (blowers, etc.), loss proportional to current (conduction), loss proportional to current squared (conduction, parasitic resistance), loss proportional to current and frequency (switching), and loss proportional to current squared and frequency (snubber). The motor loss (Figure 4.11-2) is less well behaved than the controller, but basically increases with increasing speed in PWM and remains fairly constant with speed in square wave. In square wave, the friction and windage loss increases with speed, but is partially offset by the reduced core loss as the flux level decreases. The motor loss increases with increasing current (for any constant speed). The motor loss is composed of loss due to friction and windage, stray load loss, core loss, stator and rotor resistance loss, harmonic core loss, harmonic current resistance loss, and gear box loss. The drive system loss (Figure 4.11-3) is the addition of the controller and motor losses.

The controller, motor, and drive system losses for regenerative braking operation are shown in Figures 4.11-4, -5, and -6, respectively. The transition from PWM to square wave occurs at a higher speed because the voltage is higher. The controller loss behaves similarly to motoring operation, but is somewhat larger due to the higher dc voltage and, in PWM, to the higher chopping frequency since the counter emf is small. These increases are partially offset by the lower conduction loss because the diodes carry more current. The motor loss behaves similarly to motoring operation but is somewhat lower due to lower slip.

The efficiency results for the controller and drive system in the motoring and regenerative braking modes are presented. The results are presented in the form of the efficiency versus torque at various speeds. The torque and speed are at the gear box shaft after the 2.923:1 reduction.

The controller and drive system efficiency for motoring operation are shown in Figures 4.11-7 and -8, respectively. The efficiency falls off rapidly at low torques and speeds, due

to the fixed losses (not a function of load) The peak controller efficiency of 95% occurs at 3000 to 4000 rpm (in the square wave mode) at 50 to 34 N-m (37 to 25 lb-ft), which is about one-half rated torque For speeds up to 2000 rpm, the efficiency is nearly constant past rated torque The efficiency at high speeds (3000 rpm and higher) is high, even at low torques, and falls off modestly with increasing torque The drive system efficiency behaves similarly to the controller The peak drive system efficiency of 86.9% occurs at 3000 to 4000 rpm at 49 to 38 N-m (36 to 28 lb-ft)

The controller and drive system efficiency for regenerative braking operation are shown in Figures 4-11-9 and -10, respectively The controller efficiency is lower than in motoring because of the higher losses The peak controller efficiency of 94.7% occurs at 4000 rpm and 49 N-m (36 and 53 N-m (39 lb-ft)

With the efficiency mapped over the entire torque and speed range in both motoring and regenerative braking, the efficiency for a particular load, such as the J227a-D cycle, can be found, as shown in Figure 4-11-11 This figure shows the controller and drive system efficiency plotted against the J227a-D cycle The efficiency in coasting is undefined, in regeneration, it would depend on the battery charge acceptance and the available energy from the vehicle The peak motoring controller efficiency of 94.7% and drive system efficiency of 86.5% occur from 48 to 64 km/h (30 to 40 mph) The 72 km/h (45 mph) cruise efficiencies are 92.6% and 81.0% for the controller and drive system, respectively

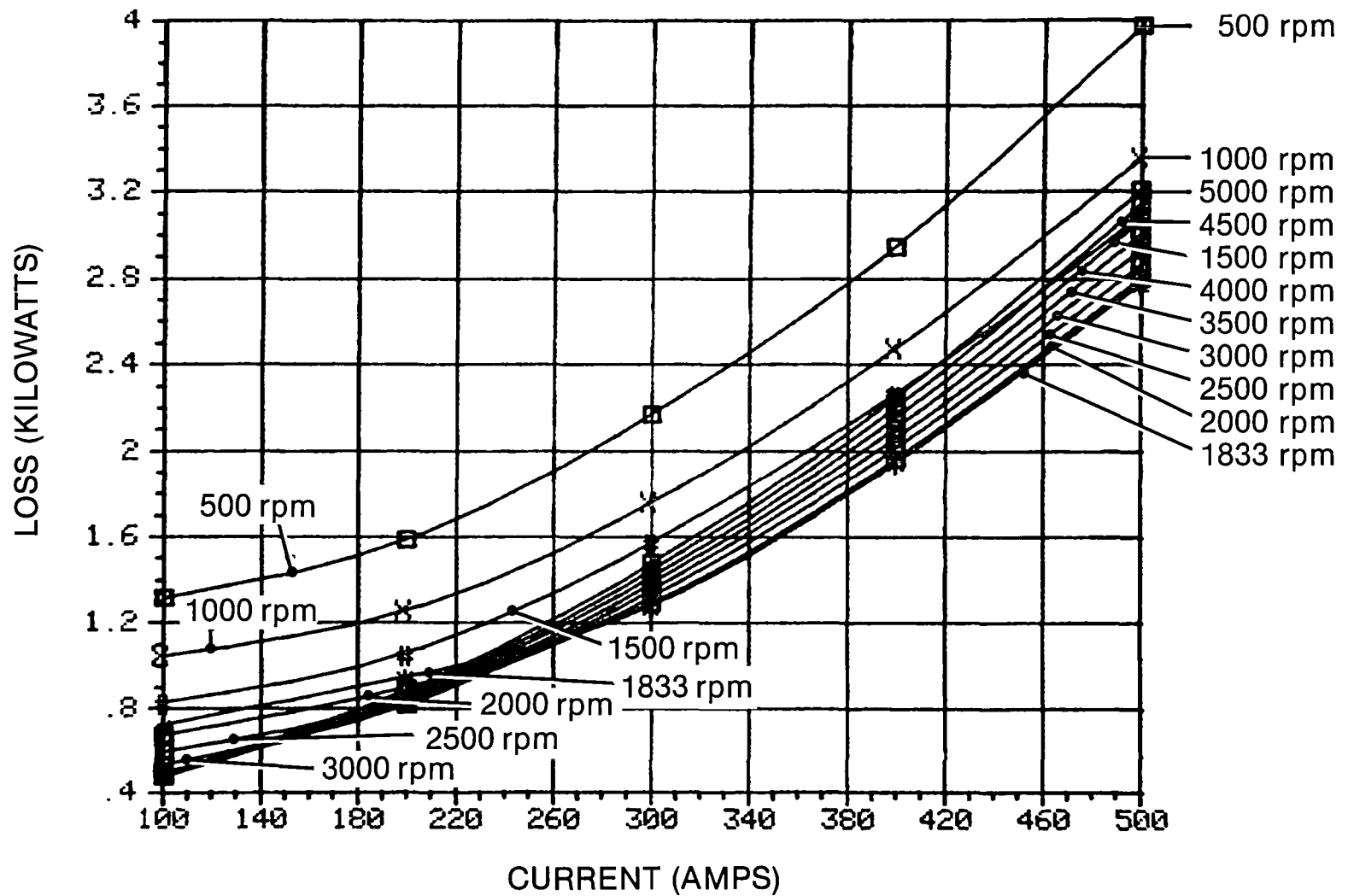


Figure 4.11-1 Controller Loss in Motoring

*Note: Current is the average of the 3-phase full wave rectified motor current. Speed is at the gear box shaft after the 2.923:1 reduction.*

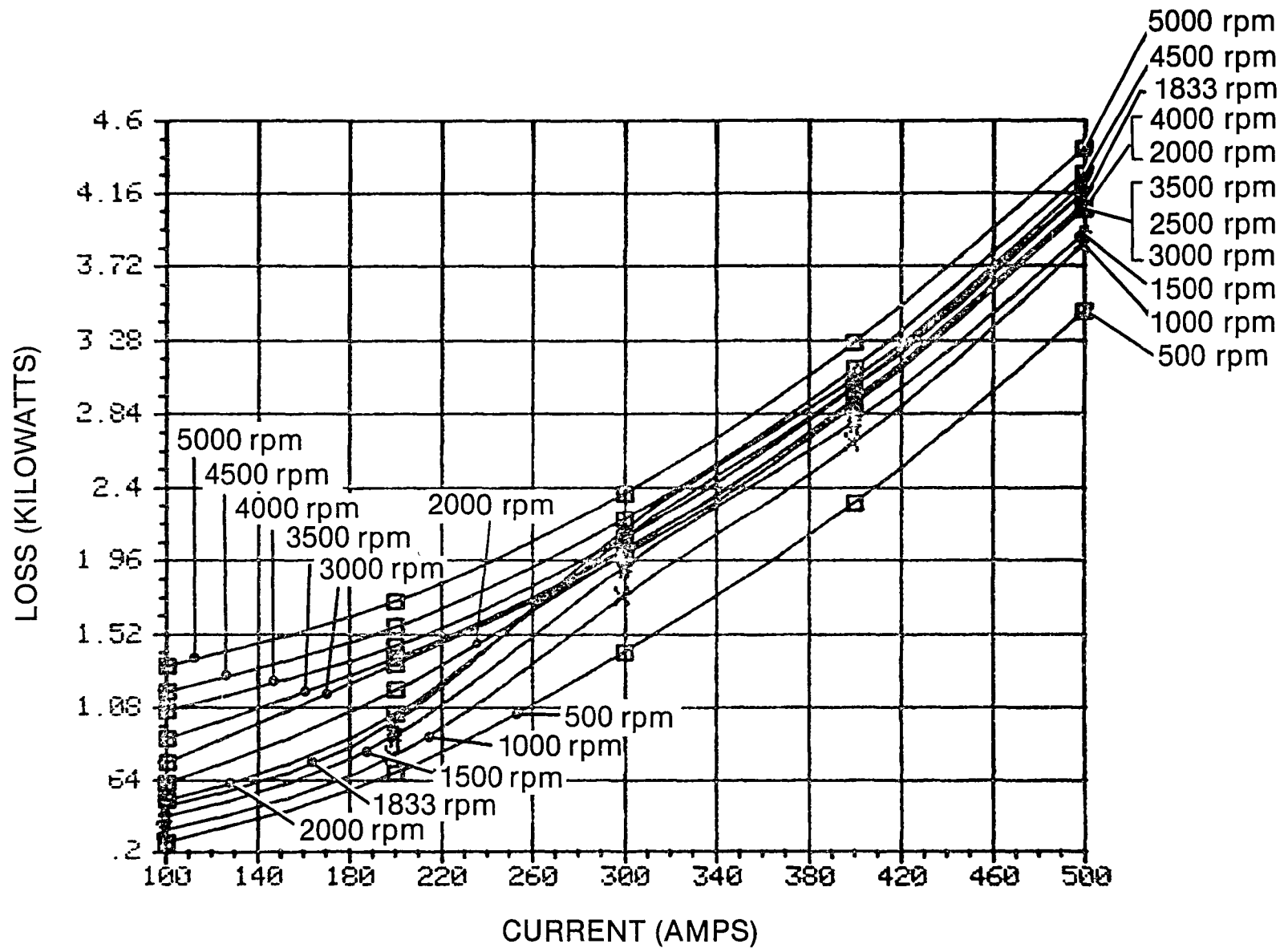


Figure 4.11-2 Motor Loss in Motoring

Note: Current is the average of the 3-phase full wave rectified motor current. Speed is at the gear box shaft after the 2.923:1 reduction.

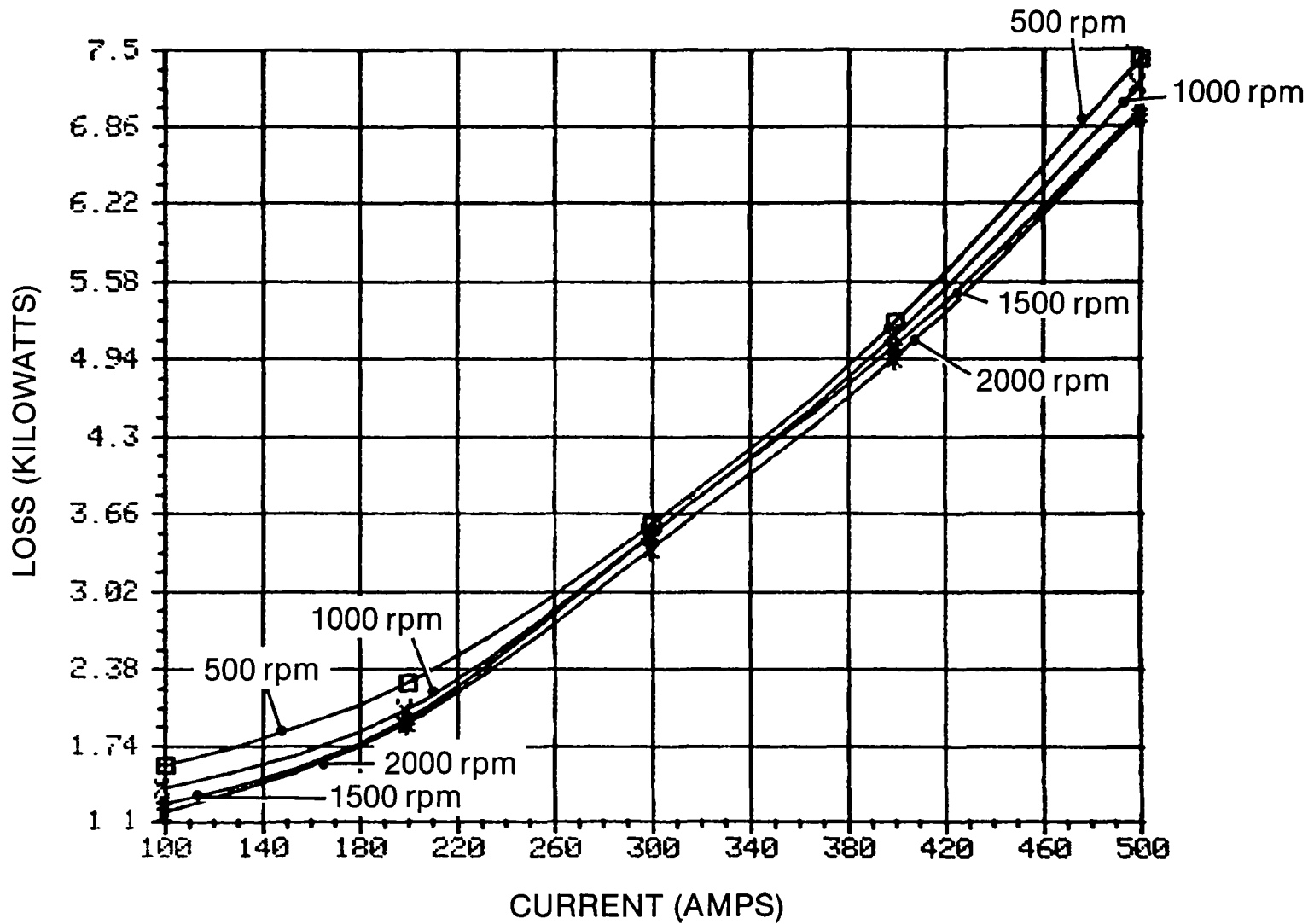


Figure 4.11-3a Drive System Loss in Motoring

*Note: Current is the average of the 3-phase full wave rectified motor current. Speed is at the gear box shaft after the 2.923:1 reduction.*

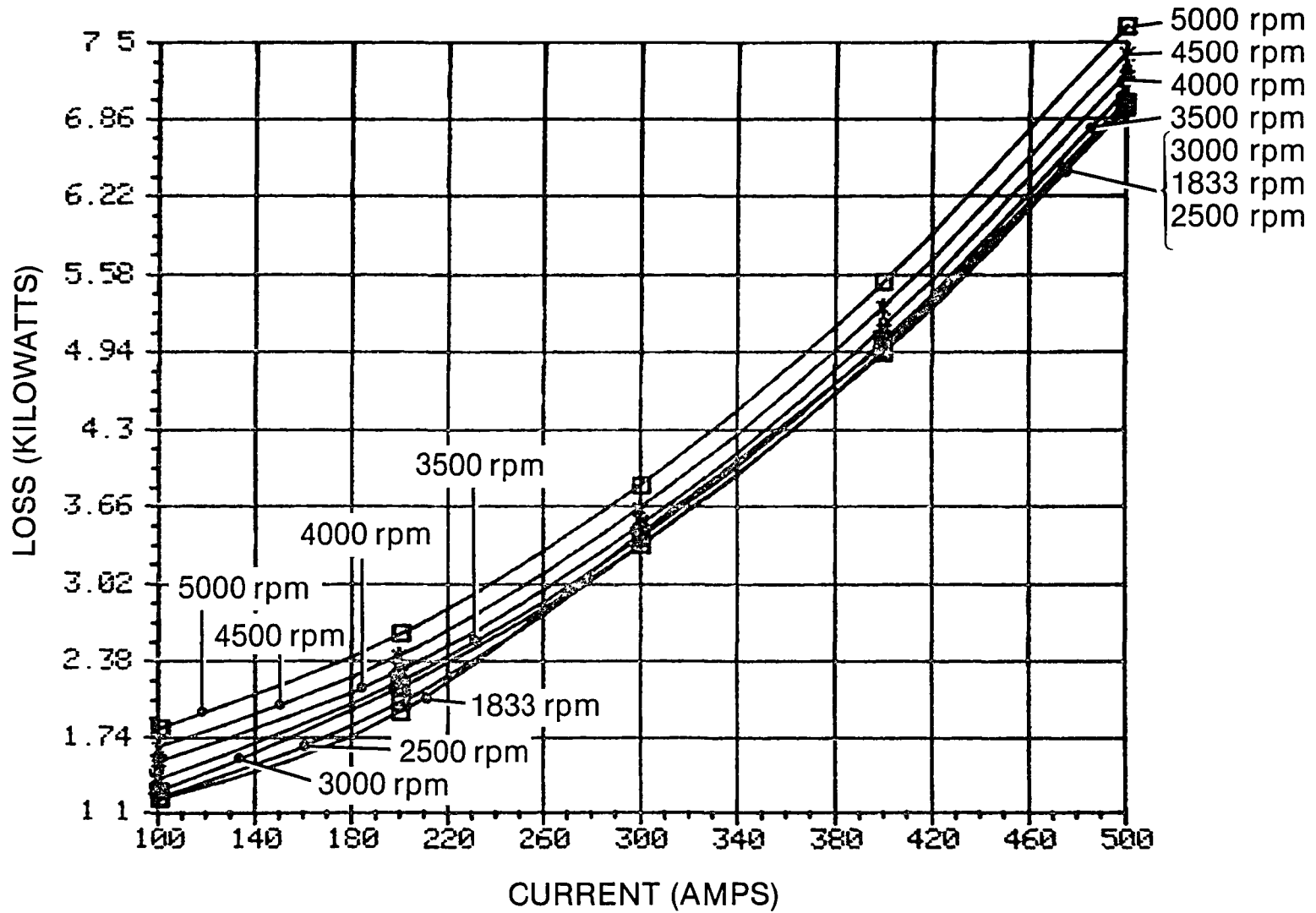


Figure 4.11-3b Drive System Loss in Motoring

*Note: Current is the average of the 3-phase full wave rectified motor current. Speed is at the gear box shaft after the 2.923:1 reduction.*

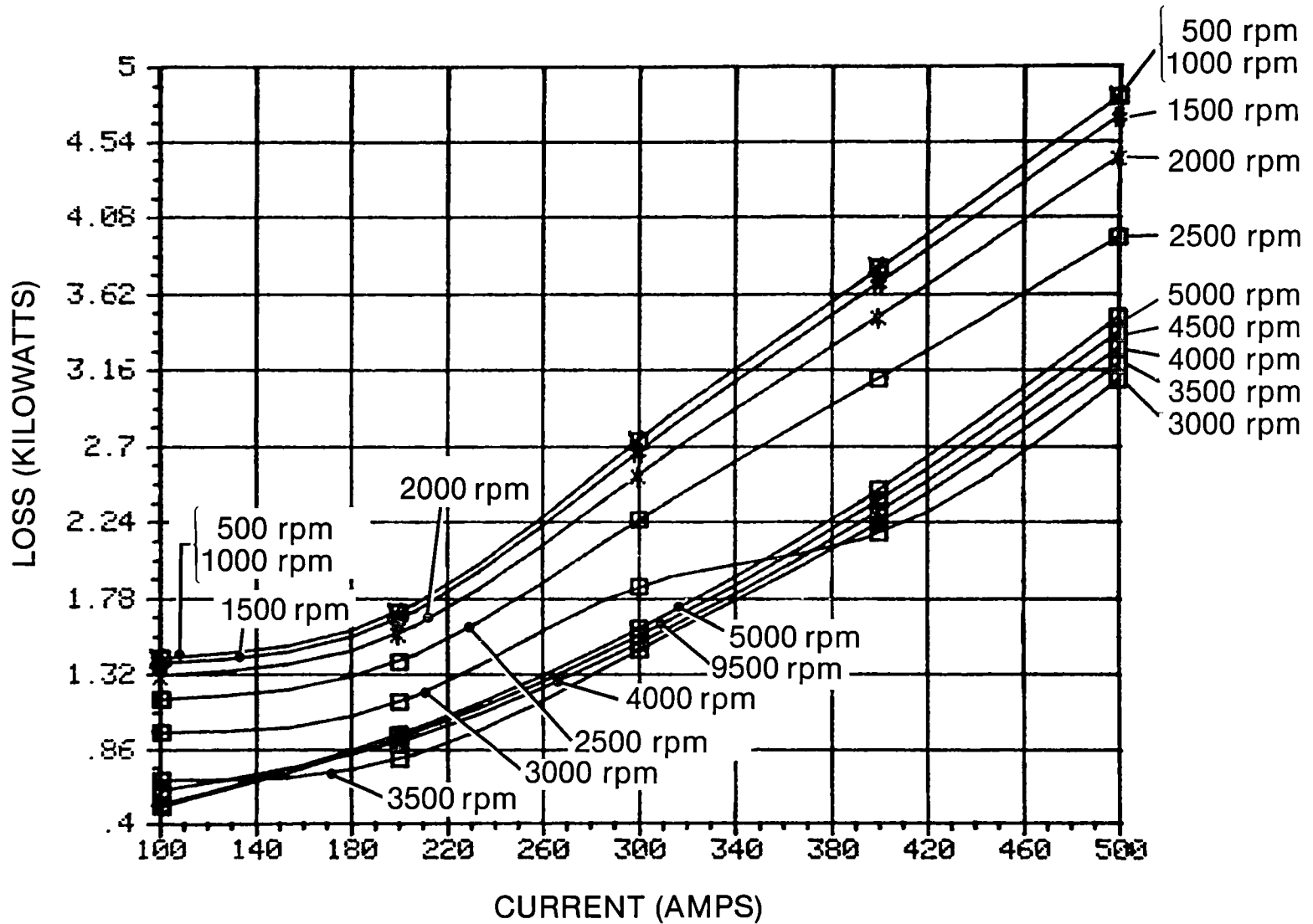


Figure 4.11-4 Controller Loss in Regenerative Braking  
 Note: Current is the average of the 3-phase full wave rectified motor current. Speed is at the gear box shaft after the 2.923:1 reduction.

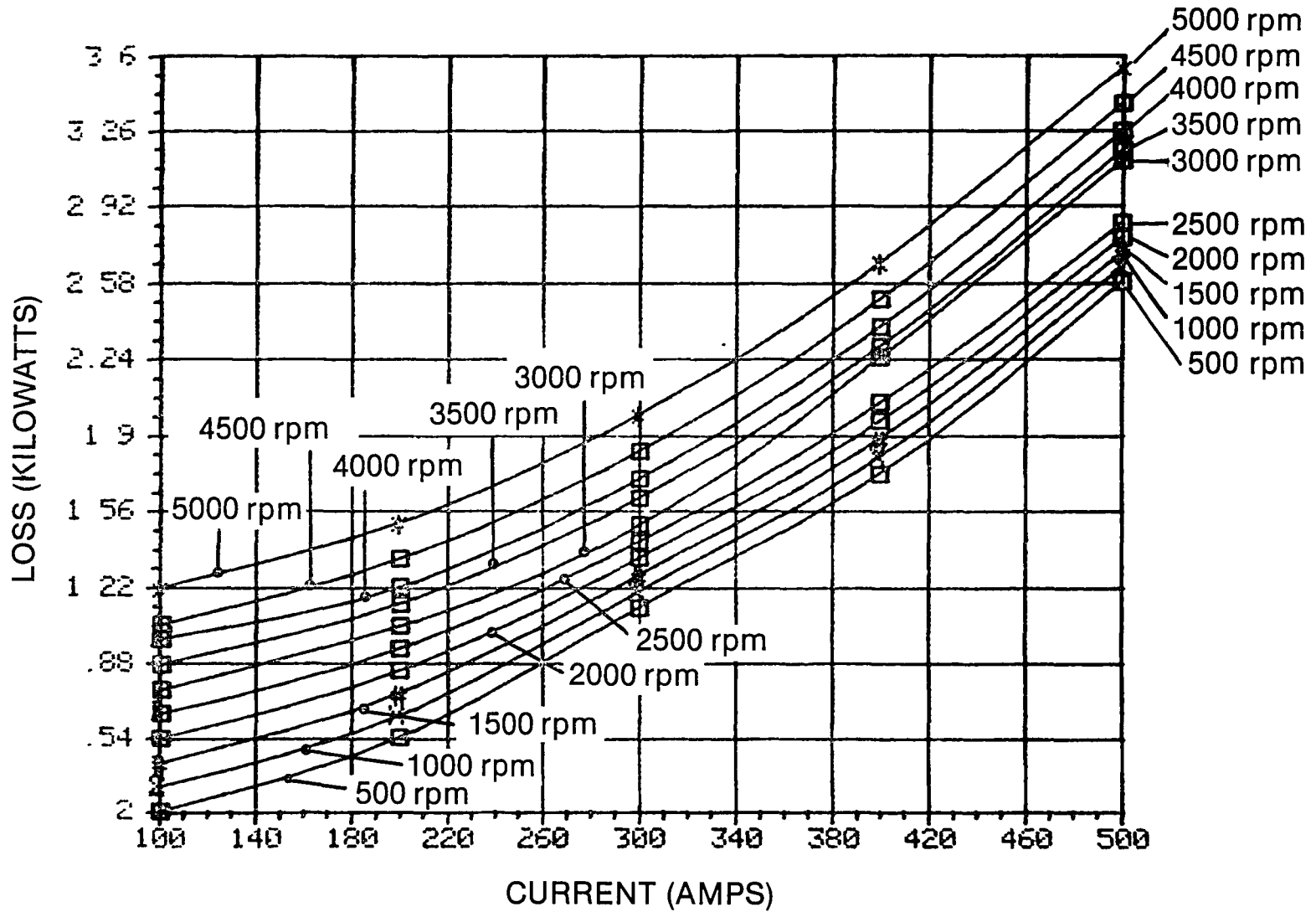
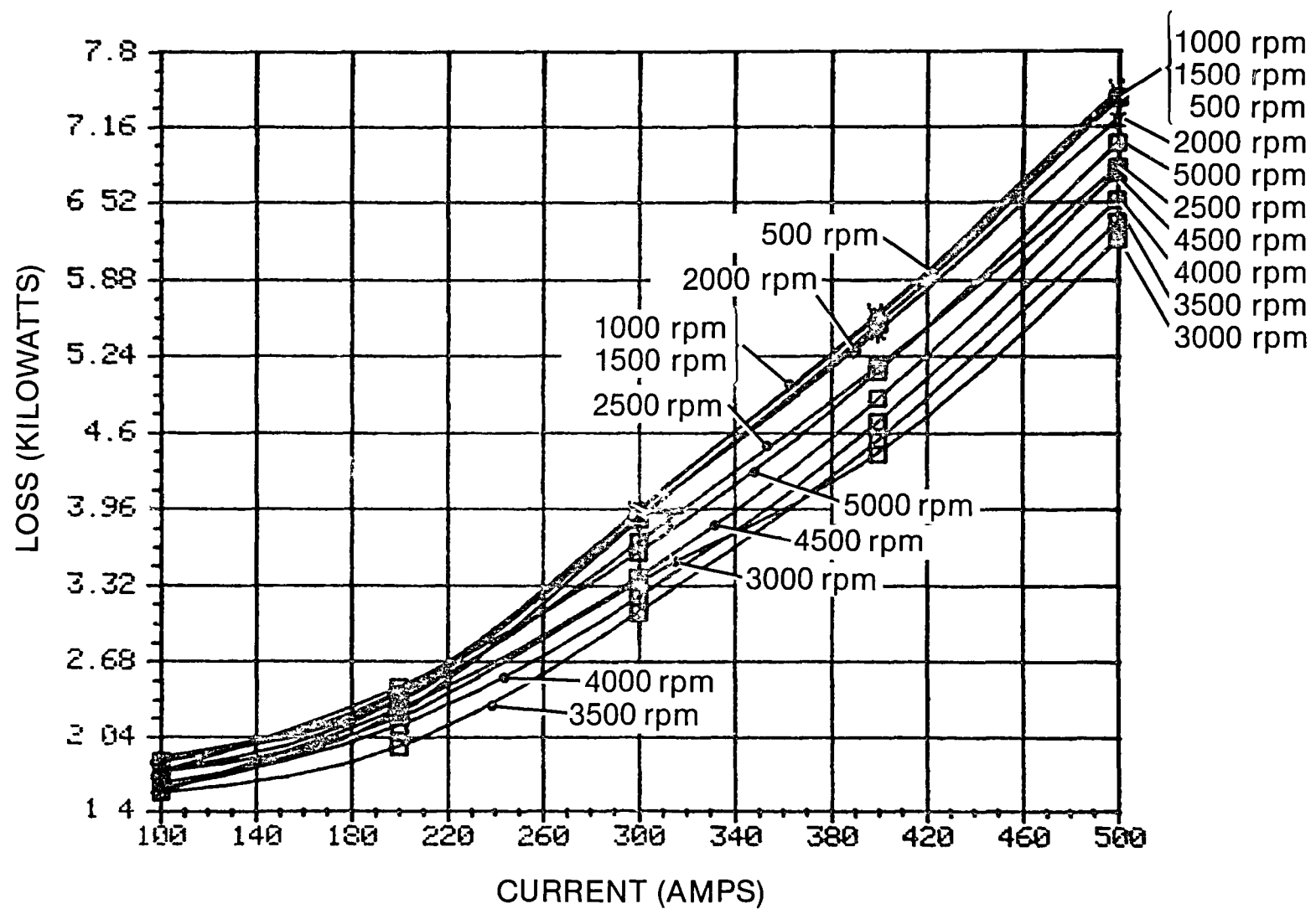


Figure 4.11-5 Motor Loss in Regenerative Braking

*Note: Current is the average of the 3-phase full wave rectified motor current. Speed is at the gear box shaft after the 2.923:1 reduction.*



**Figure 4.11-6 Drive System Loss in Regenerative Braking**  
*Note: Current is the average of the 3-phase full wave rectified motor current. Speed is at the gear box shaft after the 2.923:1 reduction.*

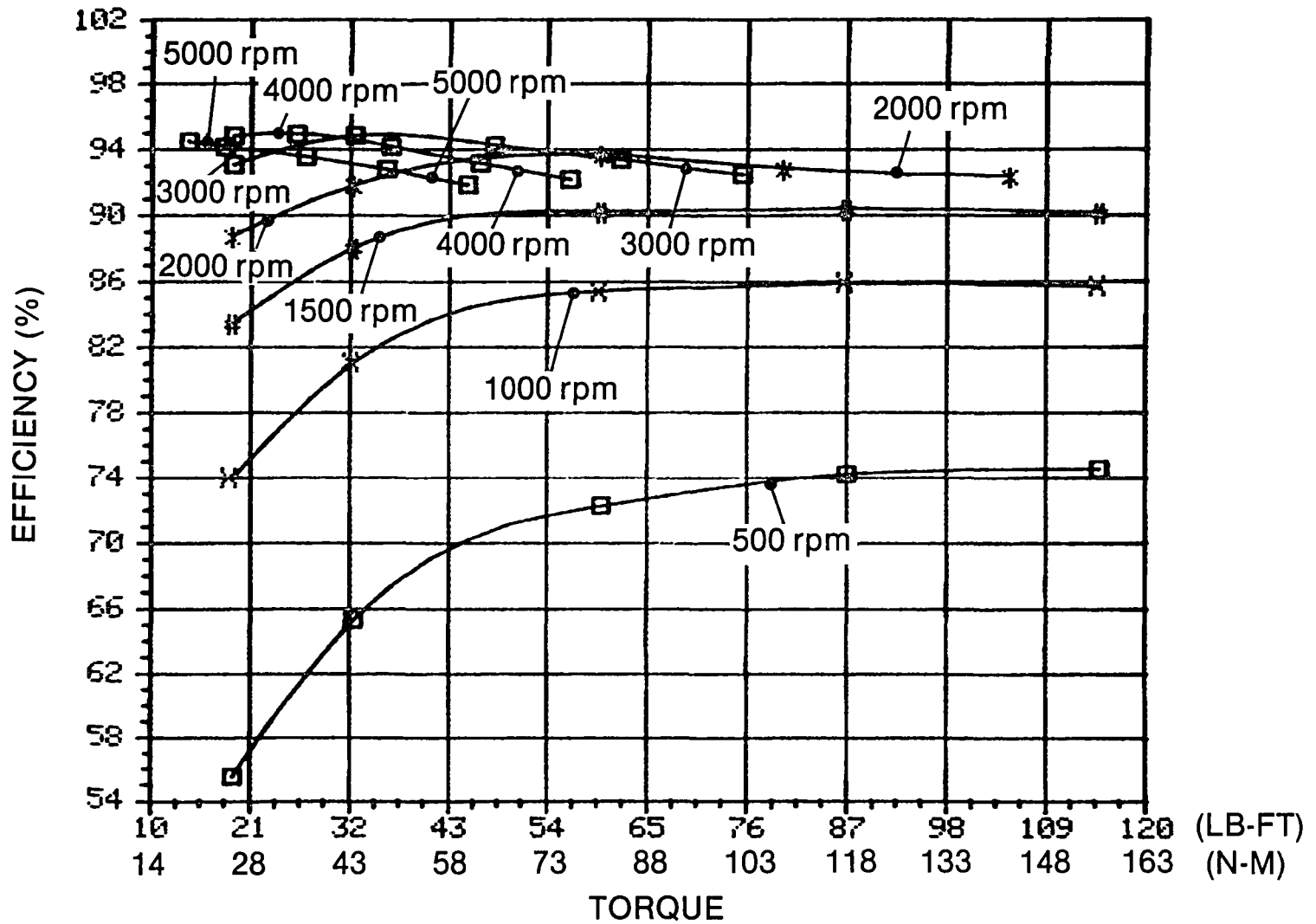


Figure 4.11-7 Controller Efficiency in Motoring  
 Note: Speed and torque are at the gear box shaft after the 2.923:1 reduction.

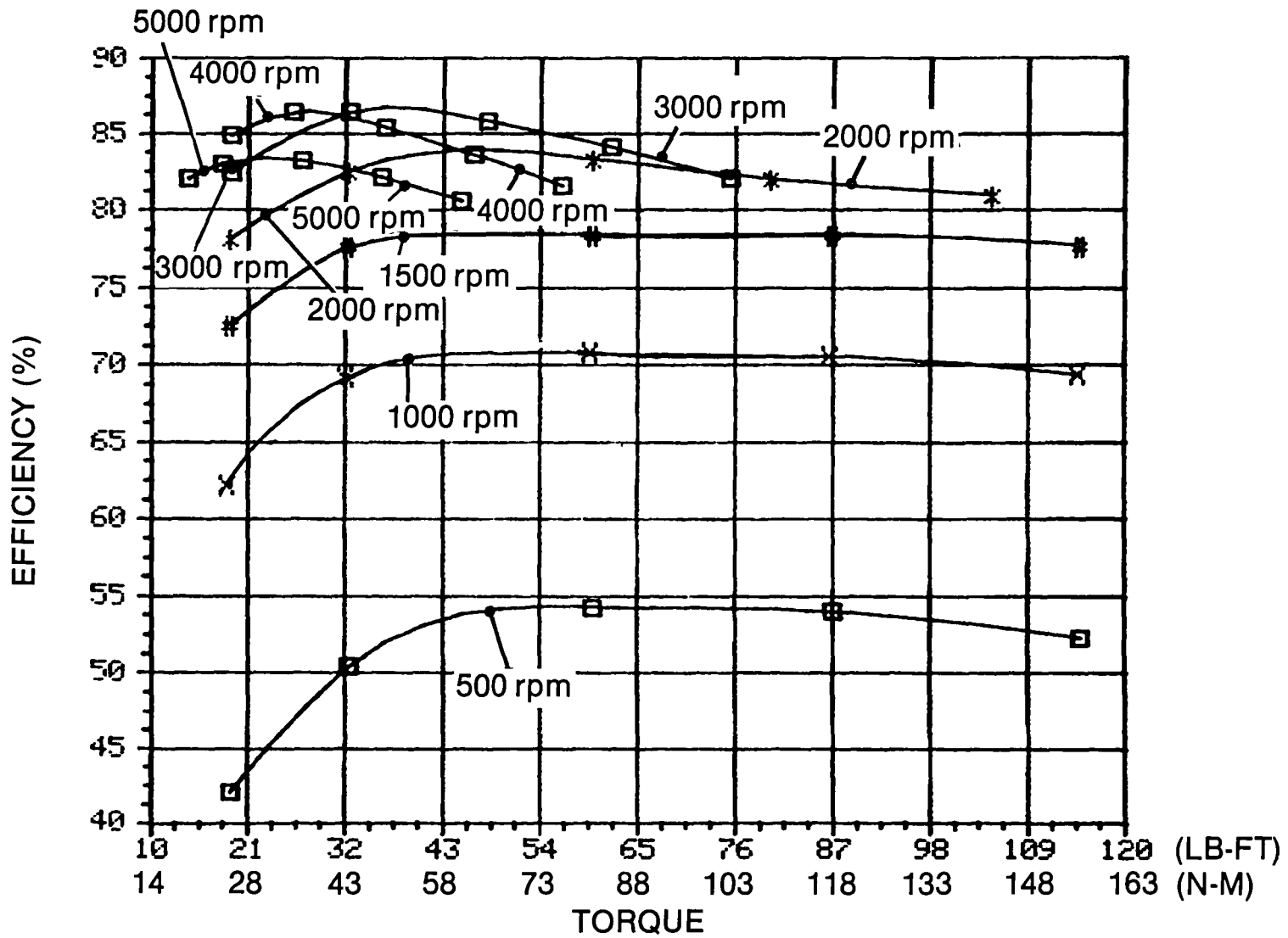


Figure 4.11-8 Drive System Efficiency in Motoring

Note: Speed and torque are at the gear box shaft after the 2.923:1 reduction.

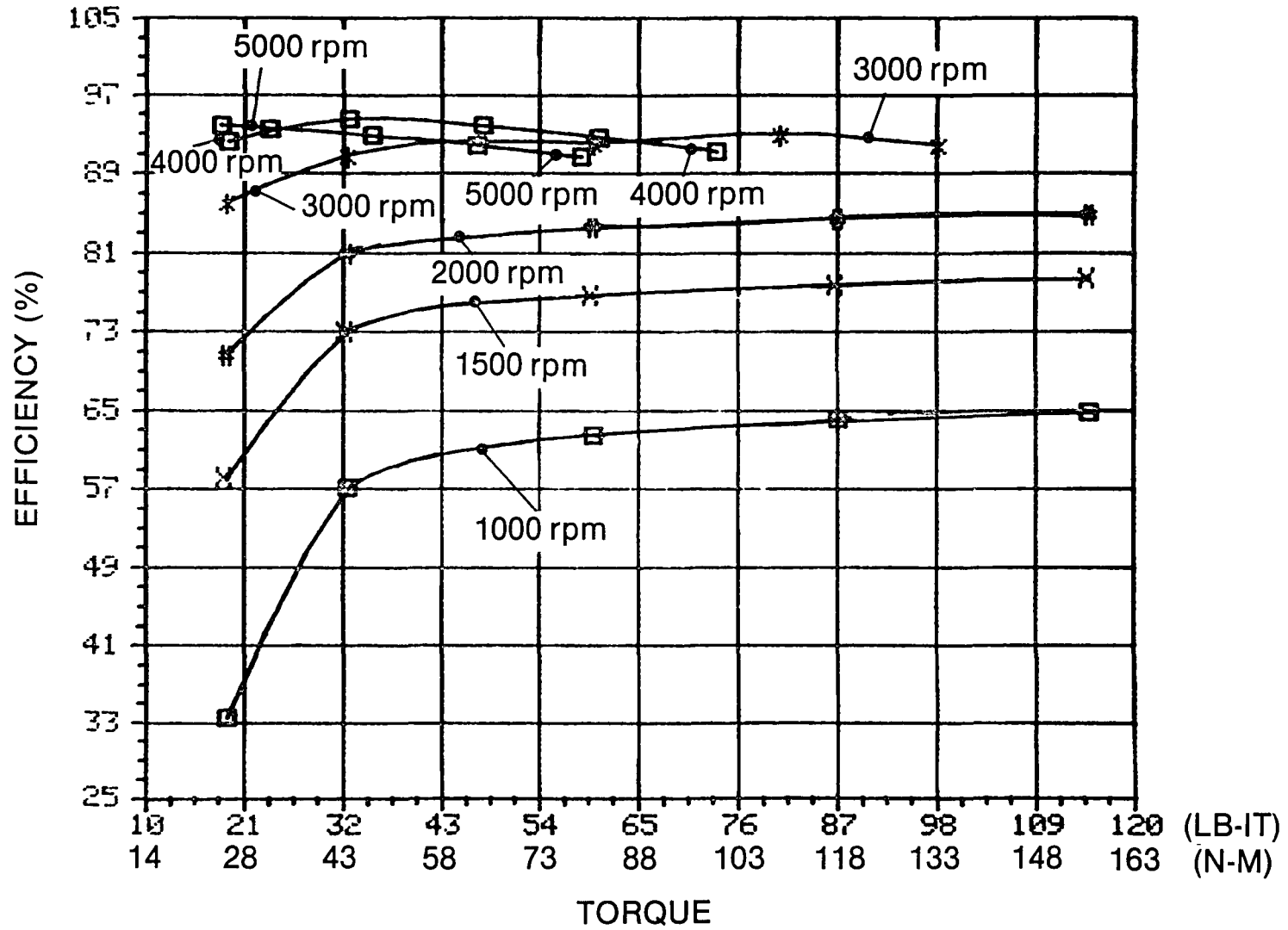


Figure 4.11-9 Controller Efficiency in Regenerative Braking

Note: Speed and torque are at the gear box shaft after the 2.923:1 reduction.

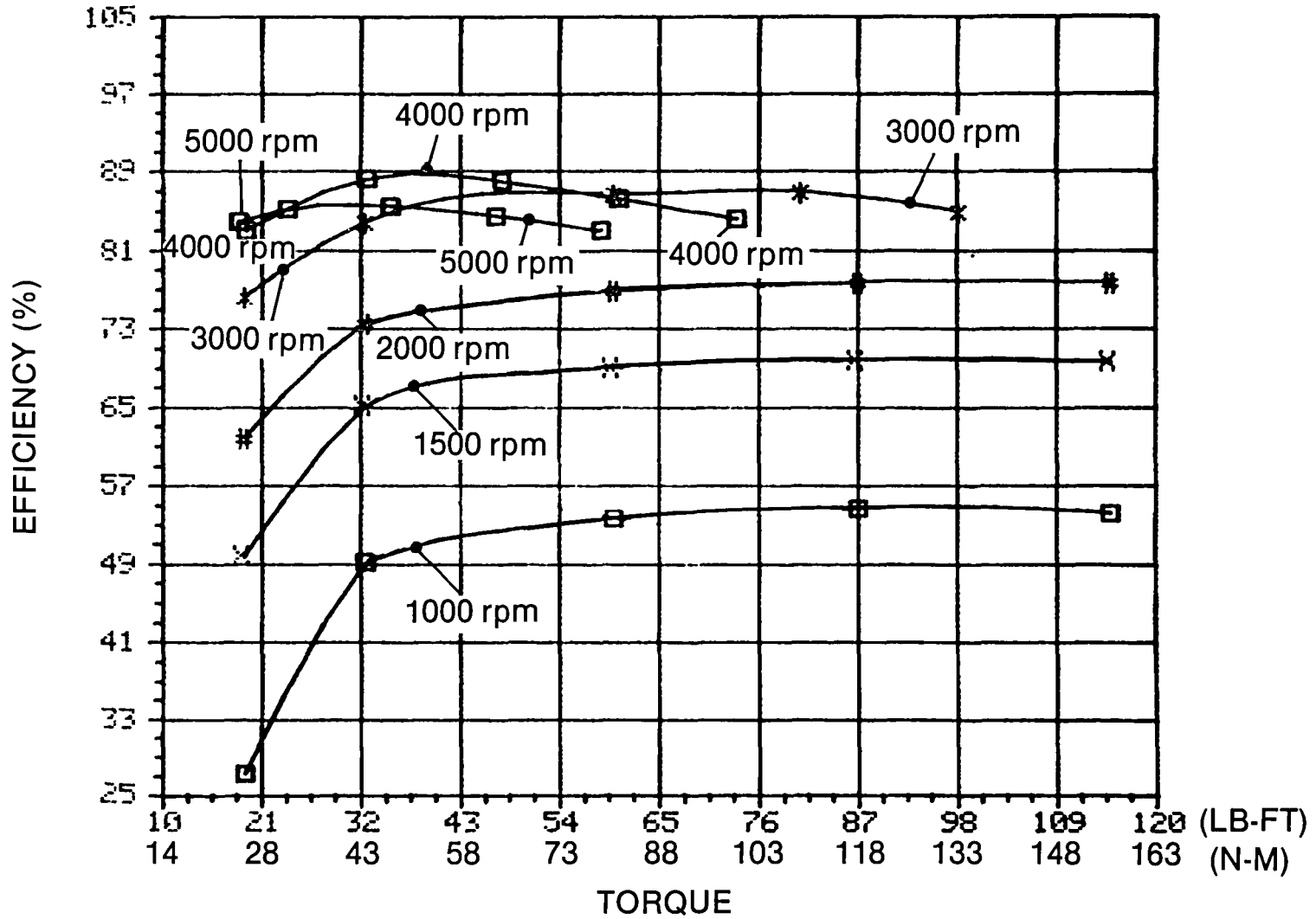


Figure 4.11-10 Drive System Efficiency in Regenerative Braking

Note: Speed and torque are at the gear box shaft after the 2.923:1 reduction.

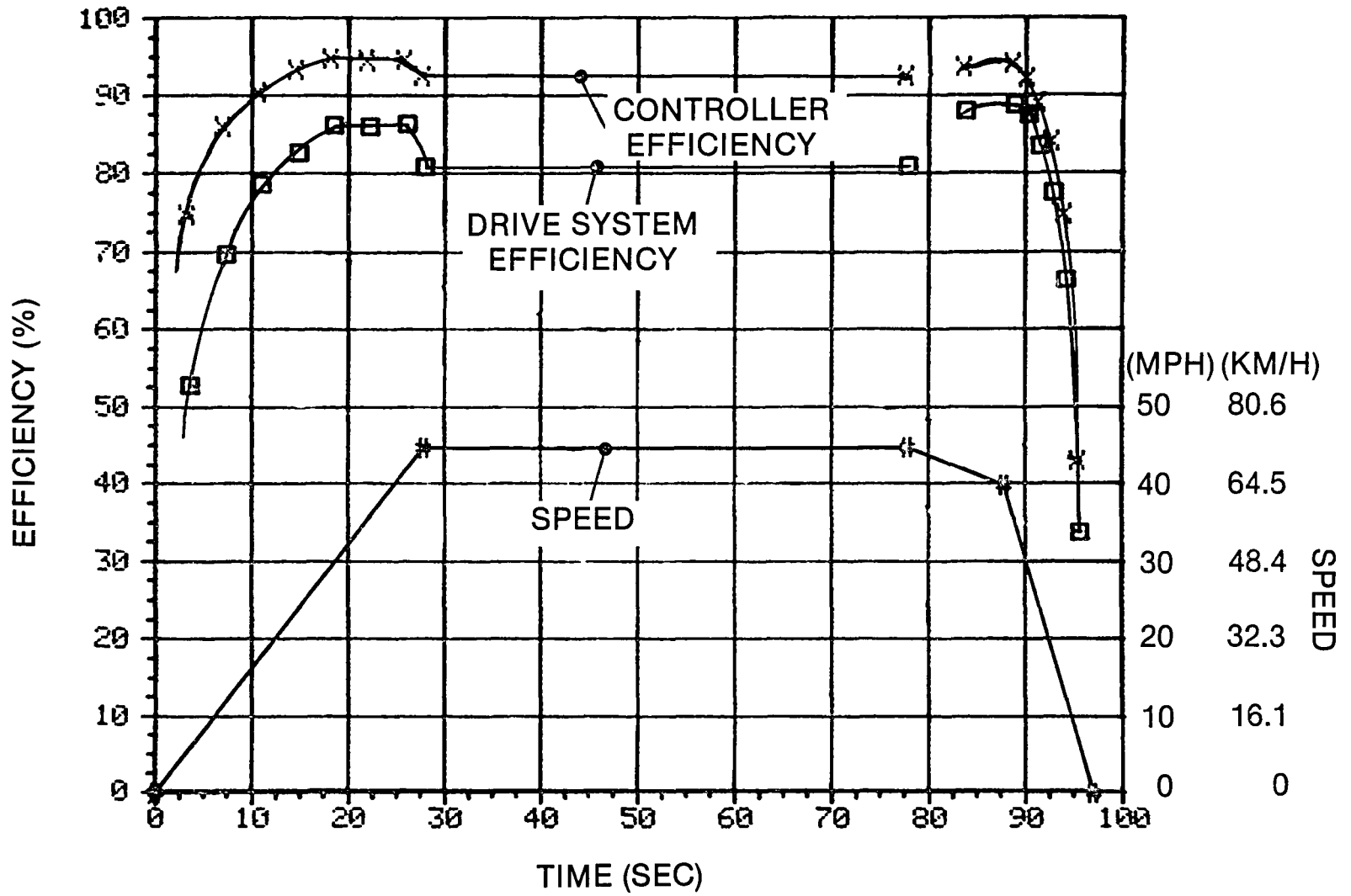


Figure 4.11-11 Efficiency over the J227 A-D Driving Cycle

## 4.12 DRIVE SYSTEM PERFORMANCE RECORDINGS

The dynamic performance of the system in both motoring and regenerating was measured. A typical run (Figure 4.12-1) is shown from zero speed to 3200 rpm with regenerative braking back to zero speed. The battery voltage is limited to 130 volts by the controls. This causes some tapering of the available braking torque at high speed when the battery charging current is high. Notice from Figure 4.12-1 that full torque is maintained in the constant torque region (0-2200 rpm) and then the torque falls off in the constant horsepower region (above 2200 rpm). The torque response is rate-limited, but is still less than one second. Also notice that the flux is constant in the constant torque region and then, when voltage amplitude control is lost (square wave mode), the flux falls off with speed. The torque angle and real current respond rapidly with little error. The stator current falls off slightly in motoring operation and is low in initial regeneration because the dc voltage rises as the battery acts as a charging capacitor. The controller is stable and has good dynamic response over the entire operating range. Note the torque, IREAL and  $\text{SIN}\theta$  are zero during the 6 second coasting time prior to regenerative braking.

Figure 4.12-2 is another run which shows the same signals as Figure 4.12-1, except the dc voltage is on channel 2 instead of IREAL. This run is at a higher torque and speed. The battery voltage sags from 110 volts to 100 volts during motoring, rises to 110 volts during coasting and rises to 130 volts during regenerative braking. The  $|I|$  reaches 400 amps during motoring, but is limited during regenerative braking by the controls to protect the batteries.

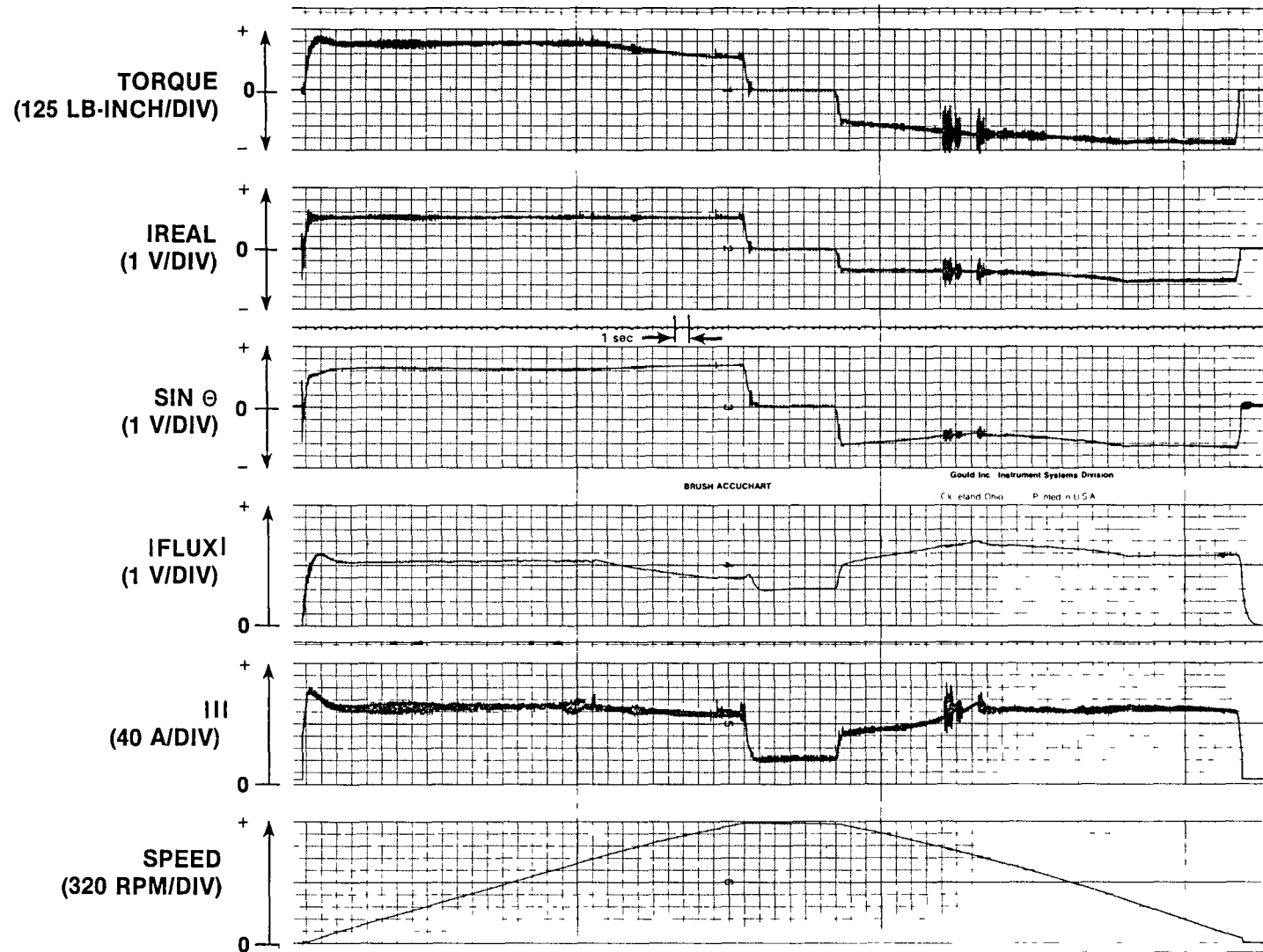


Figure 4.12-1. Typical Performance Recording

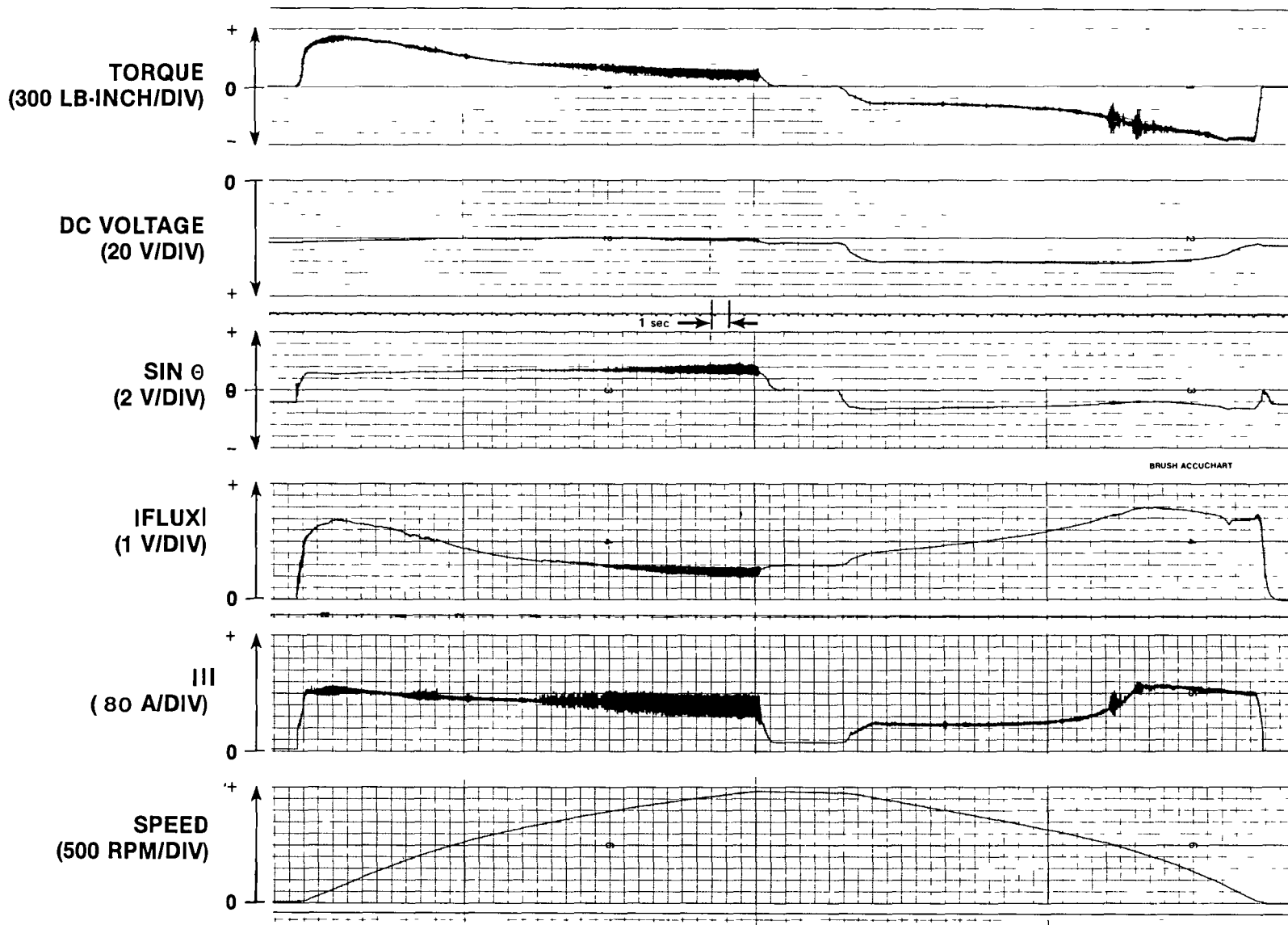


Figure 4.12-2. Typical Performance Recording with DC Voltage

## Section 5

### RESULTS AND CONCLUSIONS

The feasibility of a three-phase ac transistorized inverter for an electric vehicle ac induction motor propulsion system application has clearly been demonstrated. This type of system has potential cost and maintenance advantages over a dc chopper-based system. The ac motor has simple yet rugged construction without commutators and brushes, requires no routine maintenance, is amenable to mass production, is capable of high speeds which reduces its size, and can be totally enclosed allowing advanced packaging and cooling techniques. The power inverter in the ac controller utilizes the advances in high-power Darlington transistors to obviate the need for costly power level commutation circuits that would be needed for a thyristor approach. The inverter is consequently allowed to operate at higher switching frequencies to improve the current waveform delivered to the motor and thereby increase the motor efficiency. The control electronics in the ac controller utilize advances in microelectronics to solve the complex control of an ac inverter-induction motor drive system in relatively low cost signal electronics. The major results and conclusions drawn from the design and laboratory test of an improved ac motor controller sized for a battery powered electric vehicle weighing 1633 kg (3600 lb) are

1. The three-phase, ac transistorized inverter, GE optimized induction motor and drive system control were dynamometer tested in both motoring and regenerative braking.
2. The feasibility and improved motor current waveforms of the advanced pulse width modulation (current-controlled PWM) scheme were demonstrated.
3. A family of controllers spanning the range of 10-50 horsepower with battery voltages from 84-300 volts were scaled from the base 108-volt, 20 hp design. The basic power and control circuit concepts developed can be applied throughout this family without fundamental limitations.
4. The life cycle cost of the ac controller family was evaluated and is less than a dc chopper-based system. The life cycle cost of the base system was 2.4¢/km (3.9¢/mile).
5. The ac controller losses, motor losses, and total drive system losses were mapped over the current and speed range.
6. The efficiency of the ac controller was mapped over the speed and torque range, including the J227a-D cycle. The controller and system reached a peak efficiency of 95% and 86.9%, respectively.
7. Motor reversing was easily incorporated into the drive system controls by electrically reversing the phase sequence of the inverter.
8. An approach for the utilization of a portion of the ac controller power circuitry as a battery charger was presented.
9. The estimated ac controller costs are probably above that required for the automotive market. Cost reductions are clearly possible from a system redesign that pays special attention to system partitioning and possible performance/cost trade-offs. Common parts for various modules would lead to further cost reduction.
10. Higher horsepower systems need a higher battery voltage to reduce costs. However, some capacitor developments are needed at high voltage.
11. The ac controller cost favors a higher system voltage than the base 108-volt system. The ac controller size and efficiency also favor a higher system voltage because of the resulting lower currents. Most of the inverter losses are current or current-squared related, such as transistor forward drop and conductor drop, while few are voltage related. The size of the inverter is based on the losses that must be dissipated and the size of the components, which

are more strongly current related than voltage related. Examples are the dc filter capacitors which are sized by the ripple current requirements and the number of parallel transistors which are set by the peak currents that must be switched.

12 The feasibility of the advanced motor controls using the motor torque angle, motor stator real current, and motor flux, without a tachometer, were demonstrated.

13 The reasons for the choice of transistors for the inverter are well founded, but the main problems are their cost and availability. However, market forces and volume production are expected to result in acceptable transistor prices and sources in the future.

14 The snubber design, transistor safe-operating-area, circuit layout and system voltage need further development work to reduce the snubber complexity and snubber losses (a major source of inverter losses).

15 Further development work is needed to rationally evolve a less expensive system control hardware implementation.

16. Further development work is needed to reduce the base drive circuit and base drive power supply costs and losses. This is particularly important in the low horsepower range at low battery system voltage.



## Appendix A

# ELECTRIC VEHICLE PERFORMANCE ANALYSIS AND SPECIFICATION

### 1.0 INTRODUCTION

A method of analyzing the performance requirements of an electric vehicle is developed. The method uses the basic principles which characterize all electrical propulsion systems, regardless of the type of traction motor used. The result is a vehicle specification from which a detailed design can be generated.

### 2.0 ANALYSIS

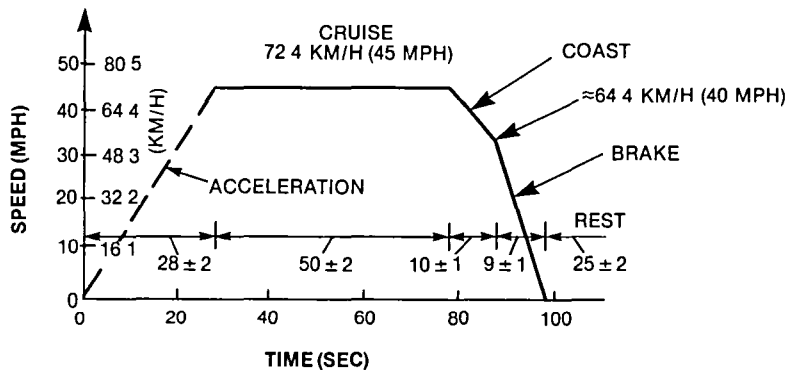
#### 2.1 PERFORMANCE GOALS

The analysis derives the vehicle tractive effort requirements to meet the maximum vehicle performance goals. These goals are:

- 1 Acceleration from 0 to 48 km/h (30 mph) in 9 seconds
- 2 Acceleration from 40 to 88 km/h (25 to 55 mph) in 18 seconds
- 3 Sustained speed on a 10% grade of 48 km/h (30 mph)
4. Initial acceleration sufficient to start on an 18% grade
5. Minimum balancing speed of 97 km/h (60 mph)

The specifications above are considered to define the maximum vehicle performance desired and to apply relatively infrequently only once or twice per battery charge. The balancing speed is the speed where the available drive power equals the vehicle friction and windage.

In addition to the above specifications, it is desired to operate the vehicle continuously on the J227a-Schedule D driving cycle. This duty cycle will determine the continuous rating of the motor and controller. The cycle is shown in Figure A-1.



NOTE: THE SHAPE OF THE ACCELERATION PORTION OF THE DUTY CYCLE CURVE IS UNDEFINED.

**Figure A-1 SAE J227a – Schedule D Driving Cycle**

## 2.2 FRICTION AND WINDAGE

An equation defining the friction and windage of the vehicle is <sup>(4)</sup>

$$R_T = 0.012W + 0.000029WV + \frac{6.08}{391} V^2$$

where,

$R_T$  = total resistance of friction and windage in lb (1)

$W$  = vehicle weight in lb (3600 lb to be assumed)

$V$  = vehicle speed in mph

The first two terms are the vehicle friction and the last term is the vehicle windage. The friction and windage are plotted separately in Figure A-2 and in total in Figure A-3.

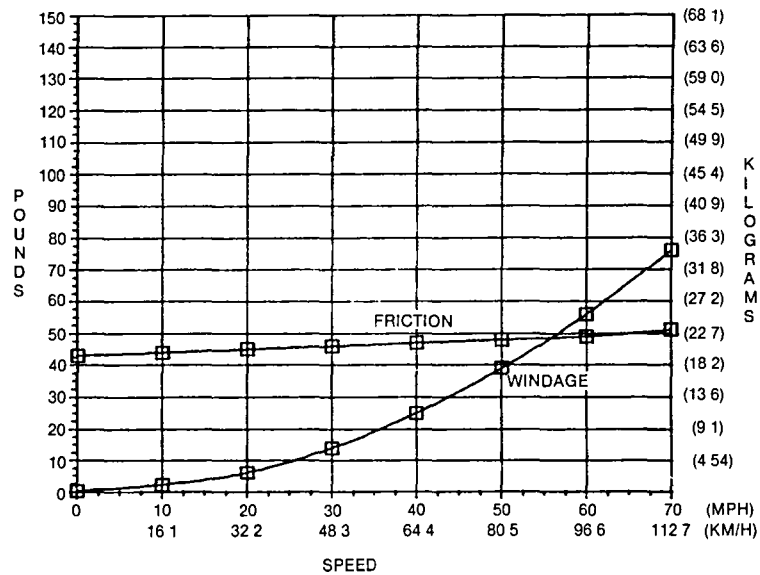


Figure A-2 Vehicle Friction and Windage

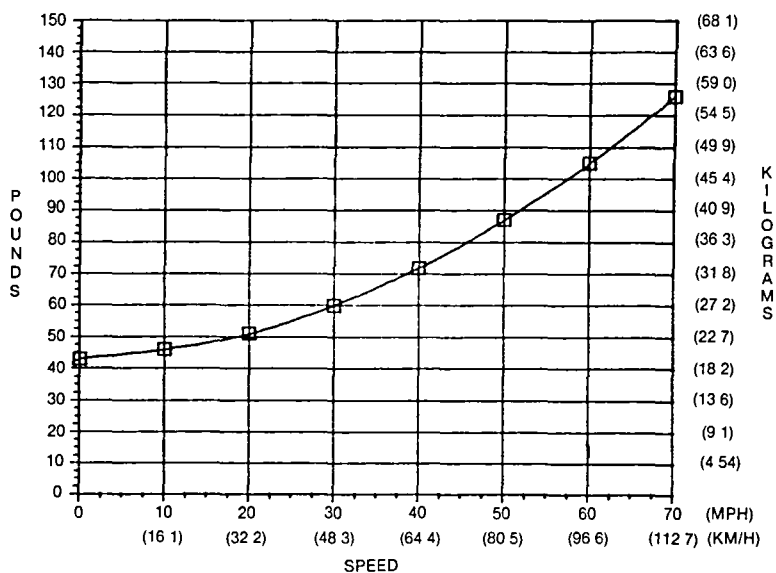


Figure A-3 Total Vehicle Friction and Windage

### 2.3 ACCELERATION

The energy required for acceleration is calculated from the formula  $F = ma$ , which, translated into vehicle terms, becomes

$$TE = 0.0456 AW + \text{Rotary Inertia Effect} \quad (2)$$

where,

$TE$  = tractive effort in lb

$A$  = acceleration in mph/sec

The normally expected value of rotary inertia for a self-propelled rail car will be equivalent to about 9% of the vehicle weight. In an automobile drive, the rotary inertia may equal or exceed 15% of the vehicle weight. This analysis assumes that rotary inertia is 10% of the vehicle weight, thus

$$TE = 0.0502 AW \quad (3)$$

when rotary inertia is included

The tractive effort can be related to power by the following equation.

$$P = 1.99 TE V \quad (4)$$

and this power can be related to the motor requirements by this equation:

$$P = 0.142 nT \quad (5)$$

where,

$P$  = power in watts

$T$  = torque in lb-ft

$n$  = motor speed in rpm

### 2.4 GRADE CLIMBING

Requirement three is the ability to climb a 10% grade at a continuous speed of 48 km/h (30 mph). Due to the absence of acceleration, the effect of rotary inertia can be neglected. The tractive effort required is given by.

$$TE = W \sin \left( \tan^{-1} \frac{G}{100} \right) \quad (6)$$

where,

$G$  = grade in percent

The required tractive effort is 163 kg (358 lb), neglecting loss. The friction and windage loss from Equation 1 at 48 km/h (30 mph) is 27 kg (60 lb), so the total tractive effort is 190 kg (418 lb). This point is shown in Figure A-5.

### 2.5 INITIAL ACCELERATION

Requirement four is the ability to start the vehicle on an 18% grade. The tractive effort required is given by Equation 6, again neglecting rotary inertia, and is 290 kg (638 lb). The friction from Equation 1 at zero speed is 20 kg (43 lb), so the total tractive effort needed is 309 kg (681 lb). This point is shown in Figure A-5.

## 2.6 VEHICLE ACCELERATION MODEL

The first and second requirements deal with the vehicle acceleration between two speeds. In order to analyze these requirements, a knowledge of the general operating characteristics of an induction motor as applied to a vehicle drive is required. Figure A-4 shows a vehicle acceleration model which can be used. This model does not include losses, but losses will be accounted for later. Note the three operating speed ranges. The first (I) is a constant acceleration region where the motor torque is constant over the speed range. The induction motor is operating at variable frequency and voltage with constant flux (constant volts/hertz) and constant slip. The second (II) is a constant horsepower region where the motor torque falls inversely with speed. The motor is operating at variable frequency with constant voltage and a variable slip frequency similar to field weakening, since the motor flux decreases with speed.  $V_1$  is the motoring corner point. The third (III) region is equivalent to series motor operation, since the motor is operating at variable frequency, but both voltage and slip are constant. The constant power speed range of the motor is  $V_2/V_1$ .

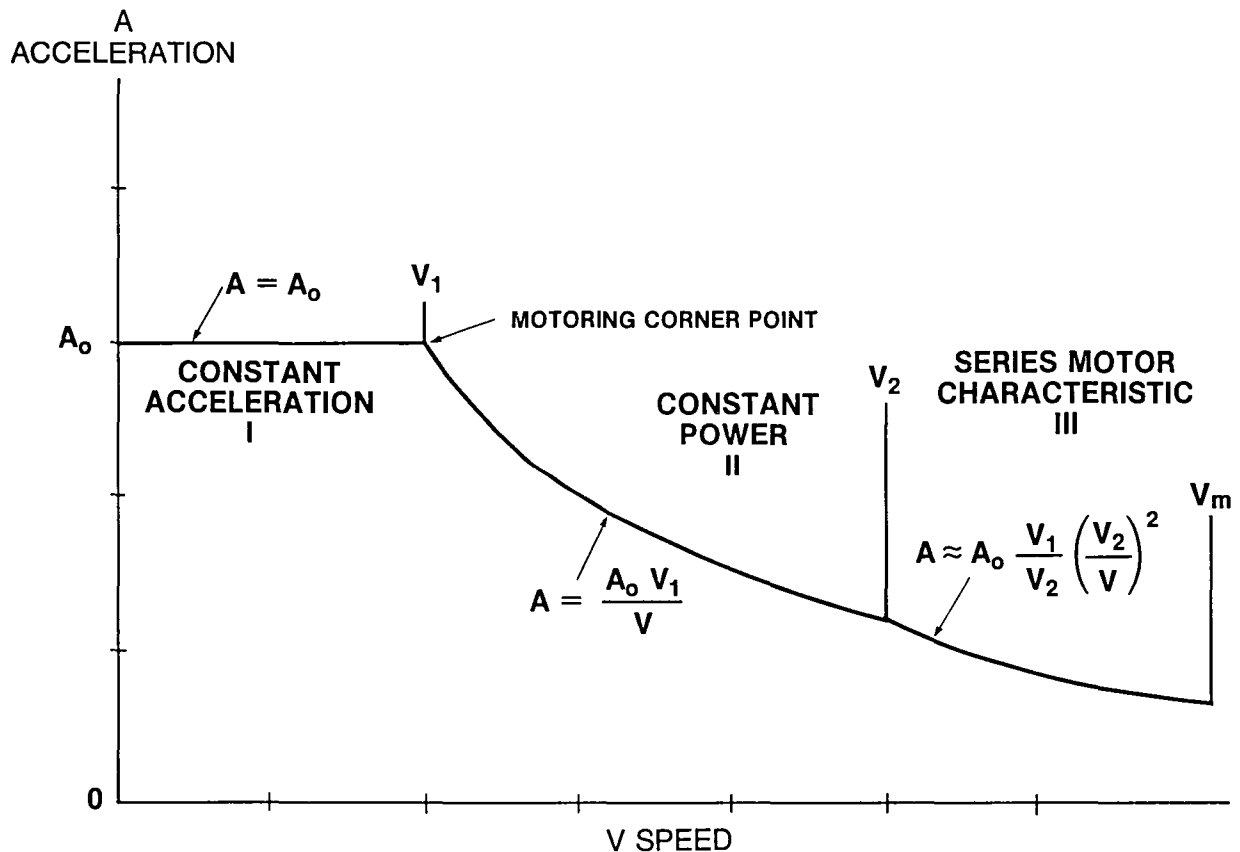


Figure A-4 Vehicle Acceleration Model

As stated earlier, this analysis approach is valid regardless of the type of traction motor used. This vehicle acceleration model is applicable to a dc drive. Region I is basically armature control with constant field as a function of speed. Region II is constant armature voltage with a field current which varies approximately as  $I_o/V$ .

Speed as a function of time is required in order to convert the vehicle requirements to motor requirements. The equation

$$A = \frac{dv}{dt} \quad (7)$$

is used for the calculations. In speed range I,  $A = A_o$ , thus

$$\int_0^{V_1} dv = A_o \int_0^{t_1} dt \quad (8)$$

and

$$V_1 = A_o t_1 \quad (9)$$

where

$V_1$  = motoring corner point speed, mph

$A_o$  = initial acceleration, mph/sec

$t_1$  = time to reach speed  $V_1$ , sec

For speed range II,  $A = \frac{A_o V_1}{V}$ , thus

$$\int_{V_1}^{V_2} V dV = A_o V_1 \int_{t_1}^{t_2} dt \quad (10)$$

and

$$t_2 - t_1 = \frac{V_2^2 - V_1^2}{2 A_o V_1} \quad (11)$$

where

$V_2$  = speed at the end of constant power, mph

$t_2$  = time at which speed is  $V_2$ , sec

For speed range III,  $A = A_o \frac{V_1 V_2}{V^2}$ , thus

$$\int_{V_2}^{V_m} V^2 dv = A_o V_1 V_2 \int_{t_2}^{t_m} dt \quad (12)$$

and

$$t_m - t_2 = \frac{V_m^3 - V_2^3}{3 A_o V_1 V_2} \quad (13)$$

where

$V_m$  = maximum speed, mph

$t_m$  = time at which speed is  $V_m$ , sec

## 2.7 MERGING ACCELERATION

In order to analyze the second requirement, accelerate from 40 to 89 km/h (25 to 55 mph) in 18 seconds, it is assumed that the entire acceleration is in the constant power speed range

Assume

$$V_x = 40 \text{ km/h (25 mph)}$$

$$V_y = 89 \text{ km/h (55 mph)}$$

$$t_y - t_x = 18 \text{ seconds}$$

Then, using Equation 11,

$$A_o V_1 = \frac{V_y^2 - V_x^2}{2 (t_y - t_x)} = 66.67 \quad (14)$$

$A_o V_1$  is a power term and, from Equations 2 and 4 the power over this constant power range, not including rotary inertia, is calculated as follows

$$P = (1.99)(0.456)(A_o V_1) W = 21,779 \text{ watts} \quad (15)$$

To account for friction and windage, the average value of friction and windage from Equation 1 over the 40 to 89 km/h (25 to 55 mph) speed range is added to the vehicle acceleration power component. Thus,

$$P = 21,779 + 6,634 = 28,413 \text{ watts} = 38 \text{ hp} \quad (16)$$

This sizes the power required at the wheels of the vehicle as delivered by the drive system. This 38 hp requirement is plotted in Figure A-5 in terms of tractive effort versus speed. This is the minimum peak horsepower to meet the vehicle acceleration maximum performance requirement. The drive system must be sized larger than this to account for rotary inertia effects under acceleration and gear losses.

## 2.8 ACCELERATION – 0 to 48 km/h (0 to 30 mph)

Requirement one is the ability to accelerate from 0 to 48 km/h (0 to 30 mph) in 9 seconds. The corner point speed  $V_1$  will probably be less than 48 km/h (30 mph), so Equations 9 and 11 will be used.

Assume,

$$V_x = 0 \text{ mph}$$

$$V_y = 48 \text{ km/h (30 mph)}$$

$$t_y = 9 \text{ seconds}$$

Then, using Equations 9 and 11,

$$t_y = \frac{V_y^2 + V_1^2}{2 A_o V_1} \quad (17)$$

Since the power term  $A_o V_1$  can be found from the previous acceleration requirement, the corner point speed  $V_1$  can be calculated. Thus,

$$V_1 = (2 A_o V_1 t_y - V_y^2)^{1/2} = 42 \text{ km/h (26 mph)} \quad (18)$$

The term  $A_o V_1$ , including friction and windage, can be found from applying Equations 2 and 4 to the power calculated in Equation 16, with the result  $A_o V_1 = 86.97$

This sets the maximum motoring corner point vehicle speed which relates directly to the base motor speed. Above base speed, for maximum tractive effort, the motor operates at constant voltage, fed by the power conditioner operating in a square wave mode. Below base speed, the motor operates at constant volts/hertz, fed by the power conditioner operating in a pulse width modulated (PWM) mode. This corner point speed is shown in Figure A-5.

### 2.9 BALANCING SPEED

The fifth requirement is for a minimum balancing speed of 97 km/h (60 mph). The friction and windage of the vehicle from Equation 1 at 97 km/h (60 mph) is 48 kg (105 lb). The drive system must have this much tractive effort available to overcome this friction and windage. This point is shown in Figure A-5. This requirement could influence the choice of speed  $V_2$ , i.e., the constant horsepower speed range, depending on the drive system's capability of meeting the balancing speed tractive effort in Region II or Region III.

### 3.0 REFERENCES

1. L. De Koranyi, "Train Resistance, Power and Energy Requirement of M-U Cars," 9th Joint ASME-IEEE Railroad Conference, May 1966
2. C.T. Hutchinson, "The Relation of Energy and Motor Capacity to Schedule Speed in the Moving of Trains by Electricity," AIEE Proceedings, January 1902.
3. A.B. Plunkett and D.L. Plette, "Inverter-Induction Motor Drive for Transit Cars," *IEEE Transactions on Industry Applications IA-13* (1), January/February 1977
4. General Electric Company, "Near-Term Electric Vehicle Phase II Final Report," March 28, 1980, DOE Contract No. DE-AC03-76CS51294
5. A.B. Plunkett and G.B. Klman, "Electric Vehicle AC Drive Development," SAE Paper 800061

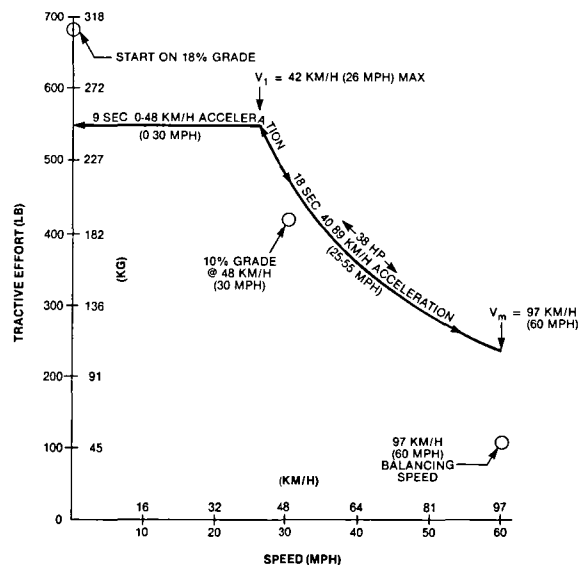


Figure A-5 Summary Vehicle Specifications



## Appendix B

### DESCRIPTION OF INDIVIDUAL CONTROL CARD OPERATION

#### 1.0 INTRODUCTION

The following discussion is a detailed description of operation for each control card in the control electronics assembly. Each control card refers to its schematic drawing contained in Appendix D. This information supplements the basic control description given in Section 3.6 and can be used for a more thorough understanding of the controls or for troubleshooting the individual control cards. Refer to Section 7.0 for the definitions of the conventions used when discussing signals on the control cards. A description of the control box used to simulate the conventional automotive driver commands is also included.

#### 2.0 DRIVER COMMAND MODULE – EP7644MDCA

The Driver Command Module is the command control box for the control electronics assembly. It simulates the conventional accelerator and brake pedals, forward and reverse, and the ignition switch. It is attached to the control electronics assembly by an 8-meter (25-foot) cable, enabling the ac controller to be operated from any number of positions, e.g., while watching another instrument.

The circuitry consists of two potentiometers buffered by voltage followers, and two toggle switches. The voltage followers are calibrated to give 0 to +10 volts for the ACCELERATE\* and BRAKE\* signal inputs. The FORWARD-REVERSE switch generates DIRECTION\*, which is a "1" for reverse and a "0" for forward. The ON-OFF switch generates ON/OFF\*, which is a "1" for on and a "0" for off and also provides a contact closure to pull in the power relay sequencing circuitry to energize the power inverter.

This box may be replaced by an interface circuit which provides two analog signals of 0 to +10 volts for ACCELERATE\* and BRAKE\*, two digital signals of 0 or +15 volts for DIRECTION\* and ON/OFF\*, and a contact closure to pull in the power contactor sequencing circuitry. The logic power supplies (+/-15 volts) are available at the P1 connector to power the interface circuitry, but it is recommended that the circuitry be isolated from the controlling equipment by isolation amplifiers for the analog signals and optical couplers or relays for the digital signals. The contact closure to energize the power inverter must be a relay contact and may include an emergency shutoff by installing a normally closed contact in series with it.

#### 3.0 CONTROL CARD DESCRIPTIONS

##### 3.1 DRIVER COMMAND AND JERK LIMIT – EP7644CDCA

This card provides several functions: the interface from the Driver Command Module to the control electronics, limiting of the rate of change of acceleration (jerk), zero-speed shutdown, and automatic reset to prevent "pullout" (too much angle between the current and flux phasors).

In the Driver Command interface, ACCELERATE\* and BRAKE\* are input buffered, corrected for polarity, and then summed by U1[E5 & E6] so that one signal is obtained. ON/OFF\* and DIRECTION\* are filtered and buffered by U8[A6] to produce /ON\* and FWD\*, respectively. Several interlock conditions are applied, the first of which is that any brake

command will override any acceleration command. BRAKE\* > 0 volts is detected by comparator U4[D6], which sets /BRK to a "0" (U7[D5]), which in turn sets NO ACC to a "1" (U10[C3]). This clamps U1[E6] output to 0 volts by way of U15[E6], preventing any effect from the ACCELERATE\* input. /BRK = "0" also turns on Q1[D1], which pulls in the brake relay in the power inverter. The second interlock condition is that if FWD\* and F/R (output which is the actual direction) do not agree, NO ACC is set to a "1" and the ACCELERATE\* input is inhibited. F/R is stored in U14[B1] and can only be changed if the system is in a shutdown condition (SD0 at U14[D2]). The difference between F/R and FWD\* is detected by U13[C1]. This sets FWD\* <> F/R = "1" which inhibits the reset input to the SD0 flip-flop (U14[D2]) and sets NO ACC = "1".

The combined ACCELERATE\* and BRAKE\* signals are rate limited by U2 [E4 & E5]. This signal (IREAL\*) is proportional to the desired real current where -10 volts is equal to full brake and +10 volts is equal to full acceleration. This circuit is scaled to slew from 0 volts to full scale (+/- 10 volts) in approximately 1 second. In addition, two clamps are applied to the signal. The first is U15[E4], which will instantly force any positive output to 0 volts in response to the NO ACC signal. This prevents a positive (acceleration) command for IREAL\* while allowing a negative (brake) command. The second is U15[E4], which clamps both polarities of the output to 0 volts at jerk limit rate in response to the RESET signal. RESET is caused by either /SD (from EP7644CPRA) or |FLUX| < MIN (U7[C5]).

Zero-speed shutdown (SD0) is generated by flip-flop U14[D2] in response to one of three sources. The first is in response to ON/OFF\* through U8[A5], U12[B3], and U11[C2] and occurs immediately. The second is the power-up reset function (P U RESET) at U8[B3], which forces the system to a reset condition at power-up. The third condition is the actual zero-speed shutdown sequence. The sequence is initiated when speed (FREQ\*) becomes less than a threshold set by R26 and 27[C6], which trips comparator U5[C6], generating S < 2 [mph]. S < 2, in either coast or brake modes, will generate SD REQ (shutdown request) at U10[C3]. This clamps IREAL\* (U15[E5]) to 0 at jerk-limit rate, causing a smooth reduction of torque. When IREAL\* reaches 0 volts, window comparator U6[B6] is tripped generating IREAL\* = 0 at U9[B5]. When both conditions exist, the sequence is complete and the SD0 flip-flop is set. Once SD0 has been set for any of the above reasons, it can only be released if ON/OFF is set for turn-on, power-up reset has timed out, and the ACCELERATE\* input is > 0 volts (and not over-ridden by BRAKE\*).

|FLUX| < MIN is generated when |FLUX| becomes less positive than a minimum threshold set by R32[C7] and R33[C6], and trips comparator U5[C6]. This condition occurs when the angle of applied voltage exceeds the pullout angle of the motor and the motor flux collapses. The resulting clamp of IREAL\* to 0 volts removes the applied torque from the motor usually fast enough to prevent pullout. As soon as the rotor flux builds up, RESET is removed and IREAL\* ramps back to the original level.

### 3.2 Current Transducer Interface – EP7644CTIA

The current transducer interface card provides two functions: the calibrated reference bias sources for the Hall effect current transducers, and the differential amplifiers for readout of the transducers. The reference source consists of a 5-volt regulator and trimmed resistors in series with the transducers' bias current input. The current sources are trimmed since the output of the transducers have a direct (1:1) sensitivity to the bias current. The transducers' output signal is very low (50 mV = 1000 amps), superimposed on a high common mode signal (approximately two volts), requiring a high gain precision amplifier to achieve a useable signal. The outputs of the card are scaled to 100 amps/volt (10 volts = 1000 amps), which

requires a gain of 200. To minimize the effect of high impedance resistors on the offset voltage, a T-network was used for the feedback resistor. In addition, the two input dividers for each op amp were trimmed to minimize the effects of resistor tolerances on the common mode rejection ratio (CMRR) of the amplifier circuit

The calibration of the card proceeds as follows

- 1 The bias current is set by selecting the trim resistor RS1 (RS2,RS3) while monitoring the bias current to the transducer. This must be done for the specific transducer in use since the bias current requirements for calibrated operation, as well as the internal impedances vary from transducer to transducer. Once the bias circuits have been calibrated, the transducer must not be replaced without re-calibrating the circuit
- 2 The output amplifier is set by selecting two resistors, RS4 (RS5,RS6) and RS7 (RS8,RS9), one in the non-inverting input network and one in the inverting input network, which is part of the feedback. The two resistor selections are interactive, so that several iterations with decade boxes or pots are required. RS4 (RS5,RS6) has a greater effect on the CMRR but some effect on gain, and RS7 (RS8,RS9) has a greater effect on gain but some effect on CMRR. A current source is required which can be accurately set and varied from 0 amps to several hundred amps. First, set the current source to 0 amps and adjust RS4 (RS5,RS6) for 0 volts on the output. Next, set the current source to the calibration point, 400 amps, and set RS7 (RS8,RS9) for 4 volts on the output. Repeat these steps until both conditions are satisfied at the same time. (A convenient test source can be achieved using 50-conductor ribbon cable and connectors so that 50 turns can be inserted through the transducer and quickly connected in series. Then 8 amps times 50 turns or 4 amps times 100 turns is equivalent to 400 amps.)

### 3.3 TORQUE CARD – EP7644CTQA

The torque card contains three major functions: the flux coil input integrators, the current transformer input amplifiers, including the high- and low-pass filters and transducer signal summing amplifiers, and the vector cross-product calculation of motor torque.

The flux coil input integrators are low offset precision amplifiers to minimize the effect of offset voltages due to the inherent high gain of an integrator. The integrators are calibrated by a series resistor in the input network. Their outputs are the flux phasor (FLUXA,FLUXB,FLUXC)

The current transformer input circuits [A4] consist of precision 50-ohm burden resistors for the 4000-turn toroidal transformers, yielding an 80-amps/volt scale factor. The three resulting signals (IA2,IB2,IC2) are high-pass filtered at 400 Hz by C22 (C23,C24) and R48 (R49,R50). The transducer interface outputs (IA1,IB1,IC1) are high-pass filtered at 400 Hz by R45 (R46,R47), R67 (R68,R69), and C25 (C26,C27). The two sets of signals are then summed by U10[B4] (U10[A4],U11[A4]) to produce the composite total current phasor (IA,IB,IC).

The vector cross-product calculation is done by first converting the three-phase current and flux signals (IA,IB,IC and FLUXA,FLUXB,FLUXC) to two-phase (d-q) equivalents as follows

$$I_d = I_A$$

$$I_q = \frac{I_C - I_B}{\sqrt{3}}$$

$$\text{FLUXd} = \text{FLUXA}$$

$$\text{FLUXq} = \frac{\text{FLUXC}-\text{FLUXB}}{\sqrt{3}}$$

The two-phase equivalents are then multiplied and summed to produce

$$(\text{FLUXq} \times \text{Id}) - (\text{FLUXd} \times \text{Iq}) = \left( \frac{\text{FLUXC}-\text{FLUXB}}{\sqrt{3}} \times \text{IA} \right) - \left( \text{FLUXA} \times \frac{\text{IC}-\text{IB}}{\sqrt{3}} \right)$$

The multiplications are done by U7[D3] and U8[C3] and summation is done by U6[D5]. The result is then filtered by U6[D6]. The four JFET transistors (Q1-Q4 [D4 and C4]) are driven in pairs by Q1 and Q2[E5] in response to F/R\*. This is to reverse polarity of the torque signal (T) when in reverse so that positive values of torque correspond to acceleration and negative values correspond to brake, regardless of direction.

### 3.4 CURRENT LIMIT – EP7644CCLA

The majority of this card is nonfunctional, being left over from early stages in the development of the system. The original use was to detect currents in excess of a maximum allowable value and to force the power inverter to switch by way of overriding inputs to the lockout card. This is now unnecessary, due to the technique of controlling current directly in the tightest inner loop of the controller. Current limit is inherent in this technique.

The portion of the card which is still used is the generation of total current magnitude (|I|) for use by the angle regulator. The diodes around U10A and U10B [D4] form a three-phase full-wave precision rectifier yielding an unfiltered full-wave rectified dc signal.

### 3.5 FLUX CONTROL – EP7644CFCA

This card has two main purposes: to generate the |FLUX| feedback signal for the angle regulator, and to control the amplitude of the inverter output by way of the amplitude control input (|I\*|) to the sine-wave reference generator.

The flux phasor signals (FLUXA, FLUXB, FLUXC) are full-wave rectified by IC1A, IC1B, and IC2B and then summed by IC2A and filtered by IC3A to generate the feedback signal |FLUX|.

The reference for the flux regulator (|FLUX\*|) is set by R25/R59 and IC4B[C4] when IREAL\* = 0 volts. This is the excitation level for the motor when no torque is being generated, and is set to reduce battery drain at coast conditions. |FLUX\*| is compared to |FLUX| by IC4A[C2], which generates |I\*|, the current amplitude command. IREAL\* is rectified by IC5A[D2] and added to |FLUX\*| at IC4B[C4] to increase the current when the motor is supplying torque. The maximum value of |FLUX\*| is set by R58/R57[D5] clamp. When IREAL\* is increased abruptly, the flux regulator cannot respond immediately and a momentary decrease in flux would result were it not for an additional input (d|FLUX|) to the regulator which is proportional to the rate of change of |IREAL\*| and causes an immediate boost in |I\*|. Additional clamps are applied to the flux regulator output by R24/R36B (minimum) and R30/R29 (maximum). These prevent the total effect of the inputs to the flux regulator from exceeding the minimum and maximum flux levels of the motor.

**NOTE:** The latter is extremely important since it defines the ultimate current limit point of the current controller. This limit can be set lower (and, indeed, it should be) when first energizing the system after any changes have been made. This is easily accomplished by connecting a resistor in parallel with R29. With R29 = 1.5 kilohms, the maximum peak current value is 600 amps. This is a safe operating point for the power inverter containing General

Electric power modules, but should be reduced to 450 amps when using Power Tech power modules by paralleling R29 with a 24 kilohm resistor.

### 3.6 ANGLE REGULATOR – EP7644CARA

The angle regulator is the most complex card in the system and contains several functions: the real current (IREAL) calculation, the real current controller, the angle (SIN  $\theta$ ) calculation, the angle controller, the traction battery under-voltage and over-voltage limits, the derivative of |SIN  $\theta^*$ | calculation for flux regulator boost, and shutdown and reset overrides to the frequency control output

The feedback signal IREAL is calculated from torque (T), flux (|FLUX|), and current (|I|) using a precision analog divider (U7[C7])

$$\text{IREAL} = \frac{T}{|\text{FLUX}| - 014 |I|}$$

This is filtered by U11[E5] and presented to the IREAL controller U3[C6] Here, it is compared to IREAL\* from U1[C7] and the error signal SIN  $\theta^*$  is generated.

The under-voltage and over-voltage limits are imposed on SIN  $\theta^*$  at U4[C5] The traction battery voltage is sampled differentially on the power inverter and input to differential amplifier U1[E7] The majority of the input resistances (190 kilohms) are on the power inverter, which limits the value of voltage entering the control electronics to a low value. The output of U1 is scaled at 20 volts/volt and is processed by two high-gain limit amplifiers These override SIN  $\theta^*$  at values predetermined by P1 and P2 potentiometers P1 sets the overvoltage limit and is presently set at 135 volts This limits the maximum voltage that the batteries will be charged to during high speed braking. P2 sets the under-voltage limit and determines the lowest that the inverter can draw the batteries during acceleration, and is presently set at 75 volts Both of these limits act to reduce power levels in a linear fashion rather than shutting the inverter down A shutdown function exists on the protection card and will be discussed in that section Clamps are applied to SIN  $\theta$  (R66/R64 and R67/R65) to limit the maximum slip angle that can be commanded to minimize pull-out of the motor.

The SIN  $\theta$  feedback signal is calculated from IREAL and |I| using another precision divider (U8[C6]).

$$\text{SIN } \theta = \frac{\text{IREAL}}{0.016 |I|}$$

SIN  $\theta^*$ , after voltage limits are applied, is compared with SIN  $\theta$  by integrator U5[D1]. The error generated is FREQ\* and controls the frequency of the sine-wave reference generator.

When flux falls below the minimum threshold defined on the driver command card, which may happen if the motor ‘pulls out’ due to excessive angle or a load torque surge, the reset signal will cause IREAL\* to be clamped to zero. It will also clamp SIN  $\theta^*$  to zero through Q1[D4] and momentarily clamp the angle regulator integrator to zero through C13, R75, and U10[E2]. The integrator will be released when C13 discharges and will integrate back toward synchronous speed at which time the flux will build back up in the motor and reset will be released.

When the inverter is commanded to shutdown (SD), the angle regulator is clamped to zero to reset the integrator to zero frequency. When SD is released, the integrator will integrate toward positive frequency If the motor is at a stand-still, the flux will build in the motor immediately and the driver command card will release IREAL\*, resulting in motor torque. If the motor is turning, the frequency will integrate upward until synchronous speed

is reached, at which time flux will build in the motor as before.

The remaining function on the card calculates the derivative of  $\text{SIN } \theta^*$  for boosting the flux regulator.  $\text{SIN } \theta^*$  is precision rectified by U12[C3] and then differentiated by U13[B2]. A clamp is applied (U13[B1]) to limit the amount of boost to a moderate level during an increase in  $|\text{SIN } \theta^*|$  and to a very small amount during a decrease in  $|\text{SIN } \theta^*|$ .

A final feature of the card is U4[C2], the driver for the SD LED on the front panel. This LED is a two-color device which is red when the controller is shut down and green when SD is released.

### 3.7 PROTECTION AND CURRENT CONTROL – EP7644CPRA

This card contains two major functions: system monitoring for automatic shutdown protection, and the current control loop comparators.

Shutdown (SD) is initiated in response to any one of eight possible fault conditions: traction battery over-voltage, traction battery under-voltage, +15 volt under-voltage, -15 volt under-voltage, interlock fault, heatsink over-temperature, zero-speed shutdown, and a spare input.

Traction battery over-voltage and under-voltage conditions are sensed by monitoring dc volts/20, which is the 20 volts/volt scaling of the traction battery from the angle regulator card. This signal is compared to thresholds scaled by R15/R17 for the over-voltage case and R16/R18 for the under-voltage case. When these thresholds are exceeded, the appropriate comparator trips (U2[B6]) and sets SD at U6[C4]. A latching LED will also be tripped (LED2[D2]) and will remain tripped by way of SCR2[D3], even if the fault condition no longer exists. This will remain to annunciate the cause of an unexpected shutdown as long as +/- 15-volt power remains valid, or the LED may be reset by pressing a button on the front edge of the card.

The +/- 15-volt power supplies are monitored by the circuitry associated with U1[D5 & D6]. If the +15-volt supply sagged, for example, the voltage at the junction of R5/R6 would become negative and trip the upper comparator. Similarly, the -15-volt supply would effect the voltage at R7/R8 and trip the lower comparator. If both supplies sagged together, the zener diodes (ZD1/ZD2) would remain biased long enough to ensure that both comparators would trip. Additional capacitors C5/C6 are diode decoupled from the main filter to ensure the protection circuitry has time to set the SD signal and stop pulses from reaching the power inverter during the loss of control logic power. This fault also sets a latching LED to annunciate the cause of an unexpected shutdown in the case where the supplies only sag in voltage rather than shut off completely.

The interlock fault detector checks for a continuous electrical path from the INTERLOCK input on the Protection card to common on the Transducer Interface card. The path uses different pin combinations on each card so that each card must be plugged into the correct slot to allow operation. Interlock faults will latch an LED.

Heatsink over-temperature will open one of two temperature sensing switches on the power inverter causing a shutdown command. The switches are located on the two heatsinks furthest from the fans since these will normally run the hottest. The switches are connected in series so that either will initiate a shutdown if too hot. There is an extra contact wired in series with the heatsink over-temperature switches, which is not related to the over-temp function directly. An auxiliary contact on the power contactor is used to hold the inverter shut down until the contactor has closed. This prevents the inverter from turning on the power inverter while the series-charging resistor is charging the main capacitors. The result if

this were not included is that the power inverter will discharge the capacitors faster than the resistor will charge them, leaving the resistor as the total load across the traction battery, a situation that the resistor is not sized to accept for more than a few seconds! The result of adding this contact is that the heatsink over-temp LED will always be tripped and latched before the power inverter is energized. If it is desired that the LED correctly announce an over-temp shutdown, the Protection card must be manually reset after the power contactor is energized.

Zero-speed shutdown (SD0) is generated on the Driver Command card as discussed in that section. This shutdown input does not have a latching LED annunciator since it is the normal mode of controlling the shutdown of the inverter.

The spare input is identical in nature to the SD0 input and is normally grounded to allow operation of the inverter. It could be used as a shutdown input if a normally closed (open = SD) contact were to be installed in place of the present jumper to common.

### 3.8 LOCKOUT AND WAVEFORM GENERATOR – EP7644CLOA

The Lockout and Waveform Generator card contains two major functions: the sine-wave reference generator, and the lockout function.

The sine-wave reference generator synthesizes three sinusoidal waveforms separated by 120 electrical degrees, whose amplitude is controlled by  $|I|^*$  and whose frequency is controlled by  $FREQ^*$ . The reference generator consists primarily of a microprocessor (U18[D3]), three digital-to-analog (D/A) converters (U19[D2], U20[C2], U21[B2]), and a voltage-to-frequency (V/F) converter (U17[B5]). The microprocessor computes the relative amplitudes of the three waveforms at a single point in the period and sends the results to three D/A converters. The amplitude of the waveforms is controlled by an analog voltage signal ( $|I|^*$ ), which is generated by the flux control loop. This signal enters the card on C12 and is inverted to form two reference voltages (+VREF & -VREF), which are then sent to the three multiplying D/A converters. The digital input sets the point on the waveform and the analog inputs (+VREF and -VREF) are the multiplying scale factor.  $FREQ^*$  (the frequency control signal) is converted by the V/F converter to a pulse train whose frequency is proportional to the desired frequency of the waveforms. This pulse train clocks the reference generator, causing it to compute successive sets of values of the waveforms. The result is three sinusoidal waveforms with discrete “staircase” values which then must be filtered (on the protection and current control card).  $F/R^*$  is used as a direct input to the microprocessor and determines whether the next point calculated is the succeeding or preceding point in the look-up table in the microprocessor’s memory. U15[D6] and U16[C6] generate clock signals used by the lockout section.

The lockout section of the card splits the phase command signals (IA COMM, IB COMM, IC COMM) into separate upper and lower power module drive commands (AU, AL, BU, BL, CU, CL) to which a lockout function is applied to force a period of time between one power module’s turn-off and the complementary power module’s turn-on. This prevents overlap of the power modules’ conduction times to prevent a “shoot-thru,” a condition which would occur if a continuous path existed through both power modules in the same phase, causing a high-fault current which would destroy the two power modules involved. The card first derives a clock pulse from both rising and falling edges of IA COMM (IB COMM, IC COMM) by clocking the waveform through flip-flops U1 (U6, U10). The flip-flops are different for one clock time as the waveform ripples through and generates a pulse through exclusive-or gate U2[D6] (U2[C6], U2[B6]). This triggers one-shot U3[D5] (U9[C5], U3[B5]) to generate the lock-out pulse. The lock-out pulse delays setting the lower module flip-flop U5[D3] (U8[C3], U12[B3]) until after the upper module flip-flop U5[E3] (U8[D3]),

U12[C3]) has been reset and vice versa. The upper and lower module flip-flops are buffered out of the system by line drivers consisting of transistors Q1/Q2 (Q5/Q6, Q9/Q10) and Q3/Q4 (Q7/Q8, Q11/Q12). These buffers drive the base driver modules (EP7644MBDA) on the power inverter assembly through coaxial cables. The base driver modules are optically coupled at the input, and are designed to source base current to the power modules when current is flowing at the input, and to sink base current from the power modules when input current is not flowing. The current sink mode of operation is intended to "sweep out" stored charge from the base junctions of the power modules for fast turn-off.

## Appendix C

### SETUP INSTRUCTIONS FOR AC CONTROLLER OPERATION

#### 1.0 INTRODUCTION

A great deal of care is required during the initial setup of the ac controller. Once the system is correctly installed, it is highly tolerant of "operator errors," but errors in the initial setup phase can cause equipment damage.

The traction battery bank must consist of series-connected battery units totalling 108 volts (e.g., 18 units at 6 volts/unit) having sufficient capacity to supply 450 amperes without significant voltage loss due to IR drops. The 108-volt positive lead is connected to the 450-amp fuse mounted on the power contactor on the power inverter, and the 108-volt common return is connected to the longer bus bar immediately adjacent to the 450-amp fuse. It is recommended that a contactor or other means of disconnecting the traction battery from the power leads at the source end as well as additional fusing be provided for safety reasons.

The 12-volt auxiliary battery must be connected to the ac controller at the power inverter through cables sufficient to carry 20 amps dc steady-state +12 volts to TB2-1 and 12 COM to TB2-2. The power inverter and the control electronics are interconnected using the multiple twisted-pair cable as follows: (1) the red and black pair is connected: red to TB2-1 and black to TB2-2 on the power inverter, and red to TB1-7 and black to TB1-8 on the control electronics unit (this applies the auxiliary battery to the power inverter first where most of the current is drawn, and to the control electronics second), (2) the white and black pair is connected: white to TB6-2 and black to TB6-1 on the power inverter, and white to TB1-1 and black to TB1-2 on the control electronics unit. This connects the traction battery voltage feedback.

*NOTE:* The traction battery should be isolated from earth ground and the 12-volt auxiliary battery connected to earth ground at the chassis of the control electronics unit. This will result in the least incidence of ground loops and will avoid high fault currents from the traction battery should a connection be made inadvertently between the traction battery power circuit and any point in the control electronics circuitry.

The remaining connections to the control electronics are straight-forward through cable connectors which are keyed so that they can only be connected to one socket. These include: P3 — current transducers, P11 — current transformers, P4 — relay control to the power inverter, P2 — flux coils in the motor, P1 — driver command module (or custom interface), and P5-P10 — the coaxial cables to the base driver modules on the power inverter.

*NOTE.* The connections for the current transformers have not been implemented on the second control electronics assembly (residual inventory). If this assembly is used, the required CT's must be connected into the Torque card as shown on EP7644MCEA and EP7644CTQA.

The motor connections are made using the Motor Terminal Board drawing — EP7644MMTA. It is important that the motor current leads and the flux coil voltage leads agree as to correct phase rotation or the torque, real current, and angle calculations will all be incorrect. If the motor accelerates in one direction and brakes in the other when no acceleration or braking torque is being called for, the probable cause is that only one set of flux coils

is connected. This will cause the flux vector to be rotated by 15-degrees which creates a 15-degree error in the angle calculation

## 2.0 INITIAL POWER APPLICATION

When power is first applied, several steps should be taken to verify that correct voltages and polarities are applied and that connections have been properly made. These should first be checked visually and then at low voltage and current levels. The following procedure is recommended as a step-by-step approach to this verification procedure

### Visual check

1. Verify that all connections on the power inverter are correct and tight. This is particularly important for the bus bar connections between half-phase modules and the bus bar connections at the dc filter capacitor bank. Also make certain that the small L-shaped bus bar from the power module to C2 is in place. This piece is easily omitted, e.g., if power modules have been changed. If so, the opposite power module will turn on once but will be destroyed at the first turn off due to over-voltage since the free-wheeling diode which protects a given power module during turn off is in the opposite power module.

### Low voltage and current checks:

2. Temporarily disconnect the traction battery supply, disconnect P1 (driver command module) and pull all of the electronic cards out at least one inch to disconnect them from the power supplies. Disconnect the 12-volt power at each base drive module (square black plug). If possible, replace (temporarily) the 12-volt auxiliary battery with a power supply capable of 12 volts and 20 amps minimum. Turn on the 12-volt auxiliary battery supply and verify that less than 1 amp of current is being drawn. Verify that the  $\pm$  15-volt dc/dc converters are functioning by measuring from P1-G to P1-J and from P1-H to P1-J. Turn off the auxiliary battery supply.
3. Plug in the electronic cards and connect P1. Connect the 12-volt power at each base drive module. With the ON/OFF switch on the driver command module in the OFF position, again turn on the auxiliary battery supply. Verify that approximately 5 amps ( $\pm$  1) are flowing. With a DVM or multimeter, measure each base drive module from B2-to-E and from B1-to-E at the output terminal board. B2-to-E should measure  $-3$  ( $\pm$  1) volts and B1-to-E should measure  $-4$  ( $\pm$  1) volts with approximately 1 volt difference between them. This indicates that all base drivers are receiving turn off commands (negative voltage) and that the power modules do not have shorted base junctions (voltages greater than 1 volt in magnitude).
4. With the traction battery still disconnected, place the ON/OFF switch on the driver command module in the ON position. The power contactor should pull in immediately and the auxiliary battery supply current should increase to approximately 10 ( $\pm$  1) amps. Place the ON/OFF switch in the OFF position and turn off the auxiliary battery supply.
5. Pull out the protection card and connect a jumper from +15 volts (card pin 32) to the end of R23 nearest to U9 to defeat the traction battery under-voltage function. Replace the protection card, turn on the auxiliary battery supply, and verify that the supply current is approximately 5 amps. With both ACCELERATE and BRAKE controls fully counterclockwise, place the ON/OFF switch in the ON position. The contactor should again pull in and the current should rise to approximately 10 amps. Turn the ACCELERATE control partially clockwise and observe the LED indicator on the front cov-

er change from red to green. The current should rise to approximately 15 amps (+/- 2). This indicates the base drivers are sourcing current into the power modules. Turn the ACCELERATE control fully counterclockwise, the ON/OFF switch to OFF, and turn off the auxiliary battery supply.

6. Connect an oscilloscope differentially across B1-to-E on A-upper base drive module and B1-to-E on A-lower base drive module (two differential input pairs). Turn the auxiliary battery supply on and observe that the oscilloscope shows two dc signals at approximately -4 volts. Place the ON/OFF switch to ON, turn the ACCELERATE control clockwise, and observe two square waves appear and smoothly increase in frequency. The waveforms should switch between approximately -4 volts and +1.5 volts. When the waveforms reach maximum frequency, expand the oscilloscope time base and observe that the two waveforms are of opposite phase and each slightly less than 50% duty cycle. The falling edge of each must occur 25 microseconds (40 for Power Tech power modules) before the rising edge of the other to prevent overlap and resulting "shoot-thru" (see section on lockout card). Repeat for B-upper and B-lower and for C-upper and C-lower.
7. Reconfigure the oscilloscope for three-channel, single-ended operation and observe B1-to-E on A-lower, B-lower, and C-lower. These should appear as three waveforms at 120 degrees phase shift from each other.
8. Using a dc current probe, observe the B1 and B2 base currents of each power module (close probe around B1 and B2 wires together). The current should have a rise-time of less than 1 microsecond to a level of approximately 4 amps and a fall-time of less than 1 microsecond to a narrow negative pulse of approximately -5 amps followed by a level of -0.5 to -1 amp. The negative pulse is the "sweep-out" of current from the base-emitter junction forcing rapid turn off of the power module. Turn the ACCELERATE control fully counter-clockwise, the ON/OFF switch to OFF, and the auxiliary battery supply off.
9. If all of the above tests have been successful, the power inverter is now ready to apply power to the motor. It is advisable to do this at very low currents and voltages however, to verify that the control electronics are fully functional. To do this, connect a power supply capable of 20-40 volts and 20-50 amps in place of the traction battery. Connect three oscilloscope channels to IA, IB, IC on the torque card (EP7644CTQA) and a fourth to IA COMM on the protection and current control card (EP7644CPRA). With the higher current supply off, turn on the auxiliary battery supply, place the ON/OFF switch ON, and turn the ACCELERATE control fully clockwise as in step (6) above. When the waveform on IA COMD reaches maximum frequency, slowly bring the high current supply up while watching IA, IB, IC. A set of three sinusoidal waveforms should appear at the same frequency as IA COMD and at 120 degrees phase shift from each other. These should grow in amplitude as the high current supply is increased. Turn the high current supply off, the ACCELERATE control fully counterclockwise, the ON/OFF switch OFF, and the auxiliary battery supply off.

Full voltage and current checks.

10. The power inverter is now ready for normal operation. Pull the protection card, remove the jumper so that the traction battery under-voltage is functional, and replace the card. Remove the flux control card (EP7644CFCA) and connect a 7.5 kohm resistor in parallel with R29 to reduce the current limit. Replace the auxiliary battery supply with the auxiliary battery, and the high current supply with the traction battery and close the appropriate breakers. Connect a multimeter across the dc filter capacitor bank or monitor

–DCV/20 on the angle regulator card. Make sure that the ACCELERATE control is fully counterclockwise, then place the ON/OFF switch to ON and this time the contactor on the power inverter should not close immediately. Instead, the capacitors will charge up, taking two or three seconds, then the contactor will close and the blowers should start. Turn the BRAKE control slightly clockwise and verify the blowers drop in speed indicating the system is in brake. Return the BRAKE control fully counterclockwise, then turn the ACCELERATE control slowly clockwise. The power inverter should start and the motor should begin to accelerate at a slow rate. Moving the ACCELERATE control fully counterclockwise should put the system in coast or, if insufficient speed has been developed, will shut the system down. If sufficient speed has been developed to remain in coast with the inverter running, turn the BRAKE control slowly clockwise and observe the motor slowing down. As brake rate is increased, observe also, a rise in the traction battery voltage indicating regeneration into the batteries. Power down the system, and remove the 7.5-kohm resistor from the flux control card to regain full current limit.

The system has now been fully checked out in a step-by-step procedure which should avoid damage, if any errors occurred in setting up. The equipment can therefore be pronounced fully operational.

## **Appendix D**

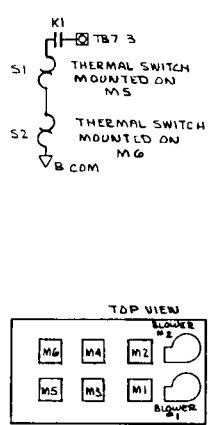
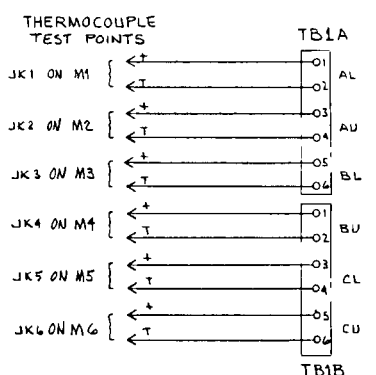
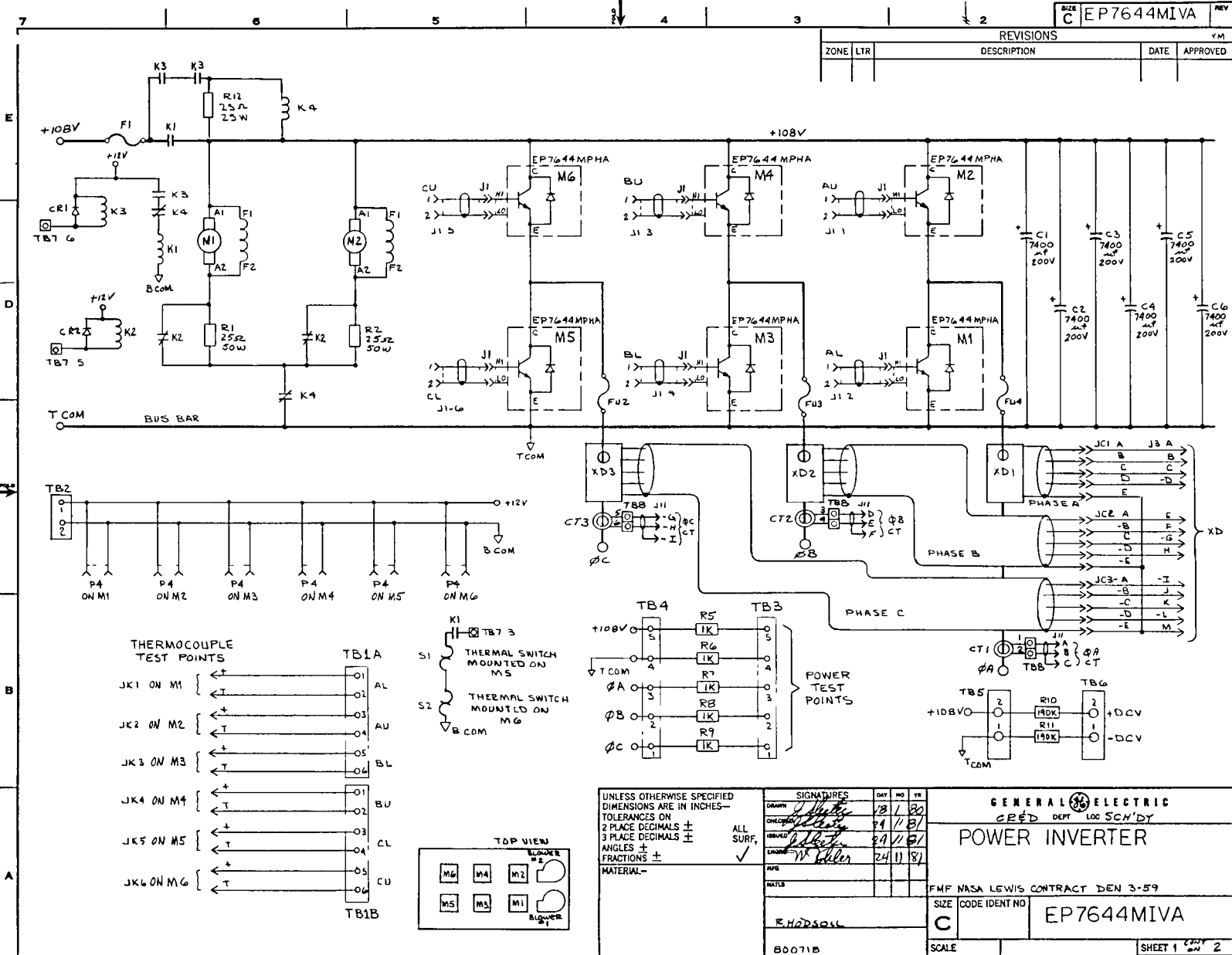
### **AC CONTROLLER DRAWINGS**

This appendix contains the following drawings for the power inverter and control electronics of the ac controller

- EP7644MIVA, Power Inverter, Schematic and Assembly, 2 sheets
- EP7644MPHA, Half Phase Module, Schematic and Assembly, 1 sheet.
- EP7644CBDA, Base Drive, Schematic, 1 sheet
- EP7644SICA, System Interconnection, Diagram, 1 sheet.
- EP7644MCEA, Control Electronics, Schematic and Assembly, 2 sheets.
- EP7644MDCA, Driver Command Module, Schematic and Assembly, 1 sheet
- EP7644CARA, Angle Regulator, Schematic and Assembly, 2 sheets
- EP7644CCLA, Current Limit, Schematic and Assembly, 2 sheets.
- EP7644CDCA, Driver Command and Jerk Limit, Schematic and Assembly, 2 sheets.
- EP7644CFCA, Flux Control, Schematic and Assembly, 2 sheets
- EP7644CLOA, Lockout and Waveform Generator, Schematic and Assembly, 3 sheets.
- EP7644CPRA, Protection and Current Control, Schematic and Assembly, 2 sheets.
- EP7644CTIA, Current Transducer Interface, Schematic and Assembly, 2 sheets.
- EP7644CTQA, Torque, Schematic and Assembly, 2 sheets

The functions of these circuits are described in Sections 3.6, 3.7, 3.8, and Appendix B.

REVISIONS				
ZONE	LTR	DESCRIPTION	DATE	APPROVED



UNLESS OTHERWISE SPECIFIED DIMENSIONS ARE IN INCHES— TOLERANCES ON 2 PLACE DECIMALS ± 3 PLACE DECIMALS ± ANGLES ± FRACTIONS ± MATERIAL—

SIGNATURES	DAY	MO	YR
DRW	18	1	80
CHKD	19	11	81
ENGRD	24	11	81
UNDR	24	11	81

ALL SURF. ✓

**GENERAL ELECTRIC**  
CRFD DEPT LOC SCH'DY

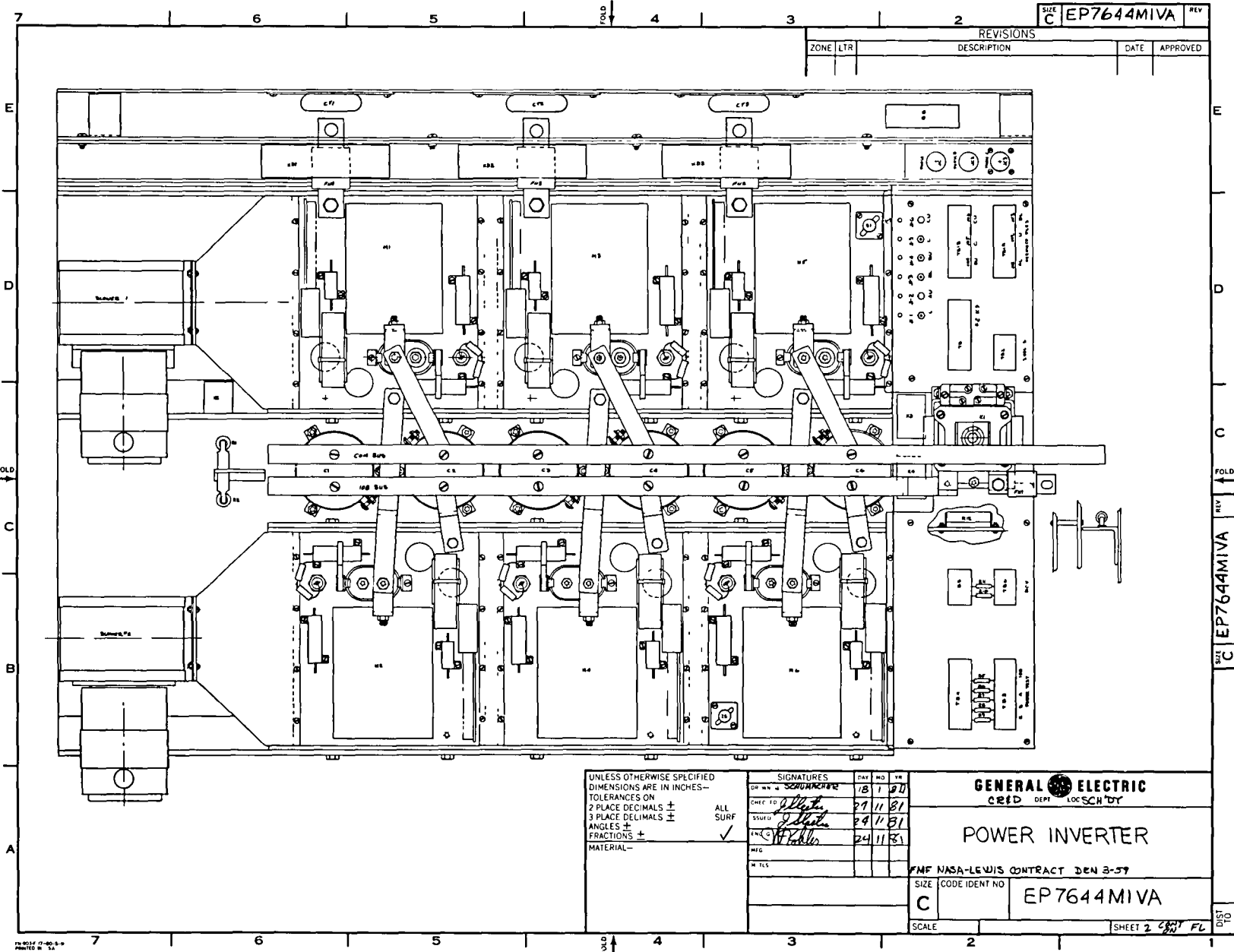
**POWER INVERTER**

FMF NASA LEWIS CONTRACT DEN 3-59

SIZE CODE IDENT NO **C** EP7644MIVA

SCALE SHEET 1 OF 2

191



SIZE	EP7644MIVA	REV
------	------------	-----

REVISIONS			DATE	APPROVED
ZONE	LTR	DESCRIPTION		

UNLESS OTHERWISE SPECIFIED  
DIMENSIONS ARE IN INCHES—  
TOLERANCES ON  
2 PLACE DECIMALS ±  
3 PLACE DECIMALS ±  
ANGLES ±  
FRACTIONS ±  
MATERIAL—

SIGNATURES		DAY	MO	YR
CHKD BY	<i>S. J. ...</i>	18	11	81
DESIGNED BY	<i>J. ...</i>	29	11	81
ENG'G	<i>J. ...</i>	29	11	81
INSP	<i>J. ...</i>	24	11	81

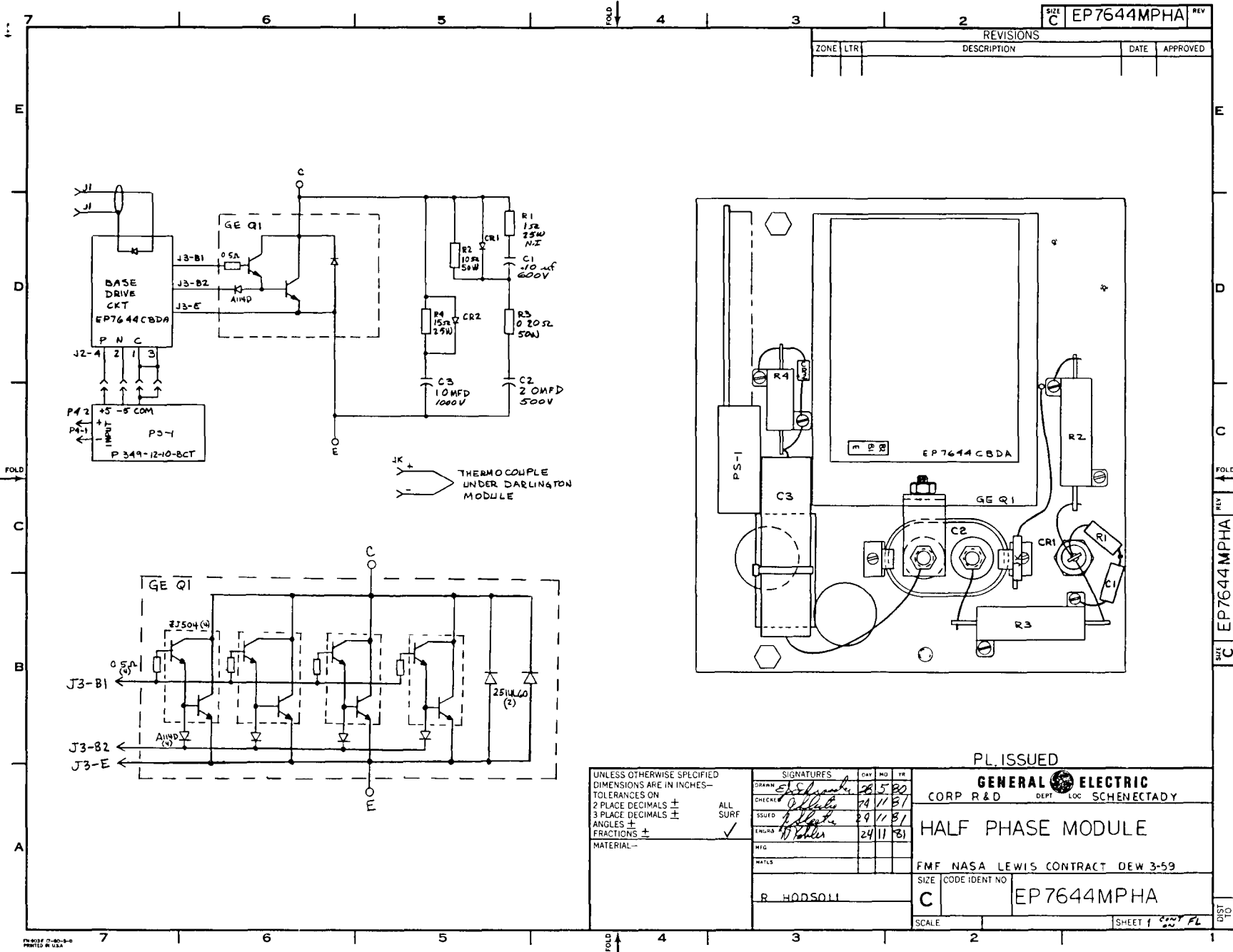
**GENERAL ELECTRIC**  
GRID DEPT LOC SCH'DY

**POWER INVERTER**

FNF NASA-LEWIS CONTRACT DEN 3-57

SIZE	CODE IDENT NO
C	EP7644MIVA

SCALE	SHEET 2	OF 2	FL
-------	---------	------	----



SIZE C EP7644MPHA REV

REVISIONS			
ZONE	LTR	DESCRIPTION	DATE APPROVED

FOLD

FOLD

C

C

B

B

A

A

PH 4037 7-60-3-0  
PRINTED IN U.S.A.

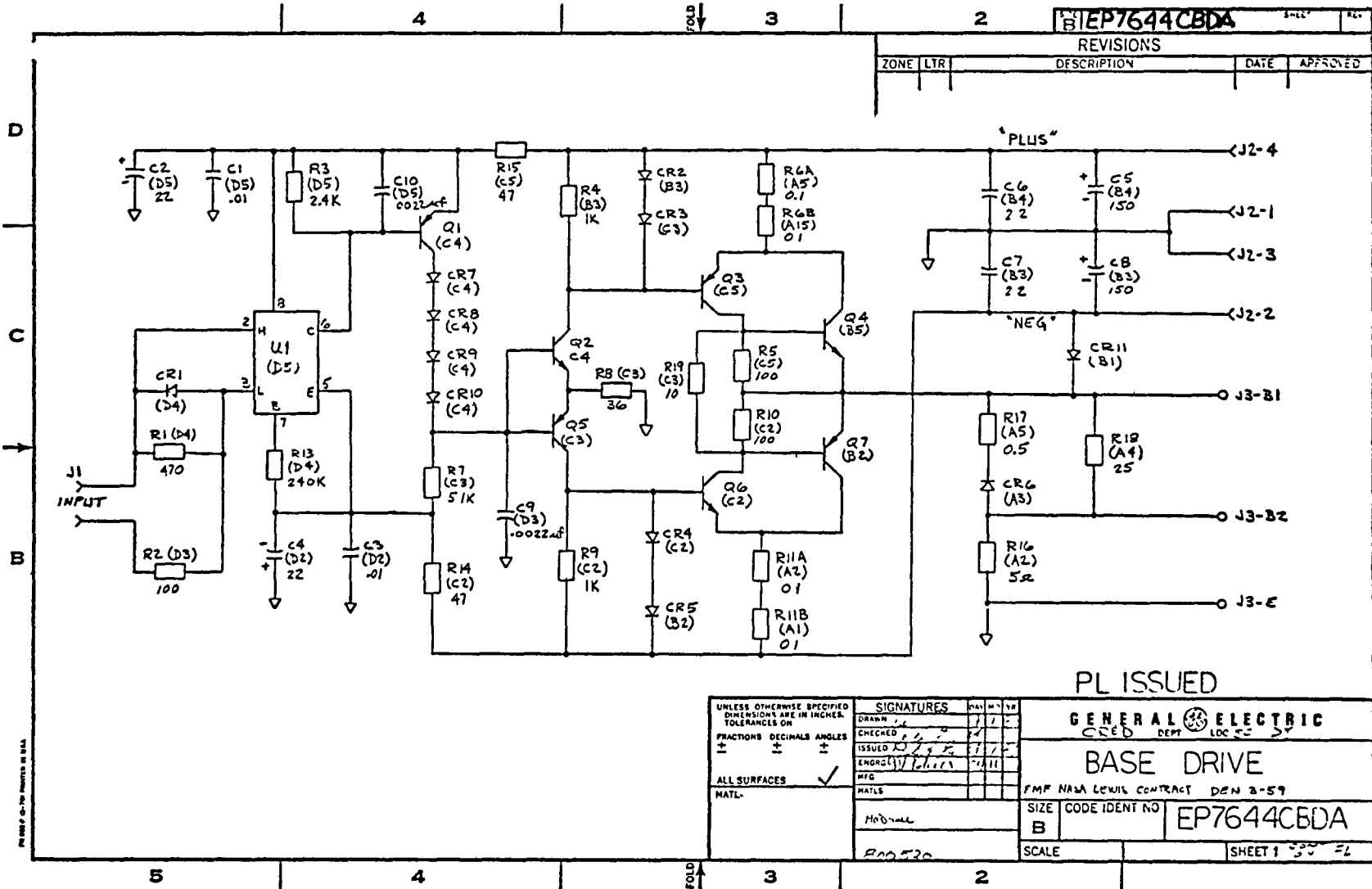
PL ISSUED

UNLESS OTHERWISE SPECIFIED DIMENSIONS ARE IN INCHES— TOLERANCES ON 2 PLACE DECIMALS ± 3 PLACE DECIMALS ± ANGLES ± FRACTIONS ± MATERIAL—	ALL SURF	✓
	SIGNATURES	DAY MO YR
	DRAWN	28 5 80
	CHECKED	24 11 81
	ISSUED	29 11 81
ENGRS	29 11 81	
MFG		
MATLS		
R HODSOLL		

GENERAL ELECTRIC	
CORP R & D	DEPT LOC SCHENECTADY
HALF PHASE MODULE	
FMF NASA LEWIS CONTRACT DEW 3-59	
SIZE	CODE IDENT NO
C	EP7644MPHA
SCALE	SHEET 1 OF 2

SIZE C EP7644MPHA REV

PL



REVISIONS			
ZONE	LTR	DESCRIPTION	DATE

PL ISSUED

**GENERAL ELECTRIC**  
CREED DEPT LOC 52

**BASE DRIVE**

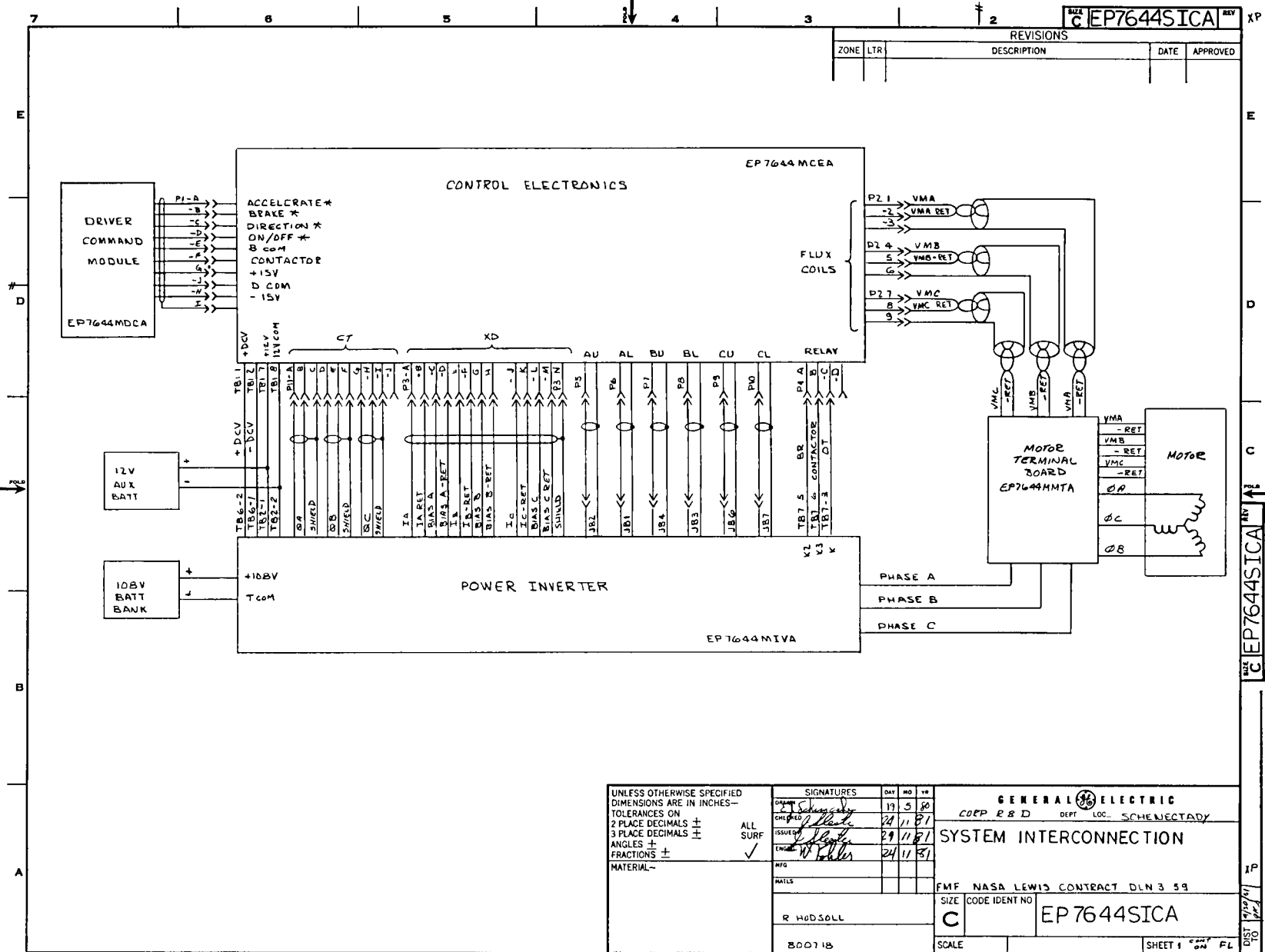
FPM NASA LEWIS CONTRACT DEN 3-59

SIZE	CODE IDENT NO
B	EP7644CBDA

SCALE: SHEET 1 OF 2

UNLESS OTHERWISE SPECIFIED DIMENSIONS ARE IN INCHES. TOLERANCES ON FRACTIONS DECIMALS ANGLES ± ± ± ALL SURFACES ✓ MATL:	SIGNATURES			DAY	MO	YR
	DRAWN					
	CHECKED					
	ISSUED					
	ENG'G					
	MATERIAL					

ALL DIMENSIONS UNLESS OTHERWISE SPECIFIED ARE IN INCHES



REV EP7644SICA XP

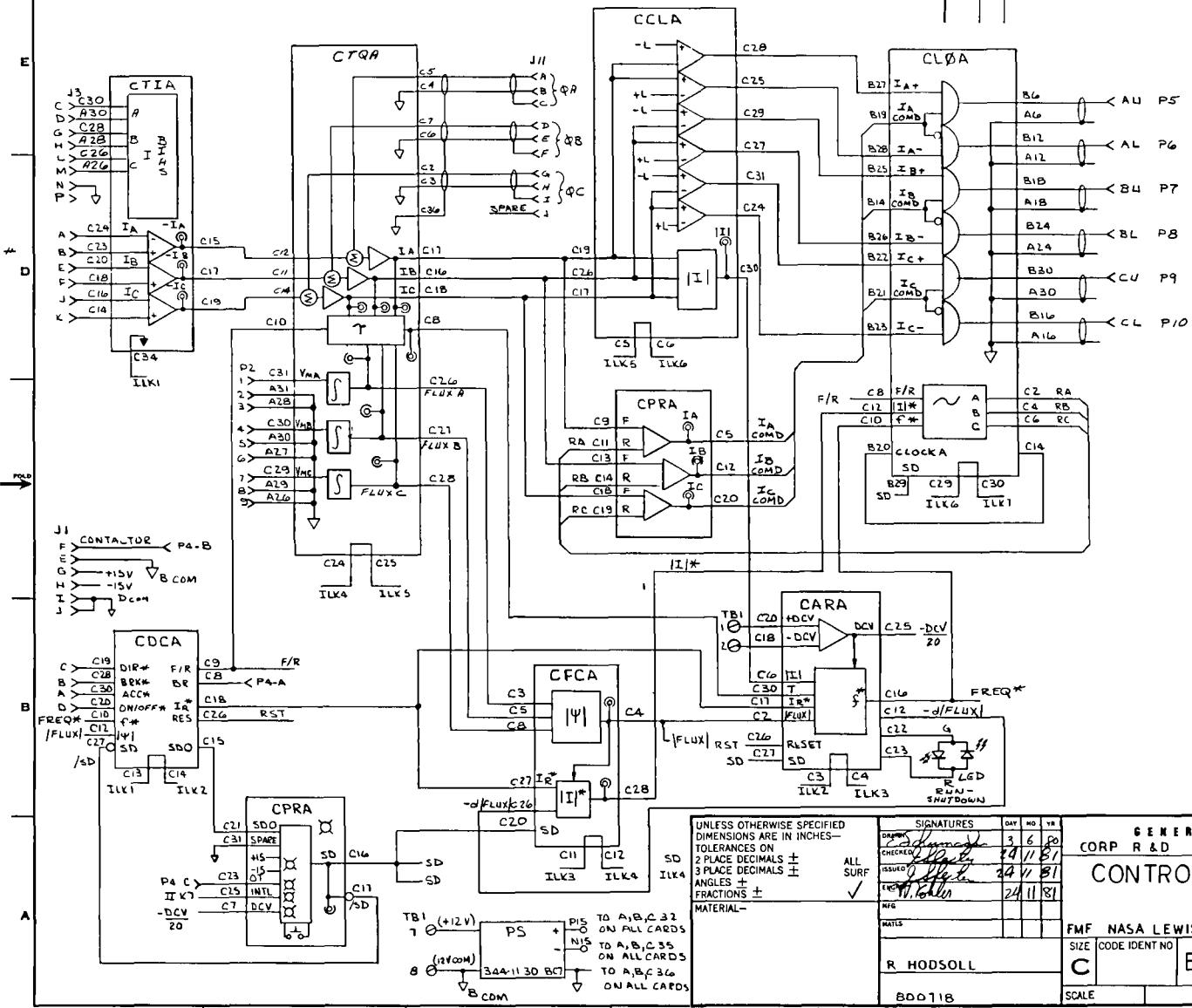
REVISIONS				
ZONE	LTR	DESCRIPTION	DATE	APPROVED

UNLESS OTHERWISE SPECIFIED DIMENSIONS ARE IN INCHES— TOLERANCES ON 2 PLACE DECIMALS ± 3 PLACE DECIMALS ± ANGLES ± FRACTIONS ± MATERIAL—	SIGNATURES			
	DESIGNED	19	5	50
	CHECKED	24	11	51
	ISSUED	29	11	51
	ENGR	24	11	51
ALL SURF ✓	MFG			
MATERIALS				
R HODSOLL				
800718				

<b>GENERAL ELECTRIC</b> CORP R & D DEPT LOC. SCHEMECTADY	
<b>SYSTEM INTERCONNECTION</b>	
FMF NASA LEWIS CONTRACT DLN 3 59	
SIZE CODE IDENT NO <b>C</b>	EP 7644SICA
SCALE	SHEET 1 OF 1 FL

SIZE **C EP7644MCEA** REV 1

REVISIONS		DATE	APPROVED
ZONE	LTR	DESCRIPTION	X P



UNLESS OTHERWISE SPECIFIED DIMENSIONS ARE IN INCHES— TOLERANCES ON 2 PLACE DECIMALS ± 3 PLACE DECIMALS ± ANGLES ± FRACTIONS ± MATERIAL—

SIGNATURES	DATE	NO	BY
<i>[Signature]</i>	24	6	80
<i>[Signature]</i>	24	11	81
<i>[Signature]</i>	24	11	81

**GENERAL ELECTRIC**  
CORP R & D DEPT. LOC. SCHEENECTADY

**CONTROL ELECTRONICS**

FMF NASA LEWIS CONTRACT DEW 3-59

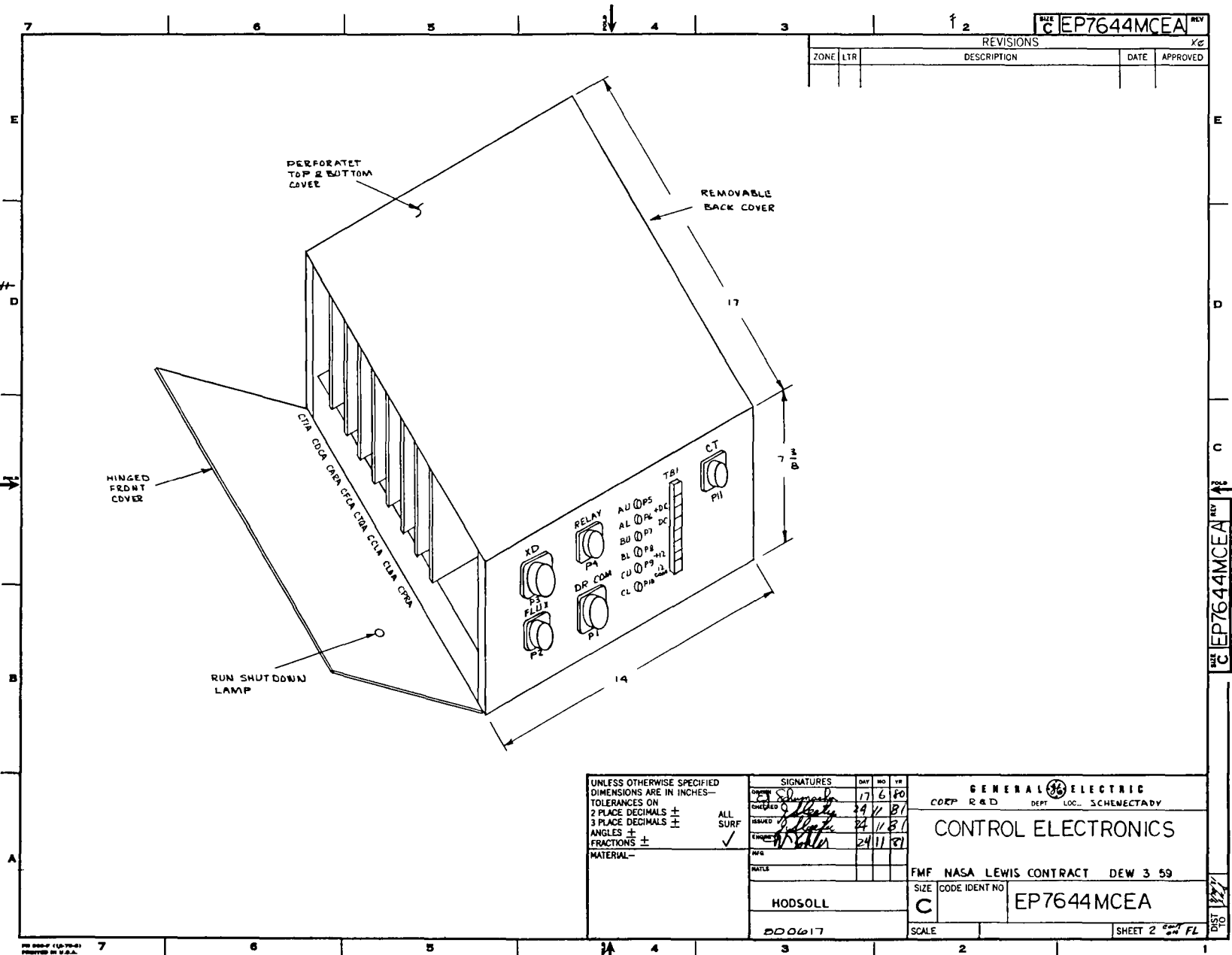
SIZE CODE IDENT NO **C EP7644MCEA**

R HODSOLL

BDD71B

SCALE

SHEET 1 OF 2



ZONE		LTR		DESCRIPTION	DATE	APPROVED

BASE **C EP7644MCEA** REV

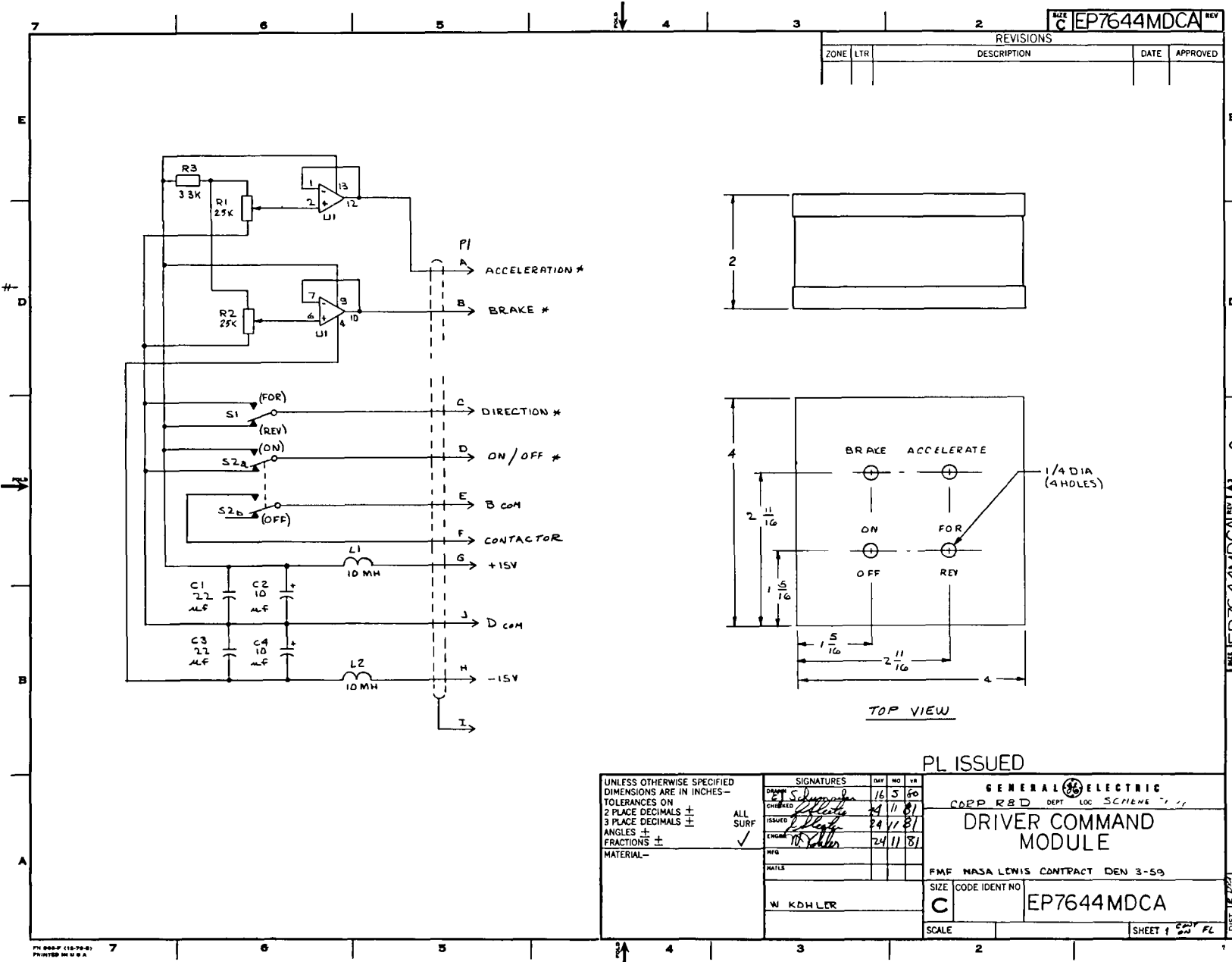
REVISIONS

KC

UNLESS OTHERWISE SPECIFIED DIMENSIONS ARE IN INCHES— TOLERANCES ON 2 PLACE DECIMALS ± 3 PLACE DECIMALS ± ANGLES ± FRACTIONS ± MATERIAL—	SIGNATURES	DAY	MO	YR	GENERAL ELECTRIC CORP R&D DEPT LOC. SCENECTADY  CONTROL ELECTRONICS  FMF NASA LEWIS CONTRACT DEW 3 59 SIZE CODE IDENT NO <b>C EP7644MCEA</b> SCALE SHEET 2 OF 2 FL
	DESIGNED <i>[Signature]</i> CHECKED <i>[Signature]</i> DRAWN <i>[Signature]</i> ENGR. <i>[Signature]</i>	17	6	80	
	ALL SURF ✓ MFG	24	11	81	
	HODSOLL DD0617	24	11	81	

BASE **C EP7644MCEA** REV

197



ZONE		LTR		DESCRIPTION	DATE	APPROVED

REV C EP7644MDCA

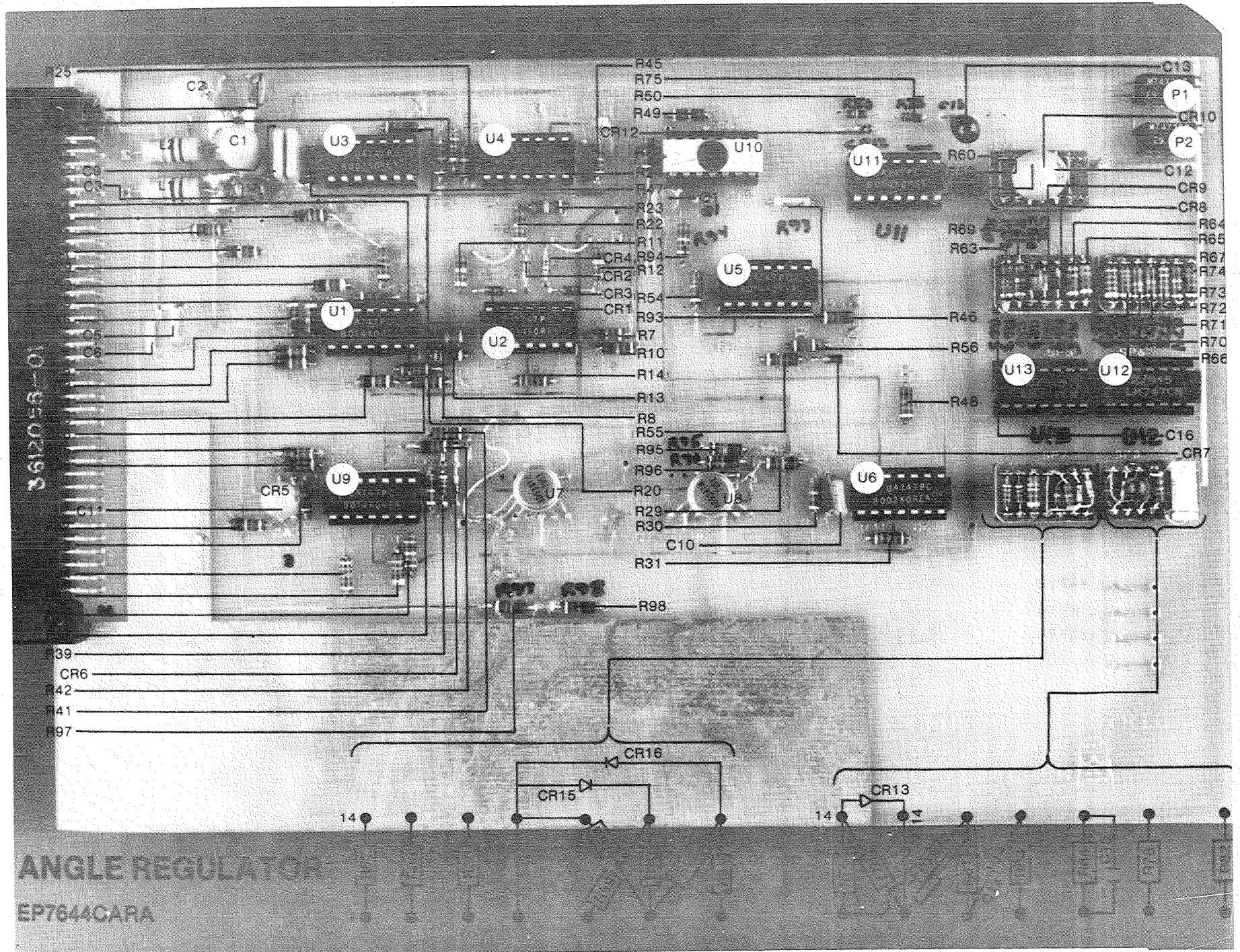
PL ISSUED

SIGNATURES	DAY	NO	YR
	DESIGNED: <i>[Signature]</i>	16	5
CHECKED: <i>[Signature]</i>	24	11	81
ISSUED: <i>[Signature]</i>	24	11	81
ENGINEER: <i>[Signature]</i>	24	11	81

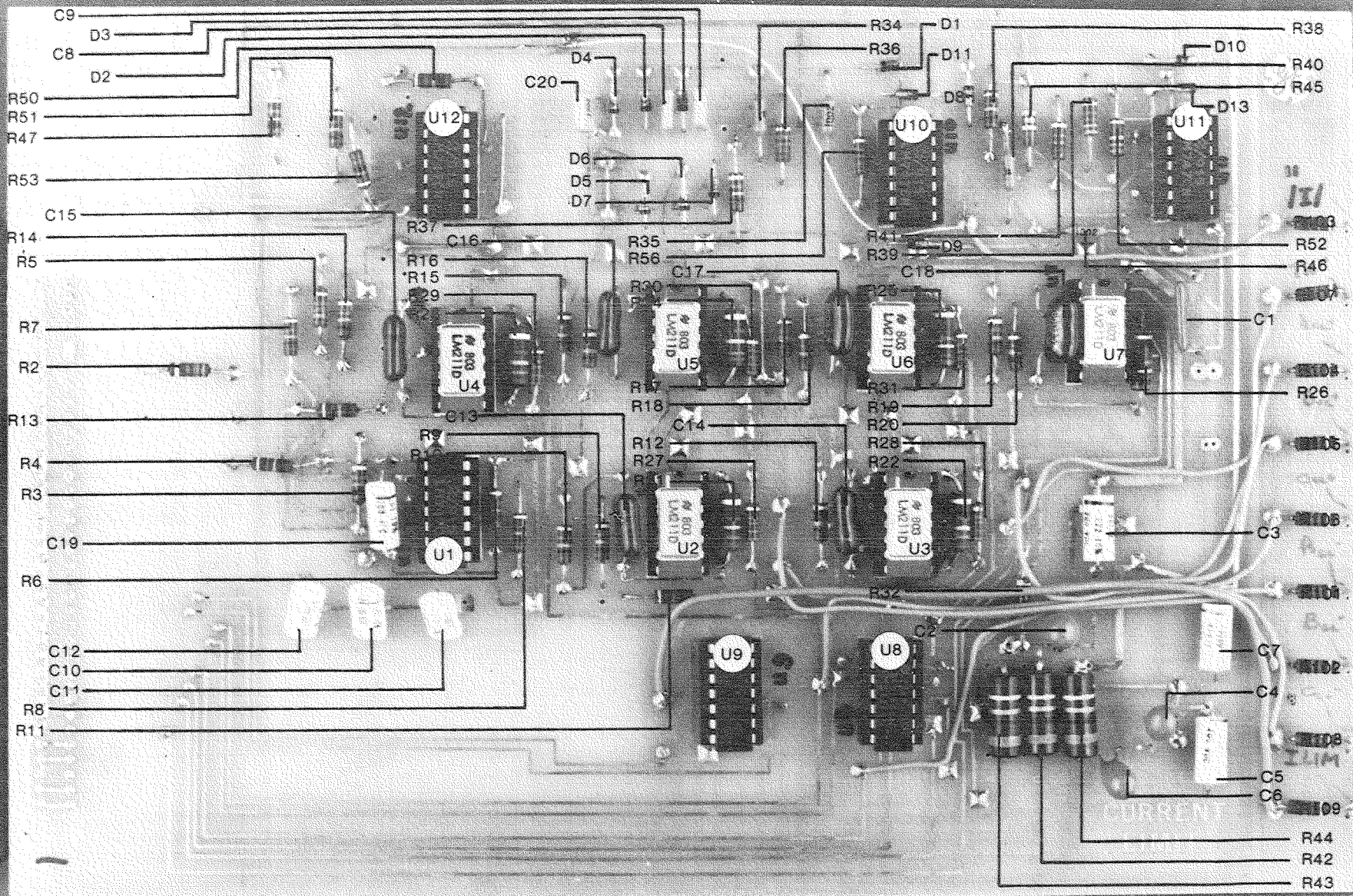
UNLESS OTHERWISE SPECIFIED DIMENSIONS ARE IN INCHES— TOLERANCES ON 2 PLACE DECIMALS ± 3 PLACE DECIMALS ± ANGLES ± FRACTIONS ±		ALL SURF ✓	MATERIAL—
GENERAL ELECTRIC CORP R&D DEPT LOG SCHEME 7, 11		DRIVER COMMAND MODULE	
FMM NASA LEWIS CONTRACT DEN 3-59		SIZE C	CODE IDENT NO EP7644MDCA
W KOHLER		SCALE	SHEET 1 OF 1 PL

REV C EP7644MDCA



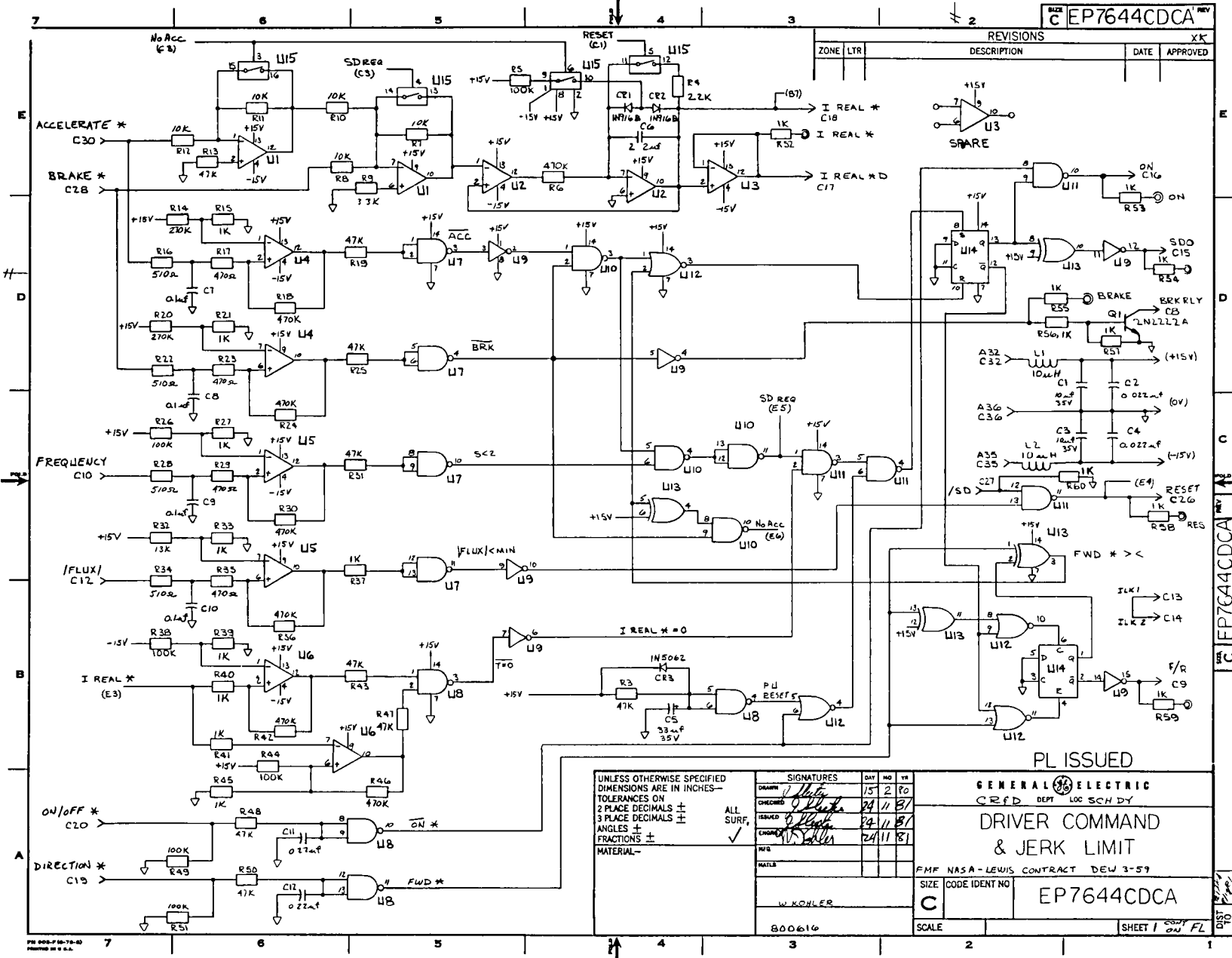






EP7644CCLA

CURRENT LIMIT



REV C EP7644CDCA

ZONE	LTR	DESCRIPTION	DATE	APPROVED

UNLESS OTHERWISE SPECIFIED  
DIMENSIONS ARE IN INCHES—  
TOLERANCES ON  
2 PLACE DECIMALS ±  
3 PLACE DECIMALS ±  
ANGLES ±  
FRACTIONS ±  
MATERIAL—

SIGNATURES  
DRAWN: *[Signature]*  
CHECKED: *[Signature]*  
ISSUED: *[Signature]*  
CHANGED: *[Signature]*  
DATE: 15 2 87  
DATE: 24 11 87  
DATE: 24 11 87

PL ISSUED

GENERAL ELECTRIC  
CRFD DEPT LOC SCH DY

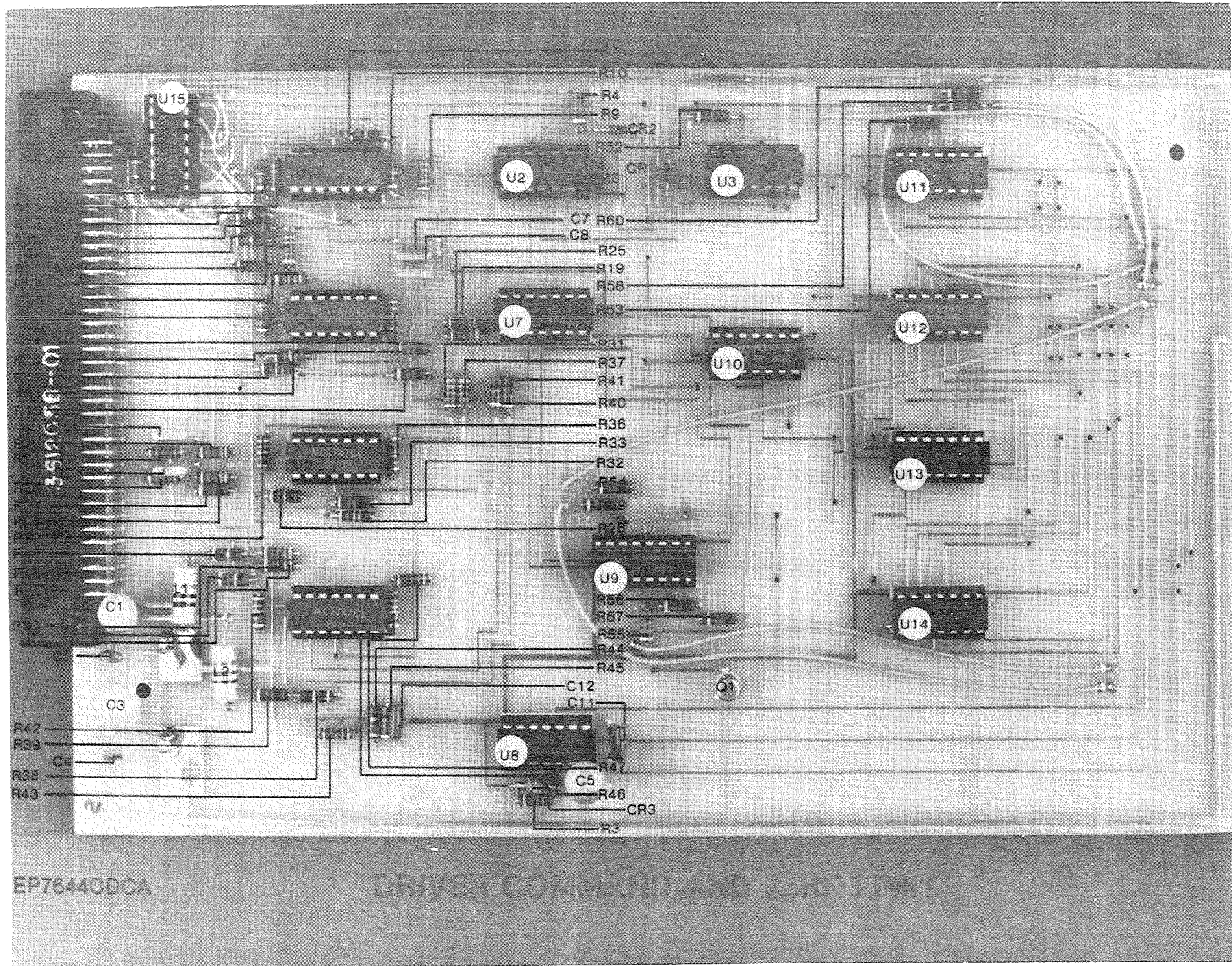
DRIVER COMMAND  
& JERK LIMIT

FNF NASA-LEWIS CONTRACT DEW 3-59

SIZE CODE IDENT NO  
C EP7644CDCA

SCALE  
800616

SHEET 1 OF 1 FL



GENE JOHNSON  
371466

XF

GENERAL ELECTRIC

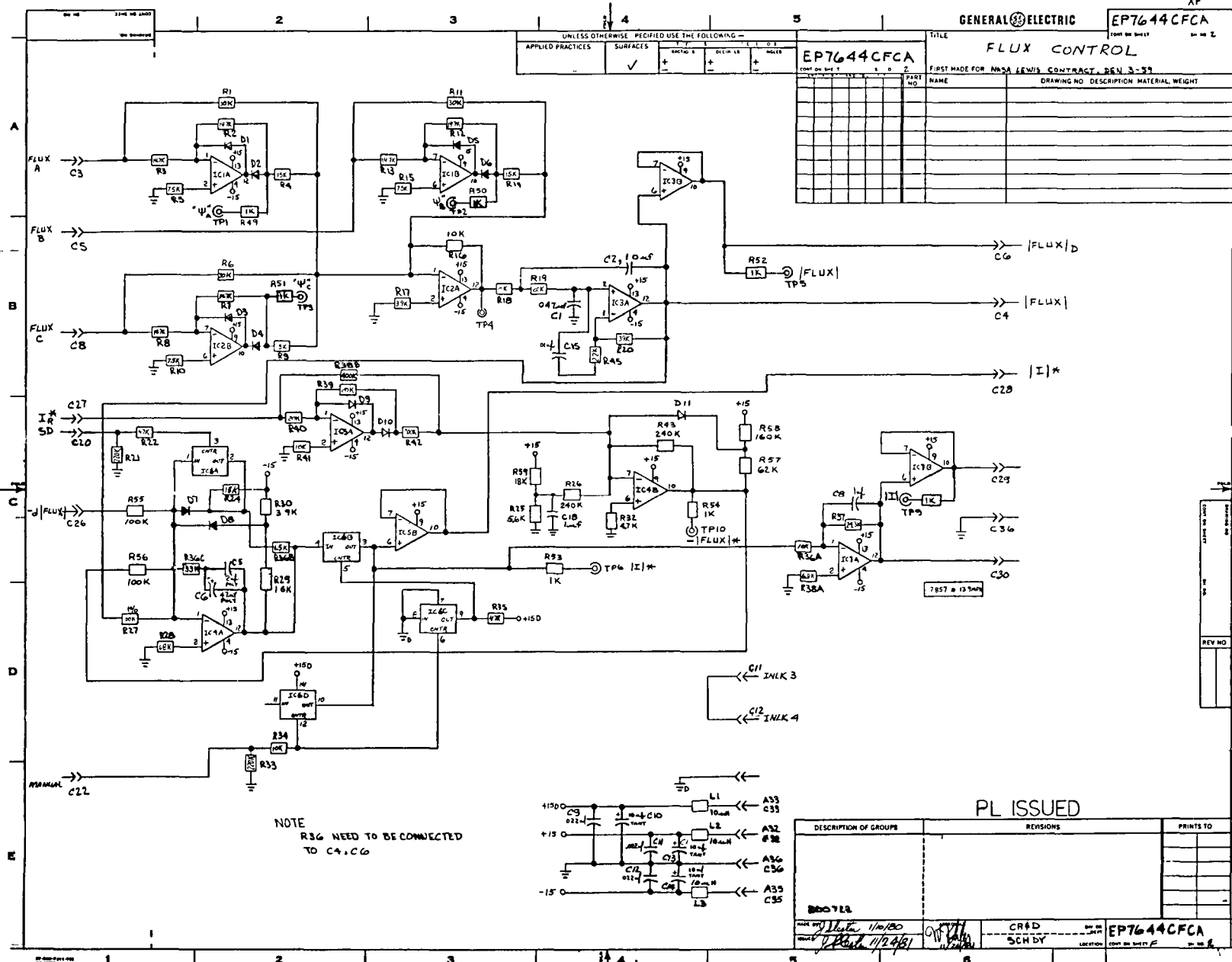
EP7644CFCA

UNLESS OTHERWISE SPECIFIED USE THE FOLLOWING—

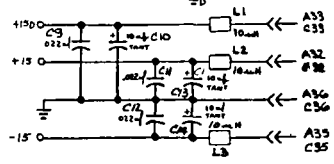
APPLIED PRACTICES	SURFACES	1	2	3	4	5

EP7644CFCA  
CONT. ON SHEET 1

TITLE		FIRST MADE FOR		DRAWING NO.		DESCRIPTION		MATERIAL		WEIGHT	
FLUX CONTROL		ANSA LEWIS CONTRACT, REV. 3-53									
NAME											



NOTE  
R36 NEED TO BE CONNECTED  
TO C4, C6

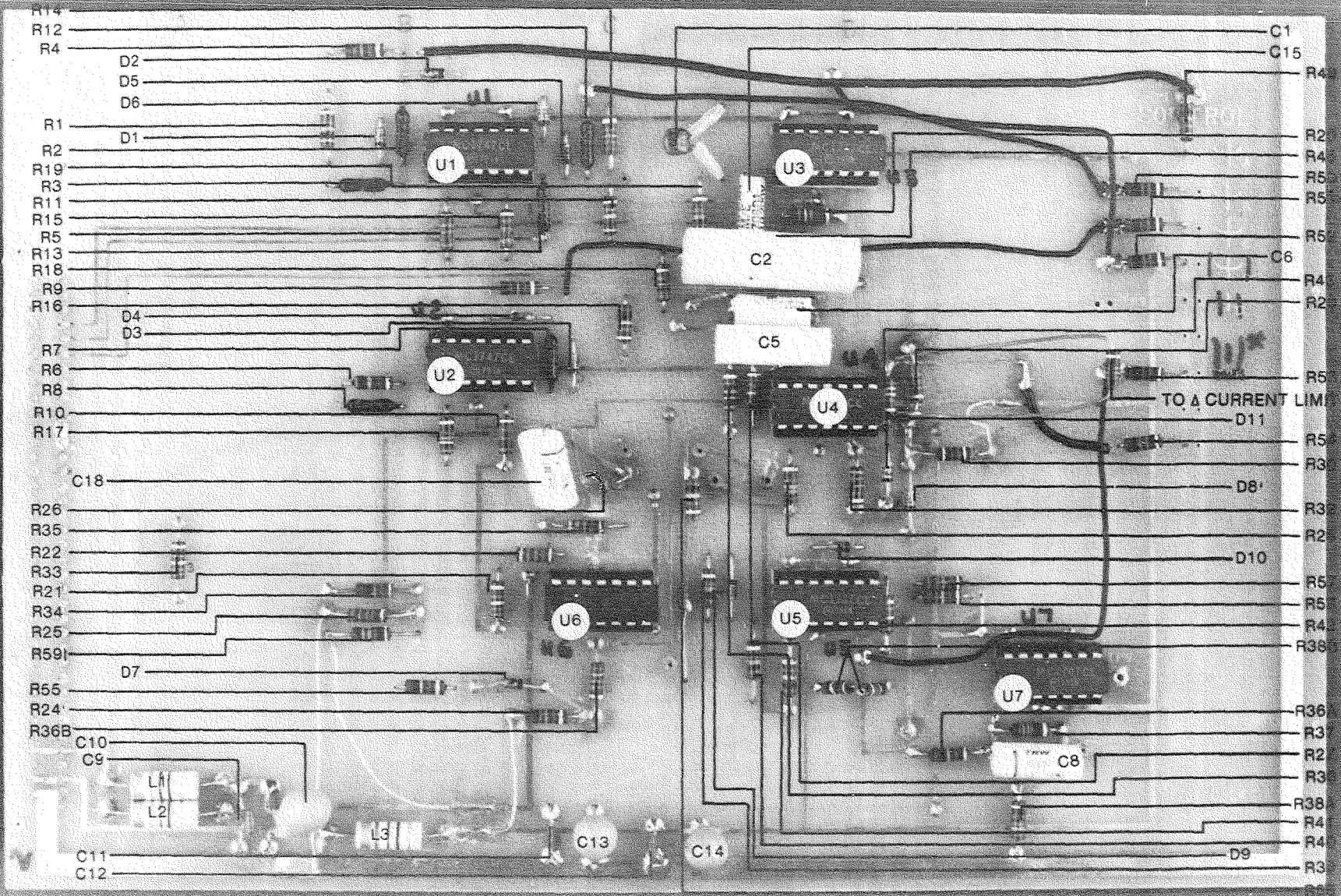


PL ISSUED

DESCRIPTION OF GROUPS	REVISIONS	PRINTS TO

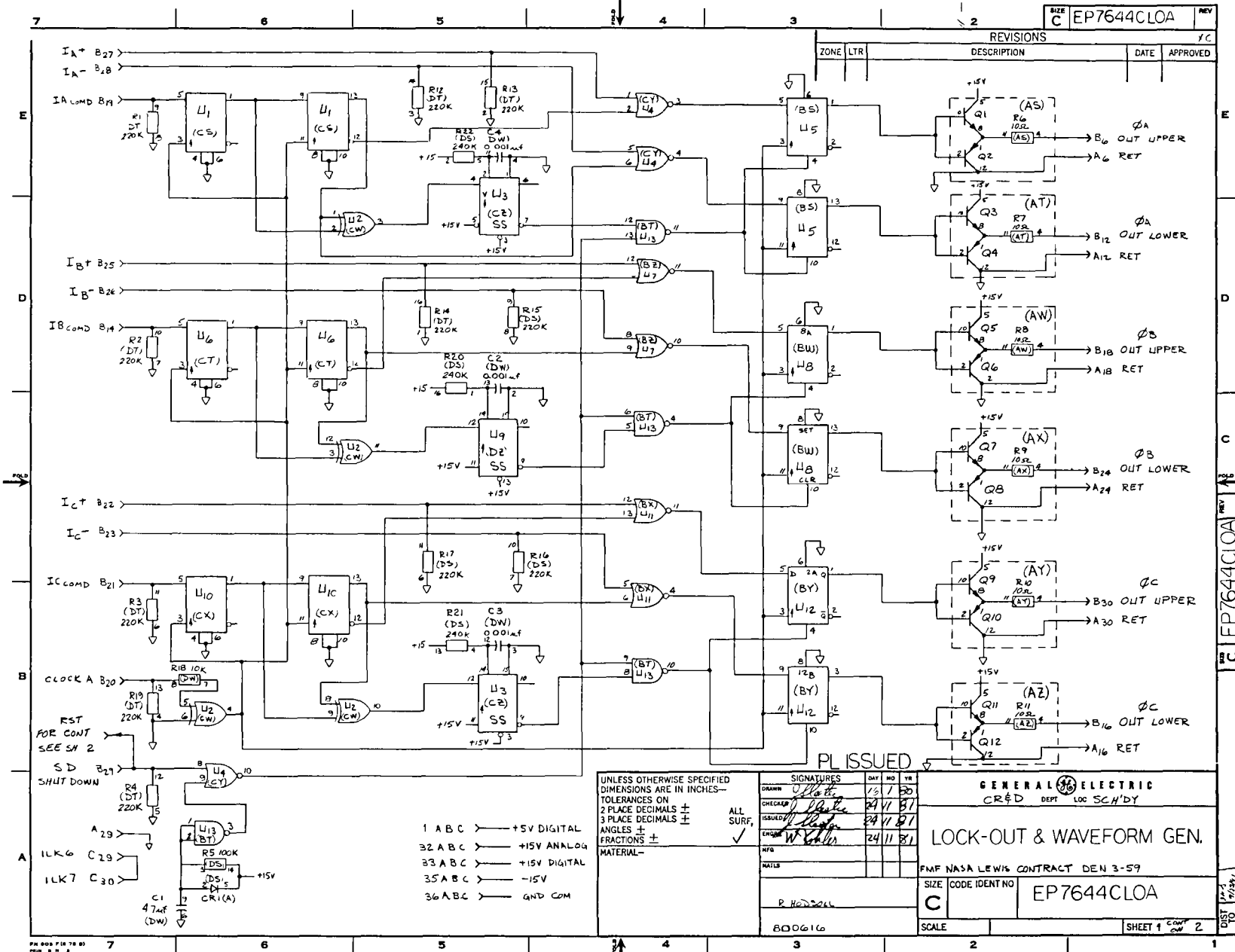
DATE BY: 1/10/50	CHKD BY: SCH BY	EP7644CFCA
REVISED BY: 1/12/51	LOC: CONT. ON SHEET F	

204



EP76440PCA

FLU CONTROL



SIZE C EP7644CLOA REV

REVISIONS			
ZONE	LTR	DESCRIPTION	DATE APPROVED

- 1 ABC > +5V DIGITAL
- 32 ABC > +15V ANALOG
- 33 ABC > +15V DIGITAL
- 35 ABC > -15V
- 36 ABC > GND COM

UNLESS OTHERWISE SPECIFIED  
DIMENSIONS ARE IN INCHES—  
TOLERANCES ON  
2 PLACE DECIMALS ±  
3 PLACE DECIMALS ±  
ANGLES ±  
FRACTIONS ±

SIGNATURES			
DRAWN	CHECKED	DATE	NO
<i>[Signature]</i>	<i>[Signature]</i>	12/7	80
<i>[Signature]</i>	<i>[Signature]</i>	24/11	81
<i>[Signature]</i>	<i>[Signature]</i>	24/11	81

GENERAL ELECTRIC  
CR&D DEPT LOC SCH'DY

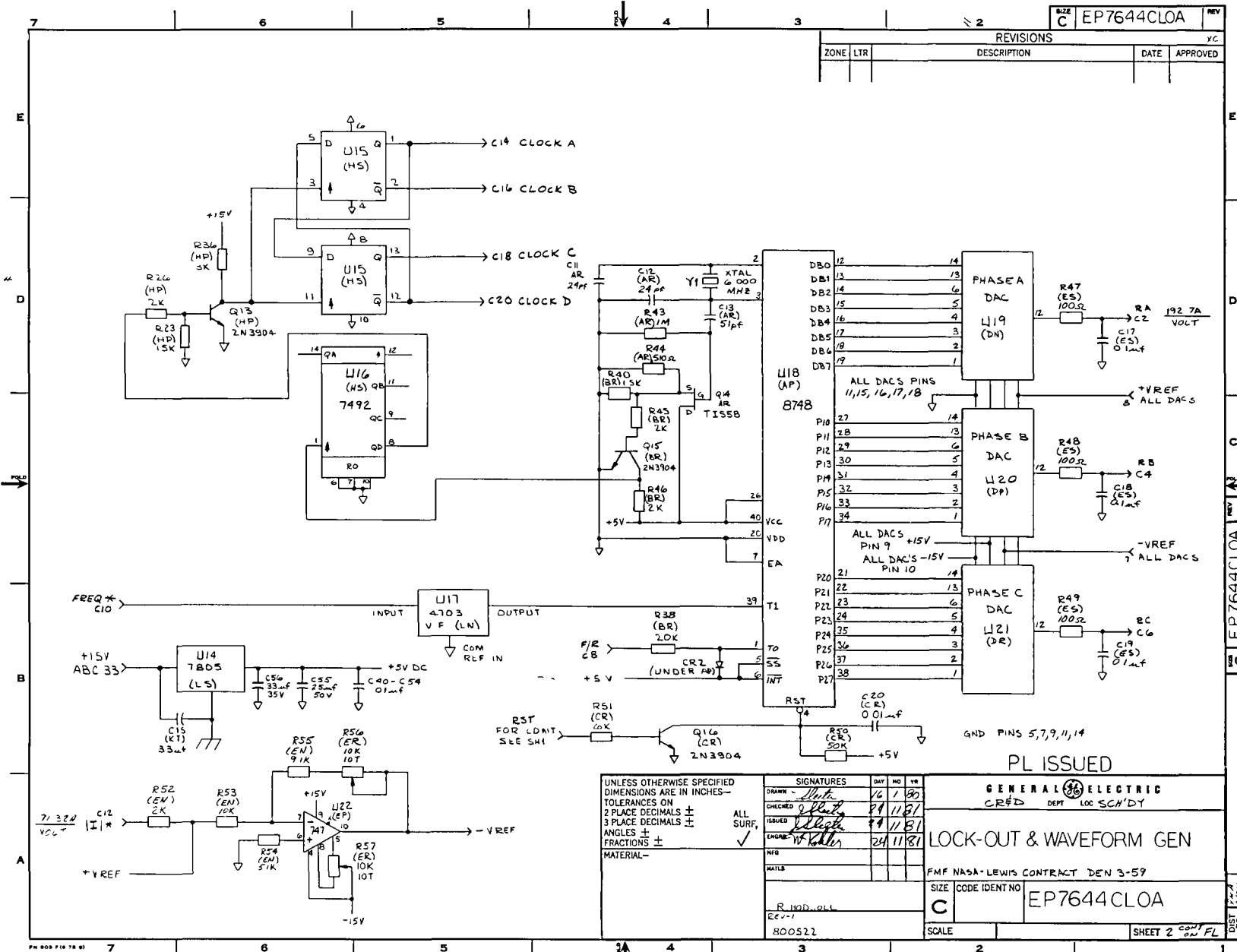
**LOCK-OUT & WAVEFORM GEN.**

FMF NASA LEWIS CONTRACT DEN 3-59

SIZE CODE IDENT NO EP7644CLOA

SCALE

SHEET 1 OF 2



SIZE		EP7644CLOA		REV
REVISIONS				
ZONE	LTR	DESCRIPTION	DATE	APPROVED

UNLESS OTHERWISE SPECIFIED DIMENSIONS ARE IN INCHES—  
 TOLERANCES ON  
 2 PLACE DECIMALS ±  
 3 PLACE DECIMALS ±  
 ANGLES ±  
 FRACTIONS ±  
 MATERIAL—

SIGNATURES	DAY	MO	YR
DRAWN <i>[Signature]</i>	14	1	81
CHECKED <i>[Signature]</i>	21	11	81
ISSUED <i>[Signature]</i>	24	11	81
ENGINEER <i>[Signature]</i>	24	11	81
DATE			
SCALE			

PL ISSUED

GENERAL ELECTRIC  
 CRFD DEPT LOC SCH'DY

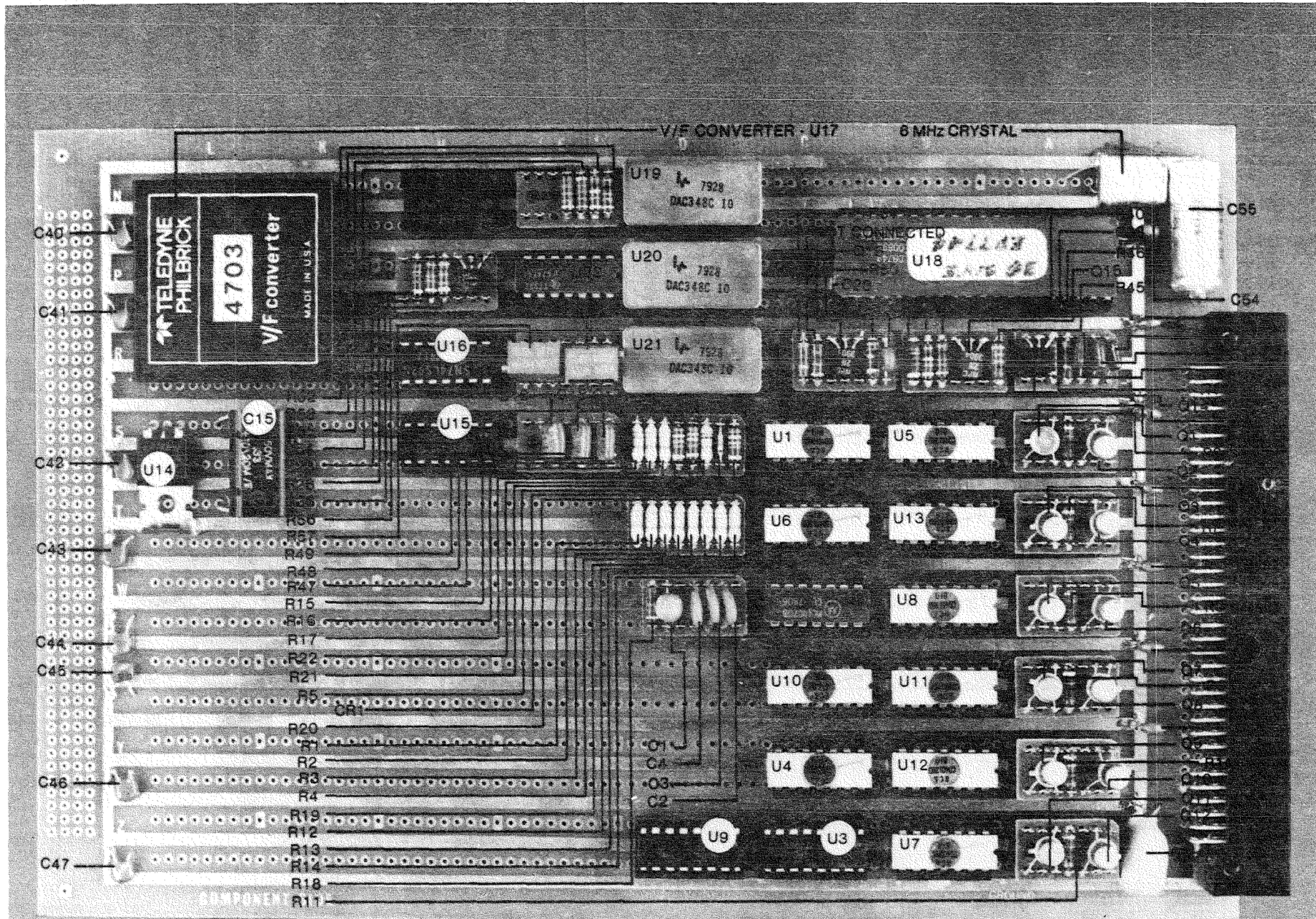
LOCK-OUT & WAVEFORM GEN

FMF NASA-LEWIS CONTRACT DEN 3-59

SIZE CODE IDENT NO  
**C** EP7644CLOA

SCALE

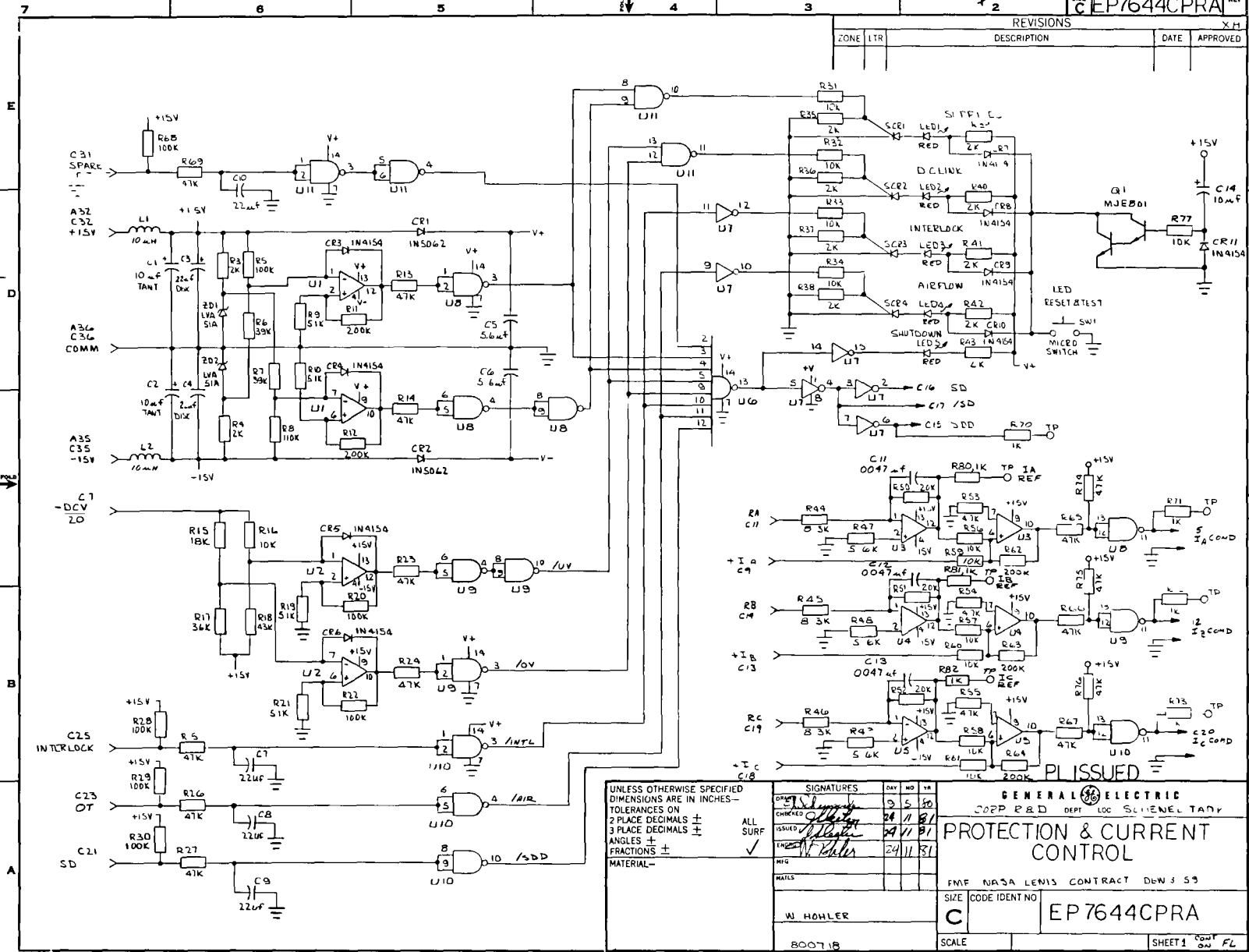
SHEET 2 OF 2



EP7644CLOA

# LOCKOUT AND WAVEFORM GENERATOR

REV X H  
DATE APPROVED  
DESCRIPTION  
LITR ZONE



UNLESS OTHERWISE SPECIFIED  
DIMENSIONS ARE IN INCHES -  
TOLERANCES ON  
2 PLACE DECIMALS ±  
3 PLACE DECIMALS ±  
ANGLES ±  
FRACTIONS ±  
MATERIAL

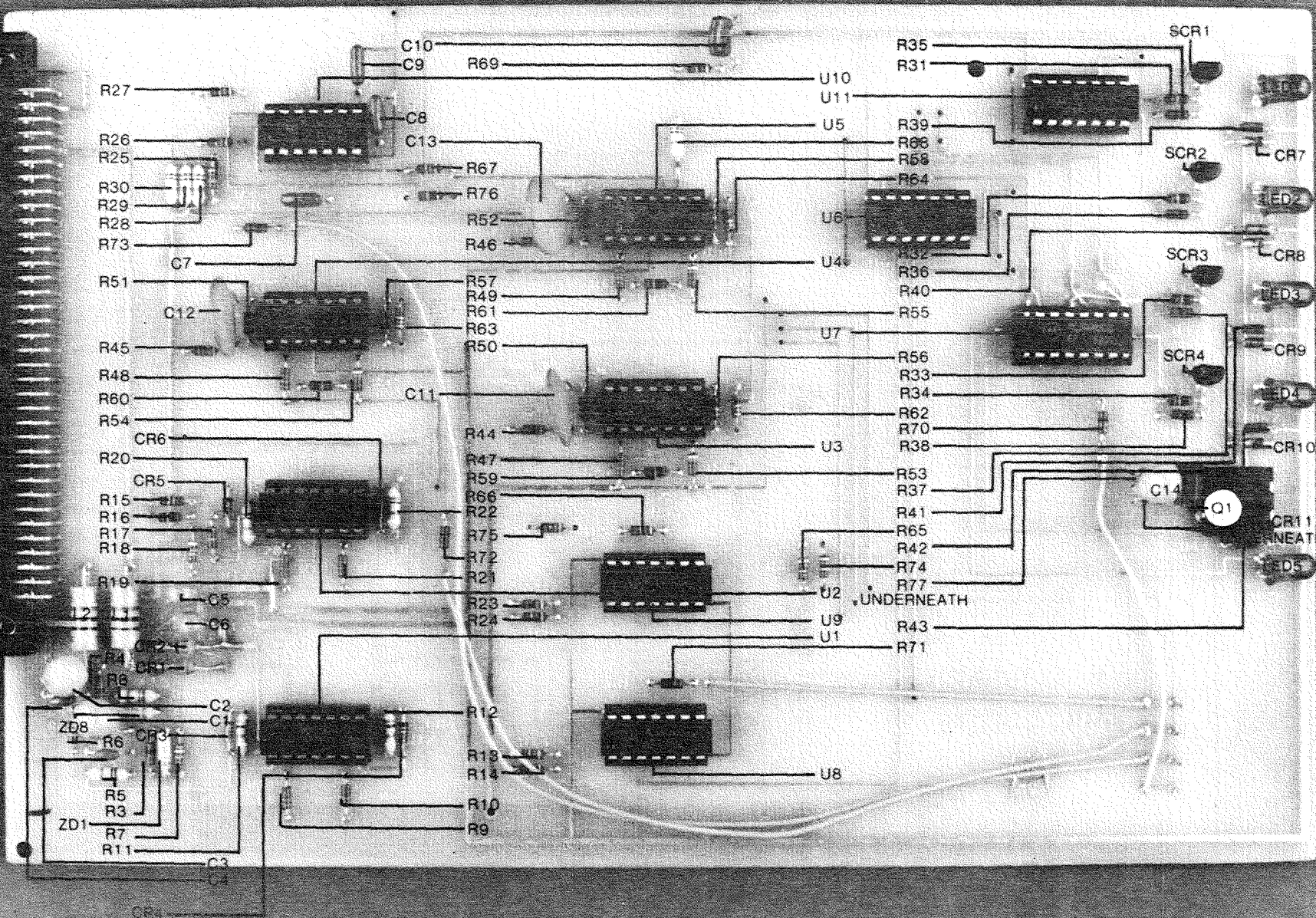
SIGNATURES		DAY	MO	YR
DESIGN	<i>[Signature]</i>	24	11	81
CHECKED	<i>[Signature]</i>	24	11	81
ISSUED	<i>[Signature]</i>	24	11	81
ENG'G	<i>[Signature]</i>	24	11	81
MFG				
MATEL				
W. HOHLER				
800718				

GENERAL ELECTRIC	
CORP R&D DEPT LOC SCIENCE TARDY	
PROTECTION & CURRENT CONTROL	
FNF NASA LEVINS CONTRACT DOW 553	
SIZE	CODE IDENT NO
C	EP 7644CPRA
SCALE	SHEET 1
	FL

REV X H  
DATE APPROVED  
DESCRIPTION  
LITR ZONE

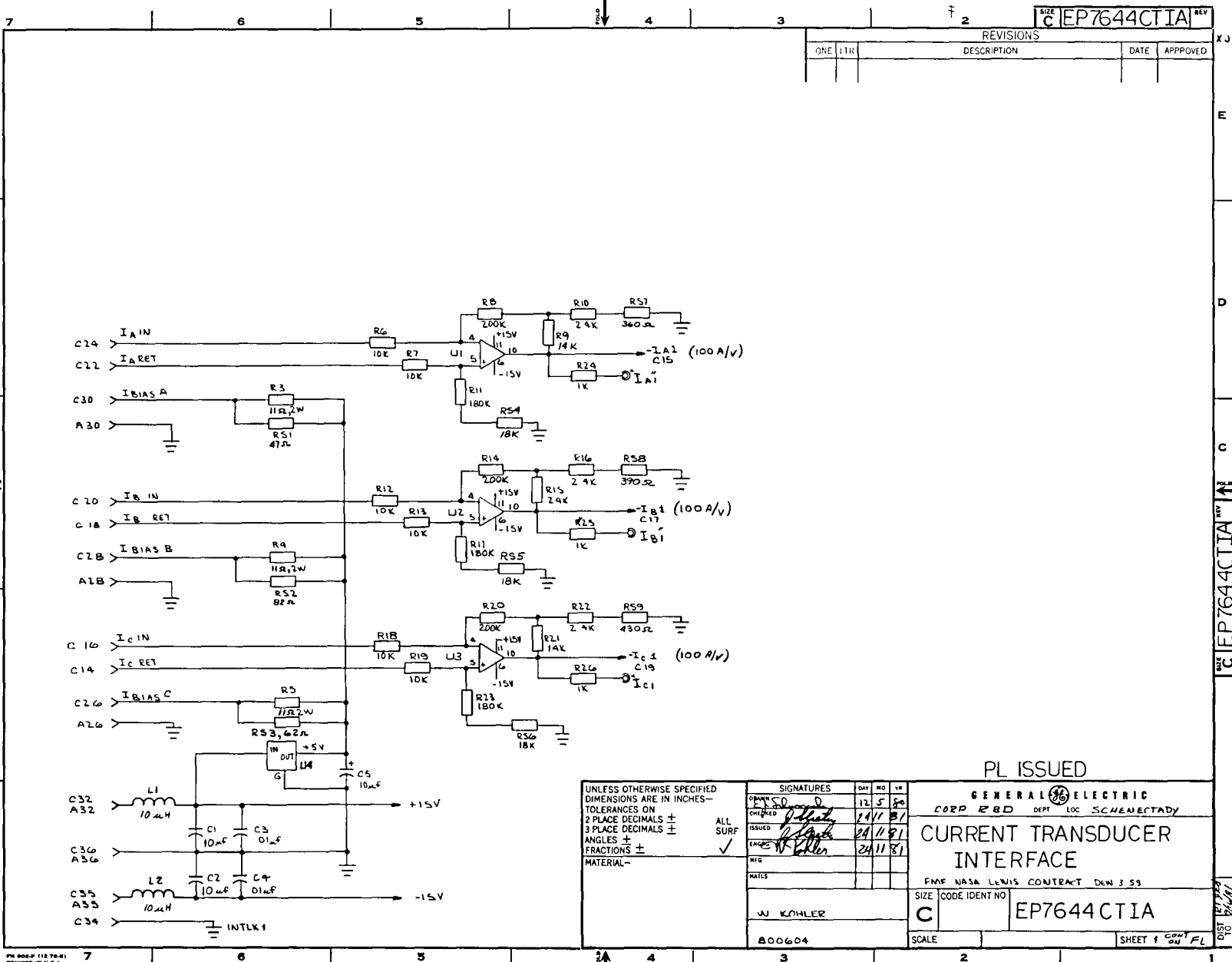
3612056-01

210



EP7644CPRA

PROTECTION AND CURRENT CONTROL



REV		C		EP7644CTIA	
REVISIONS					
ONE	ITR	DESCRIPTION	DATE	APPROVED	

UNLESS OTHERWISE SPECIFIED DIMENSIONS ARE IN INCHES— TOLERANCES ON 2 PLACE DECIMALS ± 3 PLACE DECIMALS ± ANGLES ± FRACTIONS ± MATERIAL—	SIGNATURES DESIGNED BY <i>[Signature]</i> CHECKED BY <i>[Signature]</i> ISSUED BY <i>[Signature]</i> ENGRS BY <i>[Signature]</i> DATE 12 5 80 14 11 81 24 11 81	DAY 12	MO 5	YR 80
ALL SURF ✓				
	W KOHLER			
800604				

PL ISSUED

GENERAL ELECTRIC  
CORP R&D DEPT LOC SCHENECTADY

CURRENT TRANSDUCER  
INTERFACE

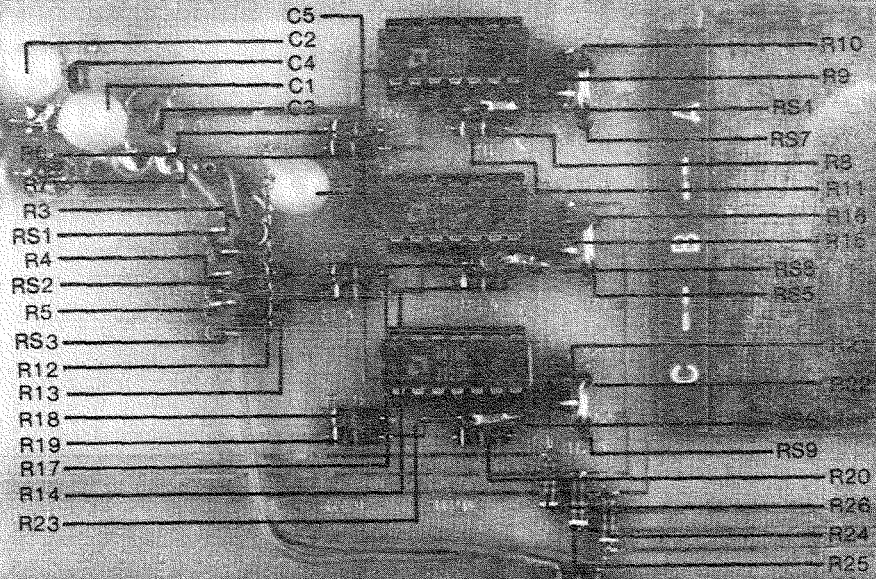
FME NASA LEWIS CONTRACT DEN 3 59

SIZE CODE IDENT NO  
C EP7644CTIA

SCALE SHEET 1 OF 1

REV C EP7644CTIA INT

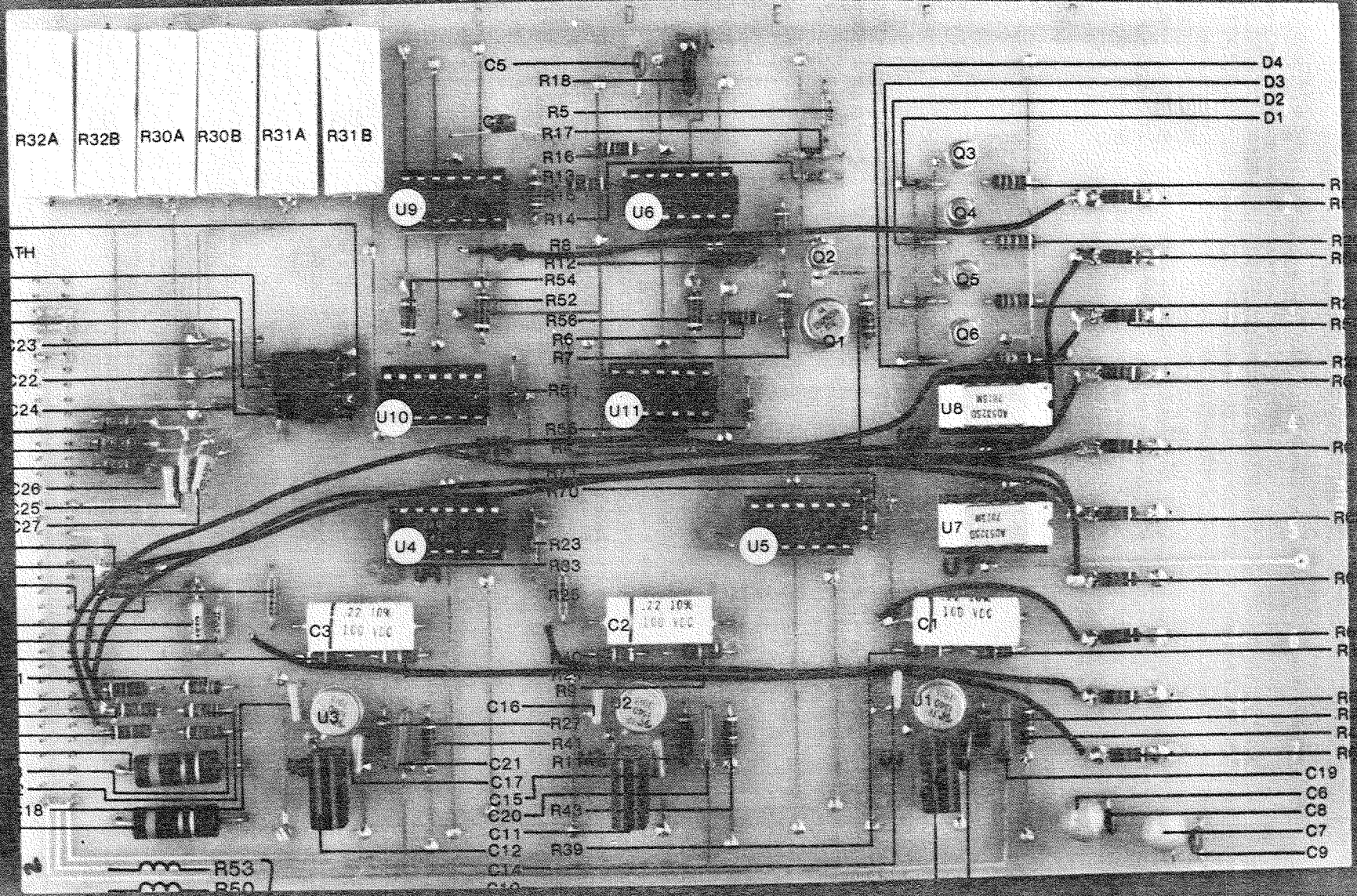
10-9502192



### CURRENT TRANSDUCER INTERFACE

EP7644CT1A





**Appendix E**  
**AC CONTROLLER PRODUCTION MODEL COSTING**

**1.0 INTRODUCTION**

A significant portion of the life cycle costs of the ac controller is the production cost of the hardware. This appendix details the ac controller costing based on the scaling done in Section 3.9. The summarized results are presented in Section 3.10. The costs presented are in 1980 dollars.

**2.0 COST CALCULATION OF MAJOR FUNCTIONS**

**2.1 INPUT CAPACITOR COSTING**

**2.1.1 Summary**

The cost of the input capacitor bank is listed in Table E-1. The cost is for each capacitor purchased in quantities of 1000 or more. The costs are extrapolated from the capacitor volume and are approximations which can vary 10-20%. Recall one capacitor bank is needed per vehicle.

**Table E-1**  
**INPUT CAPACITOR BANK COSTS PER VEHICLE**

Nominal Battery Voltage	Motor Horsepower				
	10	20	30	40	50
84	\$51	\$90	\$127	\$168	\$209
108	50	87	129	169	210
150	37	67	98	129	159
300	37	61	80	99	115

**2.1.2 Assumptions**

- 1 The capacitor bank volumes would be available as required
- 2 The capacitor is an aluminum electrolytic type
- 3 The capacitor bank is represented by six individual capacitors
- 4 The individual capacitor cost represents one sixth of the total capacitor bank cost

**2.1.3 Calculations**

After consultation with the application engineers at Cornell-Dubilier's aluminum electrolytics manufacturing facility, their information indicated that for all aluminum electrolytic type capacitors rated above 60 V, the cost appears to depend only on volume <sup>(13)</sup>. An equation representing the cost is

$$\$C = (0.476 \text{ Vol}^{0.847}) \times 6$$

Where,

\$C = capacitor bank cost in dollars

Vol = one sixth of the desired capacitor volume

## 2.2 POWER MODULE COSTING

### 2.2.1 Summary

Table E-2 lists the estimated cost range for a power module at different system ratings. The costs are approximations based on the per square inch cost of silicon, packaging, yield, and adders which are extrapolated from device costs of the General Electric D67 power Darlington transistor and a fast recovery diode. The costs are for a 60,000 to 600,000 annual quantity, recalling that six are needed per vehicle. Use the upper range for 10,000 vehicles per year and the lower range for 100,000 per year.

Table E-2  
COSTS PER POWER MODULE

Nominal Battery Voltage	Motor Horsepower				
	10	20	30	40	50
84	\$40-65	\$81-130	\$121-195	\$162-261	\$202-326
108	39-62	77-124	116-186	154-248	193-310
150	45-73	91-146	136-219	182-293	227-365
300	41-66	82-132	123-199	164-264	205-330

### 2.2.2 Assumptions

1. The silicon area of the fast recovery diode is represented by 4.5% of the silicon area of the main power device.
2. The silicon cost of the diode is 2% that of the main device.
3. The diode is packaged in the power module with the power transistors and, therefore, the effect of module yield is considered in the total cost.
4. Cost estimates are based on 1980 dollars for quantities of 60,000 to 600,000 modules annually.

### 2.2.3 Calculations

Cost estimates were obtained from the Semiconductor Products Department of the General Electric Company, Auburn, N.Y. The cost estimates are for the D67 bipolar power Darlington transistor. The costs listed in Table E-2 reflect those associated with a developing technology and such effects should be considered in "future cost" predictions, i.e., the well-known learning curve, as discussed in Section 2.6. The 300-volt rated module will still require module costs proportional to the silicon areas.

As a guideline, the silicon cost of the D67 transistor is used as a basis for module cost. The projected cost of tested transistor chips and diodes, module material costs, labor costs for

assembly, and associated module yields are combined. This combination is used to estimate the cost of a power module having 1.91 cm<sup>2</sup> (0.75 in<sup>2</sup>) of silicon area (excluding the fast recovery diode). The module cost is proportioned to represent the 1.98 cm<sup>2</sup> (0.78 in<sup>2</sup>) silicon area module for the 20 hp, 108 V application. This cost is assumed to be the base value and will be proportional in silicon area to the cost of the other drives. These costs are for volumes ranging from 60,000 to 600,000, since there are six such modules in one controller. The costs are

Silicon and packaging material costs	\$65.00 – \$105.00
Labor minutes for assembly and test = 5 min	
Labor costs at \$21.00 per hour	<u>\$ 1.75 – \$ 2.00</u>
	\$66.75 – \$107.00
Total module yield 90%	
Module cost for 1.91 cm <sup>2</sup> (0.75 in <sup>2</sup> ) of silicon	\$74.00 – \$119.00

The module cost for the 20 hp, 108-volt rating with an estimated 1.98 square cm (0.78 square inch) of silicon is within a range of

$$(0.78/0.75) \$74 = \$77$$

$$(0.78/0.75) \$119 = \$124$$

## 2.3 POWER MODULE SNUBBER COSTING

### 2.3.1 Summary

The costs of the different snubber networks are extrapolated from the 20 hp, 108-volt base values. The costs listed in Tables E-3 and E-4 are approximate because of the assumptions that are needed to make the calculations possible. Recall that six such snubbers are required for each vehicle.

**Table E-3**  
**COSTS PER SNUBBER FOR 10,000 VEHICLES PER YEAR**

Nominal Battery Voltage	Motor Horsepower				
	10	20	30	40	50
84	\$5.64	\$11.28	\$16.93	\$22.57	\$28.21
108	4.63	9.25	13.88	18.50	23.13
150	3.63	7.26	10.88	29.03	36.28
300	2.35	4.69	7.04	9.39	11.73

### 2.3.2 Assumptions

1. The present 20 hp snubber design uses components selected for their optimum characteristics.
2. The characteristic waveshape of voltage and current seen by each component does not change for different ratings, only the magnitudes change.

**Table E-4**  
**COSTS PER SNUBBER FOR 100,000 VEHICLES PER YEAR**

Nominal Battery Voltage	Motor Horsepower				
	10	20	30	40	50
84	\$4.56	\$9.12	\$13.67	\$18.23	\$22.79
108	3.74	7.47	11.21	14.94	18.68
150	2.93	5.86	8.79	11.71	14.64
300	1.89	3.78	5.68	7.57	9.46

3. The total costs of the resistors, capacitors and diodes are representative of their Thevenin equivalents and will scale appropriately
4. Cost of packaging is negligible compared with parts costs
5. The costing is based on 60,000 and 600,000 annual quantity

### 2.3.3 Calculations

Listed in Table E-5 are the individual components and their cost used in the 20 hp, 108-volt snubber network. These costs were derived from distributor catalogs and adjusted for

**Table E-5**  
**BASE SNUBBER COMPONENT COSTS**

Type/Quantity	60,000	600,000
<b>Semiconductors</b>		
1N3913R	\$5.72	\$4.62
MR856	0.79	0.64
<b>TOTAL</b>	<b>6.51</b>	<b>5.26</b>
<b>Resistors</b>		
5 $\Omega$ , 25 W	0.39	0.31
15 $\Omega$ , 25 W	0.39	0.31
0.2 $\Omega$ , 50 W	0.76	0.62
10 $\Omega$ , 50 W	0.59	0.47
<b>TOTAL</b>	<b>2.13</b>	<b>1.71</b>
<b>Capacitors</b>		
0.022 $\mu$ F, 200 V	0.080	0.064
0.22 $\mu$ F, 200 V	0.11	0.092
2.0 $\mu$ F, 200 V	0.42	0.34
<b>TOTAL</b>	<b>0.61</b>	<b>0.50</b>
<b>SUM TOTAL</b>	<b>9.25</b>	<b>7.47</b>

quantities of 60,000 and 600,000 Adjustments are made by using the graph in Figure E-1. The cost values appearing for other drive ratings is approximate Because of the complexity of an optimum snubber design, only a logical deduction of circumstance appeared as an adequate method to project costs This logical deduction is as follows

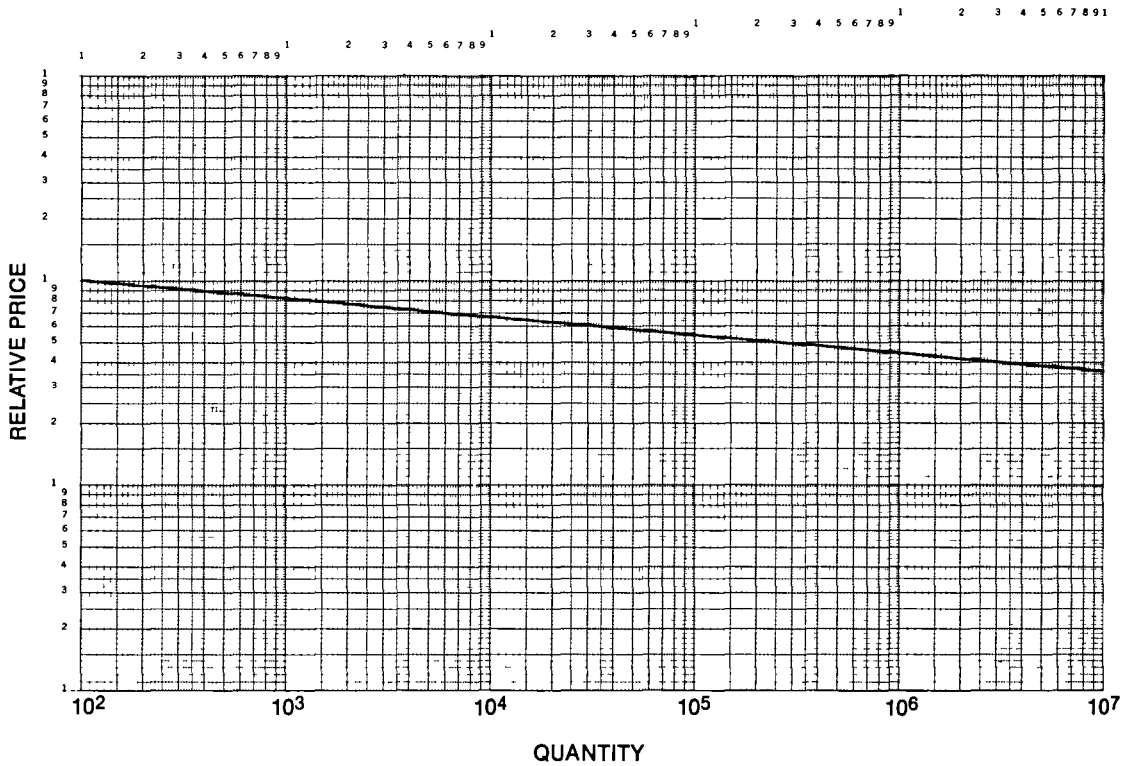


**Figure E-1 Relative Price vs. Quantity**

The snubber is assumed to absorb a constant percentage of energy from the drive system during power switching and the eventual dissipation of this energy (or a constant percentage) is done in the snubber resistance. Power dissipation in a resistor is proportional to the resistor's surface area The resistor's cost is proportional to its volume. Therefore,

$$\begin{aligned} \$ &\propto \text{Vol} \propto \text{Area} \propto \text{Power} \\ \$ &\propto \text{Power} \\ \text{thus, } \$_r &= (\text{HP}/\text{HP}_b) \$_{rb} \end{aligned}$$

Where,

- $\$_r$  = Desired cost of equivalent resistance
- $\$_{rb}$  = Base cost of snubber resistors

The absorbing of energy by the snubber is, in part, storing of energy in the snubber capacitance. If the system voltage is held constant, then, in effect, by paralleling snubbers the capacitance becomes proportional to the horsepower. Capacitor cost is traditionally proportional to its CV product (capacitance and voltage rating) Therefore, for constant system voltage

$$\$ _c = (HP/HP_b) \$ _{cb}$$

Where,

$$\$ _c = \text{desired cost of equivalent capacitance}$$

$$\$ _{cb} = \text{base cost of snubber capacitance}$$

If the system voltage is varied and system power is constant, the snubber energy storage remains constant. This indicates the capacitor value varies inversely as the square of the voltage to maintain a constant value of energy being absorbed. The capacitor cost varies as the CV product. The resulting cost change is:

$$\$ _c = (E_b/E) \$ _{cb}$$

Where,

$$E_b = \text{base value of battery voltage (108 V)}$$

$$E = \text{desired value of battery voltage}$$

The total equivalent capacitor cost is:

$$\$ _c = (HP/HP_b) (E_b/E) \$ _{cb}$$

The diodes within the snubber network should maintain constant current density within the silicon. The variation of required silicon area due to voltage change is considered negligible. Therefore, the diode is assumed to scale directly with current, increasing or decreasing the silicon area to maintain constant current density. The cost of the diode would scale as a material cost proportional to silicon area. (Packaging cost is negligible). Therefore,

$$\$ _d = (HP/HP_b) (E_b/E) \$ _{db}$$

Where,

$$\$ _d = \text{desired cost of equivalent diodes}$$

$$\$ _{db} = \text{base cost of snubber semiconductors}$$

The snubber network cost is a combination of all the equivalent components' costs. Thus,

$$\$ _{sn} = (HP/HP_b) (E_b/E) (\$ _{cb} + \$ _{db}) + (HP/HP_b) \$ _{rb}$$

Where,

$$\$ _{sn} = \text{cost of snubber network}$$

## 2.4 BASE DRIVE COSTING

### 2.4.1 Summary

The base drive costing includes both the base drive circuit costs and the base drive power supply. The base drive circuit is broken down into the common parts and the required output driver transistors. Recall six such base drives and supplies are required per vehicle. The costs over the voltage and horsepower ranges for 10,000 and 100,000 vehicles per year are shown in Tables E-6 and E-7 respectively.

**Table E-6**  
**COST PER BASE DRIVE FOR 10,000 VEHICLES PER YEAR**

Nominal Battery Voltage	Motor Horsepower				
	10	20	30	40	50
84	\$34.38	\$39.07	\$41.81	\$72.59	\$75.46
108	25.48	26.34	28.43	41.81	72.59
150	21.71	25.48	26.34	29.73	41.81
300	16.51	17.56	19.76	20.33	20.33

**Table E-7**  
**COST PER BASE DRIVE FOR 100,000 VEHICLES PER YEAR**

Nominal Battery Voltage	Motor Horsepower				
	10	20	30	40	50
84	\$26.30	\$29.91	\$32.00	\$55.48	\$57.68
108	19.54	20.20	21.81	32.00	55.48
150	16.68	19.54	20.20	22.81	32.00
300	12.70	13.49	15.15	15.59	15.59

#### 2.4.2 Assumptions

1. The base drive circuit, for costing purposes, can be separated into common parts and those parts which scale with voltage and horsepower.
2. Volumes of 60,000 and 600,000 are used since there are six base drives per vehicle.
3. The base drive power supply cost is based on its wattage rating.

#### 2.4.3 Calculations

The common components in the base drive are costed in Table E-8. These components are in reference to drawing EP7644CBDA in Appendix D. The output transistors selected in Section 3.9.6 are costed in Table E-9.

An independent study has been made of commercially available switching power supplies. The results are made available here in terms of cost per watt as shown in Figure E-2. The 1980 costs for dual supplies with some regulation with wattage ratings in the range of interest are \$1 per watt in 1000 annual quantity. This annual quantity is adjusted for the 60,000 and 600,000 quantity by using the graph in Figure E-1. The same supply will be employed over several ranges but with different heat sinking arrangements. An adder of 10% will be used for extra heat sinks and 5% more will be used for the combination heat sink and prorated blower. The base drive power supply costs are shown in Table E-10.

**Table E-8**  
**COMMON COMPONENT COST PER BASE DRIVE**

Common Items	Number	at 60 K/yr		at 600 K/yr	
		each	Total	each	Total
Optocoupler	1	\$0 60	\$0 60	\$0 50	\$0 50
Signal Diodes	9	0 05	0 45	0 04	0 36
Power Diodes	1	0 08	0 08	0 07	0 07
Electrolytic Cap (LV)	4	0 14	0 56	0 10	0 40
Bypass Capacitors	6	0 04	0 24	0 03	0 18
Signal Transistors Q <sub>1</sub> , Q <sub>2</sub> , Q <sub>5</sub>	3	0 12	0 36	0 10	0 30
Med Transistors Q <sub>3</sub> , Q <sub>6</sub>	2	0 25	0 50	0 20	0 40
Signal Resistors	11	0 01	0 11	0 01	0 11
1-Watt Resistors	7	0 03	0 21	0 03	0 21
			\$3 11		\$2 53

**Table E-9**  
**OUTPUT TRANSISTOR COST PER BASE DRIVE**

Nominal Battery Voltage	Transistor		Motor Horsepower				
			10	20	30	40	50
84	Q <sub>4</sub>	60K	\$1 34	\$2 70	\$2 70	\$5 01	\$5 01
	Q <sub>4</sub>	600K	1 06	2 16	2 16	4 00	4 00
	Q <sub>7</sub>	60K	0 97	0 97	1 82	1 82	1 82
	Q <sub>7</sub>	600K	0 77	0 77	1 45	1 45	1 45
108	Q <sub>4</sub>	60K	1 34	1 34	2 70	2 70	5 01
	Q <sub>4</sub>	600K	1 06	1 06	2 16	2 16	4 00
	Q <sub>7</sub>	60K	0 97	0 97	0 97	1 82	1 82
	Q <sub>7</sub>	600K	0 77	0 77	0 77	1 45	1 45
150	Q <sub>4</sub>	60K	0 41	1 34	1 34	2 70	2 70
	Q <sub>4</sub>	600K	0 33	1 06	1 06	2 16	2 16
	Q <sub>7</sub>	60K	0 46	0 97	0 97	1 82	1 82
	Q <sub>7</sub>	600K	0 37	0 77	0 77	1 45	1 45
300	Q <sub>4</sub>	60K	0 41	0 41	1 34	1 34	1 34
	Q <sub>4</sub>	600K	0 33	0 33	1 06	1 06	1 06
	Q <sub>7</sub>	60K	0 46	0 46	0 97	0 97	0 97
	Q <sub>7</sub>	600K	0 37	0 37	0 77	0 77	0 77

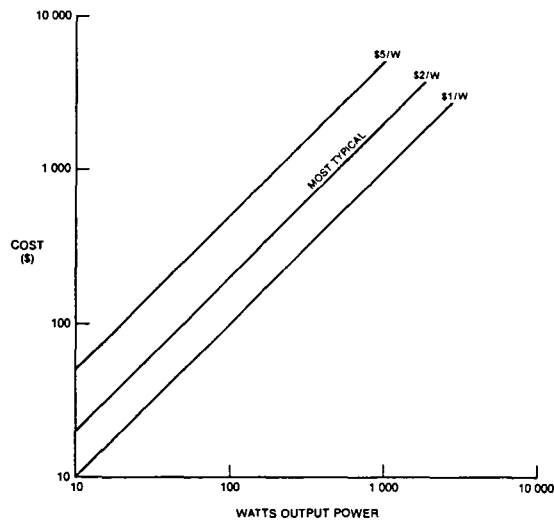


**Figure E-2 Switching Power Supply Cost**

**Table E-10****POWER SUPPLY COST PER BASE DRIVE**

Nominal Battery Voltage		Motor Horsepower				
		10	20	30	40	50
84	60K	\$17 00	\$18 70	\$19 64	\$37 40	\$39 27
	600K	13 57	14 93	15 68	29 85	31 35
108	60K	11 20	11 76	11 76	19 64	37 40
	600K	8 96	9 41	9 41	15 68	29 85
150	60K	10 18	11 20	11 76	11 76	19 64
	600K	8 14	8 96	9 41	9 41	15 68
300	60K	6 79	7 47	7 47	7 84	7 84
	600K	5 43	5 97	5 97	6 27	6 27

Circuit boards of moderate complexity of signal level components have about 75% of their material cost in readily identified components. Assembly labor and test for lower volumes in out-of-States facilities could average 15% of material costs. Thus to arrive at the expected material cost, the sum of basic material costs will be divided by 0.75. Shop costs will be accounted for by multiplying by 1.15 and 1.10 for annual volumes of 60,000 and 600,000, respectively. The results are shown in Tables E-6 and E-7.

**2.5 CONTROL COSTING**

The assumption is made that the same logic blocks will be required for all models. The variations in power handling are accomplished in the interface circuitry. The estimated control costs at the two production volumes are shown in Table E-11.

**Table E-11****CONTROL COSTS PER VEHICLE**

Logic Block	at 10 K/yr	at 100 K/yr
Driver Command and Jerk Limit	\$ 25 30	\$ 18 15
Lockout and Waveform Generator	425 24	378 02
Flux Control	8 73	6 86
Angle Regulator	313 26	195 62
Zero Speed Detector & Protection Circuits	25 30	18 15
Current Limit, Magnitude, & Controller	41 61	31 72
Torque, Current Interface & Summing	103 98	78 83
Current Transducers	281 64	229 07
Logic Power Supply	20 43	16 75
Total Expected Shop Costs	\$1,245 49	\$ 973 17
Control with Interconnections & and Housing (110%)	\$1,370 04	\$1,070 49
Control with System Assembly Labor (110% and 107%)	\$1,507 04	\$1,145 42

**2.6 FUTURE COSTS**

Cost projections can be made for this drive system by employing learning curve or experience curve techniques. "Learning Curves," sometimes called "experience curves," are projections of future prices or costs based on an extrapolation of historical pricing or cost data for manufactured products. These are empirical relationships of the cost/price to the total accumulated production volume. They are commonly used for forecasting price/cost trends in

commodity type industries (i.e., semiconductor, electronic components, plastics, consumer products, ferrous and aluminum materials, metal parts, etc ) where production volumes are large and the effects of technical innovation, manufacturing productivity and volume growth are expected to continue as driving forces to reduce costs

Learning curves are particularly applicable when the process involves

- 1) Repetitive Operations
- 2) High Direct Labor Content
- 3) High Direct Labor Skill
- 4) Long Production Runs
- 5) Reasonably Short Cycle
- 6) Complex Product

At least at the start of the production of this drive system, the learning potential is high because of the conditions indicated in Table E-12. Areas of learning potential for both portions of the fabrication process are those shown in Table E-13.

**Table E-12**

**LEARNING POTENTIAL MATRIX**

Operation	Direct Labor	Mgmt and Innovation
Man-Paced	High	High
Machine-Paced	Low	High (Between Lots)

**Table E-13**

**LEARNING POTENTIAL AREAS**

Direct Labor	Mgmt and Innovation
● Job Knowledge	● Familiarization
● Dexterity, skills	● Elimination of Bottlenecks
● Avoidance of Errors	● Product Design
● Bad Practice Avoidance	● Process Design
● Potential Trouble Detection	● Tool, Jigs, Fixtures

Some classic experience for types of assemblies are listed in Table E-14. The experience is expressed in terms of the percent of the learning curve, which is representative of the rate of price decline (slope) of a price versus volume learning curve. A typical price “learning curve” for a power semiconductor device is shown in Figure E-3. In this illustration, the modest price decline shown during the initial production phase reflected a strategy of price protection to recover the development costs. As competition increased, the price decline became steeper in order to protect market position and was more representative of the actual “cost learning curve.”

**Table E-14**  
**LEARNING % EXPERIENCE**  
**(CUM. AVE.)**

• Aircraft Industry (Ave )	~80%
WW II Fighters (Ave )	78.5
12 Post WW II Fighters	67-91
11 Post WW II Bombers	63-84
Direct Materials	90-98
• Aircraft Engines	
Machine Tool Load Hrs	86%
Internal Labor	84%
Purchased Materials	88
• Electro-Mechanical	80-85%
Assys and Some Electronics	

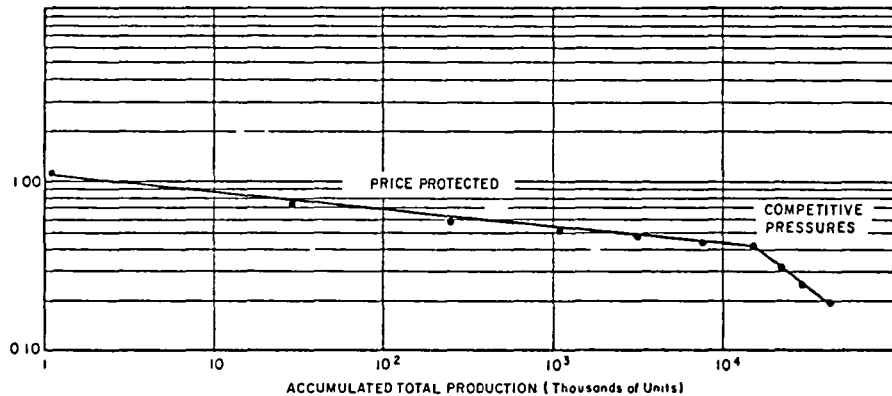


**Figure E-3 Typical Semiconductor Price Learning Curve**

This characteristic is particularly applicable for the power Darlington transistors and, to a certain extent, for the custom integrated circuits which may be employed

With competitive pressure, the original 87% learning curve illustrated above can quickly become 73% or even greater for short periods of time. It should be reemphasized that these values are for constant dollars.

**Section 7**  
**DEFINITIONS**

- 1 Propulsion System — the aggregation of all components which comprise the power train plus accessory drives and auxiliaries, with the single exception of electrochemical storage batteries
- 2 AC Controller — the subsystem as comprised of the power inverter and its associated control electronics
- 3 Power Inverter — the six-transistor inverter with associated auxiliary components
- 4 Power Inverter Assembly — as referenced to the hardware itself
- 5 Control Card — one of the printed circuit (p c ) boards in the control electronics assembly
- 6 Control Electronics — the p c boards and associated components that control the power inverter
- 7 Control Electronics Assembly — as referenced to the hardware itself
8. Life Cycle Cost — the cost per kilometer (mile) of mass produced hardware over its operating life Factors entering into this cost include but are not necessarily limited to the following
  - First cost determined and based on projected production rates of 10,000 and 100,000 per year
  - Operating lifetime of 100,000 cycles of SAE J227a, Schedule D driving cycle (approximately 3,500 hours)
  - repair and/or replacement costs over the lifetime period
  - depreciation and/or salvage value
  - energy costs directly attributable to production hardware weight
  - warranty costs
- 9 Engineering Model — an integrally assembled, representatively packaged unit which physically resembles a proposed production model in form and function and is fully responsive to its operating requirements and specifications (Engineering model design and testing is predicated on conducting comprehensive performance testing and the evaluation of all input/output interface characteristics, in situ, under controlled conditions)
- 10 Production Model — a mass produced unit assembled and fabricated using the most cost effective techniques possible and meeting all specifications and requirements
- 11 Signal Conventions —

When discussing signals, the following conventions apply

  - a. Signal names will be shown in capital letters, e.g , ACCELERATE\*. A signal name generally refers to the condition indicated by its active or most positive state For an analog signal, the active state is the most positive voltage, i.e., ACCELERATE\* = +10 volts indicates full acceleration For a digital signal, the active state would be a logic '1' or +15 volts, i.e , ACC = +15 volts indicates acceleration Logic '1' will hereafter be referred to as '1' and logic '0' as '0'

- b. An asterisk (\*) after an analog signal name indicates a command as opposed to a feedback signal, i.e., IREAL\* is the real current command, whereas IREAL is the real current feedback
- c. A slash (/) before a digital signal name indicates negation, i.e., /BRK means that the active ('1') state indicates "not brake," or conversely, the inactive ('0') state indicates "brake."
- d. The letter (D) after a signal name indicates the version of the signal which is output-buffered for external monitoring purposes (diagnostics).
- e. Reference locations on the schematic under discussion will be shown in square brackets ([]) and refer to reference marks on the left side and top edge of the schematic.
- f. A signal name enclosed in a pair of vertical lines (| |) means 'the absolute value of' or magnitude of that signal, i.e., |I| indicates the absolute value of I.

**Section 8**  
**REFERENCES**

- 1 A B Plunkett and G B Kliman, "Electric Vehicle AC Drive Development," SAE Paper 800061
- 2 A B. Plunkett and D L Plette, "Inverter-Induction Motor Drive for Transit Cars," *IEEE Transactions on Industry Applications IA-13* (1), January/February 1977, pp 26-37
- 3 P M Espelage, F G Turnbull, and J Chiera, "DC-to-AC Inverter and High-Speed Induction Motor Final Report," S-69-1037, October 18, 1968, DOA, MERDC Contract DA-44-009-AMC-1820(T)
- 4 G B Kliman and A.B Plunkett, "Development of a Modulation Strategy for a PWM Inverter Drive," IAS Conference Record of the 10th Meeting, October 1975
- 5 H C.J. DeJong, *AC Motor Design with Conventional and Converter Power Supplies*, Oxford University Press, 1976
- 6 H J. Boenig, "Optimization of Magnetic Materials Utilization in Semiconductor-Commutated Electric Machines," University of Wisconsin Doctoral Dissertation in EE, University Microfilms Inc , Ann Arbor, Michigan, 1971
- 7 J A Chiera, L Coffman, J.F. Haupt, and L Ishler, "AC Electric Wheel Design Study Final Report," February 26, 1971, DOA, MERDC Contract DAAK02-70-C-0600
- 8 General Electric Company, "Near-Term Electric Vehicle Phase II Final Report," March 28, 1980, DOE Contract No DE-ACO3-76CS51294
- 9 G B Kliman and A B Plunkett, "Development of a Modulation Strategy for a PWM Inverter Drive," *IEEE Transactions on Industry Applications*, Vol IA-15, No 1, January/February 1979
- 10 A.B Plunkett, "A Current-Controlled PWM Transistor Inverter Drive," Conference Record 1979 IEEE Industry Applications Society Annual Meeting, October 1979
- 11 G A. Kaufman and A B Plunkett, "A High-Performance Torque Controller Using a Voltage Source Inverter and Induction Machine," Conference Record 1981 IEEE Industry Applications Society Annual Meeting, October 1981
- 12 W E Rippel, "Optimizing Boost Chopper Charger Design," Proceedings of Powercon 6, May 1979
- 13 Cornell-Dubilier Electric Corporation, Class 201.87, Type FAH specification sheets
- 14 A B Plunkett, "Direct Flux and Torque Regulation in a PWM Inverter - Induction Motor Drive," *IEEE Transactions on Industry Applications*, Vol IA-13, No. 2, March/April 1977.
- 15 G.A. Kaufman and A.B Plunkett, "Steady-State Performance of a Voltage Source Inverter Synchronous Machine Drive System," Conference Record 1981 IEEE Industry Applications Society Annual Meeting, October 1981
- 16 J. Franz, "Apparatus for Regulating Magnetic Flux in an AC Machine," U S Patent No 4,011,489 assigned to the General Electric Company
- 17 T A. Lipo, D.W. Novotny, A.B. Plunkett and V.R Stefanovic, "Dynamics and Control of AC Drives," Course notes, Univ. of Wisconsin Extension, November 3-5, 1976.

- 18 A. Schonung and D. Stemmler, "Static Frequency Changers with Subharmonic Control in Conjunction with Reversible Variable Speed AC Drives," *The Brown-Boveri Review*, pp 555-577 Aug /Sept 1974
19. A Abbondanti, J Zubek and C J. Nordby, "Pulse Width Modulated Inverter Motor Drives with Improved Modulation," Conference Record 1974 IEEE Industry Applications Society Annual Meeting, October 1974
- 20 Von Konrad Heintze, Hermann Tappeiner and Manfred Weibelzahl, "Pulswechselrichter zur Drehzahlsteuerung von Asynchronmaschinen," *Siemens Review*, Vol 45, No 3, p 154, 1971
- 21 K P Phillips, "Current Source Converter for AC Motor Drives," IEEE Publication 71-C1-IGA, *Conf. Rec. 1971 IGA 6th Annu. Meet.* pp 385-392, Oct. 18-21, 1971.
22. E P Cornell and T A. Lipo, "Modeling and Design of Controlled Current Induction Motor Drive systems," *Conf. Rec. IEEE-IAS 1975 10th Annu Meet.*, Sept. 28-Oct. 2, 1975.
- 23 A B Plunkett, J D. D'Atre and T.A. Lipo, "Synchronous Control of a Static AC Induction Motor Drive," *Conf. Rec 1977 IAS Annu. Meet.*, p 609, Oct 1977
24. W McMurray, "Optimum Snubbers for Power Semiconductors," *Conference Record 1971 IEEE Industry Applications Society Annual Meeting*, October 1971
25. "A Study of Flywheel Energy Storage for Urban Transit Vehicles," 16 September 1977, General Electric Report SRD-77-121, U S Department of Transportation, Contract DOT-UT-60096T
- 26 "Regenerative Flywheel Energy Storage System, Volume III Life Cycle and Cost Benefit Analyses of a Battery — Flywheel Electric Car," June 27, 1980, General Electric Report SRD-79-148-3, U S Department of Energy under subcontract No. 8990503 from Lawrence Livermore Laboratories
- 27 Grant, Ireson, and Leavenworth, *Engineering Economy*, 6th edition, p 72
28. L L. Liston and C A Aiken, "Cost of Owning and Operating an Automobile 1976," U S. Department of Transportation, Federal Highway Administration.
- 29 B D. Bedford and R G Hoft, *Principles of Inverter Circuits*, John Wiley and Sons, N Y., 1964

1 Report No NASA CR-167978	2 Government Accession No	3 Recipient's Catalog No		
4 Title and Subtitle  Improved Transistorized ac Motor Controller For Battery Powered Urban Electric Passenger Vehicles		5 Report Date September 1982	6 Performing Organization Code 778-36-06	
		8 Performing Organization Report No SRD-81-088	10 Work Unit No	
7 Author(s)  Steven C. Peak	9 Performing Organization Name and Address General Electric Company Power Electronics Laboratory Corporate Research and Development Schenectady, New York 12345		11 Contract or Grant No DEN 3-59	
12 Sponsoring Agency Name and Address U. S. Department of Energy Office of Vehicle and Engine R&D Washington, D. C. 20585			13 Type of Report and Period Covered Contractor Report	
			14 Sponsoring Agency Code- Report No. DOE/NASA/0059-1	
15 Supplementary Notes  Final Report. Prepared under Interagency Agreement DE-AI01-77CS51044. Project Manager, F. Gourash, Transportation Propulsion Division, NASA Lewis Research Center, Cleveland, Ohio 44135.				
16 Abstract  An improved ac motor controller for an induction motor electric vehicle drive system was designed, fabricated, tested, evaluated and cost analyzed. A vehicle performance analysis was done to establish the vehicle tractive effort-speed requirements. These requirements were then converted into a set of ac motor and ac controller requirements. The power inverter is a three-phase bridge using General Electric power Darlington transistors. The induction motor is a General Electric design optimized for use with an inverter power source. The drive system has a constant torque output to base motor speed and a constant horsepower output to maximum speed. A gear shifting transmission is not required. The ac controller was scaled from the base 20 hp (41 hp peak) at 108 volts dc to an expanded horsepower and battery voltage range. Motor reversal was accomplished by electronic reversal of the inverter phase sequence. The ac controller can also be used as a boost chopper battery charger. The drive system was tested on a dynamometer and results are presented. The current-controlled pulse width modulation control scheme had improved motor current waveforms. The ac controller favors a higher system voltage. Suitable power transistors are becoming more readily available but are costly, however this is expected to change in the future. Recommendations for future work are made.				
17 Key Words (Suggested by Author(s))  Inverter, Induction motors, Power transistors, Pulse width modulation, Harmonics, Efficiency, Motor controls, Life cycle cost, Electric vehicle, Propulsion system, Powertrain, Drivetrain		18 Distribution Statement  Unclassified - unlimited STAR Category 33 DOE Category UC-96		
19 Security Classif (of this report)  Unclassified	20 Security Classif (of this page)  Unclassified	21 No of Pages  240	22 Price*  A11	

\* For sale by the National Technical Information Service, Springfield, Virginia 22161

**End of Document**